Calcium Calmodulin Dependent Protein Kinase II in the Development of Atherosclerosis

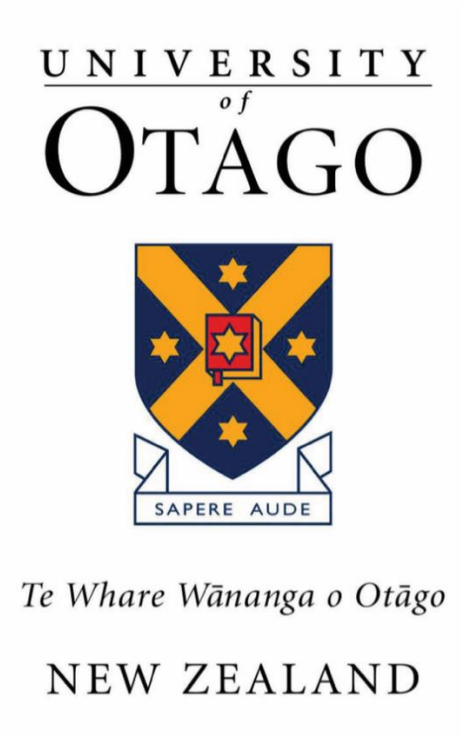

Luke P.I. Worthington

A thesis submitted in fulfilment of the requirements for the degree of Doctor of Philosophy

Department of Physiology, Otago School of Biomedical Sciences, University of Otago, Dunedin, New Zealand,

November 2020

Abstract

Atherosclerosis is the leading cause of death in the developed world. The accumulation of low-density lipoprotein cholesterol (LDL-C) in the arterial wall leads to the formation of foam cell lesions. The growth of lesions is influenced by a number of genetic and lifestyle factors. Over-time, lesions encroach the vessel lumen, impeding blood flow and increasing risk of cardiovascular events including myocardial infarction and stroke. Statins have been effective at reducing risk for cardiovascular events, however, even when target LDL-C levels are met there remains a significant residual risk. Clearly, a detailed investigation into the mechanism of foam cell lesion growth is required to explore new drug targets to ease the burden on the health care system.

Calcium/calmodulin-dependent protein kinase II (CaMKII) is a nodal signalling protein in endothelial cell (EC) and vascular smooth muscle cell (VSMC) physiology. In vascular disease, CaMKII has been shown to promote endothelial dysfunction and vascular smooth muscle cell proliferation. Both of these pathologies are involved in the early stages of atherosclerosis so it is intriguing to speculate that CaMKII also contributes to atherosclerosis. We have previously shown systemic inhibition of CaMKII in an atherosclerotic model ($ApoE^{-/-}$ mice) reduces foam cell lesion development. However, there are multiple isoforms of CaMKII (α, β, δ and γ) and associated splice variants. These sub-types are differentially expressed in the tissues of the body and have shown contrasting roles. A global inhibition of CaMKII is not a feasible target due to the important physiological functions of these multiple isoforms. Therefore, it is crucial we identify the isoform(s) contributing to foam cell lesion growth so a more specific therapeutic target can be explored.

Firstly, the predominant isoforms of CaMKII were identified in the major cell types of the vasculature. The aortic tree was dissected from $ApoE^{-/-}$ mice at 13- (early atherosclerosis) and 20-weeks (mid-atherosclerosis). In addition, human umbilical vein endothelial cells (HUVECs), human coronary artery endothelial cells (HCAECs) and human coronary artery smooth muscle cells (HCASMCs) were cultured. PCR and Western blotting was run for CaMKIIδ and γ isoforms. Results showed CaMKIIδ as the predominant isoform in human and mouse vascular cells. In addition, at the mRNA level, splice variants δ_2, δ_3 and δ_6 were detected. CaMKIIδ expression

was high at 13-weeks in the ApoE$^{-/-}$ mouse and levels persisted at 20-weeks, suggesting the δ isoform is the most likely isoform contributing to atherosclerosis.

To investigate if CaMKIIδ signalling contributed to foam cell lesion development, we next employed a genetic approach. ApoE$^{-/--}$mice were crossed with CaMKIIδ$^{-/-}$ to generate a novel ApoE$^{-/-}$CaMKII$^{-/-}$ (dKO) mouse model. At 20-weeks there was extensive atherosclerosis in the aortic sinus of female, but not male groups. Histological analysis showed there was a strikingly significant reduction in foam cell lesion content in female ApoE$^{-/-}$CaMKIIδ$^{-/-}$, compared to ApoE$^{-/-}$CaMKIIδ$^{+/+}$ litter mate controls. This indicates the CaMKIIδ isoform is a critical player in the early development of atherosclerosis.

To further test the mechanistic role of CaMKIIδ in foam cell lesion development, an opposite strategy was performed whereby an AAV-mediated overexpression approach was utilised. ApoE$^{-/-}$CaMKIIδ$^{-/-}$ mice were put on a high-fat diet at 12-weeks to accelerate atherogenesis. At 16-weeks of age, the left carotid arteries of ApoE$^{-/-}$CaMKIIδ$^{-/-}$ mice were ligated to increase shear stress and further promote foam cell lesion growth in a localised area. AAV-particles harbouring the CaMKIIδ_2 or control (scrambled) gene sequence were then introduced to the ligated left carotid artery. Ligation of the carotid artery led to a range of variation in foam cell lesion progression. Histological analysis of the carotid artery revealed the foam cell lesion area and stenosis from CaMKIIδ_2-mCherry mice showed a trend towards an increase, despite low n numbers due to adverse complications in 20% of the ligated mice.

In summary, a number of genetic and molecular biological techniques have been used to provide evidence to show CaMKIIδ contributes to the early stages of atherosclerosis. Importantly, there is still work that needs to be done to further validate this mechanism and the potential contribution of other delta variants and/or other isoforms. This novel study has provided foundation evidence of CaMKIIδ as a specific target for treatment. The results provide impetus to continue the investigation of CaMKIIδ that ultimately, could lead to a pharmacological intervention to treat the early progression of atherosclerosis.

Conferences and Meetings

Worthington L. P. I, Erickson J. R. and Heather A. K. Targeting CaMKII in Atherosclerosis **2017** MedSci Congress, Queenstown, New Zealand (poster presentation).

Worthington L. P. I, Erickson J. R. and Heather A. K. CaMKII Inhibition Reduces Foam Cell Lesion Development in the Brachiocephalic Artery of Apolipoprotein $E^{-/-}$ Mice. **2018** MedSci Congress, Queenstown, New Zealand (poster presentation).

Worthington L. P. I and Heather A. K. CaMKII in the Development of Atherosclerosis. **2018** Joint Annual Scientific Meeting of the High Blood Pressure Research Council, Australian Atherosclerosis Society and Australian Vascular Biology, Adelaide, South Australia (oral presentation).

Worthington L. P. I, Erickson J. R. and Heather A. K. CaMKIIδ Promotes Foam Cell Lesion Development in the Apolipoprotein $E^{-/-}$ Mouse. **2019** Biomedical Sciences Postgraduate Symposium, Dunedin, New Zealand (oral presentation).

Worthington L. P. I and Heather A. K. CaMKII Promotes the Early Development of Atherosclerosis. **2019** Heart Otago, Dunedin, New Zealand (oral presentation).

Acknowledgements

There is a reason why the acknowledgements appear at the beginning, not the end of the thesis. It is only fitting that I firstly express my sincere gratitude to the following people for their contribution to my research and their assistance in the completion of my work.

To Professor Alison Heather, thank you for your excellent mentoring, your professional and personal support, your leadership in creating a dynamic work environment, and your efforts to attain the funding for the research. Also to Dr Jeff Erickson, and other academics in the department who always provided great feedback and advice.

To Gill Hughes, thank you for your significant contribution to my research. From day one you shared your impressive technical knowledge and skills to set me up with the fundamentals needed to carry out independent research and I am extremely grateful for this. Also, to Alexia Kauff and Dr Zoe Ashley for your assistance in some of the more demanding methods in the project, I appreciate the expertise.

To my colleagues and friends, Dr Mike Gill, Dr Adam Denny, Dr Rachel Lund and Sam O'Hara. Thank you for providing a great environment in the lab, office or tea room and for all for your support and encouragement over the last few years. I wish you well in your careers and hope that our paths will cross often in the future. My grateful thanks also goes to all the administrative staff of the Physiology Department, who were always very approachable.

It is not always a smooth journey and this is one that would not have been possible without a caring and supportive family. Anna, Tom and Maggie, you have always inspired me to push myself through your own skills and achievements throughout your lives so far. Emily and John, I will always appreciate the home and support you have provided for me over the last couple years. Mum and Dad, thanks for your tremendous support over my life and studies. Mum, your personal strength is inspiring and I will never forget your encouragement through these last few years. Dad, you had always shown great interest in my studies and will always be a role model. The motivation and drive you have provided has been instrumental in this thesis and I will miss not being able to share this work with you. This thesis is dedicated to you.

Table of Contents

List of Figures

List of Tables

Abbreviations

AAV	Adeno-associated virus
ANOVA	Analysis of variance
$ApoE^{-/-}$	Apolipoprotein E knockout
ATP	Adenosine tri-phosphate
bp	base pair(s)
BP	Blood pressure
BSA	Bovine serum albumin
Ca^{2+}	Calcium ion
CABG	Coronary artery bypass graft
CaMKII	Calcium/calmodulin-dependent protein kinase II
CaM	Calmodulin
CAD	Coronary artery disease
cDNA	Complimentary deoxyribose nucleic acid
CHD	Coronary heart disease
CETP	Cholesterol ester transport protein
CO_2	Carbon dioxide
CT	Computed tomography
CVD	Cardiovascular disease
CVS	Cardiovascular system
DEPC	Diethyl pyrocarbonate
DES	Drug-eluting stent
DMEM	Dulbecco's modified eagle medium
DMSO	Dimethyl sulfoxide
DNA	Deoxyribose nucleic acid
ECs	Endothelial cells
ECM	Extracellular matrix
ED	Endothelial Dysfunction
EDRF	Endothelium-derived relaxing factor
EDTA	Ethylenediaminetetraacetic acid
EEL	External elastic lamina
eNOS	Endothelial nitric oxide synthase

ER	Endoplasmic reticulum
FBS	Fetal bovine serum
g	Grams
G	Gravity
GAPDH	Glyceraldehyde 3-phosphate dehydrogenase
GFP	Green fluorescent protein
HCl	Hydrochloric acid
HDL	High-density lipoprotein
HFD	High-fat diet
Hrs	Hours
Hu	Human
HCAECs	Human coronary artery endothelial cells
HCASMCs	Human coronary artery smooth muscle cells
HMG-CoA	Hydroxy-methylglutaryl coenzyme A
HUVECs	Human umbilical vein endothelial cells
H_2O_2	Hydrogen peroxide
HSF-1	Heat shock factor-1
IEL	Internal elastic lamina
ICAMs	Intracellular cell adhesion molecules
IFN-γ	Interferon-γ
IL-1β	Interleukin-1β
IL-6	Interleukin-6
IL-10	Interleukin-10
IMA	Internal mammary artery
kDa	Kilo Dalton
KO	Knock out
L	Litre
LAD	Left anterior descending coronary artery
LCx	Left circumflex artery
LDL-C	Low-density lipoprotein cholesterol
LFA-1	Lymphocyte function-associated antigen-1
LSA	Left subclavian artery
M	Molar

Mac-1	Macrophage-1-antigen
MACE	Major adverse cardiac event
MAPK	Mitogen activated protein kinase
M-CSF	Macrophage colony stimulating factor
MEF-2	Myocyte enhancer factor-2
mg	Milligram
MI	Myocardial infarction
mL	Millilitre
MMP-9	Matrix metalloproteinase-9
mRNA	Messenger ribonucleic acid
Ms	Mouse
MSRA	Methionine sulfoxide reductase
mins	Minutes
N_2	Nitrogen
NADPH	Nicotinamide adenine dinucleotide phosphate
ND	Normal diet
NaCl	Sodium chloride
NF-κB	Nuclear factor-kappa B
ng	Nanogram
nM	Nanomoles per litre
NO	Nitric oxide
NOS	Nitric oxide synthase
NLS	Nuclear localisation signal
NTC	No template control
O_2	Molecular oxygen
Ox-LDL-C	Oxidised low-density lipoprotein cholesterol
PBS	Phosphate buffered saline
Pen/Strep	Penicillin/ Steptomycin
PCI	Percutaneous coronary intervention
PCR	Polymerase chain reaction
PDGF	Platelet-derived growth factor
PFA	Paraformaldehyde
PFU	Plaque forming units

PP1	Protein Phosphatase-1
PTM	Post-translational modification
PVDF	Polyvinylidene fluoride
RCA	Right coronary artery
RSA	Right subclavian artery
RNA	Ribose nucleic acid
ROS	Reactive oxygen species
rSAP	Recombinant shrimp alkaline phosphatase
RT-PCR	Reverse transcription polymerase chain reaction
RyR2	Ryanodine receptor 2
SEM	Standard error measurement
TBS	Tris buffered saline
TBST	Tris buffered saline tween 20
TLRs	Toll-like receptors
TNF-α	Tumour necrosis factor-alpha
VCAMs	Vascular cell adhesion molecules
VCAM-1	Vascular cell adhesion molecule-1
VLA-4	Very late antigen-4
VLDL	Very low-density lipoprotein
VSMCs	Vascular smooth muscle cells
WB	Western blot
U/ml	Units per millilitre
µg	Microgram
µg/kg	Microgram per kilogram
µL	Microlitre
µm	Micrometre
µmol	Micromole
°C	Degrees Celsius
3’	Three prime
5’	Five prime

Chapter 1: Introduction

Cardiovascular disease (CVD) is the most significant health problem and burden on the health care system in the developed world. Atherosclerosis or coronary artery disease (CAD) is the major CVD characterised by 'fatty' arteries. Atherosclerosis manifests into a range of pathologies as well as life threatening events including myocardial infarction (MI) and stroke. In 2017, CVD was estimated to be responsible for 17.8 million deaths globally [1]. Clearly there is a major burden on the health care system that, in turn, provides strong impetus for research into the pathogenesis of atherosclerosis.

1.1 The cardiovascular system

The cardiovascular system (CVS) is composed of the heart and a number of specialised vessels which supply the tissues and vital organs around the body [2]. Oxygenated blood is ejected out of the heart at high pressure (~120mmHg) into the systemic circulation and travels to organs by a pressure gradient through a diverging network of arteries [3]. The arterial network diverges further at the target organ into a fine network of vessels, termed capillaries, which are specialised for gas exchange and diffusion of nutrients [4]. As well as providing nutrients to the organ at the capillary bed, the systemic circulation is just as vital for the removal of CO_2 and other byproducts of cellular metabolism. Following gas exchange at the capillary bed, de-oxygenated blood rich in CO_2 is collected via venules and converges into a lower pressure network of vessels called veins and returned to the heart [2]. At the heart, blood is pumped into the pulmonary circulation to offload CO_2 and to become re-oxygenated (**Figure 1.1**) [3].

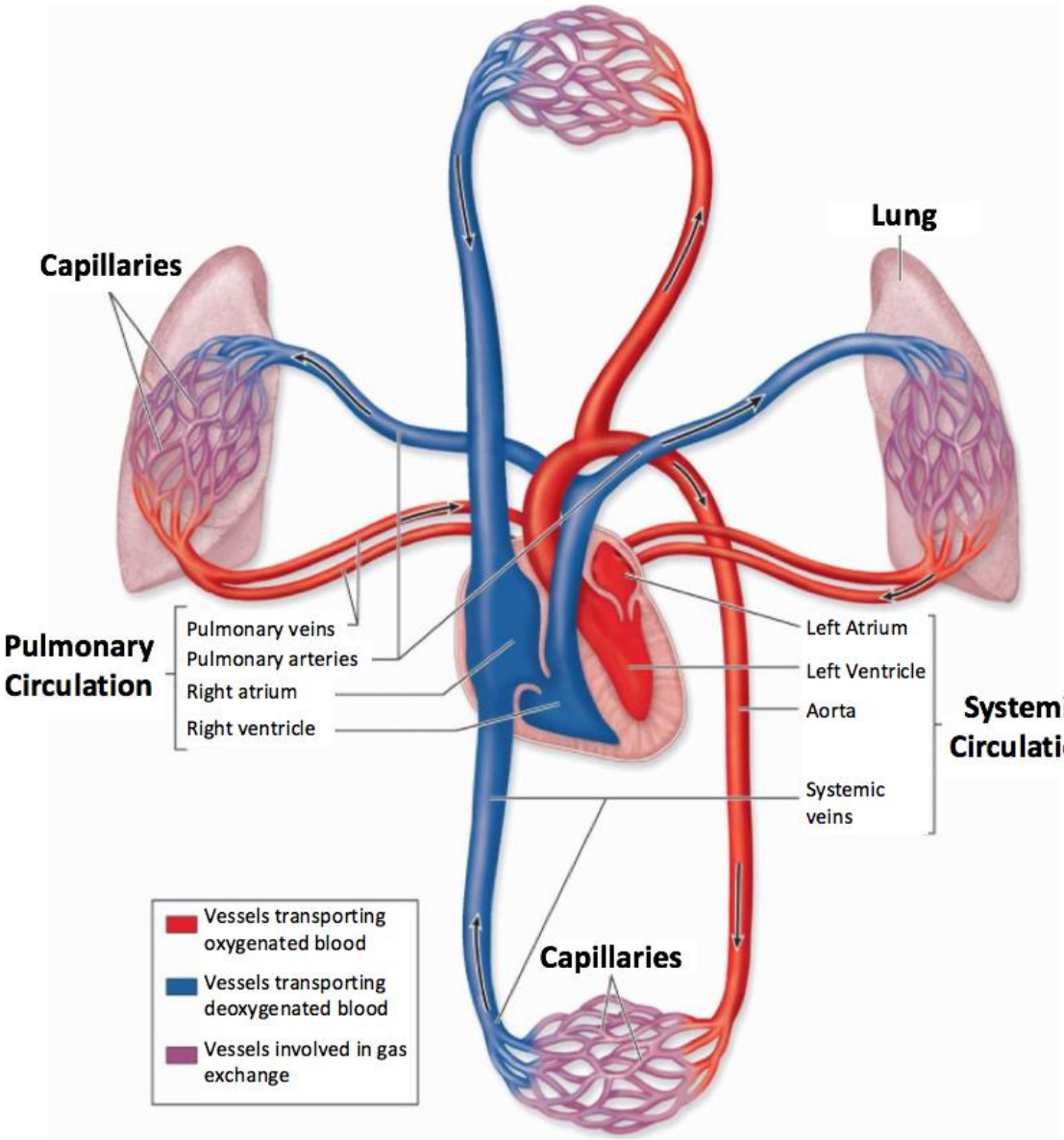

Figure 1.1: Basic schematic of the cardiovascular system (CVS). *The CVS is made up of the heart and blood vessels including arteries and veins. Oxygenated blood (red) is ejected out of the heart into the systemic circulation and is conducted to the organs around the body via arteries. At the organ the artery diverges into a fine network of blood vessels termed capillaries (purple). Deoxygenated blood (blue) is drained via venules and collected into the systemic veins to be returned to the heart. At the heart deoxygenated blood is pumped into the pulmonary circulation to offload CO_2 and pick up O_2. Figure adapted from https://basicmedicalkey.com/the-circulatory-system-2/.*

1.1.1 Structure of the Vessel Wall

The blood vessels, which compose the CVS supplying the organs around the body have three main layers. Both arteries and veins have the same layers, however the composition and size of each specific layer varies allowing different functions. The arteries are specifically adapted to provide an efficient delivery network in a high-pressure environment.

The three layers of an artery include the tunica intima, media and adventitia (**Figure 1.2)** [5]. The tunica intima is the inside layer of the artery exposed to the vessel lumen. This layer consists of a single layer of endothelial cells (ECs) on an extracellular matrix rich in elastic fibres called the internal elastic lamina (IEL). The endothelium plays a key role in both restricting and facilitating the entry of substances between the blood and sub-intimal space [6]. The ECs also release a number of substances that have anti-adhesive and antithrombotic properties to allow laminar flow of blood [7].

The middle layer of the artery wall is the tunica media. In an artery, this region, occupied by vascular smooth muscle cells (VSMCs), makes up the bulk of the total vessel size [8]. VSMCs have a critical role in the generation of vascular tone to maintain physiological blood pressure (BP) through constriction and relaxation [9]. Modulation of tone is critical in regulating blood flow in response to a change in metabolic demand. This is regulated mainly by extrinsic mechanisms such as the autonomic nervous system and locally released growth factors and vasoactive substances [10].

The outer most layer of the artery wall is the tunica adventitia which is separated from the tunica media by a tight bundle of elastin fibres, termed the external elastic lamina (EEL). This layer is composed of tightly bound collagen and elastin, important for providing structural support [8]. Additionally, in the larger arteries, the adventitia contains a network of micro blood vessels, important for providing nutrients to the muscular wall [11].

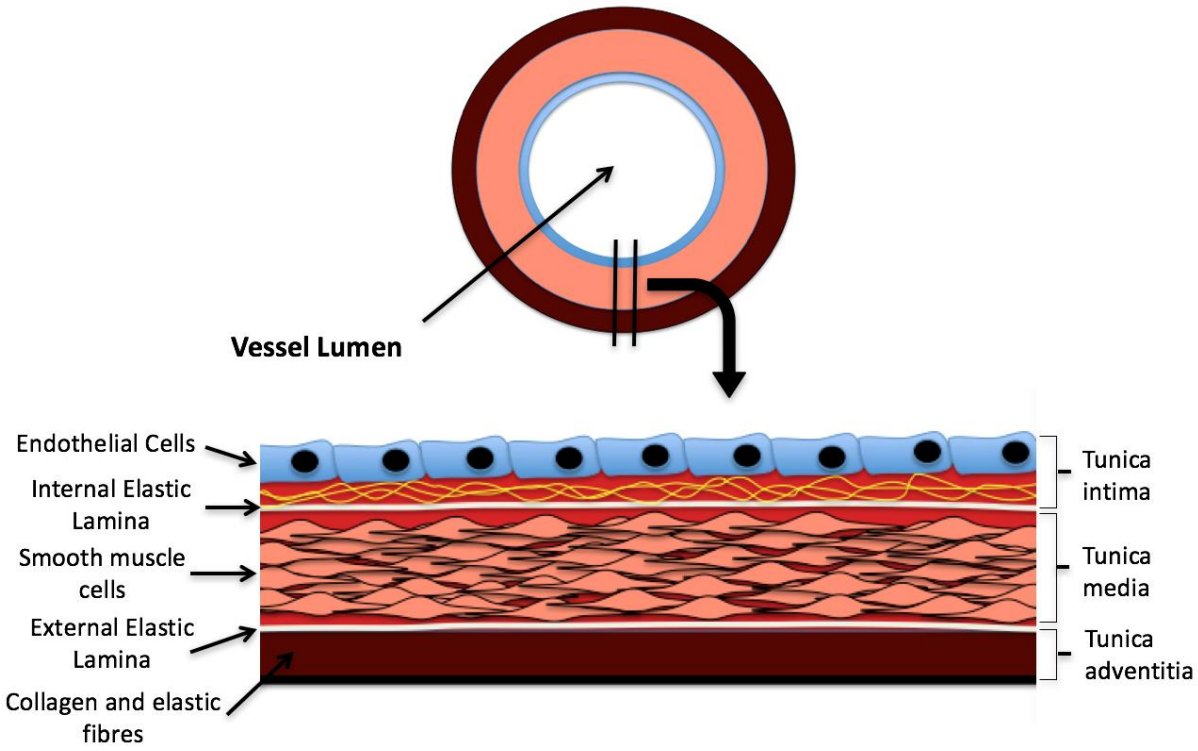

Figure 1.2: Structure of an artery. *The artery wall is composed of three distinct layers. The tunica intima consists of a single layer of endothelial cells which sits on a matrix of elastin fibres called the internal elastic lamina. The tunica media is the largest layer of the vessel wall and contains smooth muscle cells. The tunica adventitia is the outside layer of the artery and consists of collagen and elastin fibres. Worthington, 2016.*

The maintenance of a healthy artery is critical to provide efficient transport of blood around the organs of the body. The arteries are exposed to a volatile high pressure environment. The ECs and VSMCs are equipped with a number of inherent defense mechanisms through the release of active substances which promote vascular health. Over time, cumulative insult to the vascular wall reduces proper functioning of the cells of the vasculature and promotes the emergence of vascular pathology such as atherosclerosis [12].

1.2 Pathogenesis of Atherosclerosis

Atherosclerosis is a vascular pathology characterised by the formation of lipid-laden lesions (atheroma) on the inner layer of the artery wall (**Figure 1.3**). Atherosclerosis is multifactorial, meaning the disease progression is a cumulative effect from a number of genetic and environmental risk factors [13]. The most significant risk factor for the development of atherosclerosis is elevated plasma low-density lipoprotein cholesterol (LDL-C) [14-16]. Other risk factors include hypertension, type II diabetes, smoking and physical inactivity [17-19].

The two main hypotheses describing how atherosclerosis is initiated include the LDL-C and the response to injury (endothelial dysfunction) hypothesis [20, 21]. In the LDL-C hypothesis, the atherosclerotic lesion starts as a small streak of LDL-C in the artery wall [22]. LDL-C becomes oxidised and promotes an inflammatory response leading to the recruitment of monocytes to the vascular wall. Monocytes differentiate into macrophages and carry out phagocytosis of LDL-C/ox-LDL-C. In the process of lipid accumulation, macrophages transform into foam cells. Additionally, inflammatory signaling molecules promote migration and proliferation of VSMCs from the media to the sub-intima driving lesion growth. Over-time the atherosclerotic lesion can undergo further compositional changes that make the lesion vulnerable to rupture. Thrombolysis of atherosclerotic lesions are responsible for ischaemic attack including myocardial infarction (MI) and stroke [23]. For the purpose of this thesis, the early mechanisms of atherosclerosis which promote foam cell lesion growth are of the most interest.

1.2.1 Endothelial Dysfunction – the initiation of atheroma

The endothelial cells (ECs) that line the lumen of the artery wall play a critical role in vascular health. In a healthy artery, endothelial cells regulate the entry and exit of substances between the blood and vessel wall. These include hormones, nutrients and cells of the immune system. ECs release vasoactive substances such as nitric oxide (NO), prostacyclin and bradykinin for dilation and endothelin and angiotensin II for constriction [24] [25] [26] [27] [28] [29]. Additionally, NO has added protective functions to promote a non-adhesive surface for laminar blood flow [30, 31]. Over time, cumulative damage to the endothelial wall leads to a loss of function of these defense mechanisms and ECs become unable to maintain vascular homeostasis [32]. Endothelial dysfunction is a primary event in vascular disease such as atherosclerosis [20, 33].

Atherosclerosis is predisposed in curved and bifurcating sites around the aortic tree [26]. These regions are exposed to turbulent oscillatory patterns of shear stress which promote endothelial dysfunction [34, 35]. In mammalian arteries, these regions include the aortic arch, brachiocephalic artery, coronary arteries and the carotid artery bifurcation [36]. Endothelial dysfunction is associated with a change in appearance of the endothelial cell structure from a thin elongated to a contracted appearance [37]. This is associated with increased permeability properties promoting the deposit of circulating atherogenic substances such as LDL-C into the vessel wall [22, 38]. Alongside increased permeability properties, the endothelial cells express adhesion molecules such as vascular cell adhesion molecule 1 (VCAM-1) and intracellular cell adhesion molecule 1 (ICAM-1) [39, 40]. These adhesion molecules allow ligation of circulating immune cells such as monocytes to the vessel wall. Collectively, increased adhesion and permeability of the endothelial wall are critical steps in the early events of atherosclerosis.

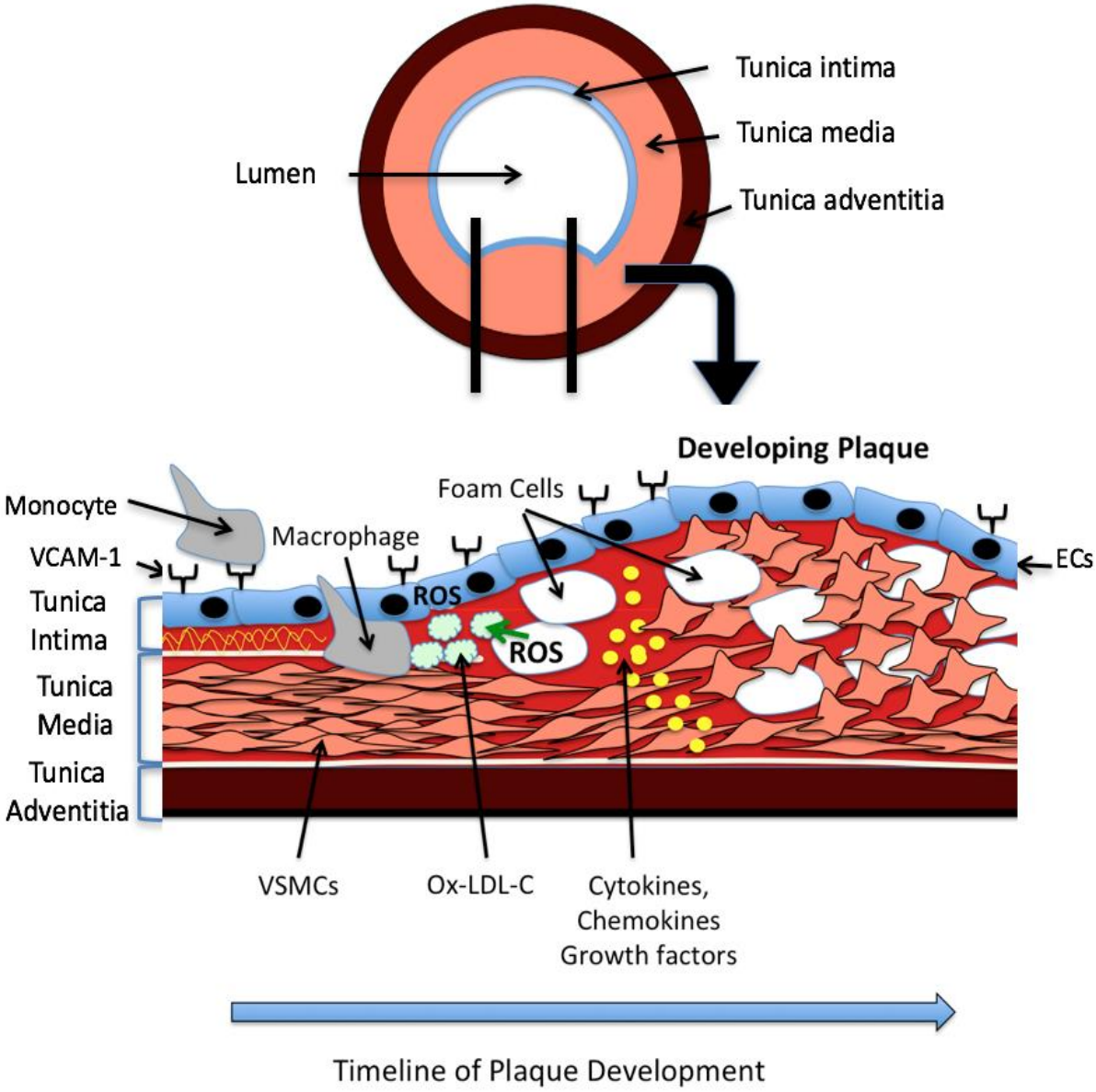

Figure 1.3: The pathogenesis of atherosclerosis. *Endothelial dysfunction leads to the expression of cell adhesion molecules including VCAM-1. Circulating LDL cholesterol becomes deposited in the artery wall leading to an inflammatory response. Over time, LDL cholesterol becomes oxidised and promotes the recruitment and infiltration of monocytes into the sub-intima. Monocyte-derived macrophages engulf the oxidised LDL-C and differentiate into foam cells. Foam cells release cytokines, chemokines, growth factors and reactive oxygen species (ROS) which promote a switch in VSMC phenotype from contractile to synthetic. In the synthetic phenotype, VSMCs migrate to the sub-intima space and proliferate driving atherosclerotic lesion growth. Worthington, 2016.*

1.2.2 The Inflammatory response – monocytes to macrophage-foam cells

Atherosclerosis is a chronic inflammatory disease that involves a complex environment of signalling molecules including chemokines, growth factors and reactive oxygen species (ROS). These signalling molecules culminate to drive an inflammatory response to ameliorate insult to the vessel wall. However, with sustained insult to the vascular wall the immune response loses the ability to maintain vascular health and atherosclerotic lesions present throughout the arterial tree. There are two main populations of monocytes that are important in the initiation and progression of atherosclerosis. These include resident macrophages and circulating monocytes [41, 42].

In the healthy artery there is a small population of macrophages that reside in the vascular wall [41]. Over time, LDL-C within the artery wall becomes oxidised triggering a local inflammatory response [43]. This is mediated, in-part, through the activation of toll-like receptors (TLRs) on macrophages and other cell groups of the vasculature [44, 45]. The activation of TLRs leads to pro-inflammatory signalling through the expression of cytokines like TNF-α and transcription factors such as nuclear factor kappa B (NF-κB) [46]. NF-κB is a transcription factor critical for regulating the expression of a large number of genes involved in the inflammatory response. In resident macrophages, activation of TLRs promotes phagocytic activity for LDL-C clearance [47]. Additionally, macrophages release TNF-α and IL-1β, which diffuse into the local environment and have effects such as promoting adhesion molecule expression in ECs [40, 48]. Collectively, this early inflammatory response functions to stimulate phagocytic activity of resident macrophages but also promote the recruitment of circulating monocytes.

Circulating monocytes in the blood are recruited to the endothelial wall through an increased expression of the adhesion molecules, VCAM-1 and ICAM-1. Monocytes express a variety of integrins on the cell surface including lymphocyte function-associated antigen-1 (LFA-1), macrophage-1-antigen (Mac-1) and very late antigen 4 (VLA-4). LFA-1 and Mac-1 interact with ICAM-1 whereas VLA-4 primarily interacts with VCAM-1 [49-51]. Once the monocyte is bound to the endothelial wall via a specific integrin, migration of the monocyte into the sub-intima space can occur. This migration can be either transcellular, requiring transport through both the apical and basolateral membrane, or paracellular, between cells [52].

As monocytes migrate into the sub-intima, they are exposed to a new environment of cytokines and growth factors which stimulate differentiation into macrophages. Some of these signalling molecules include interferon γ (IFN-γ), ox-LDL-C, TNF-α, IL-10 and macrophage colony stimulating factor (M-CSF) [53]. As differentiation occurs, macrophages increase expression of a range of scavenger receptors which have the ability to take up LDL-C and ox-LDL-C [54, 55]. Additionally, macrophages carry out pinocytosis, or the incorporation of the extracellular environment by endocytosis including cytokines and LDL-C [56, 57]. In the process of LDL-C uptake, macrophages transform into foam cells [58, 59]. Foam cells also contain ATP binding cassette transporters, ABCA1 and ABCG1, that are important for cholesterol efflux [60, 61]. The balance between lipid transport into and out of foam cells is critical to prevent the cytotoxic effects of excess LDL-C uptake [62, 63]. When lipid accumulation overtakes storage capabilities, lipid pooling occurs in the extracellular matrix (ECM). Histologically, this is observed as the lipid core [64].

With disease progression, excessive foam cell lipid accumulation leads to endoplasmic reticulum (ER) stress and the activation of apoptotic cell pathways [65, 66]. This triggers efferocytosis (phagocytosis) of the apoptotic cell by neighbouring macrophages to clear cellular debris [67]. With lesion progression, the increase in lipid pooling and apoptotic cell bodies becomes too much for phagocytic activity and secondary necrosis occurs [68]. This is at an advanced stage of lesion progression and histologically classified as the necrotic core [69].

1.2.3 Vascular smooth muscle cells – driver of lesion size

The vascular smooth muscle cells (VSMCs) are another major cell group critical to the development of atherosclerosis. VSMCs can display two distinct structural and functional ends of diversity as well as a number of intermediates [10]. In a healthy artery, VSMCs display a contractile phenotype important for the maintenance of arterial tone. In contrast, in development or disease, VSMCs switch to a synthetic phenotype characterised by increased migration and proliferation [10].

In the contractile phenotype, VSMCs have a long spindle-like structure. Additionally, contractile VSMCs maintain a high expression of ion channels and molecular machinery which facilitate VSMC contraction [70, 71]. In response to certain stimuli or environmental cues, the phenotypic state of VSMCs is modulated to a synthetic state. In the synthetic state, VSMC loses the contractile filaments and has an increase in the factory organelles including endoplasmic reticulum (ER) and Golgi apparatus [72]. Functionally, VSMC have increased proliferation and migration as well as the ability to synthesise ECM.

Macrophage-foam cells in the sub-intima release cytokines, like TNF-α, which activates the NF-κB transcription factor to promote the expression of a specific subset of cytokines such as interleukin-6 (IL-6) [73]. IL-6 diffuses into the local vessel wall environment and acts in a paracrine manner to stimulate production of platelet-derived growth factor (PDGF) in VSMCs [74]. PDGF is a potent mitogen that activates a range of signalling pathways including mitogen-activated protein kinase (MAPK). Activation of MAPK stimulates a series of phosphorylation events that trigger the VSMCs into the cell cycle [75]. Alongside proliferation, the MAPK pathway promotes cytoskeletal rearrangements to drive migration [76]. VSMCs also produce matrix degrading enzymes such as matrix metalloproteinase 9 (MMP-9), which facilitate migration from the tunica media to the intima [77, 78]. Collectively, proliferation and migration of the VSMCs to the tunica intima is a major mechanism for lesion growth [79].

The dynamic modulation of VSMC phenotype is further highlighted when VSMCs migrate to the sub-intima. At the tunica intima VSMC can carry out phagocytic activity similar to neighbouring macrophages and foam cells [80]. This is achieved through expression of cholesterol transporters [81, 82]. As the lesion develops VSMCs are responsible for the synthesis and secretion of the ECM. This includes a number of glycoproteins which can influence stability of developing lesion. For example, IFN-γ released by macrophages leads to the production of collagen to promote the development of the fibrous cap over the growing lesion [83].

In summary, VSMCs display a range of synthetic phenotype functions that all promote atherosclerosis. These include proliferation, migration, lipid accumulation and ECM synthesis. Ultimately, VSMCs are the major cell group responsible for growth of the lesion as well as the composition.

1.2.4 Classification of Atherosclerotic Lesions

Atherosclerotic lesion growth is dynamic and progresses over decades. There is an extensive classification system that details the different lesion phenotypes throughout disease progression [69, 84]. However, for simplicity, this extensive system can be more broken down into four main lesion categories. Each lesion type is categorised based on lesion size and the physical composition of lesion components. The four types include; fatty streak, intermediate lesion, fibrous plaque and advanced plaque (**Figure 1.4**).

The fatty streak is the first clinical indication of atherosclerosis indicated by expansion of the tunica intima alongside the accumulation of fat droplets in the sub-intima space. These early lesions have been identified in children and teenagers from post-mortem examination [85]. The intermediate lesion contains lipid droplets and foam cells derived from monocytes and VSMCs. The intermediate lesion progresses to the fibrous lesion at the appearance of a fibrous cap over the developed lipid core [84, 86]. At this point, other cells of the immune system are recruited to the lesion [87, 88]. An advanced plaque is characterised by a necrotic lipid core [69]. Other components include calcification, infiltration of blood vessels and thinning of the fibrous cap. These components all culminate to influence the stability of a lesion and thrombolytic activity [89, 90].

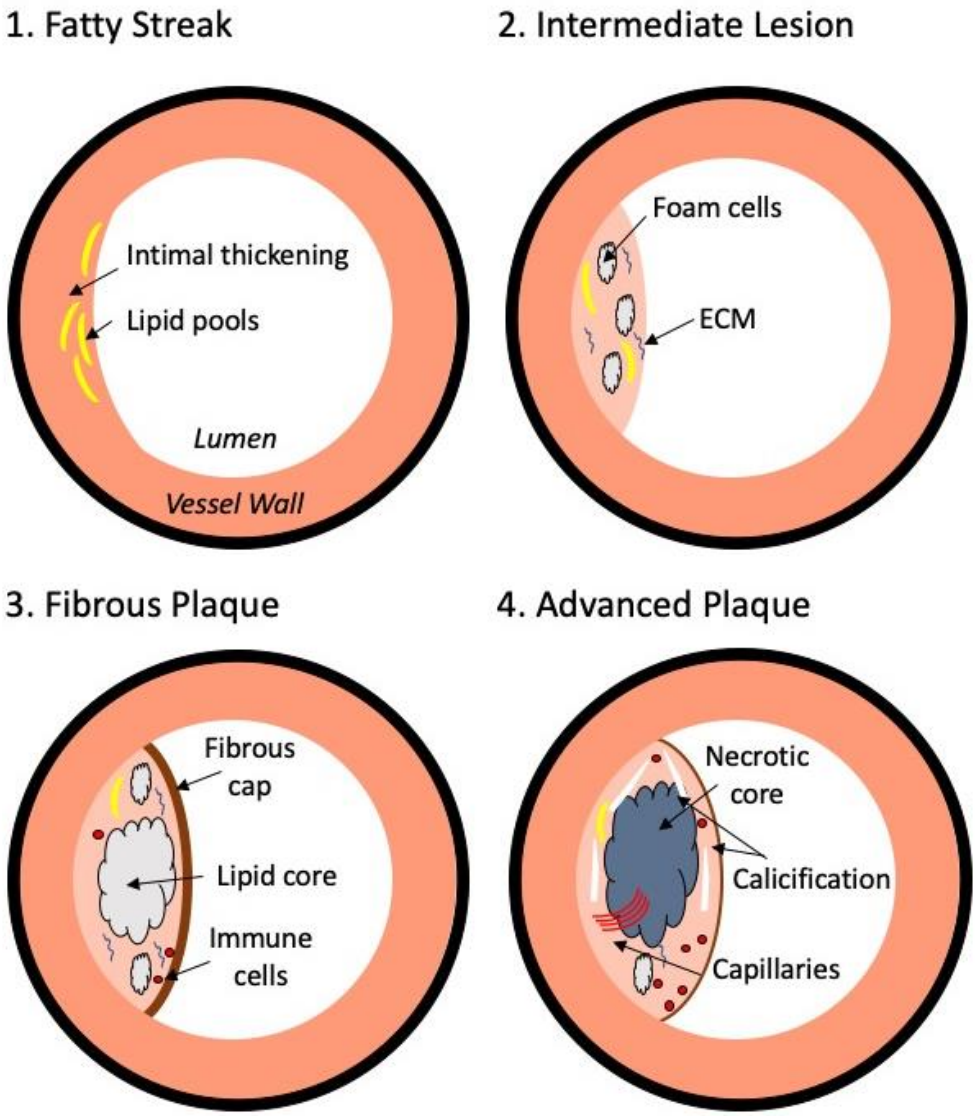

Figure 1.4: Classification of atherosclerotic lesions. *Intimal thickening and lipid droplet accumulation (1). Intermediate lesion consists of foam cells in a growing sub-intima (2). Lipid core, presence of immune cells and developed fibrous cap (3). Necrotic core, capillary infiltration and calcification and thinning of the fibrous cap (4). Original Figure, Luke Worthington, 2020.*

1.3 Atherosclerosis – a clinical perspective

Atherosclerotic lesions remain stable and asymptomatic for decades [91, 92]. The progression of lesion development is influenced by a number of genetic and environmental factors including elevated LDL-C, hypertension, type II diabetes and smoking [14, 16, 18, 19, 93, 94]. Controlling the progression of atherosclerotic lesion growth is not the only issue. With disease development, morphology of the lesion also changes toward a phenotype that is susceptible to rupture [95]. The rapid thromboembolic complications that arise from lesion rupture including myocardial infarction (MI) and stroke are life-threatening and present a challenge to the clinic.

The progressive build-up of atherosclerosis in the coronary arteries leads to a reduction in blood flow exerting metabolic stress on the heart, termed angina [96]. Angina is an early clinical symptom of CAD, and patients commonly described experiencing shortness of breath and tightness across the chest [97]. However, angina is not always the first clinical symptom of CAD and in fact death can be the first symptom with no previous warnings [98, 99]. The asymptomatic nature of lesion growth prior to any clinical symptoms means the disease is poorly monitored in its early stages [92]. Instead, patients will receive treatment only after they have come into the clinic with angina, or after a major adverse cardiac event (MACE) including myocardial infarction and stroke [100, 101]. Therefore, clinical treatment for atherosclerosis only occurs at a very late stage in its progression.

1.3.1 Pharmacological treatment of CAD

The benefits of improving lifestyle factors such as increasing exercise for decreased cardiovascular risk has been exhausted in the literature [86, 102, 103], and both lifestyle and pharmacological intervention to improve cardiovascular outlook is promoted and used in the clinic [104-106]. CAD is multifactorial and many patients have pre-existing co-morbidities such as type II diabetes and hypertension which need to be considered for drug selection [15, 107, 108]. Therefore, in reality, there is not a blanket subset of drugs for treatment of CAD in every patient. Instead, a range of drug classes including anticoagulants, antiplatelet therapy, nitrates, Ca^{2+} channel blockers, statins and beta-blockers are used to treat CAD and improve

vessel health [109-113]. This results in a cocktail of pharmaceuticals needing to be tailored to the needs of each patient [114, 115].

For the acute management of unstable angina, relief is best achieved with dual anti-platelet therapy, commonly clopidogrel and aspirin [116, 117]. This provides an effective mechanism to prevent blood clots while reducing blood viscosity and vessel wall shear stress [118-120]. For relief against angina which persists for extended periods, additional drugs are also effective at ameliorating symptoms. Ca^{2+} channel blockers and nitrates are used to promote relaxation and inhibit contraction of VSMCs to increase vessel diameter and improve blood flow [24, 121, 122]. Beta-blockers are also sometimes used in patients with CAD to decrease the metabolic demands of the heart and also increase the diastole phase of the cardiac cycle, when blood is circulating through the coronary arteries [109, 123]. In summary, the action of these drugs aim to improve CAD by augmenting coronary blood flow, while limiting myocardial oxygen demands.

The gold standard drug therapy for the treatment of coronary artery disease is the use of statins [124, 125]. Statins inhibit 3-hydroxy-methylglutaryl coenzyme A (HMG-CoA) reductase, an essential enzyme in the production of LDL-cholesterol [126]. LDL-cholesterol is the major promoter of atherosclerotic lesions and strongest risk factor for cardiovascular disease related morbidity and mortality [14-16]. The use of statins and the resulting reduction in serum LDL lipid profile has been shown to be beneficial in reducing risk for CAD and MACE [113, 124, 125, 127]. The implementation of lifestyle modifications and pharmacological approaches to treat CAD has been successful in improving prognosis [109-112]. However, these approaches are not sufficient for patients with severe CAD, or after a MACE and will require surgical intervention to restore adequate blood flow [128].

1.3.2 Tools for evaluating Atherosclerosis

Upon arrival in the clinic, doctors will evaluate the magnitude and extent of CAD in each patient to decide what surgical intervention is required to re-vascularise diseased vessel segment. The coronary artery angiogram was pioneered by Mason Sones in the early 1960s [129]. Today, it remains the gold standard method for the evaluation of coronary artery

disease [105]. In this technique, a catheter is inserted into the radial or femoral artery and guided to the aortic root where a contrast dye is released. By normal haemodynamics, the dye flows through the left and right main coronary arteries and subsequent diverging branches around the heart. An X-ray is then taken to capture the coronary arteries and any degree of stenosis that may be present (**Figure 1.5**).

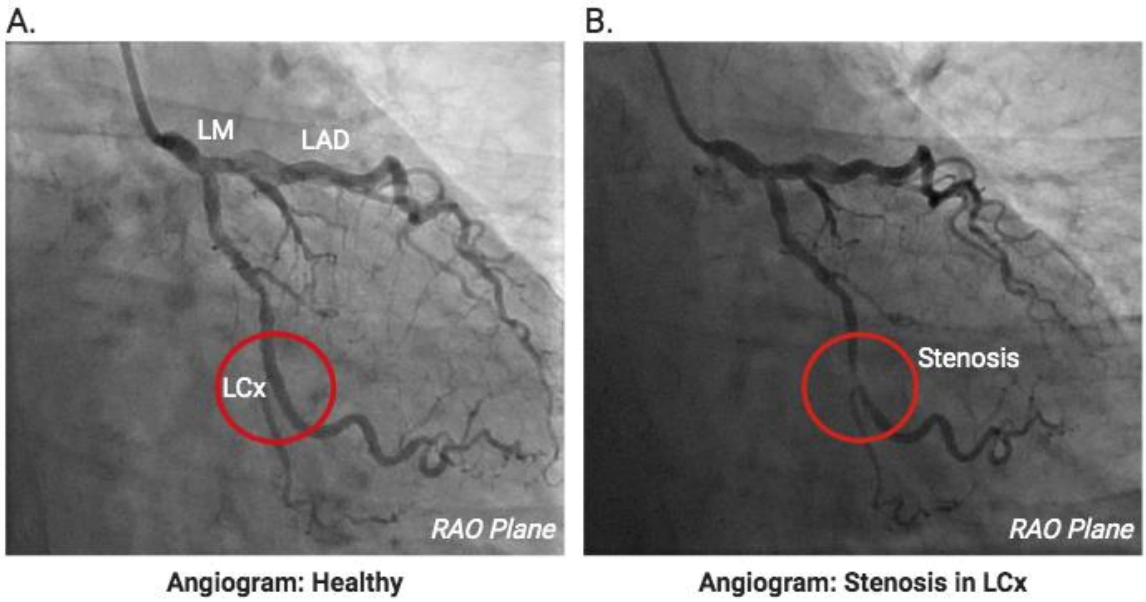

Figure 1.5: Coronary angiogram to detect narrowing of the left circumflex artery. *Contrast dye is released into the coronary network and an X-ray photo captured in the right anterior oblique (RAO) plane. The LCx artery in (A) is shows no signs of narrowing compared with the LCx artery in (B) which highlights a significant stenosis present (red ring). Images adapted from https:// www.heartfoundation.org.nz/shop/heart - healthcare / angiography - and -angioplasty-2018.pdf.*

While the coronary artery angiogram provides an excellent tool for the evaluation of stenosis, it is limited to this. Lesion progression is associated with increased calcification [130] which stems from both trans-differentiation of vascular smooth muscle cells to an osteogenic phenotype and vesicle mediated mineralisation due to apoptosis of macrophages and VSMCs within the necrotic core [131, 132]. The effect this plays on lesion stability is still a topic of debate [133]. While studies have shown contradictory findings, it is very likely the impact of calcification on lesion stability is additionally influenced by the geometric location of the artery as well as lesion type [26, 34]. Regardless of this, epidemiological evidence has shown

increased levels of calcium in the coronary arteries is a strong marker for coronary artery disease and associated MACE [134, 135].

The use of cardiac computed tomography (CT) scan technology can provide structural data on vascular calcification (**Figure 1.6**) [136, 137]. One of the advantages of this method is visualisation of arteries in 3D without the need of any X-ray dyes. Clinicians have developed complex scoring systems that rank magnitude and severity of CAD within patients for risk of MACE [138]. This is based on a number of variables including genetics, extent of atherosclerosis, presence of calcification, and the location within the coronary network. Taken together, the coronary angiogram and cardiac CT scan provide a good prognostic tool for the assessment of CAD and in making a decision about what surgical intervention is most suitable.

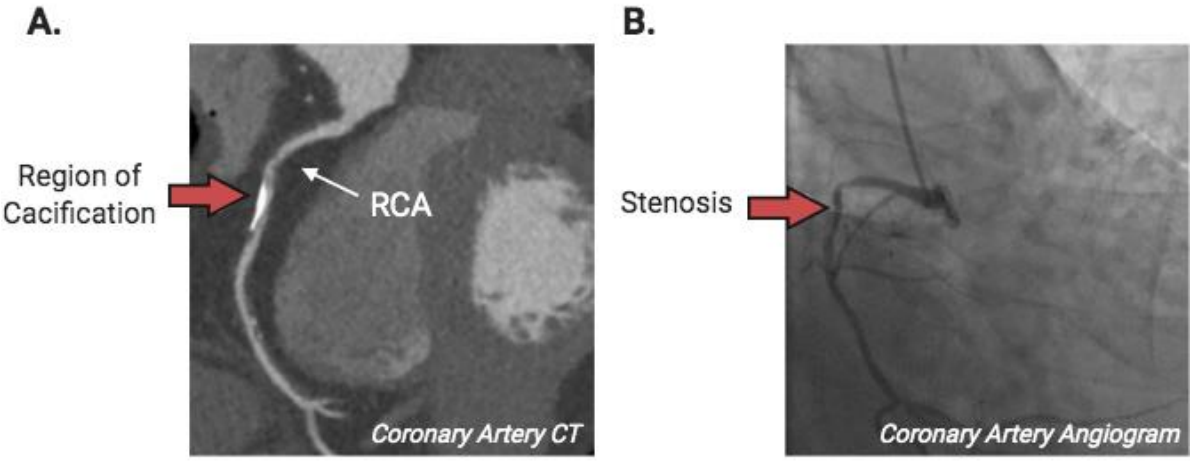

Figure 1.6: Comparing coronary CT scan with traditional coronary artery angiogram. *Coronary artery CT scan showing a segment of extensive calcification (white) in the RCA, marked by the red arrow (A). Coronary artery angiogram of the same RCA shows stenosis in region of calcification. Images adapted from [139].*

1.3.3 Surgical intervention to treat CAD

The two most common forms of heart revascularisation by surgical intervention are coronary artery bypass grafting (CABG) and percutaneous coronary intervention (PCI) (stenting). CABG has become one of the most commonly performed surgeries since its introduction in 1968 [140]. The procedure involves the removal of a donor vessel from another part of the body, which is then grafted from the aorta to the coronary artery, distal to the diseased segment (**Figure 1.7**). This restores blood flow through the ischaemic tissue and alleviates stress on the heart muscle. The extent of grafts required reflects the magnitude of CAD and there are several commonly used graft donors, including the radial artery, saphenous vein and internal mammary arteries (IMA). The IMA are useful as only one side needs to be grafted as it originates off the subclavian close to the aortic arch. **Figure 1.7B-C** shows a single vs triple bypass surgical approach.

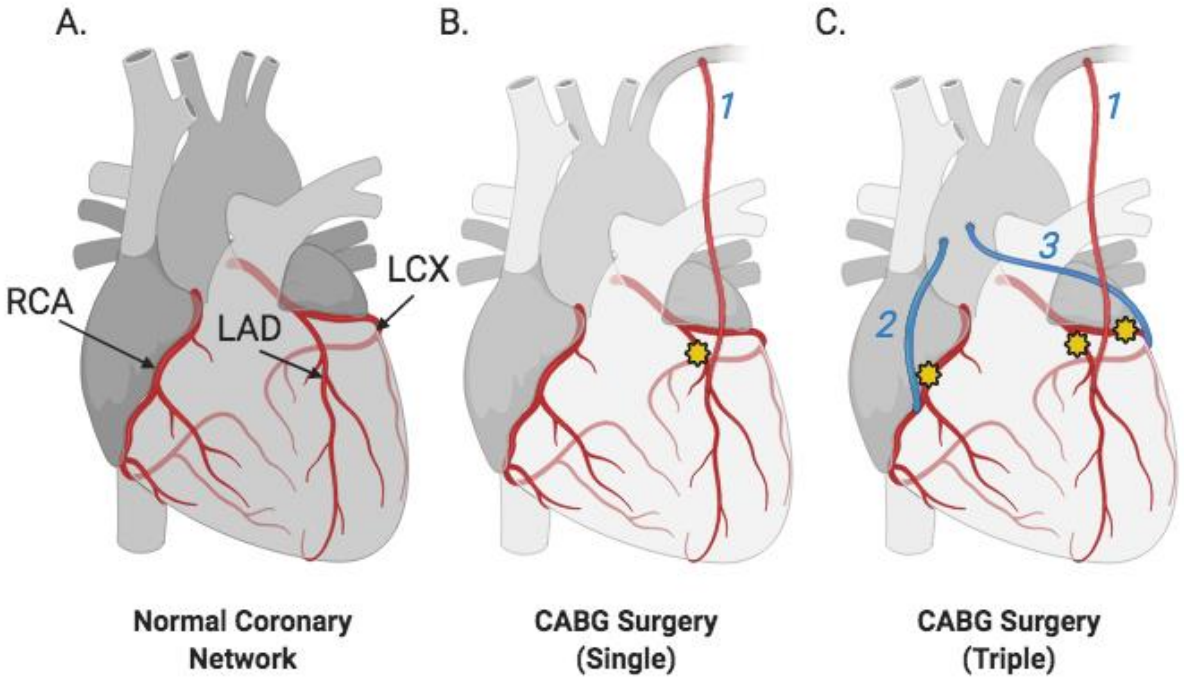

Figure 1.7: Common coronary artery bypass graft surgical approaches. *The three main coronary arteries which supply the heart are the right coronary artery (RCA), left anterior descending coronary artery (LAD) and left circumflex artery (A). The extent of surgical intervention, whether it is a single or triple CABG (B-C,) reflects amount and location of atherosclerosis (yellow stars). 1: Left internal mammary artery is grafted onto the LAD distal to the diseased segment. 2: The saphenous vein (blue) removed from the leg is grafted from the aorta to the right coronary artery. 3: The radial artery has been removed from the hand and grafted from the aorta to the LCx.*

The other common procedure for restoring blood flow through diseased arteries is PCI [141]. A balloon tip catheter is inserted via the femoral or radial artery and guided to the narrowed artery. The catheter is positioned adjacent to site of atherosclerosis and the balloon is inflated to expand the stent. The balloon is deflated, catheter removed and blood flow is restored to the ischaemic region (**Figure 1.8**) [142]. One of the main issues with PCI is restenosis (recurrence of stenosis). The physical force of the stent against the atherosclerotic vessel wall can cause physical damage which stimulates a local inflammatory response [143]. This leads to VSMC proliferation and migration toward the intima, a common step in the pathophysiology of atherosclerosis. Importantly, restenosis puts patients at risk of MACE, so revascularisation by CABG is the next option [144]. In more recent times, the development of drug-eluting stents (DES) has reduced restenosis and ultimately the need for repeat surgery [145]. Common pharmacological agents present in DES include anti-proliferative effects (e.g. paclitaxel).

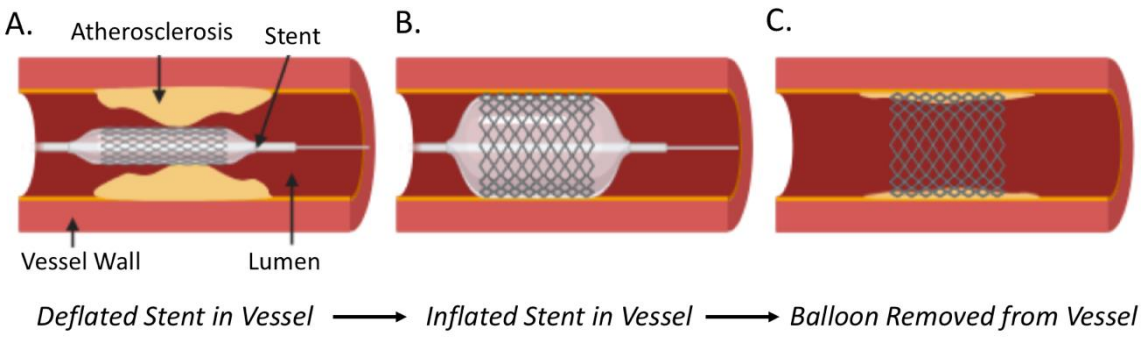

Figure 1.8: Percutaneous coronary intervention (PCI). *The stent is navigated through the arterial network to the site of stenosis (A). The stent is expanded using a balloon tip catheter and fixed in place (B). The balloon is deflated, removed and blood flow is restored (C). Original Figure (2020, Luke Worthignton).*

The 'SYNTAX Trial' is a prospective study started in 2005 evaluating the effectiveness of CABG vs PCI with DES, where 1800 patients were randomly assigned to either CABG or PCI group [146]. Over the 10-year period following up, there has been no significant differences in deaths between CABG, 212 (24%) and PCI, 248 (28%) [147]. Interestingly, there were differences for CABG vs PCI groups with respect to the severity of coronary artery disease. In patients with three-vessel disease, there were significantly fewer deaths in CABG compared to PCI group. However, no differences were seen in patient deaths with left main CAD between CABG and

PCI group. Collectively these results suggest both CABG and PCI are effective at preventing MACE, however CABG is more protective for patients with severe CAD.

The majority of interventions discussed are for the treatment of atherosclerosis in the context of the coronary arteries. However, the coronary arteries are not the only region prone to extensive atherosclerosis. The carotid artery also has a high burden of atherosclerosis (**Figure 1.9**) [148, 149], where the build-up of plaque in the carotid artery is associated with increased risk of stroke and other ischaemic brain injuries [150]. There are two main interventions to treat atherosclerosis in the carotid arteries; carotid angioplasty with stent, previously described, and carotid endarterectomy [151, 152]. To carry out the carotid endarterectomy, the carotid artery is cut open and the lesion surgically scraped away from the vessel wall to restore blood flow. While the surgical procedure is invasive and requires ongoing pharmaceutical management, for patients with extensive carotid atherosclerosis, it remains one of the last lines of treatment.

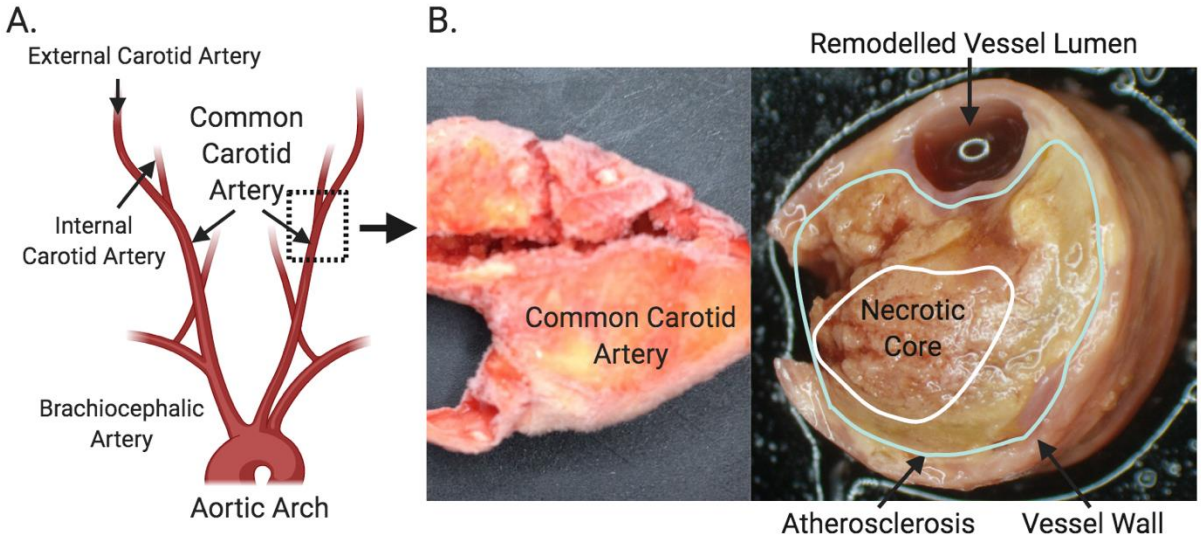

Figure 1.9: Atherosclerotic disease in the carotid artery. *The left and right common carotid artery branch from the aortic arch and brachiocephalic artery, respectively. Each common carotid artery further bifurcates into the internal and external carotid artery (A). Frozen segment of the common carotid artery from a 79-year old male (B). Cross section of the carotid artery shows extensive atherosclerosis occupying majority of vessel with characteristic necrotic core. The vessel lumen has been significantly reduced. Original photos.*

In conclusion, there are a number of methods to diagnose the extent and severity of atherosclerosis. Alongside pharmacological intervention to ameliorate symptoms of CAD, arteries prone to atherosclerotic disease can be re-vasculated by surgical intervention. The introduction of these surgical approaches has had a significant impact at reducing the number of MACE. However, the lesions responsible for ischaemic events are of an advanced phenotype late in disease progression. This highlights the importance of researching the cellular mechanisms which promote early foam cell lesion development. The ability to target atherosclerosis in an earlier stage of its progression would have a positive impact on all the clinical manifestations that arise from atherosclerotic disease. Without screening of early lesions and the ability to treat them at an earlier stage these surgical interventions will remain heavily utilised in the clinical treatment of atherosclerosis.

1.4 Research tools in atherosclerosis – ApoE$^{-/-}$ mouse model

In the research world there are a number of excellent tools for studying the pathogenesis of atherosclerosis. *In vitro* studies have been a useful model at providing insight into the cellular mechanisms that contribute to atherosclerosis. However, the environment that promote lesion growth is difficult to establish in an artificial setting. Atherosclerosis is a chronic inflammatory disease involving an interplay of autocrine and paracrine signalling between cells of the immune system and vascular wall. For this reason, the research field has adopted a number of animal models which has exponentially increased our knowledge of the mechanisms and therapeutic targets around lesion growth.

The first use of animals for atherosclerosis research was in 1908, when Ignatowski showed that rabbits fed a diet high in protein and fat displayed atherosclerotic lesions within the vessel wall of the aorta [153]. Since then, a variety of animal models have contributed to our understanding of the pathophysiology of atherosclerosis, however the mouse has become the gold standard model [154]. Like Ignatowski, other groups utilised the major risk factor for atherosclerosis by putting mice on a high fat diet (HFD) to induce hyperlipidaemia and lesion development [155-157].

One of the main issues with wild-type mice on the HFD is their inherent resistance to atherosclerosis [158]. This stems from the fact mice have a cholesterol metabolism that allows efficient clearance of LDL-C [159]. It was not until the evolution of the molecular biology field and discovery of gene editing techniques where the mouse emerged as the gold standard model for atherosclerosis research. Scientists targeted proteins involved in reverse cholesterol transport, the removal of cholesterol from peripheral tissues via biliary excretion [160]. The most successful genetic manipulations to induce hyperlipidaemia in mice is the knockout of the ApoE or the LDL receptor (LDLR) gene [160]. Targeted deletion of these genes interrupts the uptake of chylomicrons and LDL-C by the liver resulting in the net accumulation of LDL-C in the blood [161, 162]. The resulting hyperlipidaemia in both models drives the development of atherosclerotic lesions throughout the arterial tree that are characteristic with the human disease [162, 163]. The main advantage of the ApoE$^{-/-}$ model is the development of lesions on a normal chow diet (ND) at a faster rate relative to LDLR$^{-/-}$ mice

[164, 165]. In our own lab and others around the world, the ApoE$^{-/-}$ mouse model has been consistently used to unravel some of the mechanisms driving atherosclerotic lesion growth.

The wild-type mouse has plasma cholesterol of 75-110 mg/dl on a ND [162]. By knocking out the ApoE gene these cholesterol levels are elevated to an average of 600 mg/dl on a ND [162]. Additionally, supplementation of ApoE$^{-/-}$ mouse with the HFD augments plasma cholesterol levels to >1000 mg/dl [162, 166]. One of the major differences between mice and humans is a differential lipoprotein expression [167]. Mice transport the majority of cholesterol bound to HDL and have only small concentrations of LDL-C and VLDL-C [168]. Furthermore, the high levels of the anti-atherogenic lipoprotein HDL is thought to provide the inherent protection from atherosclerosis in the wild-type strain [158]. In contrast, humans transport the majority of cholesterol on the atherogenic LDL and VLDL particles [169]. Even with these differences in lipid profile between species, ApoE$^{-/-}$ mice rapidly develop atherosclerotic lesions with a physiology and anatomy comparable to humans [84, 170].

In humans, atherosclerosis is present in the coronary and carotid arteries whereas the ApoE$^{-/-}$ mouse lesions are primarily located in the aortic arch, aortic sinus and brachiocephalic artery (**Figure 1.10**) [171, 172]. This is likely to reflect differences in shear stress across the vessel wall between species. At 6 weeks, ApoE$^{-/-}$ mice exhibit monocyte adherence to the endothelial cell wall as well as sub-intimal deposits of LDL-C [162]. This progresses to pockets of foam cell lesion growth throughout the aortic tree at 15-weeks, visible to the naked eye. At 20-weeks, extensive lesions are present containing macrophages, foam cells, VSMC, ECM and a distinct fibrous cap [162]. Even as the lesion progresses to an advanced phenotype the disease remains comparable between humans and mice. This advanced stage of the lesion is characterised by pockets of calcification and a growing necrotic core with infiltrating blood vessels [162, 171].

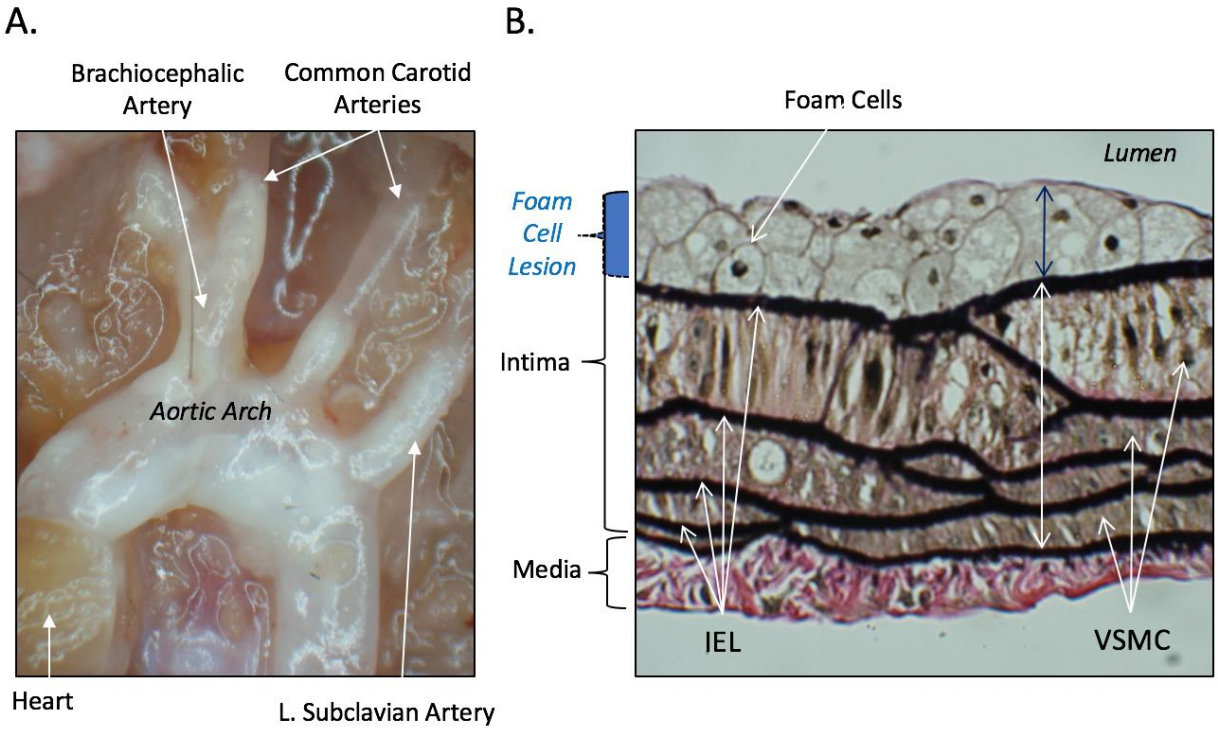

Figure 1.10: Atherosclerosis in the ApoE$^{-/-}$ mouse. *Dissection of a 20 week female ApoE$^{-/-}$ mouse highlights atherosclerosis indicated by the opaque vessel wall. Extensive atherosclerosis is present in the brachiocephalic artery, carotid arteries, left subclavian artery and the lesser curvature of the aortic arch (A). A 4µm section of the aortic arch vessel wall was treated with Verhoeff van Gieson stain. Features of the vessel wall include VSMCs (brown), internal elastic lamina (black), extracellular matrix (pink) and foam cells (grey). At 20-weeks expansion of the intima (white double arrow) and foam cell lesion development (blue double arrow) is evident. Original images, figure created on Microsoft PowerPoint.*

A limitation of this model is that at a very advanced stage of atherosclerosis, there is no spontaneous lesion rupture and thrombo-embolic complications which manifest at the advanced stage of the human disease [173]. However, for us, and other labs around the world who are interested in unravelling the cellular mechanisms that drive atherosclerotic lesion development, the ApoE$^{-/-}$ mouse serves as an excellent tool.

1.5 Calcium calmodulin-dependent protein kinase II (CaMKII)

The development of foam cell lesions is an early event in the pathogenesis of atherosclerosis driven by a combination of ECs, VSMCs and macrophages [13]. More specifically, when the pathology is broken down to the specific functional changes occurring in each cell type, it includes endothelial dysfunction, macrophage lipid accumulation and a synthetic VSMC function [13, 20, 22, 79]. A number of signalling pathways have been identified, which promote these cellular changes to drive foam cell lesion growth [75, 174]. However, many of these pathways are incomplete and lack important detail about intermediate signalling proteins that will be involved. These intermediate signalling proteins could provide novel drug targets.

Calcium calmodulin-dependent protein kinase II (CaMKII) is a nodal signalling protein in cellular physiology [175, 176]. CaMKII translates upstream Ca^{2+} signals to downstream cellular response by phosphorylation of target proteins [177, 178]. These responses include acute cellular changes in activity and gene transcription events. CaMKII activity has been strongly associated with cardiac dysfunction and increasing evidence suggests a role in vascular disease [179-182].

1.5.1 CaMKII Structure and Function

CaMKII is a holoenzyme composed of 10-12 subunits [183]. There are four separate genes that encode the α, β, δ and γ isoforms [184, 185]. Each subunit contains a catalytic, regulatory and a C-terminal association domain, which orchestrates multimerisation of the holoenzyme. The catalytic domain is at the N-terminal and carries out serine/threonine kinase activity (the addition of a phosphate group to molecule). The regulatory domain links the two terminal ends and contains a binding pocket for the catalytic region. In the inactive state the catalytic domain is folded over in a 'hinge-like' fashion and bound to the regulatory pocket [186].

Increases in the intracellular Ca^{2+} concentration leads to the formation of a Ca^{2+}-calmodulin complex. Ca^{2+}-calmodulin bind a specific region in the regulatory domain inducing a conformational change [187]. The conformational change relieves the interaction between

the catalytic and regulatory domain, allowing serine/threonine kinase activity (**Figure 1.11**). Therefore, while Ca^{2+} levels are elevated, CaMKII can carry out target phosphorylation of proteins [178]. Importantly, when Ca^{2+} is removed from the intracellular environment, calmodulin dissociates and the enzyme is inactive. This mechanism of auto-inhibition in the presence and absence of Ca^{2+} allows for tightly regulated kinase activity.

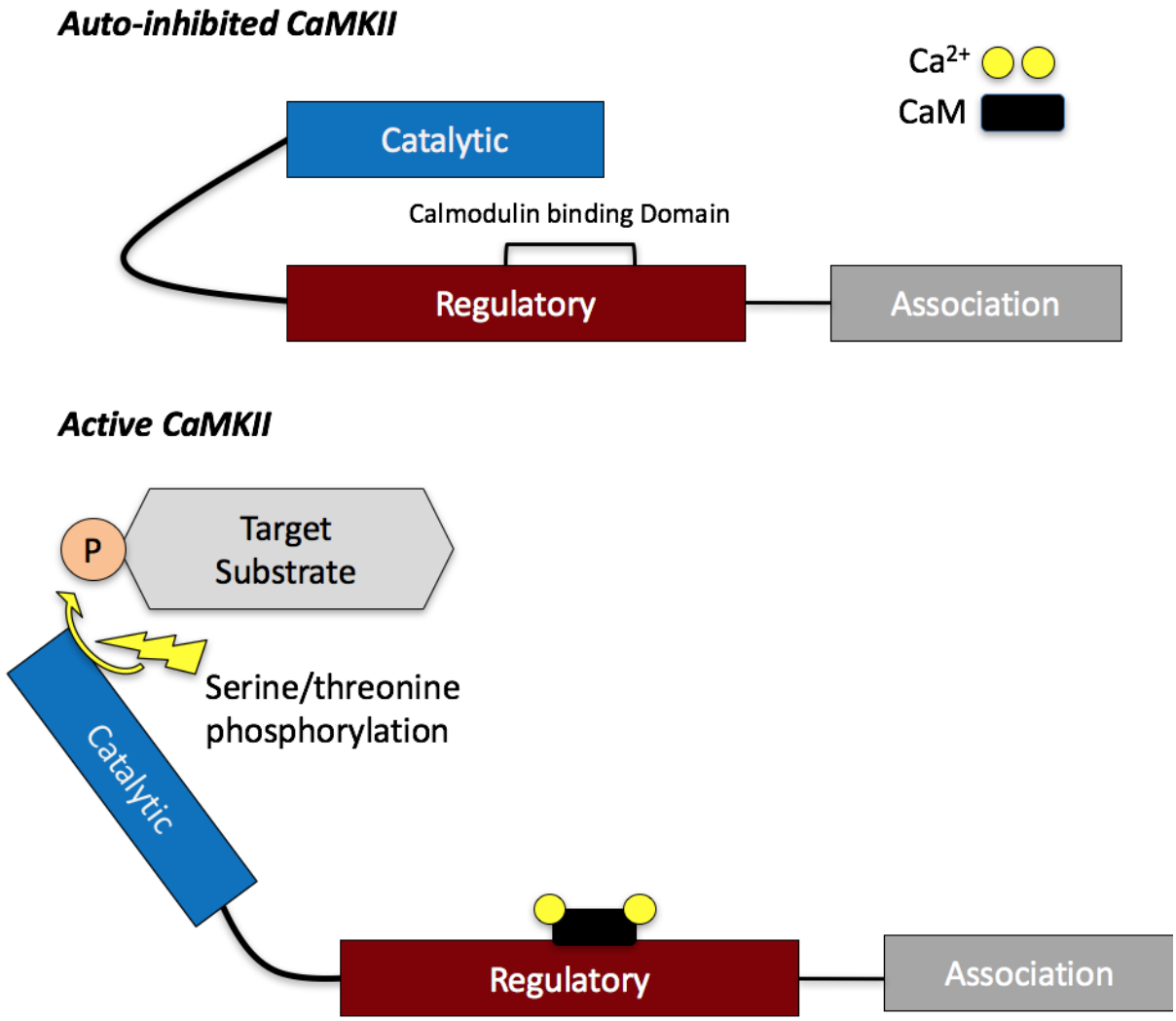

Figure 1.11: Structure and function of CaMKII monomers. *CaMKII monomers are composed of a catalytic, regulatory and association domain. In physiological conditions the catalytic domain is bound to the regulatory domain and the enzyme is inactive. Increases in Ca^{2+} stimulates binding of calmodulin to the regulatory domain relieving the interaction with the catalytic domain. In this active state CaMKII carries out phosphorylation of target substrates. When Ca^{2+} is extruded out of the environment, CaM dissociates and the catalytic domain binds to the regulatory domain. Original figure (Worthington, 2020).*

1.5.2 Chronic activation of CaMKII

Even though CaMKII activity is tightly regulated by auto-inhibition, prolonged activation of the holoenzyme leads to inter-subunit auto-phosphorylation of adjacent subunits (**Figure 1.12**). More specifically, a phosphate group is added to threonine residue 287 (Thr^{287}) within the regulatory domain of CaMKII (P^{287}-CaMKII) [188, 189]. The presence of this phosphate group prevents the auto-inhibitory properties of the enzyme even in the absence of Ca^{2+}. In this state, the enzymes activity is unregulated and requires the activity of protein phosphatases to de-phosphorylate Thr^{287} [190].

In addition to phosphorylation, prolonged activation of CaMKII in an environment of elevated ROS leads to the oxidation of methionine residues 281 and 282 $M^{281/282}$ within the regulatory domain ($ox^{281/281}$-CaMKII) [180]. The oxidative modification of these residues also prevents auto-inhibition of the kinase in a similar mechanism to phosphorylation, and the enzyme's activity becomes chronic [180] (**Figure 1.12**). Since the discovery of phosphorylation and oxidation to the enzyme, there have been additional post-translational modifications described. These include nitrosylation and O-GlyNAcylation and have similar consequences on CaMKII activity [191, 192].

CaMKII gained significance in the cardiovascular research world after the discovery that this chronic activity of CaMKII attributable to post-translational modifications (PTMs), was associated with the development of cardiac pathology. Prolonged P^{287}-CaMKII activity has been shown to promote hypertrophy in cardiomyocytes [179]. Additionally, increases in the phosphorylation status of Ca^{2+} handling proteins are observed. More specifically, P^{287}-CaMKII has been shown to increase the phosphorylation status of the ryanodine receptor 2 (RyR2) [193]. This leads to altered Ca^{2+} handling in cardiomyocytes, leading to impaired contraction, a hall mark of heart failure [194]. Alongside phosphorylation, oxidation of CaMKII is linked to CVD [180]. $Ox^{281/282}$-CaMKII is linked to cardiomyocyte apoptosis and arrhythmia [195, 196]. Collectively, PTM of CaMKII leading to chronic activity is a mechanism for promoting cellular changes that drive cardiac disease.

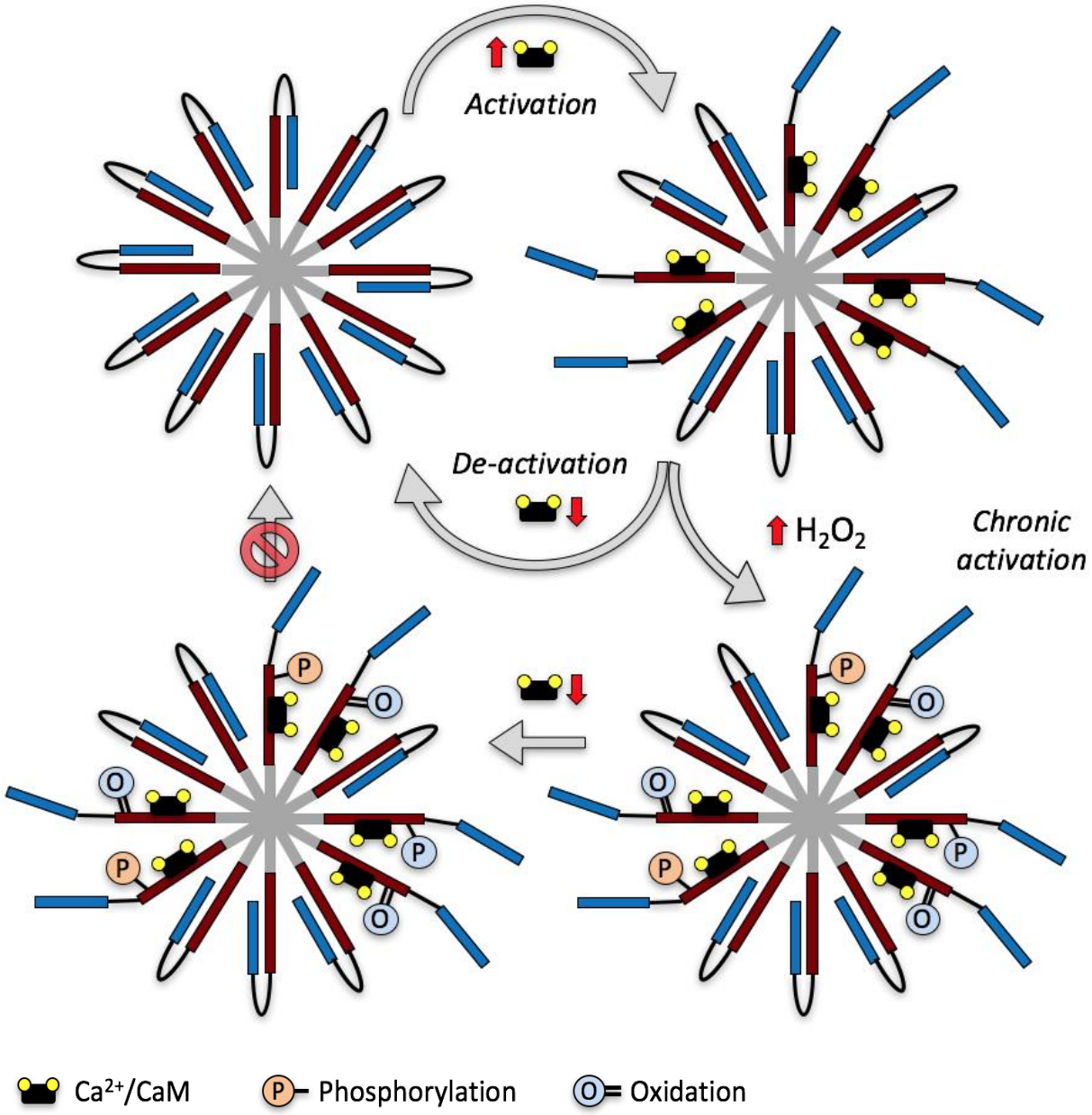

Figure 1.12: Chronic activation of the CaMKII holoenzyme. *CaMKII is activated and de-activated by the presence and absence of Ca^{2+}/calmodulin (CaM), respectively. Prolonged activation of CaMKII results in inter-subunit auto-phosphorylation of adjacent subunits within the regulatory domain. In addition, chronic activation of the kinase under conditions of elevates oxidative stress leads to oxidation of the regulatory domain. Under this chronic activation state driven by phosphorylation and oxidation, CaMKII remains active even in the absence of Ca^{2+}/CaM. Worthington (2017).*

1.5.3 CaMKII isoform diversity

While chronic activation of CaMKII plays a role in cardiovascular pathology, it is only one small part of the CaMKII story. The CaMKII family is diverse and contains four separate genes that encode the 4 main isoforms α, β, δ and γ [184, 185]. CaMKIIα and β isoforms are expressed in neuronal tissue, whereas the δ and γ isoforms are ubiquitously expressed. CaMKIIδ and γ are the predominant isoforms expressed in the CVS [197, 198].

The CaMKIIδ isoform family also contains eleven alternatively spliced products under the regulation of alternative splicing factor/ pre mRNA splicing factor 2 (ASF/SF2) [197, 199-202]. Of the eleven variants discovered, δ_2, δ_3 and δ_6 have been investigated in relation to function and pathology. The other cardiovascular isoform CaMKIIγ also contains three splice variants 1-3, however, no group is yet to investigate any differences between these subtypes [203].

Sequence homology is highly conserved in the catalytic, regulatory and association domain between CaMKIIδ variants. However, there is a variable region between the association and regulatory domain that is alternatively spliced prior to translation and results in the different δ variants [200]. There has been evidence to suggest there are functional differences between subtypes, best exemplified by the δ_2 and δ_3 variants in cardiomyocytes. An early study by Srivnovasan et al., (1994) showed that the δ_2 and δ_3 subtypes were primarily located in either the cytosol or nucleus, respectively. A sequence comparison of the variants showed an eleven amino acid insert sequence in the variable region of the δ_3 subtype which was not present in the δ_2 subtype [204]. The insert sequence contained the lysine-lysine-arginine-lysine (KKRK) motif, a well-established nuclear localisation signal (NLS) [205].

Over-expressing CaMKIIδ_2 in cardiomyocytes results in an increased expression of total CaMKIIδ in the cytosolic compartment [204]. This is associated with dysfunction of excitation-contraction coupling due to its phosphorylation effects on the major Ca^{2+}handling proteins [206-208]. In contrast, over expressing CaMKIIδ_3 in cardiomyocytes leads to increased nuclear localisation of total CaMKIIδ [204]. This was associated with increased hypertrophy of the heart through activation of myocyte enhancer factor 2 (MEF-2) GATA-4 and heat shock factor 1 (HSF-1) transcription factors [209, 210]. In patients with developing heart failure there is an

upregulation of the CaMKIIδ_3 variant [211]. Clearly, both CaMKIIδ_2 and δ_3 variants are important in the development of cardiac pathology. This suggests that the balance of CaMKIIδ subtypes in the cytosol and nucleus compartments is critical for cellular homeostasis.

1.5.4 CaMKII – an emerging player in vascular disease

Outside the heart in the vasculature, CaMKII is emerging a critical player in health and disease. The predominant cardiovascular CaMKII isoforms δ and γ are expressed in the ECs and VSMCs which make up the vascular wall [185, 198, 203]. As a general summary, the literature suggests CaMKIIδ drives cellular changes that drive the development of vascular pathology [181, 212]. Interestingly, in contrast, CaMKIIγ signalling promotes vascular health [213].

In ECs, CaMKIIδ has been shown to phosphorylate NADPH oxidase to increase production of the ROS superoxide ($O_2^-\bullet$) [214]. Furthermore, in oxidant conditions, CaMKII promotes the expression of endothelial nitric oxide synthase (eNOS) [215]. Phosphorylation of eNOS at serine residue 1177 (P-eNOS^{1177}) also promotes production of $O_2^-\bullet$ [216, 217]. We have shown *in vivo* that systemic inhibition of CaMKII results in a reduction of P-eNOS^{1177} (*unpublished data, 2017*). Alongside an increase in ROS production, CaMKII has been shown to increase EC permeability and VCAM-1 expression [212, 218]. Taken together, CaMKII promotes a number of cellular changes that promote endothelial dysfunction.

CaMKII isoforms have clear opposing roles in VSMCs. During vascular injury, CaMKIIδ expression increases and this is associated with increased proliferation and migration of VSMCs, evidenced by neo-intimal hyperplasia (the expansion of the tunica intima) [181, 219]. A deeper investigation highlighted CaMKIIδ_2 stimulation of proliferation through the activation of the MAPK pathway [181, 219, 220]. In contrast, during vascular injury CaMKIIγ expression decreases [181]. As far as physiological roles have been investigated, CaMKIIγ has been shown to be involved in ion channel regulation and contraction of VSMC, mediated via extracellular signal-related kinase (ERK) and phosphorylation of myosin filaments [213, 221-223]. Collectively, the delta and gamma variants promote the synthetic and contractile pathway, respectively.

In summary, transcriptional regulation of CaMKII generates an extensive isoform family that displays a differential pattern of gene expression in different cell types. A limitation of this research is that many groups have focused on total CaMKII rather than specific isoforms. When conclusions have been drawn in relation to CaMKII function, it is not known whether it is the δ, γ or a combination of isoforms that is/are the main player/s. Identifying the specific isoform is important, at least, in the vasculature, where δ and γ have contrasting roles in promoting the synthetic or contractile phenotype, respectively. The pathological effect of the CaMKIIδ is also observed in the ECs by the increased expression of markers of endothelial dysfunction. Thus, CaMKII isoforms play a critical role in vascular health and dysregulation of activity and its expression, at least of CaMKIIδ, promotes vascular disease.

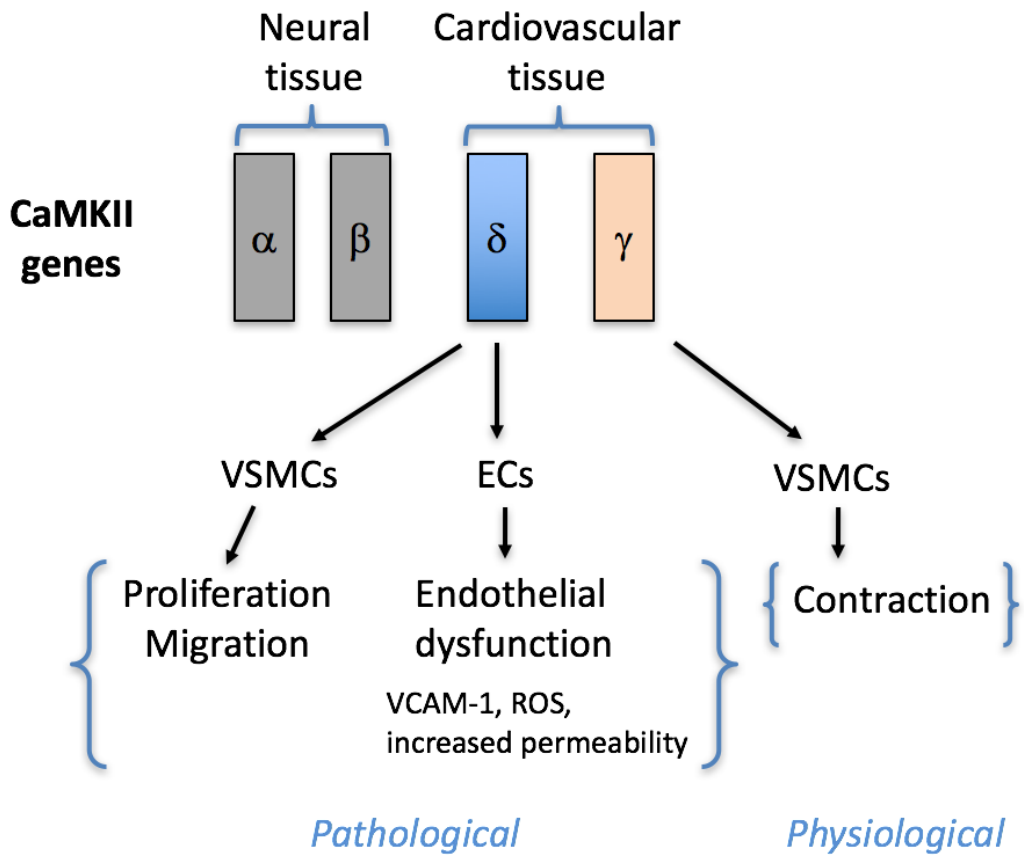

Figure 1.13: Basic summary of CaMKII isoform function in the vasculature. *There are four separate genes that encode CaMKII isoforms α, β, δ and γ. The α and β isoforms are predominantly expressed in the nervous system and have important roles in brain function. The δ and γ isoforms are expressed in cardiovascular tissue. Furthermore, δ has pathological roles in promoting endothelial dysfunction and increasing the synthetic phenotype in VSMCs. In contrast, the γ isoform has received little attention, however it has important functions in VSMC contraction and maintenance of the contractile phenotype.*

1.6 Rationale, Aims and Hypotheses

Cardiovascular disease (CVD) is the most significant health problem in the developed world. In New Zealand, CVD contributes to 33% of annual deaths and continues to burden the health care system (Ministry of Health, 2015). The implementation of lipid-lowering therapies (statins) has been beneficial in reducing risk for cardiovascular disease (CVD). However, even when lipid targets are achieved, there remains a significant residual risk for CVD and surgical revascularisation (CABG, PCI) is often required [224]. This is of significance in the Maori population, as the Heart Otago data bank shows that Maori undergo coronary artery bypass procedures up to 17 years earlier than NZ Europeans. Clearly, there is need for alternative therapies to target atherosclerosis in its early stages.

The development of lipid-filled lesions on the inner layer of the arterial wall, is driven by pathological changes in ECs, macrophages and VSMCs [13]. CaMKII has been highlighted as a nodal signalling protein in EC, macrophage and VSMC physiology and pathology. CaMKIIδ and γ are the predominant isoforms expressed in the cardiovascular system and research suggests δ has a pathological role under certain disease states, whereas γ is protective [181, 212, 213, 218]. CaMKIIδ regulation is complex and alternative splicing results in a differential pattern of sub-type expression in different cell groups of the vasculature [200]. While the majority of the sequences that encode these sub-types are conserved, there are small differences in the variable region which has been shown to display different functions [204]. Since then the research field has readily focused on total CaMKII without taking into account the specific isoforms and different contributions to functions they may be playing. This is important in VSMCs, where δ and γ may promote the synthetic and contractile phenotype, respectively [213, 220]. Regardless, in the studies that have focused on specific isoforms, what is striking is that CaMKIIδ promotes cellular signalling pathways in ECs and VSMCs that collectively contribute to atherosclerosis.

Previously we have showed a systemic inhibition of CaMKII with the inhibitor drug KN-93, reduces foam cell lesion development in the ApoE$^{-/-}$ mouse (**Figure 1.14**). However, this was a total blockade of all CaMKII isoforms and did not preserve the important physiological functions of CaMKII. In order to better understand CaMKII function, especially in the context

of future drug development, it is now required to investigate the specific isoform contributing to foam cell lesion development.

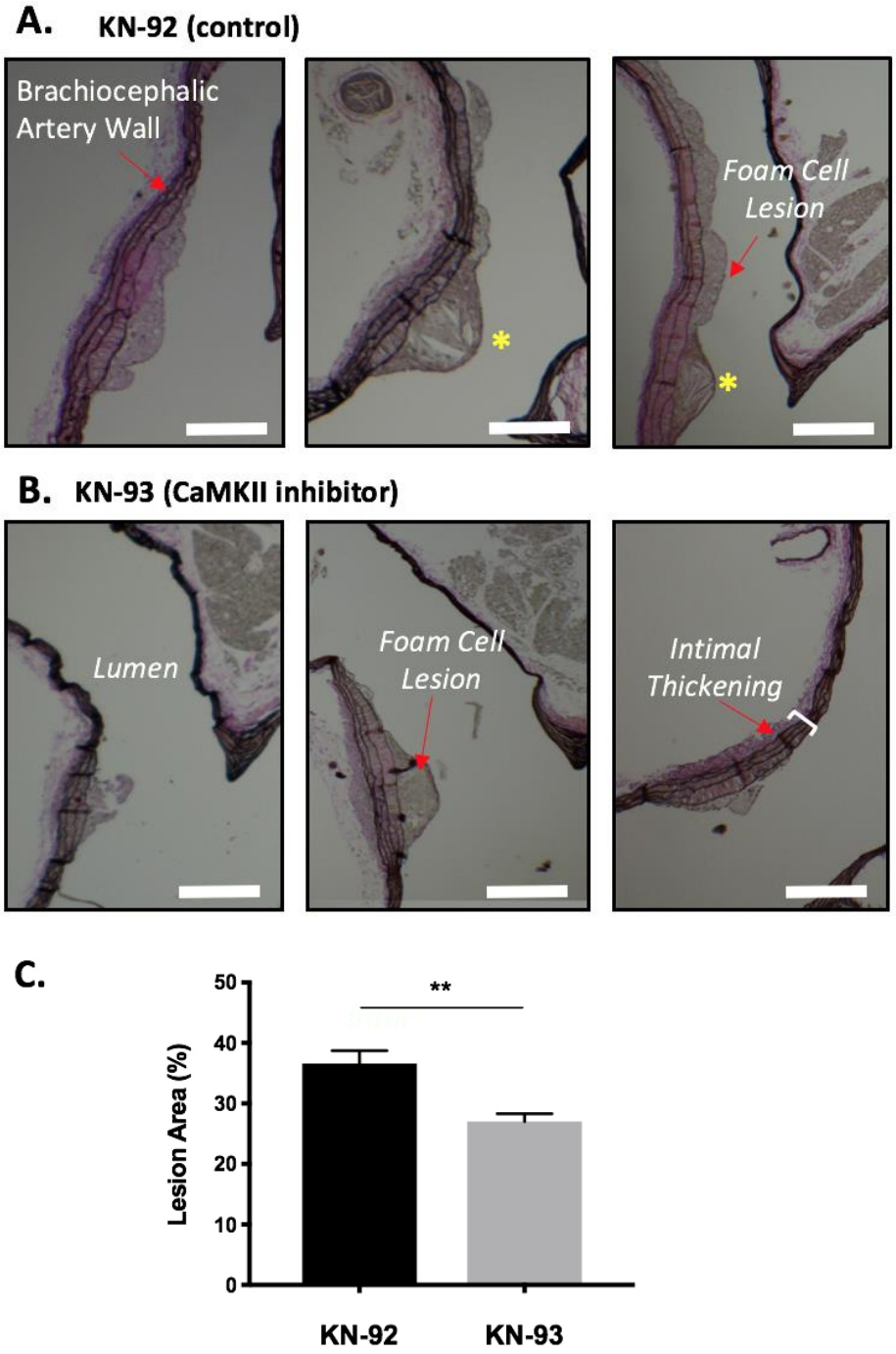

Figure 1.14: CaMKII inhibition in the ApoE mouse reduces foam cell lesion development in the brachiocephalic artery. *Mice were treated with KN-92 (10µg/kg) or KN-93 (10µg/kg) from 16- to 20 weeks. Mice were perfusion fixed with PFA and the aortic arch dissected. Longitudinal sections containing the brachiocephalic artery were subject to Verhoeffs van Gieson staining for plaque analysis. Panels **A-B** are three representatives of a 20-week brachiocephalic artery after treatment with KN-92 or KN-93, respectively. Foam cell lesion area including intimal thickening was calculated in the brachiocephalic artery by subtracting luminal area from the total brachiocephalic area (**C**). *P<0.05, (n=11) as determined by unpaired Students T-test.*

The overarching aims of this PhD are to

1. Identify the major isoforms and splice variants of CaMKII in human cells of the vasculature and the arteries of atherosclerotic mice ($ApoE^{-/-}$). (*Chapter 2*)

2. To knockout the predominant CaMKIIδ isoform in $ApoE^{-/-}$ mice and generate the $ApoE^{-/-}$CaMKII$\delta^{-/-}$ mouse model to identify the contribution of this specific isoform to foam cell lesion development. (*Chapter 3*)

3. To over-express CaMKIIδ by AAV, in surgically-ligated carotid arteries of $ApoE^{-/-}$ CaMKII$\delta^{-/-}$ mice to examine the impact of CaMKIIδ in foam cell lesion development. (*Chapter 4*)

It was hypothesised that CaMKIIδ would be the predominant isoform expressed in the arteries of atherosclerotic mice. Furthermore, knock-out of the CaMKIIδ isoform in $ApoE^{-/-}$ mice would lead to a reduction in total foam cell lesion development. In contrast, overexpressing CaMKIIδ in the carotid arteries of $ApoE^{-/-}$CaMKII$\delta^{-/-}$ mice would exacerbate atherosclerosis.

The following thesis does not contain a general methods chapter. Instead, the protocols specific for each experiment, are described in detail in the approach section of each chapter.

Chapter 2

Investigating CaMKII Isoforms in Human and Mouse Vascular Cells

Contents

2.1 Introduction

The calcium/calmodulin-dependent protein kinase II (CaMKII) family are important regulators of cell signalling in normal physiology and disease. CaMKII has four isoforms α, β, δ and γ, each encoded by an independent gene. The α and β isoforms are expressed in neuronal tissue and have important roles in brain function and learning, whereas δ and γ are more ubiquitously expressed [184, 185, 225, 226] [197]. As the focus of the thesis was on atherosclerosis, a disease of the arteries, the more ubiquitously expressed CaMKIIδ and γ were the focus of this investigation.

CaMKII activity is driven by Ca^{2+} transients which relieve an auto-inhibitory interaction between the regulatory and catalytic domain of the kinase [187]. In this form, CaMKII carries out phosphorylation of target substrates for an acute cellular response or a downstream gene transcription event [227]. Under conditions of prolonged CaMKII activation, the regulatory domain is subject to a number of post-translational modifications (PTMs), including phosphorylation, oxidation, nitrosylation and O-GlyNAcylation [180, 188, 189, 191, 192]. Importantly, these PTMs are on residues within the regulatory domain, which prevent the auto-inhibitory properties of the kinase in the absence of Ca^{2+}, and its activity becomes chronic (*Section 1.5.2*) [180, 188, 228]. Chronically active forms of CaMKII have been associated with the development of cardiac pathology [193, 195, 196, 228].

Research into functions of CaMKII within the cardiovascular system has mainly focused on total CaMKII, without investigating the specific isoforms δ and γ, that are expressed within the cardiovascular system [185, 200, 225]. This is a significant limitation, as subsequent studies that did focus on a specific isoform highlighted that CaMKIIδ and γ appear to play opposing roles [213, 219-221]. Early studies in the heart demonstrated that it was the δ isoform that was the main contributor in driving cardiomyocyte pathology. This ranged from, hypertrophy, apoptosis to arrhythmia [195, 196, 211].

Outside the heart in the arteries, CaMKIIδ has been shown to promote vascular pathology. CaMKIIδ drives proliferation of VSMCs via the MAPK pathway, a function of the synthetic VSMC phenotype [219, 220]. In contrast, the other cardiovascular isoform CaMKIIγ, promotes the contractile VSMC phenotype through ion channel regulation and localisation within the

contractile apparatus [221-223]. Not only does δ promote dysfunction in VSMC, but also in the ECs. More specifically, CaMKIIδ signalling leads to increased adhesive and permeability properties of the endothelial wall, a phenotype of endothelial dysfunction [212, 218]. CaMKIIγ, has been identified in ECs, however there is no evidence for a function in health and disease [185, 198, 203]. So far, the literature would suggest CaMKIIδ promotes vascular disease, whereas, CaMKIIγ is protective against vascular disease.

The story is not as simple as two isoforms with two opposing functions in vascular health and disease. CaMKIIδ and γ are targeted for post-transcriptional regulation resulting in a subset of alternatively spliced isoform variants [197, 204]. There have been eleven CaMKIIδ variants described in the literature [200, 202, 211]. Of interest δ_{2-3} have been shown to have roles in hypertrophy, heart failure and restenosis (VSMC proliferation in the intima) [181, 193, 206, 229]. Moreover, δ_6 is involved with thrombin-induced increases in endothelial cell permeability [212].

In contrast, CaMKIIγ has three variants identified, however there has been little research into any relation to variant-specific functions [198]. Collectively, this suggests it is not only isoforms that are important to differentiate apart, but also the splice variants of each isoform. At least in the CaMKIIδ variant family there has been evidence to suggest splice variants can display different functions [204]. This is best highlighted between the δ_2 and δ_3 variants, which are identical apart from a nuclear localisation signal present within the variable region of the δ_3 variant [204]. This, in turn, primarily locates the δ_3 variant to the nucleus whereas the δ_2 is present in the cytoplasm where they interact with different targets carrying out different functions. Clearly, CaMKII regulation is complex and we are only beginning to appreciate the importance of investigating isoforms and their splice variants. A growing body of evidence for CaMKIIδ functions, compared to CaMKIIγ which has not been extensively studied in the context of function, would suggest CaMKIIδ is the most likely contributor to vascular disease such as atherosclerosis.

Previously, we have shown that systemic inhibition of CaMKII in $ApoE^{-/-}$ mice leads to a significant reduction in foam cell lesion development in the brachiocephalic artery (**Figure 1.14)** (unpublished; *Worthington, 2016*)**.** However, this inhibition blocked the activity of all the isoforms and the cumulative physiological role they play. This would include the off target

effects in the brain and other nervous tissue. Consequently, a global inhibition of CaMKII is not a feasible drug target for the treatment of atherosclerosis. A more detailed investigation into the CaMKII isoform family is required for a more targeted strategy to combat the complex pathogenesis of atherosclerosis. Therefore, the aim here was to describe the CaMKII isoforms present in vascular cells.

2.2 Approach

Human vascular cells and the atherosclerotic mouse ($ApoE^{-/-}$) were the models used to identify which isoform/s of CaMKII contribute to the pathogenesis of atherosclerosis. Firstly, three major cell groups of the vessel wall; human coronary artery smooth muscle cells (HCASMCs), human umbilical vein endothelial cells (HUVECs) and human coronary artery endothelial cells (HCAECs) were cultured. Additionally, $ApoE^{-/-}$ mice were aged for 13- or 20-weeks, which reflect two different stages of atherosclerosis disease pathology. At 13-weeks, the arteries of $ApoE^{-/-}$ mice show intimal thickening and small pockets of lesion development. In contrast, at 20-weeks of age, extensive foam cell lesions present throughout the arterial tree. In this study, the aortic arch and carotid arteries were isolated as they are regions prone to atherosclerosis.

Total RNA and protein were extracted from vascular cell cultures and aortic arch/carotid artery homogenates (**Figure 2.1**). RT-PCR was used to demonstrate the mRNA levels of the cardiovascular isoforms, CaMKIIδ and γ. Further to this, RT-PCR was used to identify what variants of the CaMKIIδ isoforms were present in the human and mouse samples. To validate the RT-PCR results, Western blotting (WB) was completed to show total CaMKIIδ and γ levels and identify whether the expression profile changes with lesion progression.

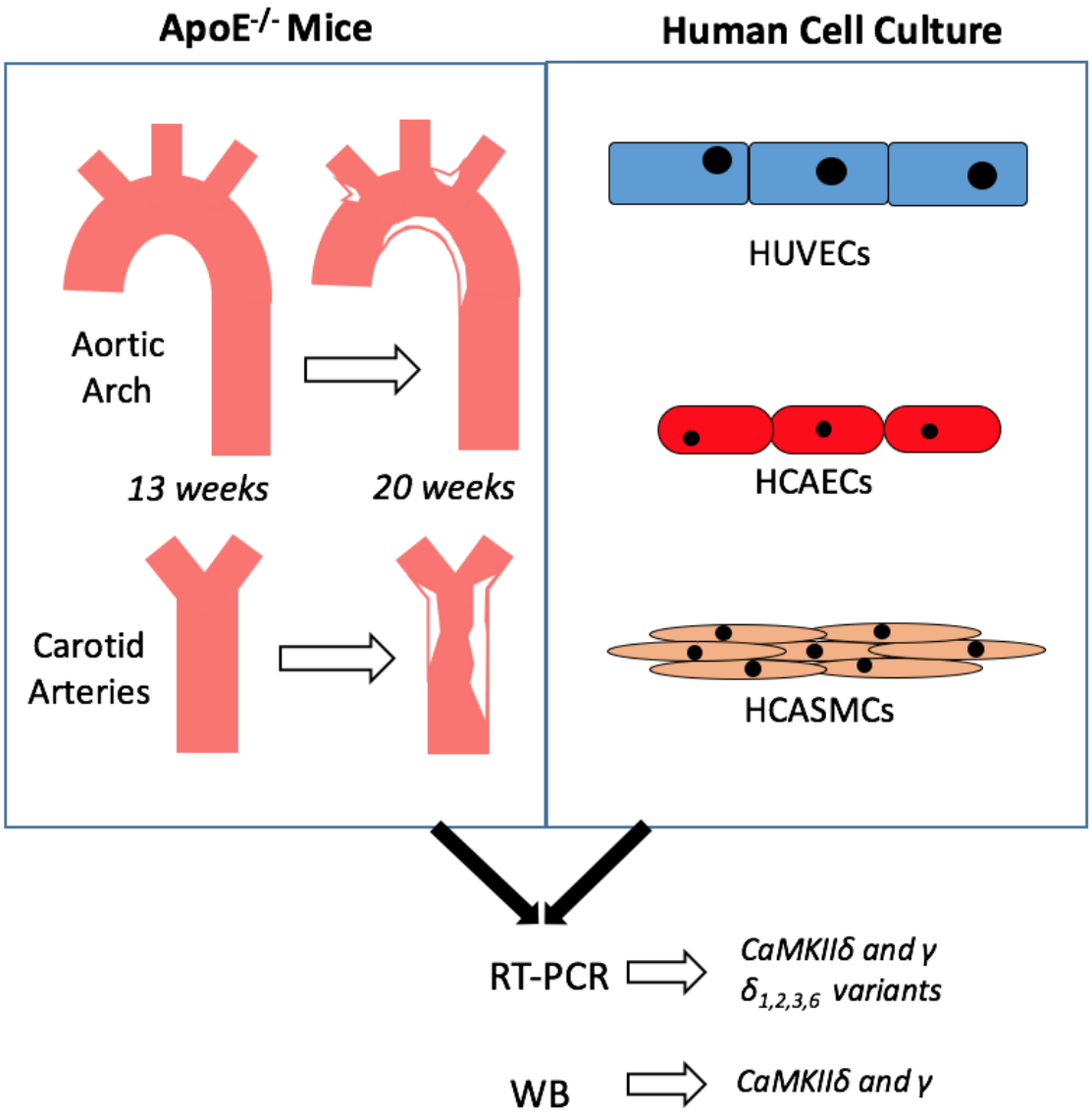

Figure 2.1: Schematic summary of Chapter 2 methods. *The aortic arch and carotid arteries were harvested from 13- and 20-week-old ApoE$^{-/-}$ mice. Human umbilical vein endothelial cells (HUVECs), human coronary artery endothelial cells (HCAECs) and human coronary artery smooth cells (HCASMCs) were cultured. Total RNA and protein were extracted and used for RT-PCR (total CaMKIIδ, $\delta_{1,2,3,6}$ variants and total γ) or western blotting (WB) (CaMKIIδ and γ), respectively. Original figure, Worthington (2020).*

2.2.1 Cell Culture

Human coronary artery smooth muscle cells (HCASMCs), human umbilical vein endothelial cells (HUVECs) and human coronary artery endothelial cells (HCAECs) were cultured in specialised growth medium with 10% fetal bovine serum (FBS) and 1% penicillin/streptomycin (pen/strep) as shown in **Table 2.1**.

Table 2.1: Cell lines and respective growth media/factors.

Cell Line	Media	Growth factors
HCASMC (cat.no.C0175C)	231 (cat.no.M231500)	Smooth muscle differentiation supplement (cat.no.S00725)
HUVEC (cat.no.C0035C)	200 (cat.no.M200500)	Low serum growth supplement (cat.no.S00310)
HCAEC (cat.no.C12221)	MesoEndo Cell Growth Medium (cat.no.212-500)	-

Cells were grown in T75cm^2 culture flasks and maintained in an incubator at 37°C with 5% CO_2, hydrated with milliQ H_2O. To sustain each cell line, cells were washed with pre-warmed PBS and media changed every 24 hours. Once cells reached 80-90% confluence, they were passaged or used for an experiment. All experiments were carried out between passage number 4-8. All cell lines were seeded at 5 x 10^5 cells/ml in 6-well plates for protein and RNA extraction.

2.2.2 Animal Work

The apolipoprotein E (ApoE) knockout mouse is the gold standard model for atherosclerosis research [154, 160, 162]. ApoE$^{-/-}$ mice on a C57/Bl6 background were housed at the Hercus-Taieri Research Unit (HTRU) under a 12:12 hr lighting schedule with *ad libitum* access to food and water. All experiments were approved by the Otago Animal Ethics and Welfare Committee (AEC#: 05/16).

Sixteen mixed-sex ApoE$^{-/-}$ mice were randomly assigned into either the 13- or 20-week-old group. This sample size was used to provide pilot data on the predominant CaMKII isoform involved in early atherogenesis before a more detailed approach. Mice were housed at the Hercus-Taieri Research Unit (HTRU) under a 12:12 hr lighting schedule with ad libitum access to food and water until 13- or 20- weeks of age. At the end of the experimental time point, mice were euthanised by carbon dioxide (CO_2) overdose at a flow rate of 8.5 L/min. Once breathing had ceased, mice were left for an additional 2 mins of CO_2 and then death was confirmed by the pedal withdrawal reflex. Each mouse was weighed and set on a dissection board with chest and stomach exposed.

2.2.2.1 Cardiac Perfusion

The following perfusion was carried out within 10 mins of confirmed death to avoid blood clotting. The mouse was sprayed with 70% ethanol. Using a pair of forceps and surgical scissors, an incision was made below the sternum to expose the abdominal cavity. The diaphragm muscle was carefully blunt dissected away from the ribcage to access the thoracic cavity. Either side of the ribcage was cut and folded back in a hinge-like manner to expose the heart. The right atria was located by following the superior vena cava to the heart, and cut using spring scissors to allow the venous return to drain. Shortly after, a 27 G needle was inserted into the left ventricle via the apex of the heart and perfused with 30 ml of heparinised PBS (40 U/ml).

The aortic tree was cut out of the mouse and set under a dissection stereomicroscope (Motic Ltd, Hong Kong, China) (**Figure 2.2**). The carotid arteries were identified and isolated off the aortic arch using micro spring scissors. The carotid arteries and aortic arch were further divided into four segments. One piece of the divided carotid and aortic arch samples was stored for RNA extraction while the other three segments were stored for protein extraction. Samples were snap frozen in liquid nitrogen and stored at -80°C until RNA/protein isolation.

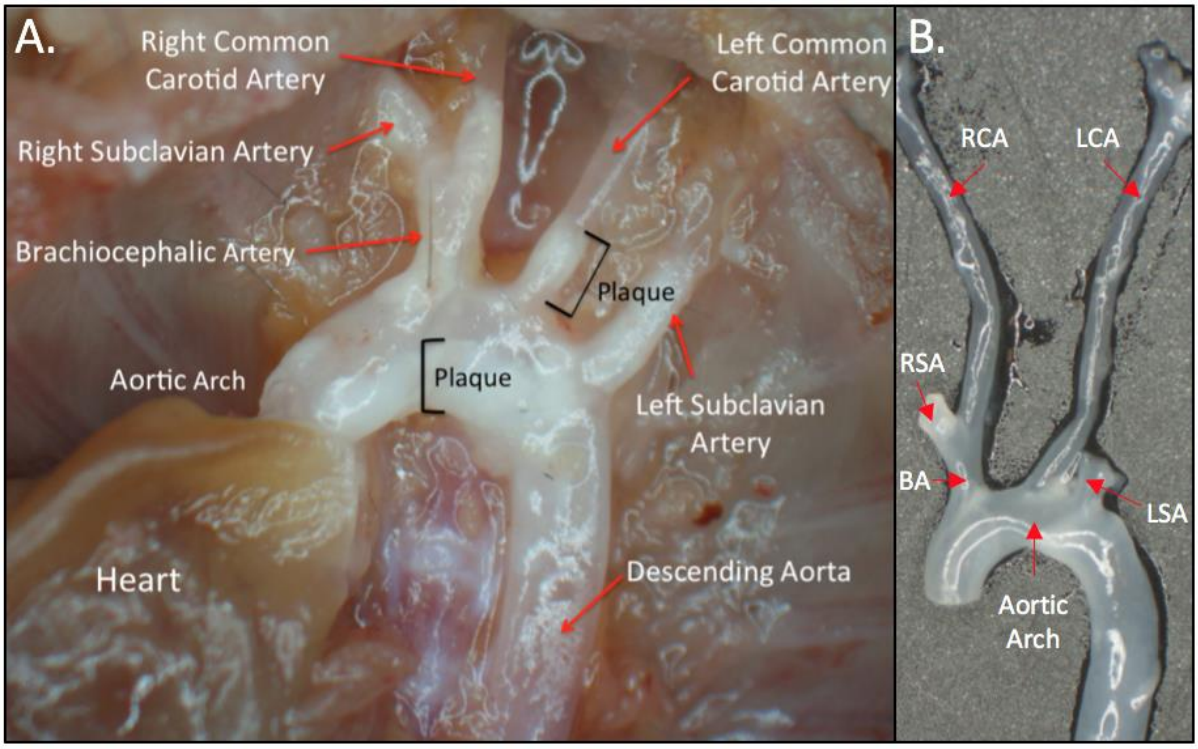

Figure 2.2: Intact aortic arch (A) in the chest cavity and (B) dissected. *ApoE$^{-/-}$ mouse was perfusion fixed with 40U/ml heparinised PBS and 50 ml 4% PFA. Excess adipose tissue was carefully trimmed away from the aortic arch and associated branches using a pair of micro spring scissors under a stereomicroscope **(A)**. The aortic tree was dissected from mouse and set under a microscope to isolate vessels **(B)**. Red arrows indicate the anatomy of the aortic tree. Right common carotid artery (RCA), left common carotid artery (LCA), brachiocephalic artery (BA), aortic arch, right subclavian artery (RSA), left subclavian artery (LSA). Black brackets show opaque regions in the vessel wall indicating foam cell lesion (plaque).*

2.2.3 RT-PCR and Gel Electrophoresis

Total RNA was extracted from human cells (HCASMCs, HUVECs, HCAECs) and the aortic arch and carotid arteries of ApoE$^{-/-}$ mice using TRIZOL reagent (Sigma-Aldrich, Munich, Germany). Total RNA concentration was quantified by measuring absorbance at 260/280 nm using the Maestro nanodrop (MaestroGen Inc, Taiwan). 1 µg RNA was reverse transcribed using the SuperScript®VILO™ cDNA Synthesis Kit (ThermoFisher Scientific, Waltham, USA, cat.no. 11754050) as shown in **Table 2.2**.

Table 2.2: Reverse transcription protocol.

Reagent	**Volume/reaction**	**Reaction**
5X ViLO reaction mix	4 µL	25°C, 10 mins 42°C, 60 mins 85°C, 5 mins
10X Superscript (ViLO) enzyme mix	2 µL	
RNA	1 µg	
DEPC – treated H_2O	Adjusted to total volume of 20 µL	

100 ng of cDNA was used for RT-PCR using the KAPA HiFi HotStart ReadyMix (Cape Town, South Africa). The reaction components are described in **Table 2.3**. A list of primers used for respective human (Hu) and mouse (Ms) species and target products are provided in **Table 2.4**. Primers were either designed for this project or obtained from the scientific literature [212]. PCR amplification was performed in a thermal supercycler (Kyratec, Queensland, Australia). A no template control (NTC) was performed for each RT-PCR experiment where cDNA was replaced with DEPC-water. This was to control for any contaminating DNA that may be present in the other components of the PCR reaction mix. GAPDH was used as the reference gene for RT-qPCR and WB as it is routinely used in our lab as a stable house-keeping gene under disease conditions.

Table 2.3: PCR mastermix reaction.

Reagent	**Volume/reaction (µL)**
KAPA HiFi Hot Start Ready Mix (KAPA Biosystems, cat.no. KRO370)	12.5
Forward primer	0.75
Reverse primer	0.75
DEPC-treated H_2O	9
cDNA	2 (100 ng)

Table 2.4: Primer sequences and cycling conditions for human cells and mouse arteries.

Primer		Sequence	Cycling	Target Size
MsCaMKIIδ	F	5'-GCTAGGGACCATCAGAAACTG-3'	98°C (10s) 55°C (20s) 72°C (30s) X35	150 NM_001025438
	R	5'-GTCTTCAAACAGTTCGCCAC-3'		
MsCaMKIIγ	F	5'-CGACTACCAGCTTTTCGAG-3'	98°C (10s) 55°C (20s) 72°C (40s) X35	150 NM_178597.5
	R	5'-GCCTCTCGTTCTAGTTTCTGATG-3'		
MsV2 (CaMKIIδ variants 1,2,3,6)	F	5'-TCGGCTCACACAGTACATGGACGG-3'	98°C (10s) 58°C (20s) 72°C (30s) X30	227 δ_1 NM_001025439.2 δ_3 NM_023813.4 316 δ_2 NM_001025438.2 δ_6 NM_001293665.1
	R	5'-GAAACATGCATGAAGAGGAGAGGA-3'		
MsGAPDH	F	5'-AACTTTGGCATTGTGGAAGG-3'	98°C (10s) 58°C (20s) 72°C (20s) X30	223 NM_001289726.1
	R	5'-ACACATTGGGGGTAGGAACA -3'		
HuV1 (CaMKIIδ variants)	F	5'-GCCATCTTGACAACTATGCTGGCT-3'	98°C (10s) 57°C (20s) 72°C (30s) X35	173 δ_6 NM_172114.1 131 δ_2 NM_172128.3
	R	5'-CGTGCTTTCACATCTTCATCCTCA-3'		
HuV2 (CaMKIIδ variants 1, 2, 3)	F	5'-TAGGCTCACACAGTACATGGATGG-3'	98°C (10s) 57°C (20s) 72°C (30s) X25	325 δ_3 NM_001221.4 229 δ_2 NM_172128.3 273 δ_1 NM_172127.2
	R	5'-ACATGCATGAAGAGGAGGAGA GGA-3'		
HuCaMKIIγ	F	5'-GACTTCTGAAACATCCAAAC-3'	98°C (10s) 52°C (20s) 72°C (40s) X35	431 NM_172171.2
	R	5'-CACCAGGAGGATATACAGGA-3'		
HuGAPDH	F	5'-AATGGGCAGCCGTTAGGAAA-3'	98°C (10s) 58°C (20s) 72°C (20s) X30	168 NM_001256799.3
	R	5'-GCGCCCAATACGACCAAATC-3'		

Agarose gels were used for electrophoresis to separate and visualise PCR products. Gels ranged from 1-4% agarose in TAE buffer (40mM Tris, 20mM acetate, 1mM EDTA (Calbiochem, San Diego, USA, cat.no. 16G145210)) depending on the number and size of target products. The gel was microwaved to dissolve agarose and left to cool before adding 6 µL of SYBR safe DNA stain (ThermoFisher, cat.no. S33102). The gel was poured into the tray and left to cool. Products of PCR reactions were mixed with BlueJuice™ Gel Loading Buffer (10X) (ThermoFisher Scientific, cat.no. 10816015) and loaded onto an agarose gel alongside the NTC. The size of each amplified product was confirmed by comparing with a 100 kb DNA marker (ThermoFisher, cat.no. 15628050) that was electrophoresed in parallel with samples. For primer pairs with one target, a low percentage agarose gel (1-2%) was used with electrophoresis at 100 V for 2 hr. In contrast, for primer sets that amplify a number of products of different sizes, a higher percentage agarose gel was used (2.5-4%) for electrophoresis at 60 V for 2 hr. Agarose gels were placed in the tray of the PXi 4 Touch Multi-Application Gel Imaging System (Syngene, PXi 4 Touch, Bangalore, India) and images digitally captured.

2.2.4 Western Blots

Total protein was extracted using RIPA lysis buffer (50 mM Tric-HCl, 150 mM NaCl, 0.1% SDS, 1% Triton X-100, 1 mM EDTA, milliQ H_2O, pH 7.4). 40 µg samples were mixed with Bolt™ LDS sample buffer (4X) (ThermoFisher, cat.no. B0007) and Bolt™ reducing agent (10X) (ThermoFisher, cat.no. B0004) and heated at 70°C for 10 mins. Denatured samples were then loaded in a 10% Bolt Bis-Tris Plus Gel (Invitrogen, Carlsbad, USA, cat.no. NW00105) alongside the SeeBlue® Plus 2 Pre-stained Protein Standard (Invitrogen, cat.no. LC5925). The gel tank was plugged into the power pack and electrophoresis performed at 150 V for 90 mins.

The gel was placed on a piece of PVDF membrane and sandwiched between four pieces of blotting paper. The transfer sandwich was submerged in transfer buffer (25 mM Tris, 0.2 mM Glycine, 10% methanol) in a Mini-PROTEAN Tetra Cell (Biorad, Hercules, USA) system. The tank was connected to a power pack and 90 V was applied for 90 mins to transfer proteins from gel to PVDF membrane. After transfer, the PVDF membrane was removed and blocked in 5% milk powder in TBST (10 mM Tris, 100 mM NaCl, 5% Tween 20) for 1 hr. The membrane was then probed with primary and secondary antibodies as shown in **Table 2.5**. Primary antibodies were added to the membrane and incubated overnight at 4°C. The following day, membranes were

washed in 5 min intervals for 30 min with TBST. Secondary antibodies were then incubated for an hour and washed with TBST in a similar manner. Supersignal West Pico Chemiluminescent Substrate (ThermoFisher, cat.no. 34087) was used to detect conjugated secondary antibody and imaging of the membrane was performed using the Syngene PXi 4 Touch.

Table 2.5: Primary and secondary antibodies with respective dilutions.

Primary Antibody	Dilution Factor		Secondary Antibody	Dilution Factor
CaMKIIδ (ThermoFisher Cat. No. PA5-22168)	1:3500		Goat anti-rabbit HRP (Novex™ Cat. No. A16104)	1:2500
CaMKIIγ (ThermoFisher Cat. No. PA5-14035)	1:2000			
GAPDH (GeneTex® Cat. No. GTX627408)	1:7000		Goat anti-mouse HRP Novex™ (Cat. No. A16072)	1:10,000

2.2.5 Statistical Analysis

All data was analysed on GraphPad Prism 8 and expressed as mean ± SEM. Significant differences were determined by Students T-Test or 2-way ANOVA with Tukey's multiple comparisons post-hoc test. Significant (*$p<0.05$, ****$p<0.0001$) and non-significant (NS) comparisons indicated on graph.

2.3 Results

2.3.1 CaMKIIδ mRNA levels in the aortic arch and carotid arteries of 13- and 20-week old ApoE$^{-/-}$ mice.

CaMKIIδ is suggested to be the pathological isoform that contributes to vascular disease [181, 212, 218, 219]. To show the relative mRNA levels of CaMKIIδ during the progression of atherosclerosis, the aortic arch and carotid arteries of 13- and 20-week-old ApoE$^{-/-}$ mice were dissected (**Figure 2.3**). The homogenates will contain all cell groups of the vascular wall including endothelial cells, smooth muscle cells and foam cells (macrophages). Total RNA was extracted and RT-PCR targeting the total MsCaMKIIδ and MsV2 (CaMKIIδ$_{1,2,3,6}$) [212] primer sets were completed in a thermocycler. PCR products were visualised by agarose gel electrophoresis (*Section 2.2.3*).

Figure 2.4 shows the relative mRNA level of CaMKIIδ in the aortic arch of 13- and 20-week-old ApoE$^{-/-}$ mice. The presence of a band at 150 bp in each sample lane is indicative of the CaMKIIδ product (NM_001025438). The faint band below 150 bp is likely to be primer dimer as the same band is present in the no-template control (NTC).

CaMKIIδ mRNA was detected in the aortic arch of 13- and 20-week ApoE$^{-/-}$ mice. Next, it was identified what specific δ variants are present. **Figure 2.5** shows the products of MsV2 (CaMKIIδ$_{1,2,3,6}$) [212] targeted primers in the aortic arch of 13- and 20-week ApoE mice. The presence of bands at 227 bp and 316 bp are indicative of a combination of either the δ$_{1/3}$ or δ$_{2/6}$ variants, respectively. CaMKIIδ$_{1,2,3,6}$ variants were present before the onset of lesion development in the aortic arch of 13- week ApoE$^{-/-}$ mice. Furthermore, the same variants were present at 20-weeks, where lesions are more developed.

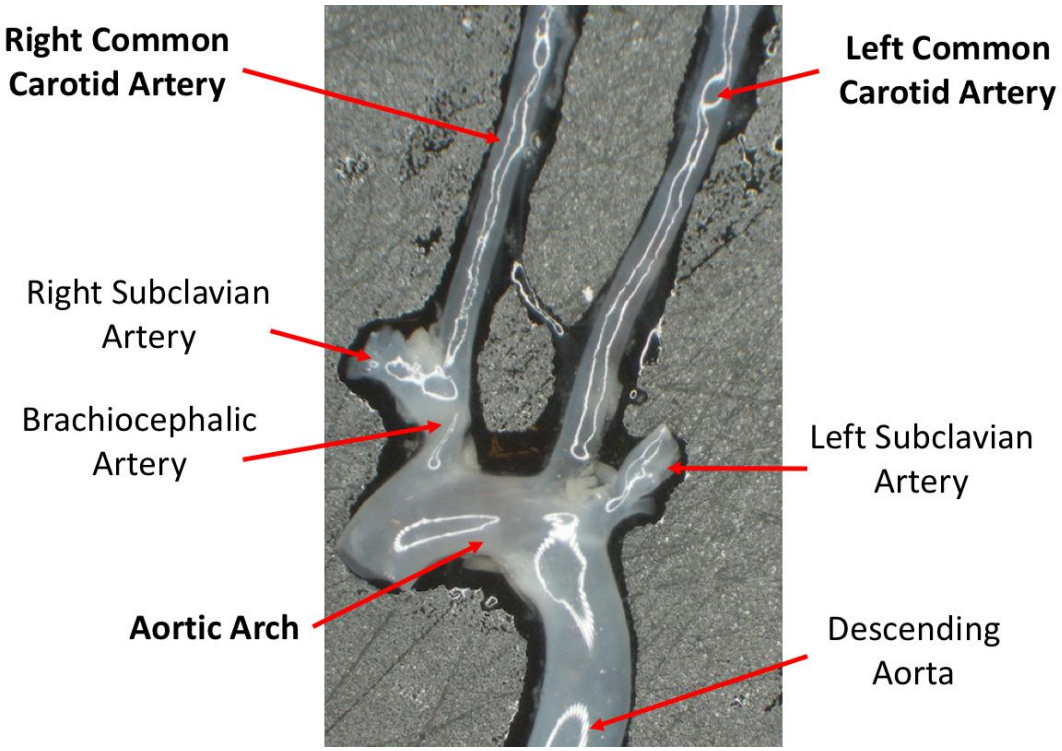

Figure 2.3: Dissected aortic tree of a 20-week ApoE$^{-/-}$ mouse. *The mouse was euthanised by CO_2 overdose at 20-weeks of age. The mouse was fixed with 4% PFA via cardiac perfusion. The aortic tree with carotid arteries were dissected out. The carotid artery and aortic arch were isolated and snap frozen in liquid N_2. Red arrows indicate the anatomy of the aortic arch. Photo taken on a stereomicroscope (10X objective). Representative image of one aortic tree from a 20-week ApoE$^{-/-}$ mouse, n=8. Photo taken on a Motic stereomicroscope (10X objective).*

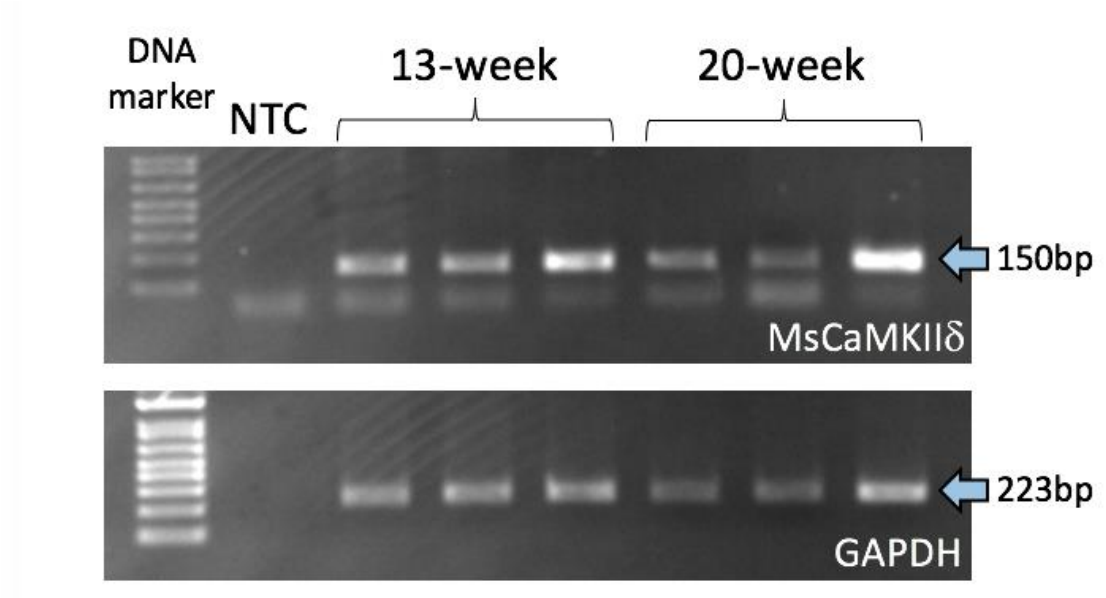

Figure 2.4: DNA agarose gel showing total CaMKIIδ levels in the aortic arch of 13- and 20-week ApoE$^{-/-}$ mice. *Total RNA was extracted and 100 ng cDNA was used in RT-PCR targeting the total MsCaMKIIδ primer set. PCR products were loaded onto a 1.5% agarose gel and electrophoresis run at 100 V for 1 hr. GAPDH was used as a reference gene. No template control (NTC) contains reaction mix with DEPC-H_2O replacing DNA sample. 100 bp DNA marker (Invitrogen cat.no. 15628019). Representative gel shows data for 3 of 8 independent mice from each age group (n = 8).*

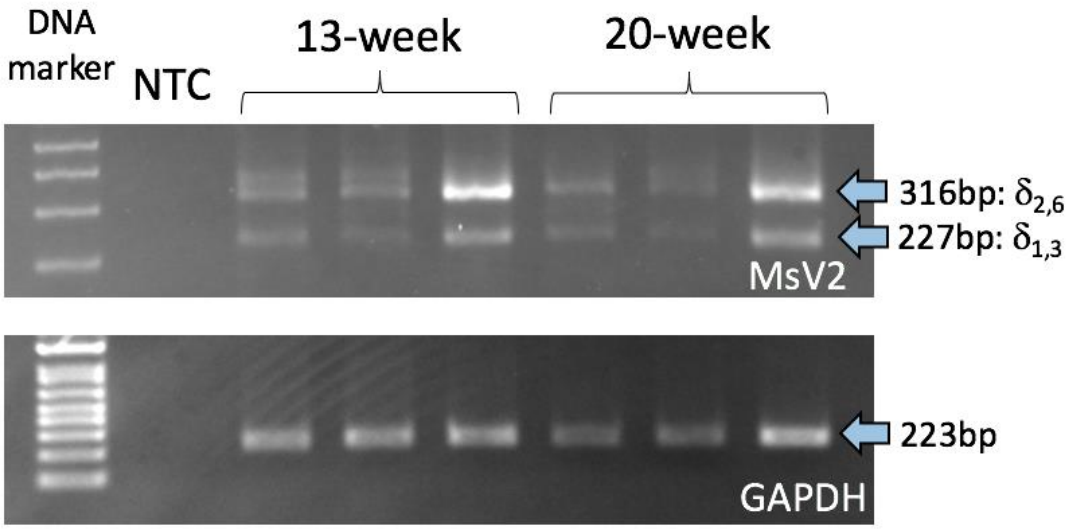

Figure 2.5: DNA agarose gel showing CaMKIIδ variant levels in the aortic arch of 13- and 20-week ApoE$^{-/-}$ mice. *Total RNA was extracted and 100 ng cDNA was used in RT-PCR targeting the MsV2 primer set. PCR products were loaded onto a 3.5% agarose gel and electrophoresis run at 60 V for 2 hr. GAPDH was used as a reference gene. No template control (NTC) contains reaction mix with DEPC-H_2O replacing DNA sample. 100 bp DNA marker (Invitrogen cat.no. 15628019). Representative gel shows data for 3 of 8 independent mice from each age group (n = 8).*

To validate these observations, CaMKIIδ and its spliced variants were also measured in the carotid artery. **Figure 2.6** shows CaMKIIδ is present in the carotid arteries of 13- and 20-week ApoE$^{-/-}$ mice, evidenced by the presence of a band at 150 bp. **Figure 2.7** shows the relative level of CaMKIIδ variants in the carotid arteries of 13- and 20-week ApoE$^{-/-}$ mice. The presence of bands at 227 bp and 316 bp are indicative of a combination of the $\delta_{1/3}$ and $\delta_{2/6}$ variants. Therefore, like the aortic arch, CaMKII$\delta_{1,2,3,6}$ are expressed in the carotid artery of 13- and 20-week ApoE$^{-/-}$ mice.

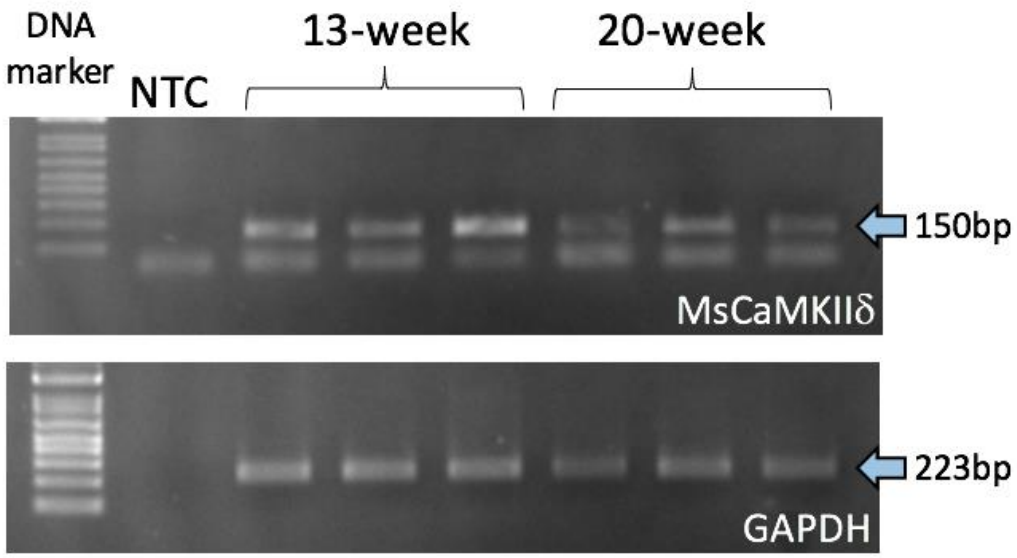

Figure 2.6: DNA agarose gel showing total CaMKIIδ levels in the carotid arteries of 13- and 20-week ApoE$^{-/-}$ mice. *Total RNA was extracted and 100 ng cDNA was used in RT-PCR targeting total MsCaMKIIδ primer set. PCR products were loaded onto a 1.5% agarose gel and electrophoresis run at 100 V for 1 hr. GAPDH used as a reference gene. No template control (NTC) contains reaction mix with DEPC-H_2O replacing DNA sample. 100 bp DNA marker (Invitrogen cat.no. 15628019). Representative gel shows data for 3 of 8 independent mice from each age group (n = 8).*

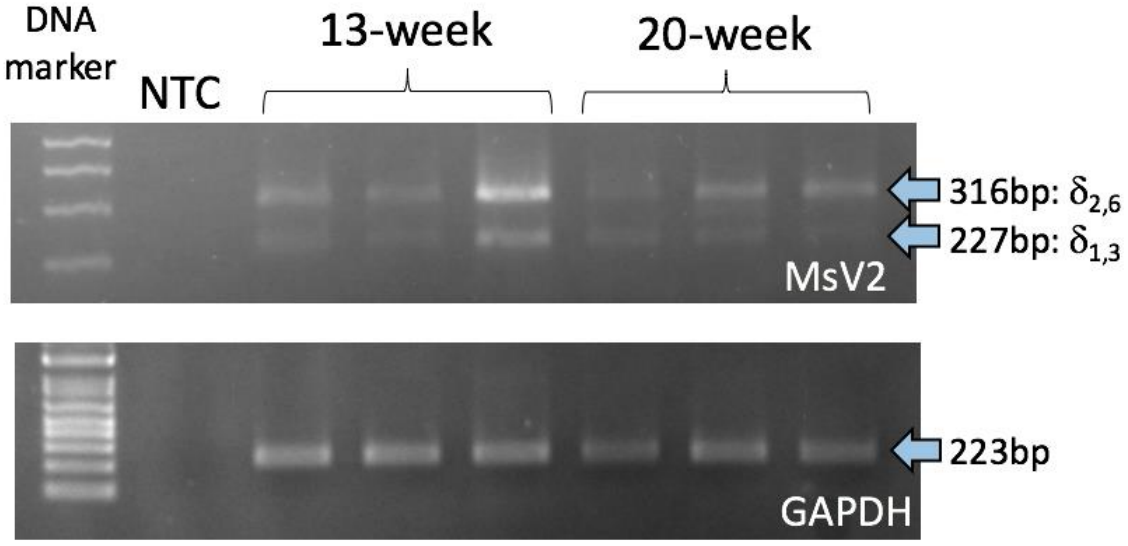

Figure 2.7: DNA agarose gel showing CaMKIIδ variant levels in the carotid arteries of 13- and 20-week ApoE$^{-/-}$ mice. *Total RNA was extracted and 100 ng cDNA was used in RT-PCR targeting the MsV2 primer set. PCR products were loaded onto a 3.5% agarose gel and electrophoresis run at 60 V for 2 hr. GAPDH was used as a reference gene. No template control (NTC) contains reaction mix with DEPC-H_2O replacing DNA sample. 100 bp DNA marker (Invitrogen cat.no. 15628019). Representative gel shows data for 3 of 8 independent mice from each age group (n = 8).*

2.3.2 CaMKIIδ mRNA levels in the human vascular cell.

Results so far have shown that CaMKIIδ mRNA is present in the arteries of ApoE$^{-/-}$ mice during the progression of atherosclerosis. In particular, CaMKII$\delta_{1,2,3,6}$ variants were detected by RT-PCR. To determine whether the variants in the ApoE$^{-/-}$ mouse are the same as those found in human vascular cells, CaMKIIδ variant levels were analysed in HUVECs and HCASMCs using the huV1 and huV2 primer set(s) [212]. The huV1 primer set is specific for CaMKIIδ_2 and δ_6 variants, whereas the huV2 primer set is specific for CaMKIIδ_1, δ_2, and δ_3 [212]. These cell models are commonly used for studying endothelial and smooth muscle cell physiology [35, 39, 48, 212, 220, 230, 231].

Figure 2.8 shows CaMKIIδ variant levels in HUVECs and HCASMCs. For the huV1 targeted PCR primer set, the presence of a band at 130 bp or 190 bp indicates the CaMKIIδ_2 and δ_6 variants, respectively. For the huV2 targeted RT-PCR, the presence of a band at 229 bp, 275 bp and 350 bp shows the CaMKIIδ_2, δ_1, and δ_3 variants, respectively. In HUVECs and HCASMCs CaMKII$\delta_{1,2,3}$ variants were detected. Furthermore, HCASMCs had a faint band at the 190bp marker indicating CaMKIIδ_6 mRNA.

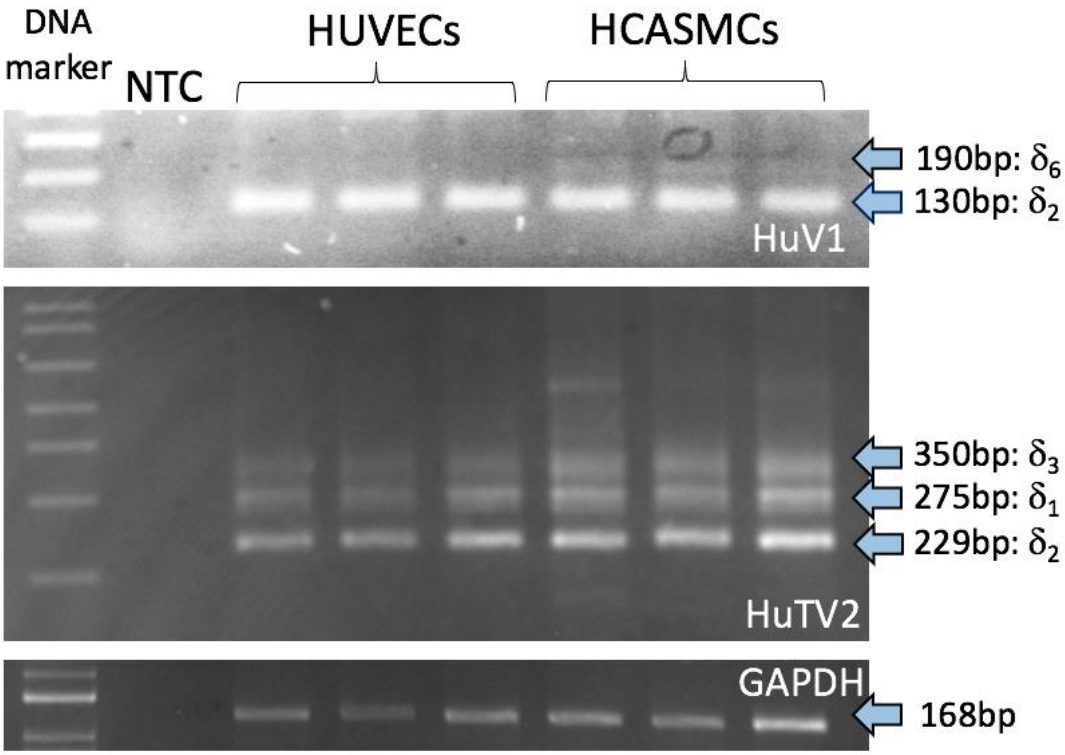

Figure 2.8: DNA agarose gel showing CaMKIIδ variant levels in human cells of the vasculature. *Total RNA was extracted from HUVECs and HCASMCs. 100 ng cDNA was used in RT-PCR targeting CaMKIIδ variants with huV1 and huV2 primer sets. PCR products were loaded onto a 2.5% (huV1), 4% (huV2) and 1% (GAPDH) agarose gel and electrophoresis run at 60 V for 2 hr. GAPDH was used as a reference gene. No template control (NTC) contains reaction mix with DEPC-H_2O replacing DNA sample. 100 bp DNA marker (Invitrogen cat.no. 15628019). Representative gel shows data for 3 of 6 independent HUVEC and HCASMC experiments (n = 6).*

2.3.3 CaMKIIγ mRNA Levels in human and mouse vascular cells.

So far, it has been shown that CaMKIIδ mRNA is present in cultured human ECs, VSMCs and the atherosclerotic aortic arch and carotid arteries of ApoE$^{-/-}$ mice. In particular CaMKIIδ$_{1,2,3,6}$ variants were detected in extracts from both human vascular cells and the arteries of ApoE$^{-/-}$ mice. However, CaMKIIδ is not the only isoform specific to the vasculature. CaMKIIγ is the other predominant isoform expressed in the vasculature [203] and has been shown to play a contrasting protective role against vascular disease [181, 213]. Therefore, it was next determined what the CaMKIIγ mRNA levels were in ECs and VSMCs and the aortic arch of ApoE$^{-/-}$ mice.

Figure 2.9 shows the relative mRNA level of CaMKIIγ in the aortic arch of 13- and 20-week ApoE$^{-/-}$ mice. CaMKIIγ was detected before and during the development of atherosclerosis indicated by the presence of a band at 150 bp in the 13- and 20-week sample lanes. **Figure 2.10** shows the relative mRNA level of CaMKIIγ in HUVECs and HCASMCs. The presence of a band at 431 bp is indicative of CaMKIIγ mRNA expression in the cells.

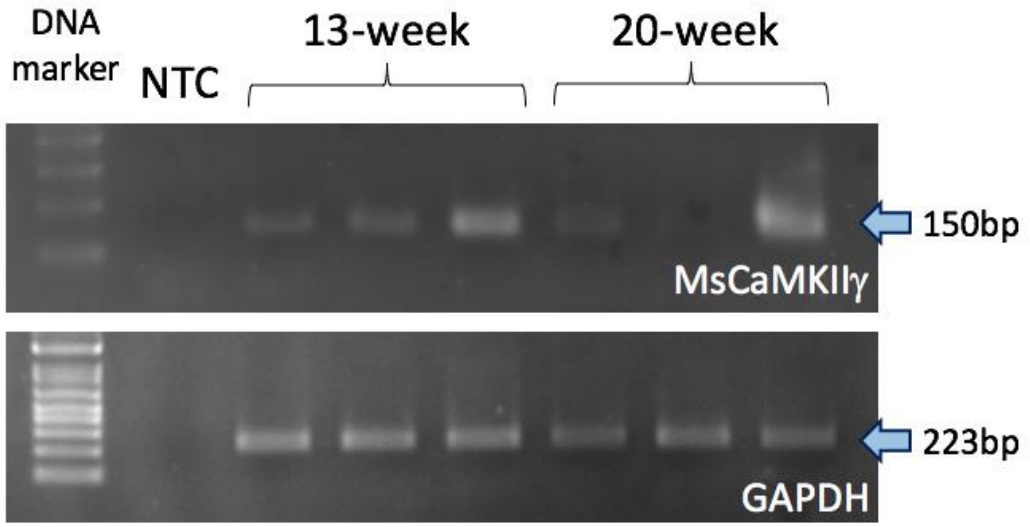

Figure 2.9: DNA agarose gel showing total CaMKIIγ isoform levels in the aortic arch of 13- and 20-week ApoE$^{-/-}$ mice. *Total RNA was extracted and 100 ng cDNA was used in RT-PCR targeting CaMKIIγ. PCR products were loaded onto a 1.5% agarose gel and electrophoresis run at 100 V for 1 hr. GAPDH was used as a reference gene. No template control (NTC) contains reaction mix with DEPC-H_2O replacing DNA sample. 100 bp DNA marker (Invitrogen cat.no. 15628019). Representative gel shows data for 3 of 8 independent experiments from each age group (n = 8).*

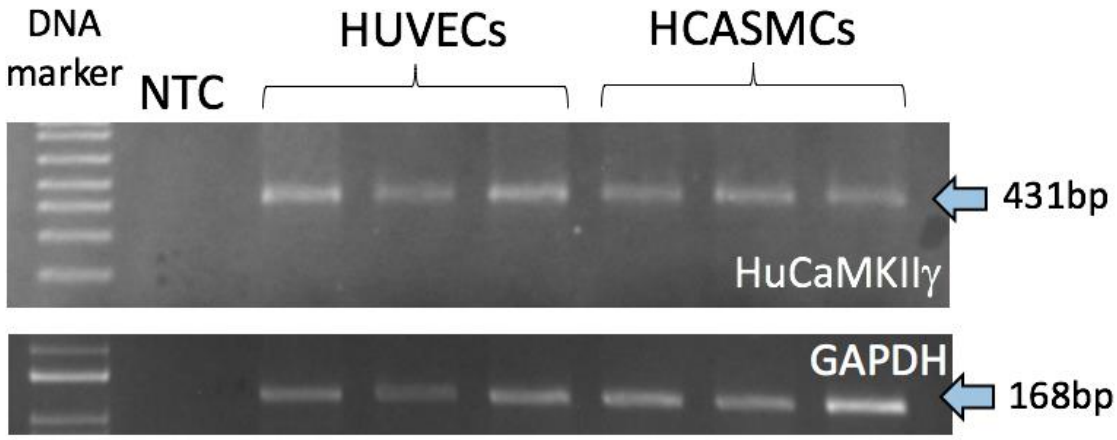

Figure 2.10: DNA agarose gel showing total CaMKIIγ isoform levels in human cells of the vasculature. *Total RNA was extracted from HUVECs and HCASMCs. 100 ng cDNA was used in RT-PCR targeting CaMKIIγ. PCR products were loaded onto a 1.5% agarose gel and electrophoresis run at 100 V for 1 hr. GAPDH was used as a reference gene. No template control (NTC) contains reaction mix with DEPC-H_2O replacing DNA sample. 100 bp DNA marker (Invitrogen cat.no. 15628019). Representative gel shows data for 3 of 6 independent HUVEC and HCASMCs experiments (n = 6).*

2.3.4 CaMKIIδ and γ protein levels in human and mouse vascular cells.

The CaMKIIIδ and γ isoforms are expressed in human ECs, VSMCs, and the aortic arch and carotid arteries of ApoE$^{-/-}$ mice at the mRNA level. To identify whether the transcript level extends to protein expression, human cells were cultured and lysates subject to Western blotting (WB) targeting CaMKIIIδ and γ. HUVECs were used in previous experiments as they are a validated EC model, however, to more closely represent the coronary artery, for the next set of experiments, human coronary artery endothelial cells (HCAECs, Sigma Aldrich, 300-05a) were obtained from a commercial source. HUVECs were compared HCAECs to confirm the similarity of EC CaMKII isoform expression.

Figure 2.11A shows CaMKIIδ expression in HUVECs, HCAECs and HCASMCs evidenced by the presence of a band indicated by the blue arrow above the 49 coda marker. The HUVEC and HCAEC mean band intensities were pooled as representative of EC and compared with HCASMC. GAPDH was used as a loading control to account for any global protein expression differences between cell groups, as well as total protein concentration differences. The band intensity for CaMKIIδ in HCASMC groups was visually stronger that the endothelial cell groups (N.S, n = 3) (**Figure 2.11B**).

CaMKIIγ expression was also detected in vascular endothelial cells and HCASMCs indicated by the presence of a band above the 49 coda, indicated by the blue arrow (**Figure 2.12A**). The other faint bands present may be non-specific targets or other CaMKII isoforms. Unlike the different CaMKIIδ expression pattern observed between ECs and HCASMCs, here, CaMKIIγ expression was relatively similar between cell types (N.S, n=3)(**Figure 2.12B**). The high SEM in the EC group is most-likely an effect of pooling HCAEC and HUVEC densitometry data.

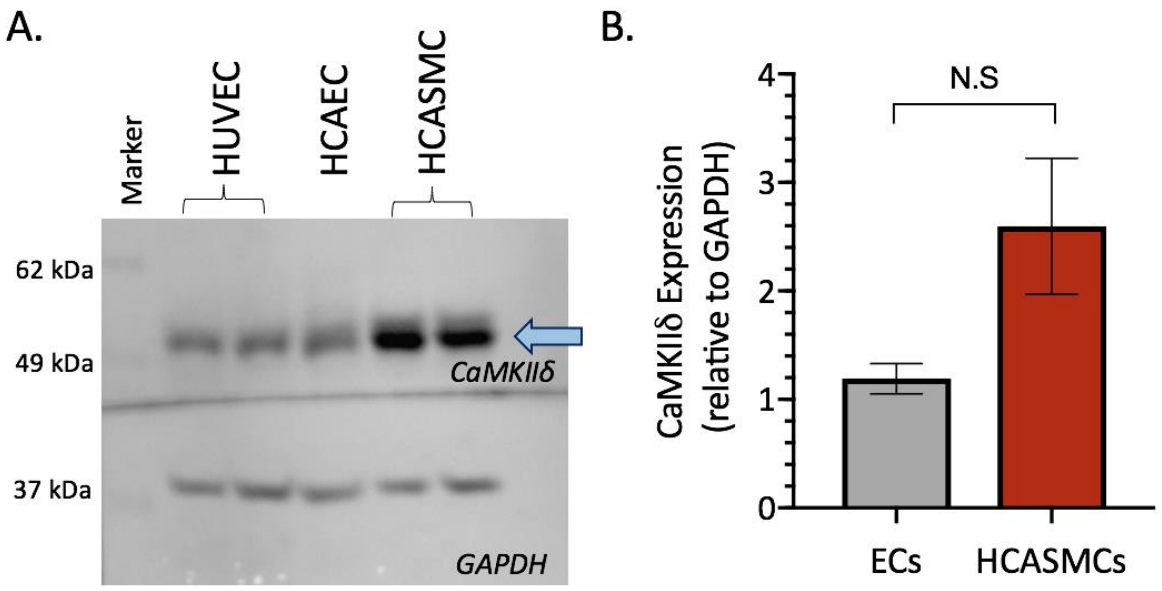

Figure 2.11: Western blot membrane showing CaMKIIδ and GAPDH protein levels from human cells of the vasculature (A). Quantification of CaMKIIδ in vascular endothelial cells (ECs) and human coronary artery smooth muscle cells (HCASMCs) (B). *Protein lysates were extracted from HUVECs, HCAECs and HCASMCs. 40 µg samples were subject to PAGE electrophoresis for 1 hr. Proteins were transferred to a PVDF membrane, blocked and incubated with antibodies targeting CaMKIIδ and GAPDH. Bands were detected using the Super signal West Pico Chemiluminescent Substrate (ThermoFisher, cat.no. 34087) and digital images captured on a Syngene PXi 4 Touch. The positions of the kDa marker weights are shown to the left (ThermoFisher, cat.no. 15628050) (A). Histograms show mean band densitometry level $\pm$ S.E.M (n = 3)(B). Non-significant (N.S) as determined by Students unpaired T-test.*

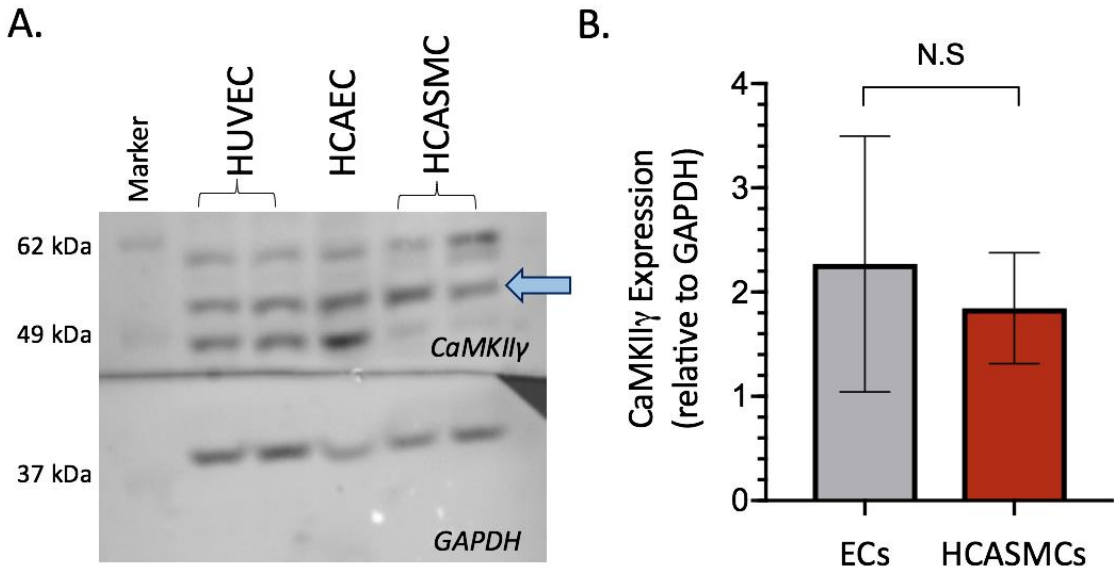

Figure 2.12: Western blot membrane showing CaMKIIγ and GAPDH protein levels from human cells of the vasculature. Quantification of CaMKIIγ in endothelial cells (ECs) and human coronary artery smooth muscle cells (HCASMCs) (B). *Protein lysates were extracted from HUVECs, HCAECs and HCASMCs. 40 µg samples were subject to PAGE electrophoresis for 1 hr. Proteins were transferred to PVDF membrane, blocked and incubated with antibodies targeting CaMKIIγ and GAPDH. Bands were detected using the Supersignal West Pico Chemiluminescent Substrate (ThermoFisher, cat.no. 34087) and digital images captured on a Syngene PXi 4 Touch. The positions of the kDa marker weights are shown to the left (ThermoFisher, cat.no. 15628050) (A). Histograms show mean band densitometry level ±S.E.M (n = 3)(B). Non-significant (N.S) as determined by Students unpaired T-test.*

CaMKIIδ and γ expression was detected in human cells of the vasculature. Furthermore, δ levels were greater in HCASMCs compared to ECs. Next, it was tested which isoform of CaMKII was dominantly expressed in the vasculature of ApoE$^{-/-}$ mice throughout the development of atherosclerosis. Western blot analysis was used to target CaMKIIδ and γ in aortic arch homogenates of 13- and 20-week old ApoE$^{-/-}$ mice.

CaMKIIδ expression levels were detected at 13-weeks indicated by the strong band above the 49 markers as indicated by blue arrow (**Figure 2.13**). CaMKIIδ levels remained high at 20-weeks and no changes were seen when compared to densitometry of 13-weeks data. Compared to CaMKIIδ, CaMKIIγ expression levels were lower as evidenced by faint bands above the 49 kDa marker ($p<0.0001$). At 20-weeks, CaMKIIγ levels remained low (N.S, ANOVA, n=7) *(***Figure 2.13B**). Collectively, this data indicates that CaMKIIδ is the most likely isoform that is driving foam cell lesion development.

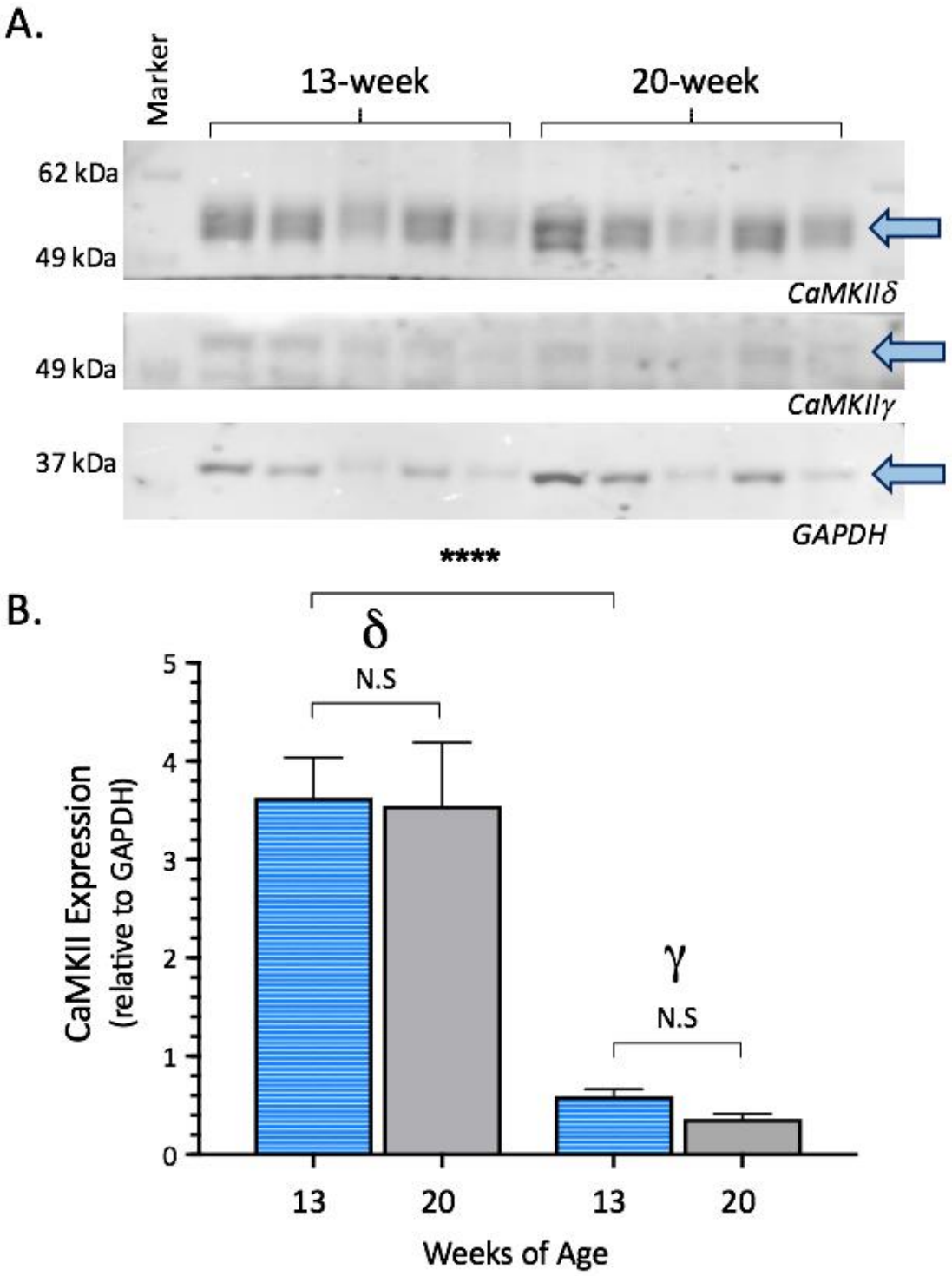

Figure 2.13: CaMKIIδ is the predominant isoform present in the vasculature of ApoE$^{-/-}$ mice. *Protein lysates were extracted from the aortic arch of 13- and 20-week od ApoE$^{-/-}$ mice. 40 µg samples were subject to PAGE electrophoresis for 1 hr. Proteins were transferred to a PVDF membrane, blocked and incubated with antibodies targeting CaMKIIδ, CaMKIIγ and GAPDH. Bands were detected using the Supersignal West Pico Chemiluminescent Substrate (ThermoFisher, cat.no. 34087) and digital images captured on a Syngene PXi 4 Touch. The positions of the kDa marker weights are shown to the right (ThermoFisher, cat.no. 15628050) (A). Representative blot showing five out of seven independent mice for 13-week and 20-week age groups. Histograms below show mean band densitometry level $\pm$S.E.M (n=7) (B).****P<0.0001, non-significant (N.S), as determined by two-way ANOVA with Tukey's multiple comparisons post-hoc test.*

2.4 Discussion

A molecular approach has been used employing RT-PCR and Western blotting to identify what isoform of the CaMKII family was the most likely key player in early atherogenesis. An investigation of CaMKII isoform expression in human ECs and VSMCs, and aortic arch/carotid artery tissue from a mouse model of atherosclerosis ($ApoE^{-/-}$) identified CaMKIIδ as the predominant isoform.

The two regions of the aortic tree selected for investigation in the $ApoE^{-/-}$ mouse was the aortic arch and carotid arteries. These regions are prone to the development of extensive atherosclerosis, and at 20-weeks of age in the $ApoE^{-/-}$ mouse, both regions have reported foam cell lesions [160, 162, 172]. CaMKIIδ mRNA was expressed in the aortic arch and carotid arteries of $ApoE^{-/-}$ mice as well as cultured HUVECs and HCASMCs (*Section 2.3.1-2*). Other observational and mechanistic studies that have focused on a specific CaMKII isoform have identified the δ form as the predominant type expressed in the cells of the heart and vasculature [185, 197, 200]. Activation of CaMKIIδ has been identified in promoting EC dysfunction and a proliferative response of VSMCs [212, 219, 220]. This finding is important because endothelial dysfunction and VSMC proliferation are key contributing mechanisms in the development of foam cell lesions [13].

Given that δ was the dominant isoform, it was next investigated what splice variants of CaMKIIδ were present. Identifying the specific variants is important as in previous research it has been shown at least in cardiomyocytes, the δ_2 and δ_3 types display different functions due to differential localisation to the cytoplasm and nucleus, respectively [204, 229]. CaMKIIδ variants 1, 2, 3 and 6 were present in HUVECS and HCASMCs, as well as in the aortic arch and carotid arteries of $ApoE^{-/-}$ mice. What seemed to stand out across each experiment and be consistent between species was the CaMKIIδ_2 variant (*Section 2.3.1-2*). The specific CaMKIIδ_2 has already been identified in the development of cardiac disease and more recently, in the vasculature it is emerging a player in vascular pathology [181, 193, 229]. CaMKIIδ_2 is involved in proliferation of VSMCs, a key event in the development of foam cell lesions [219, 220]. While the CaMKIIδ_2 was becoming the variant of increasing interest in atherogenesis, the similar mRNA profile of variants between species was important in further validating the $ApoE^{-/-}$ mouse for atherosclerosis research in a translational aspect. For the purpose of these

observational pilot GAPDH was a suitable reference gene. In future studies it would be useful to use a combination of reference genes as GAPDH expression levels have been shown to fluctuate under certain conditions [232].

Of interest, CaMKIIδ_6 mRNA was detected in ApoE$^{-/-}$ mice but it was only just observable in HUVECs and HCASMCs after overexposing the agarose gel (**Figure 2.8**). This is likely to reflect differences in the local environment between the two models. In the arteries of ApoE$^{-/-}$ mice, ECs and VSMCs are exposed to inflammation (atherosclerosis) and the physical forces associated with blood flow (shear stress) [26, 34]. In contrast, human cells were cultured under standard non-inflammatory conditions. An increase in CaMKIIδ_6 has been shown to be involved in increasing the permeability of the endothelial wall, a common phenotype of endothelial dysfunction and atherosclerosis [212]. The lack of cell culture conditions that mimicked an atherosclerotic milieu is a probable reason for the lack of CaMKIIδ_6 transcript. In a future experiment it would be interesting to investigate whether exposing HUVECs and HCASMCs to an inflammatory milieu with TNF-α and H_2O_2 would induce CaMKIIδ_6 transcription.

The major difference between the cell culture and animal model is that the individual vascular cells were investigated in humans, whereas aortic arch and carotid artery homogenates of the ApoE$^{-/-}$ mouse contained a combination of ECs, SMCs and any other immune cells that are present in the vascular wall. This meant that in the human cell cultures, CaMKIIδ and γ expression was observed in individual ECs and VSMCs. In contrast, CaMKIIδ and γ expression profile in artery homogenates from ApoE$^{-/-}$ mice is the cumulative expression profile from ECs, VSMCs and foam cells (macrophages). However, for the purpose of this study, the primary objective was to identify the predominant isoform likely contributing to atherosclerosis rather than what cell group was the main contributor.

CaMKIIδ protein expression was significantly higher than γ expression in the arteries of ApoE$^{-/-}$ mice at both 13- and 20-weeks (**Figure 2.13**). These two time points reflect two different stages in the disease progression of atherosclerosis, a pre-lesion phase (13-weeks) and lesion phase (20-weeks) [162]. While CaMKIIδ expression was high at 13-weeks, the levels persisted at 20 weeks and no differences were observed. The hypothesis of this study was that CaMKIIδ was the most likely isoform expressed in vascular cells and the most likely player contributing

to the pathogenesis of atherosclerosis. Therefore, this result was surprising as it was anticipated that δ expression levels would increase with disease progression. Firstly, this suggests the 13-week time point was not early enough in the disease progression. At 13-weeks ApoE mice already present with ED and small pockets of intimal lipid accumulation [162]. If there is an increase in CaMKIIδ expression, it could be occurring at a time before there are any gross changes to the vascular wall. Secondly, if CaMKIIδ expression is not changing then the activation state of the enzyme could be. In previous work, our lab showed that the level of P^{287}-CaMKII increases over this lesion growth phase (*Unpublished; Worthington 2016*). This activated form of CaMKII has been well-established in the development of cardiovascular pathology [178, 180, 228].

The individual cell groups that compose the vascular wall of $ApoE^{-/-}$ mice were not investigated for their relative contribution to CaMKIIδ expression and potentially atherosclerosis. However, pilot data can be provided from the human cell culture studies. HCAECs, HUVECs and HCASMCs were cultured and analysed for CaMKIIδ by WB. Across cell groups, HCASMC had saturated CaMKIIδ expression compared with EC samples (**Figure 2.11**). This was not significant due to a low n-number and densitometry saturation, which is likely to be masking a more dynamic range. Regardless, these three experiments provided enough observational data that δ was the dominant CaMKII isoform in VSMCs.

While it was becoming increasingly evident that CaMKIIδ is the predominant isoform expressed and the most likely player in atherogenesis, it is important to reflect on the other major isoform present in the vasculature [225]. In our cell culture model gamma expression was observed in HCAECs, HUVECs and HCASMCs (**Figure 2.10**). For mouse arterial tissue, CaMKIIγ expression levels were low at 13-weeks, compared with the δ isoform levels, and expression remained low at 20-weeks (**Figure 2.9**). In contrast with CaMKIIδ, CaMKIIγ been shown to be protective against vascular disease [213, 221]. In VSMCs that make up majority of vascular wall, CaMKIIγ protects against vascular pathology by promoting the contractile phenotype. This is achieved via regulation of critical ion channels and the specific isoform localisation within the contractile machinery of VSMC [221-223]. In the context of an atherosclerotic model, it is therefore not unexpected that the level of CaMKIIγ is relatively low. As discussed previously, CaMKIIδ expression may increase earlier than any visible lesion growth. In turn, there may be a dramatic drop in gamma prior to the development of foam

cell lesions. If this is the case and there is an increase in the “pathological” delta isoform alongside a drop in the “protective” gamma isoform, then this would be a double edged sword in lesion development. The gamma isoform clearly warrants future investigation as a protective mechanism.

In summary, the results observed in this chapter showed that CaMKIIδ is the major isoform present in vascular tissue and a likely player in atherosclerosis. Furthermore, RT-PCR analysis at the transcript level revealed that between both mouse and human species CaMKIIδ 1, 2, 3 and 6 variants are present. Now it has been identified that human vascular cells and artery homogenates of ApoE$^{-/-}$ mice express the same splice variants, the investigation can continue in the ApoE$^{-/-}$ mouse that encompasses all the physiological/pathological variables of atherosclerosis. Also the similar expression profile across species is of interest in a translational aspect for drug target discovery. To advance our understanding of the contribution of CaMKIIδ in foam cell lesion development, an ApoE$^{-/-}$ model is required that has a genetic deletion of the δ isoform while maintaining the expression of the other three isoforms.

Chapter 3

Generation of a Novel Mouse Model to Investigate the Role of CaMKIIδ in Atherosclerosis.

Contents

3.1 Introduction

The calcium/calmodulin-dependent protein kinase II (CaMKII) family is comprised of four isoforms, α, β, δ and γ as well as associated splice variants [184, 185, 197]. The isoforms are differentially expressed in the tissues of the body. CaMKII carries out cellular signalling by phosphorylation of target proteins and has emerged a critical regulator of cell signalling in health and disease.

The CaMKIIα and β isoforms are predominantly expressed in the brain and nervous tissue [184]. Studies have shown these isoforms play critical roles in synaptic plasticity and neuro-physiological processes such as long term potentiation (LTP) [233-235]. In the cardiovascular system (CVS), the predominant isoforms expressed are the δ and γ type [197, 198]. Interestingly, the δ isoform has been associated with the development of cardiovascular pathology, whereas, γ has been shown to promote vascular health [181, 213].

CaMKIIδ has been shown to be important in the regulation of Ca^{2+} handling proteins as well as the regulation of inflammatory and survival pathways [175, 227]. CaMKIIδ has an important physiological role in mediating β-adrenergic stimulation. This is best exemplified in the heart where CaMKIIδ mediates β-adrenergic signalling by the phosphorylation of key Ca^{2+} handling proteins to improve contraction of the heart [175, 178]. However, prolonged activation of the kinase has emerged as driver of cellular dysfunction and cardiovascular pathology [195, 196]. Increasing evidence for CaMKIIδ would suggest the compounding pathological effects of the kinase in cardiovascular pathology outweigh any main physiological effect, which is a key consideration for drug discovery and development.

CaMKIIδ is expressed in ECs and VSMCs, which are the main cell types that compose the artery wall [185, 200]. Like the heart, CaMKIIδ has been associated with the development of cellular pathology. In ECs, CaMKIIδ promotes phenotypes of endothelial dysfunction by increasing permeability and expression of adhesion molecules e.g. VCAM-1 [212, 215, 218]. Furthermore, in VSMCs, CaMKIIδ promotes the synthetic phenotype by the stimulation of migration and proliferation pathways in a number of *in vivo* and *in vitro* approaches [181, 219, 220]. In contrast, the other cardiovascular isoform CaMKIIγ has been shown to oppose this

synthetic function by promoting contraction of VSMCs [181, 213]. This is through the regulation of specific ion channels and localisation around myosin filaments [221-223]. Collectively, this suggests CaMKIIδ promotes vascular pathology whereas, CaMKIIγ is protective.

Still, many of the studies that have investigated CaMKII in the vasculature lack detail about what specific isoform is being targeted so many of these functions remain incompletely understood. The effects of CaMKIIδ on EC and VSMC dysfunction are common mechanisms in the pathogenesis of atherosclerosis, however CaMKII signalling has not been investigated in a model of atherosclerosis. To further understand CaMKIIδ function in atherosclerosis, a specific genetic approach is required in a model of atherosclerosis such as the ApoE$^{-/-}$ mouse.

The ApoE$^{-/-}$ mouse is the gold standard model used for atherosclerosis research. This mouse model contains a knockout in the apolipoprotein E (ApoE) gene, essential for cholesterol metabolism and transport. ApoE$^{-/-}$ mice develop elevated plasma LDL-C levels and develop atherosclerotic lesions throughout the aortic tree [160]. The ApoE$^{-/-}$ mice generally develop atherosclerosis in the aortic sinus, aortic arch and brachiocephalic artery whereas, in humans, the disease tends to manifest in the coronary and carotid arteries [162, 165, 171]. What is important though is that between species the lesions develop with a similar phenotype and physiology to human [162, 172]. This includes intimal thickening, foam cell lesions, lipid deposits and later in the disease progression, a necrotic core and calcification.

Interestingly, male ApoE$^{-/-}$ mice are more resistant to the development of atherosclerosis than females. This sex difference is observed over a number of genetic backgrounds for ApoE models, including the C57/Bl6-ApoE$^{-/-}$ which is commonly used in our lab and others in the atherosclerosis research world [236-238]. For example, lesion content in the aortic sinus of female ApoE$^{-/-}$ mice on a C57/Bl6 background is more developed than males at 20-weeks age [239]. The mechanisms that promote this sex difference are not fully understood and many labs are investigating how the genetic component of ApoE gene may influence this. One thought, is that the anti-atherogenic particle HDL concentration is higher in males than females so protection may be conferred here [236]. Regardless of these differences in disease timeline, both male and female mice display atherosclerotic lesions with a similar physiology

to humans and remain a great model for investigating the pathogenesis of atherosclerosis [162, 172].

Previously, we have shown that a systemic inhibition of CaMKII in ApoE$^{-/-}$ mice leads to a significant reduction in foam cell lesion development in the brachiocephalic artery. While CaMKII clearly plays a role in lesion progression the isoform family is extensive. Furthermore, a global inhibition of CaMKII is not feasible as a clinical target with the physiological roles other isoforms play in the other systems of the body. For this reason, it is important that the critical subtype(s) of CaMKII which plays a role in atherosclerotic disease pathology is identified.

In Chapter 2, we saw that CaMKIIδ was the predominant isoform expressed in cell of the human and mouse vasculature. Furthermore, during the development of atherosclerosis CaMKIIδ expression was relatively high in contrast to CaMKIIγ, and levels persisted with disease progression. This suggests from an observational point, that it is the CaMKIIδ isoform most likely contributing to atherosclerosis, but to answer this, a mechanistic study is required where CaMKIIδ expression can be manipulated.

3.2 Approach

In order to investigate the specific role of CaMKIIδ in atherosclerosis, there needed to be a model that blocked CaMKIIδ expression while keeping the other isoforms α, β, and γ intact. For this work, a good mouse model would be a CaMKIIδ knockout (KO). However, in order to study CaMKIIδ function in the pathogenesis of atherosclerosis, this model had to be introduced into an ApoE$^{-/-}$ background. Therefore, the second aim of this PhD was to develop and characterise atherosclerosis in the double knockout (dKO) (ApoE$^{-/-}$CaMKIIδ$^{-/-}$) mouse.

3.2.1 Animal work

CaMKIIδ$^{-/-}$ mice were generated as previously described [240] by the Joan Heller-Brown lab and donated for the following experiment. Initially, ApoE$^{-/-}$CaMKIIδ$^{+/+}$ and ApoE$^{+/+}$CaMKIIδ$^{-/-}$ mice were bred to give rise to a litter heterozygous for ApoE and CaMKIIδ (F2). Following this, breeding pairs of mice with an ApoE$^{-/-}$CaMKIIδ$^{+/-}$ genotype were selected for and bred as the F3 generation (**Figure 3.1**). Tail tips from the litters of the F3 breeding pairs were used for RT-PCR to confirm genotype. Twelve ApoE$^{-/-}$ CaMKIIδ$^{+/+}$ (control) and ApoE$^{-/-}$CaMKIIδ$^{-/-}$ (dKO) male and female mice (total n = 48) were housed until 20-week of age at the Hercus Taieri Research Unit (HTRU), under a 12:12 hr lighting schedule with *ad libitum* access to food and water. Twelve male and female mice per group were selected for the sample size as this is the number previously used in our lab to determine significant differences. This experiment was approved by the Otago Animal Ethics and Welfare Committee (AEC # 17/02 & 19/172).

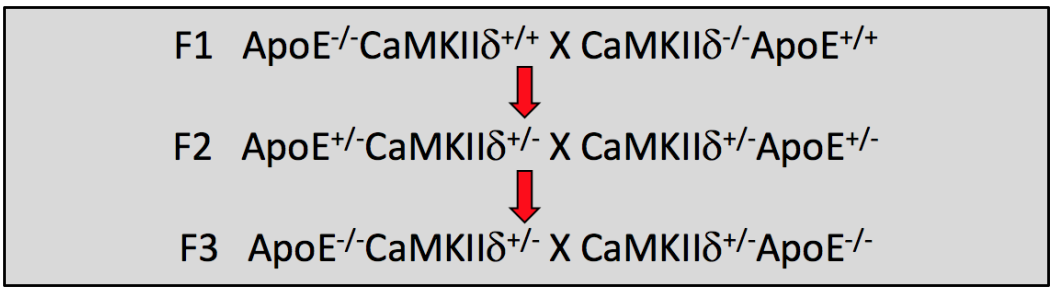

Figure 3.1: Summary of breeding generations to develop the ApoE$^{-/-}$CaMKIIδ$^{-/-}$.

3.2.1.1 DNA extraction and genotyping

The tail tips from litters of ApoE$^{-/-}$CaMKII$\delta^{+/-}$ (heterozygous) mice were put in a microcentrifuge tube with 200 µL DNA extraction buffer (100 mM Tris, 5 mM EDTA, 200 mM NaCl, 0.2% SDS, 100 µg/ml proteinase K, pH 8.5). The tubes were incubated at 55°C for 2 hr and then 98°C for 15 min. The samples were stored at 4°C until RT-PCR.

0.5 µL of DNA extract from tail tips was used for RT-PCR using the KAPA HiFi HotStart ReadyMix. The reaction components are described in **Table 3.1**. A list of primers used for ApoE$^{-/-}$, CaMKIIδ wild-type (*wt*) and KO genes are provided in **Table 3.2**. PCR amplification was performed in a thermal supercycler (Kyratec). A no template control (NTC) was performed for each RT-PCR experiment, where the DNA sample from the tip is replaced with ready mix. This was to control for any contaminant DNA that might be present in the other components of the PCR reaction mix.

Table 3.1 PCR mastermix reaction.

Reagent	**Volume/reaction (µL)**
KAPA HiFi HotStart ReadyMix (KAPA Biosystems, cat.no. KRO370)	12.5
Forward primer	0.75
Reverse primer	0.75
DEPC-treated H_2O	10.5 (9.75 for ApoE$^{-/-}$ reaction as has 3 primers)
DNA	0.5

Table 3.2 Primer sequences and cycling conditions for genotyping.

Primer		Sequence	Cycling	Target Size
ApoE	180	5'-GCCTAGCCGAGGGAGAGCCG-3'	98°C (10 sec) 68°C (15 sec) 72°C (20 sec) X35	Wt allele 180 & 181 = 155 bp Mutant allele 180 &182 = 245 bp [241]
	181	5'-TGTGACTTGGGAGCTCTGCAGC-3'		
	182	5'-GCCGCCCCGACTGCATCT-3'		
CaMKIIδ *wt*	F	5'-GGAGCATTTCATCTGTAGGTG-3'	98°C (10 sec) 62°C (20 sec) 72°C (30 sec) X40	220 bp [240]
	R	5'-CAGATGTGCCTGACCAATATG-3'		
CaMKIIδ KO	F	5'-AATGGGCTGACCGCTTCCTCGT-3'	96°C (20 sec) 70°C (20 sec) 68°C (20 sec) 72°C (60 sec) X35	350 bp [240]
	R	5'-CGATCAAGCTGAACAGCTGC-3'		

Following RT-PCR, reaction products were mixed with BlueJuice™ Gel Loading Buffer (10X) (ThermoFisher, cat.no. S33102) and run alongside the NTC on 1.5% agarose gels for 60 min, as previously described in *Section 2.2.3.* The size of each amplified product was confirmed by comparing with a 100 kb DNA marker (Thermofisher, cat.no. 15628050) that was electrophoresed in parallel with samples. Agarose gels were placed in the PXi 4 Touch Multi-Application Gel Imaging System (Syngene, PXi 4 Touch) and images digitally captured.

3.2.1.2 Dissection of the aortic sinus

At 20-weeks of age ApoE$^{-/-}$ (control) and ApoE$^{-/-}$CaMKIIδ$^{-/-}$ (double knock-out (dKO)) mice were euthanised by carbon dioxide (CO_2) overdose and death was confirmed by pedal withdrawal reflex. The mouse was weighed and set on a dissection board with chest and stomach exposed. Each mouse was then perfused with 30 mL heparinised PBS (40 U/mL) via the apex of the heart, as previously described in *Section 3.2.2*. The perfusion solution was then changed to 4% paraformaldehyde (PFA) and the aortic tree was perfused for a further 10 min.

To isolate the aortic sinus, the heart was cut in a transverse plane below the level of the left and right atria. The heart was then trimmed around the ventricular outflow tract and atria to

identify the aortic sinus (**Figure 3.2**). The aortic sinus was returned to 4% PFA for 48 hr for further fixation and then stored in 70% ethanol.

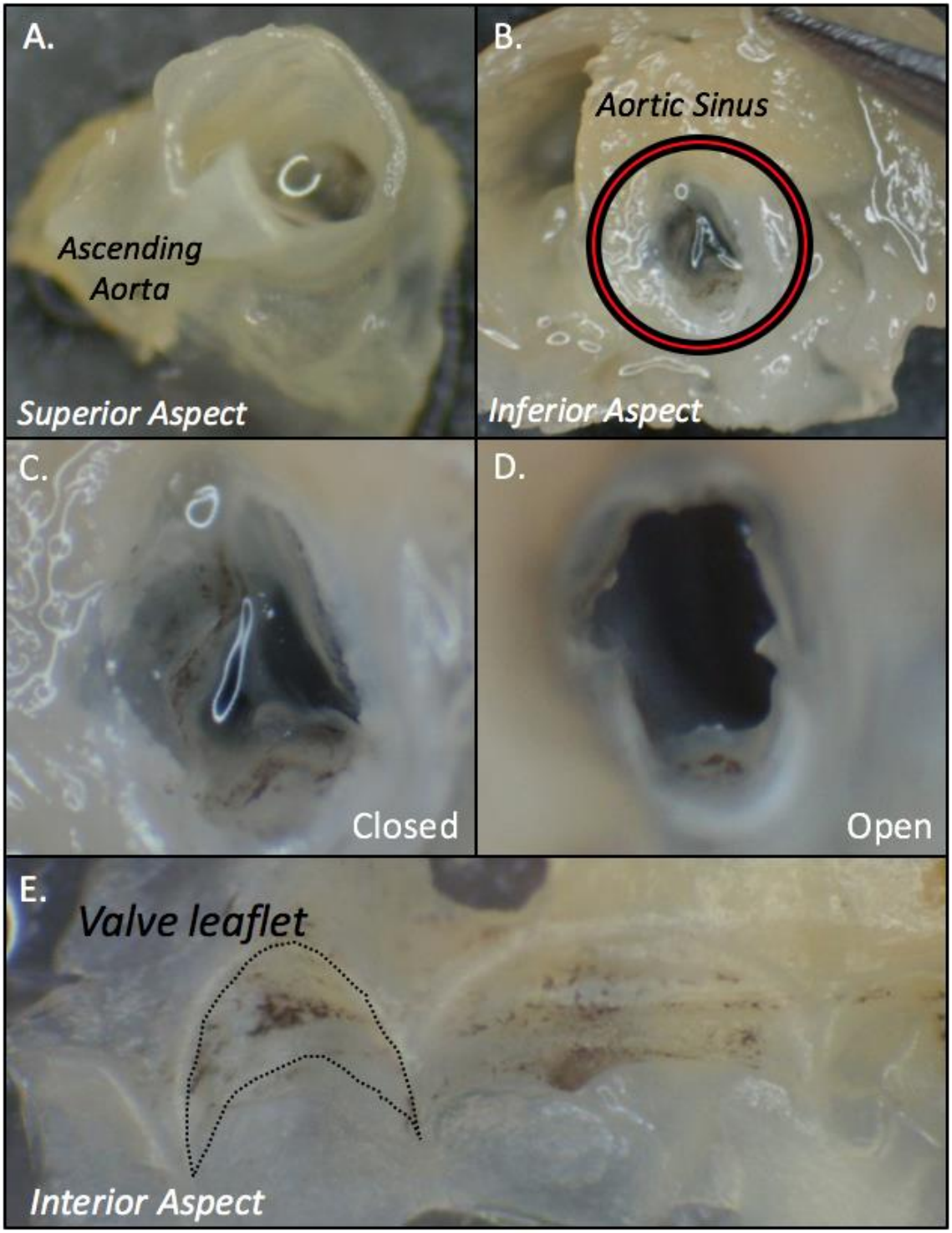

Figure 3.2: Anatomy of the aortic sinus. *Mice were perfusion fixed with 4% PFA and the heart dissected. The heart was cut in a transverse plane below the level of the atria and trimmed to isolate the aortic sinus. Views of the aortic sinus from a superior and inferior aspect* ***(A-B)****. The red ring highlights the aortic sinus which is zoomed in on* ***C-D*** *indicating the closed and open position of valve leaflets. Aortic sinus was cut longitudinally and pinned flat to observe the valve leaflets.*

3.2.1.3 Total cholesterol ELISA

To investigate total cholesterol levels in both control and dKO mouse groups, an ELISA was performed using the HDL and LDL/VLDL Cholesterol Assay Kit (Abcam, cat.no.65390). Firstly, a set of cholesterol standards were diluted to a total volume of 50 µL using cholesterol assay buffer. The standards ranged from 0 to 5 µg/50 µL by intervals of 1 µg. Secondly, 2 µL of serum was diluted 1:25 by mixing with 48 µL cholesterol assay buffer. 50 µL of standards and samples were added to a 98 well plate in triplicate. 50 µL of the reaction mix, described in **Table 3.3**, was added to standards and samples before being incubated at 37°C for 1 hr.

Table 3.3 Cholesterol reaction mix.

Component	**Total cholesterol reaction mix (µL)**
Cholesterol assay buffer	4
Cholesterol probe	2
Enzyme mix	2
Cholesterol esterase	2

Post-incubation, the plate was removed from the incubator and output was measured on a microplate reader at optical density (OD) 570 nm. The mean absorbance (A_{570}) value was calculated between triplicates for standards and samples. Using GraphPad Prism 8, absorbance values for standards were plotted against concentration (**Figure 3.3**). A line of best fit (y = mx + c) was generated from the data points and used to calculate cholesterol in serum samples. The value was then multiplied by the initial dilution factor to calculate serum cholesterol concentration in µg/mL.

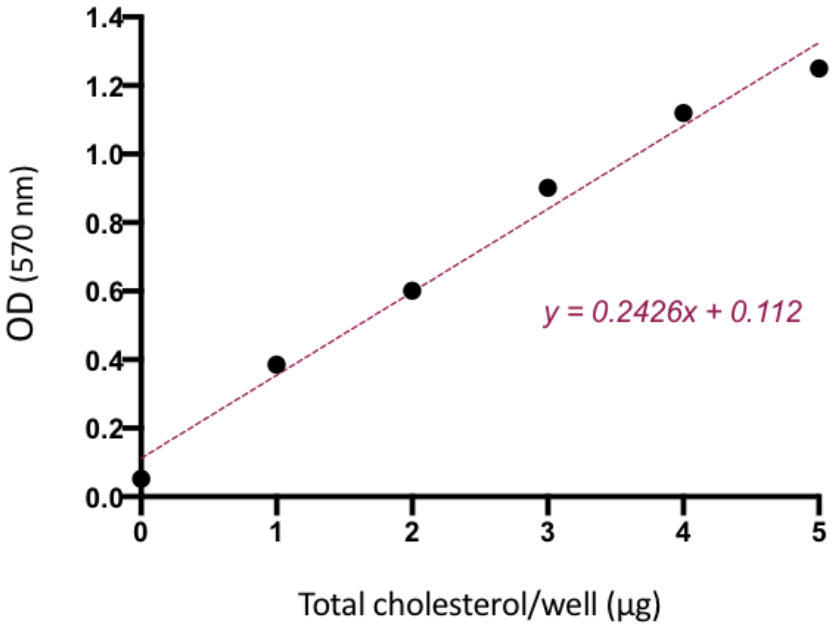

Figure 3.3: Example standard curve for total cholesterol. *Six cholesterol standards were diluted ranging from a concentration of 0 to 5 µg in 50 µL assay buffer. The cholesterol standards were added to a 98-well plate in triplicate. 50 µL of the cholesterol reaction mix was added to each standard well and the plate was incubated at 37°C for 1 hr. Optical density (OD) was measured at 570 nm. Mean absorbance values were calculated and plotted against cholesterol using GraphPad Prism 8. A line of best fit equation was generated.*

3.2.2 Histology

3.2.2.1 Tissue processing and embedding

The aortic sinus was removed from 70% ethanol and placed in a histological cassette for tissue processing. This process dehydrates the tissue through a series of wash steps from ethanol to xylene and finally, paraffin wax, as shown in **Table 3.4.**

Table 3.4 Short tissue processing cycle.

Stage	Solvent	Time (min)
1.	70% ethanol	15
2.	900% ethanol	15
3.	100% ethanol	105
4.	Xylene	85
5.	Paraffin wax	105

Post-tissue processing, the cassettes were transferred to a tray of paraffin wax at 60°C for 1 hr. This was to allow the wax to melt around the tissue so the aortic sinus could be manipulated for embedding. The aortic sinus was placed in a block tray flat against the transverse plane it was cut on during dissection. For further confirmation, the lumen of the ascending aorta was visible and pointed directly upwards. Each block mould was filled to the top with additional paraffin wax and placed on a cold plate for 1 hr to set.

3.2.2.2 Tissue Sectioning

The Paraffin blocks containing aortic sinus tissue were pre-cooled in the fridge to harden wax prior to sectioning. Each block was clamped into the microtome and the cutting dial adjusted to 20 µm. The block was trimmed until at least two valve leaflets of the aortic sinus were present in the section with the aid of a light microscope (**Figure 3.4A**). Once this region was located, the cutting dial was adjusted to 5 µm. A section was collected and transferred to 30% ethanol to reduce surface tension and prevent folding. The section was transferred to a 37°C water bath to melt surrounding wax. A microscope slide with a poly-lysine coat was used to collect and adhere the section and placed on a heating rack. Four more sections were collected at 100 µm intervals throughout the aortic sinus as shown in **Figure 3.4**. Slides containing sections were baked at 60°C for 1 hr and stored for staining and lesion analysis.

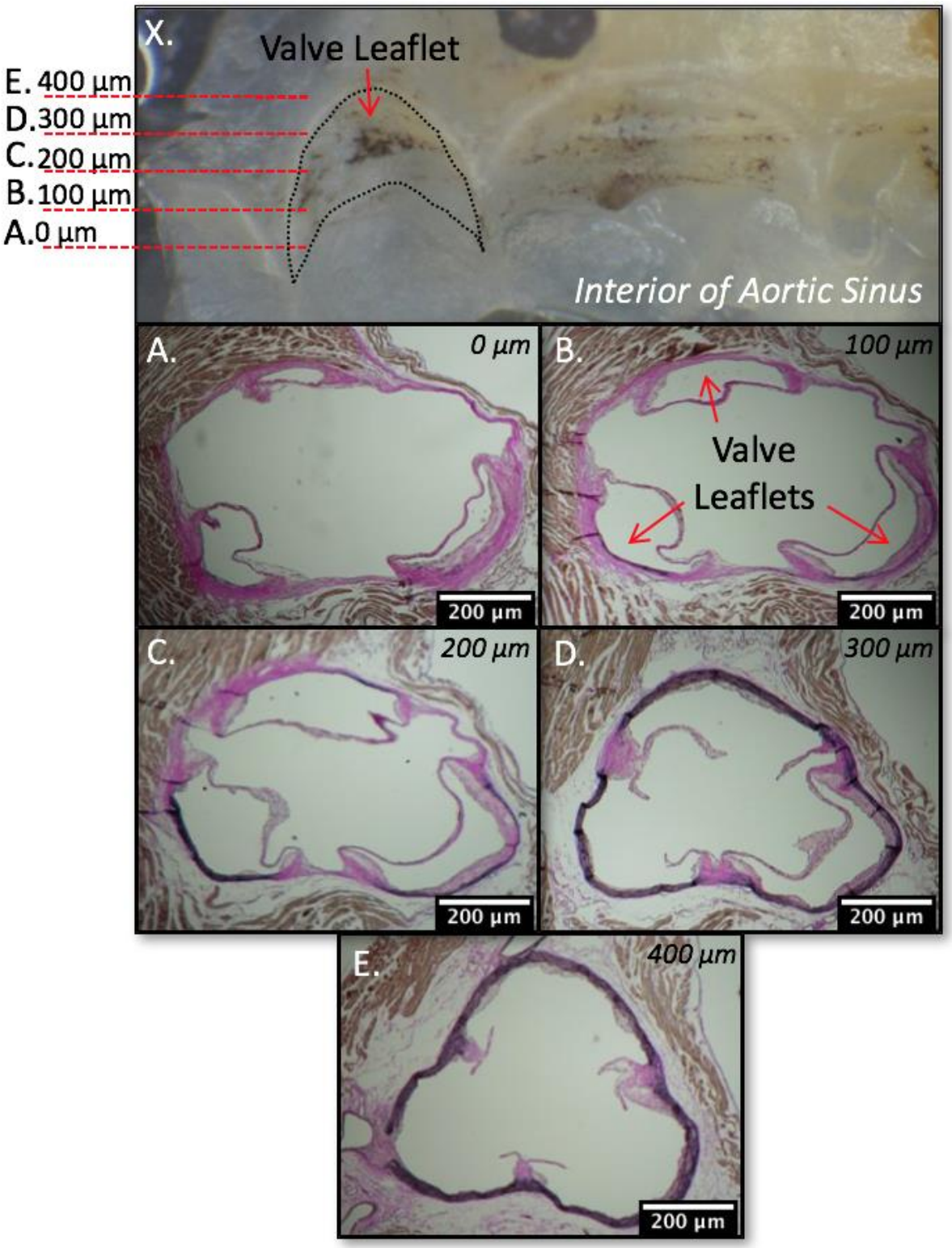

Figure 3.4: Sectioning of the aortic sinus in a representative ApoE$^{-/-}$ mouse. *The aortic sinus was cut along the longitudinal plane and pinned flat **(X.)**. Indicated by the black trace is one of three valve leaflets. Red dotted lines provide each target location along the aortic sinus for sectioning. At the appearance of the first two valve leaflets a 5 µm section was collected **(A.)**. Four more sections were collected at 100 µm intervals throughout the aortic sinus **(B-E)**. Sections stained with Verhoeff van Gieson. Histology images taken with a light microscope.*

3.2.2.3 Verhoeff van Gieson stain

The Verhoeff van Gieson staining method is useful in identifying major components of the vascular wall [242]. In particular, this approach is useful in identifying elastin fibres, vascular smooth muscle cells and extracellular matrix (ECM). Prior to staining, each slide was rehydrated through a series of washes from xylene to alcohol and then water, as shown in **Figure 3.5**.

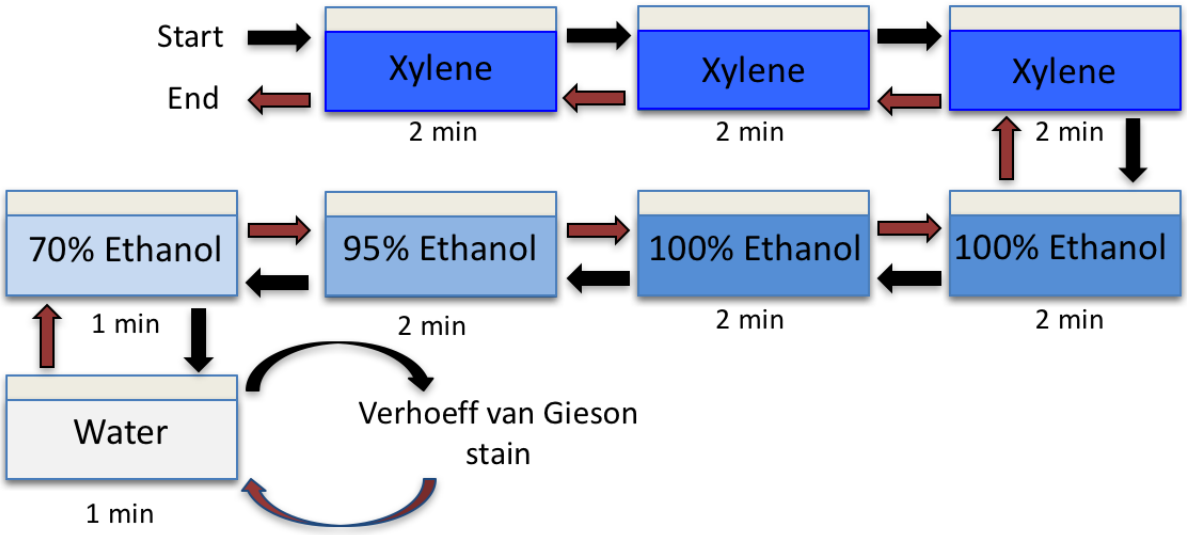

Figure 3.5 Rehydration and dehydration of aortic sinus sections. *Prior to staining, slides containing aortic sinus sections were run through a series of washes from xylene, through a reducing concentration of ethanol to water. Once sections were at this point they were stained with Verhoeff van Gieson stain. Post-staining, slides were dehydrated in the opposite manner and cover-slipped. Original, Worthington (2017).*

Components for the Verhoeff van Gieson staining method are described in **Table 3.5**. Slides were submerged in Verhoeff's haematoxylin solution for 20 min to saturate the tissue section. The slide rack was then drained, washed under tap water and placed in distilled water. Individually, each slide was carefully submerged in 2% ferric chloride from 45-60 sec to strip the Verhoeff's haematoxylin so the stain is only retained in the elastin fibres. The slides were washed in distilled water and rinsed in 95% alcohol. The slide rack was then dipped in Van Gieson solution for 30 sec. Slides were then dehydrated back to xylene, in the reverse order of rehydration method and cover-slipped (**Figure 3.5**).

Table 3.5 Components of the Verhoeff van Gieson staining method.

Solution	Components	Volume (ml)
Verhoeff's haematoxylin working solution	Alcoholic haematoxylin (5%)	125
	Ferric chloride (10%)	50
	Lugols iodine	50
Van Gieson	Saturated aqueous picric acid	500
	Acid fuschin (1%)	90
	Distilled water	500
2% Ferric chloride	Ferric chloride (10%)	100
	Distilled water	400

3.2.2.4 Lesion area and volume analysis

Lesion area was measured in five points along the aortic sinus of ApoE$^{-/-}$ and ApoE$^{-/-}$CaMKII$\delta^{-/-}$ as described in *Section 3.2.2.2*. This is an effective method of analysis as it provides detail on the distribution of lesion growth in the aortic sinus as well as total lesion content.

Images were captured digitally using a Motic® Microscope (BA130 Motic Inc. LTD) at 20X magnification so the whole aortic sinus was in the field of view. Digital images were analysed using Image J (imagej.nih.govt/ij/download/2016). Using the free hand trace tool, one area was drawn around the internal boundary of the internal elastic lamina (A) (stained black from VVG). A second area was then drawn within the lumen area (B). Foam cell lesion area was calculated by the difference in these two areas as shown in **Equation 3.1**.

Equation 3 1: Calculating foam cell lesion area.

Foam cell lesion area = A – B

Foam cell lesion area measurements were calculated on GraphPad Prism 8 and expressed as mean $\pm$ SEM for each group along each point (100 µM intervals) along the aortic sinus. The area under the curve was measured for each group to calculate foam cell lesion volume in the aortic sinus. Foam cell lesion volume measurements were graphed as mean volume $\pm$ SEM.

3.2.3 Statistics

All data was analysed on Graphpad Prism 8 and expressed as mean ± SEM. Significant differences were determined by Students unpaired t-test. For body weight and total cholesterol of the $ApoE^{-/-}CaMKII^{-/-}$ significant differences were determined using a two-way ANOVA with Tukey's multiple comparisons post-hoc test.

3.3 Results

3.3.1 Development of a new ApoE$^{-/-}$CaMKII$\delta^{-/-}$ mouse model.

To identify the impact of CaMKIIδ on the pathogenesis of atherosclerosis, ApoE$^{-/-}$ mice were crossed over a series of breeding pairs to generate the ApoE$^{-/-}$CaMKII$\delta^{-/-}$ mouse model as described in *Section 3.2.1*. DNA was extracted from the tail tips of each litter of the F3 breeding pairs and used in RT-PCR targeting ApoE, CaMKIIδ *wt* allele and CaMKIIδ mutant (KO) allele. Products of PCR were electrophoresed on a 1.5% agarose gel for an hour and digital images were captured using the Syngene PXi 4 touch.

Shown in **Figure 3.6**, an example experiment confirming the genotypes of eight mice from a new litter. In gel A targeting ApoE, if the *wt* allele is present the primer pairs 180-181 yield product of 155 bp in the PCR reaction [241]. Furthermore, if the mutant allele (KO) is present primer pairs 180-182 yield a product size of 245 bp [241]. In the case of the CaMKIIδ gene, the presence of *wt* and mutant (KO) alleles is indicated by product sizes of 220 bp and 350 bp, respectively [240].

After confirmation of genotype, ApoE$^{-/-}$CaMKII$\delta^{+/+}$ (control) and ApoE$^{-/-}$CaMKII$\delta^{-/-}$ (dKO) mice were housed in HTRU until 20 weeks of age. What was evident in some of the litters with a dKO phenotype was the appearance of ataxic behaviour. This included head nodding and an inconsistent gait. These were only moderate signs of ataxia and did not significantly affect animal welfare and these mice were used for experiments.

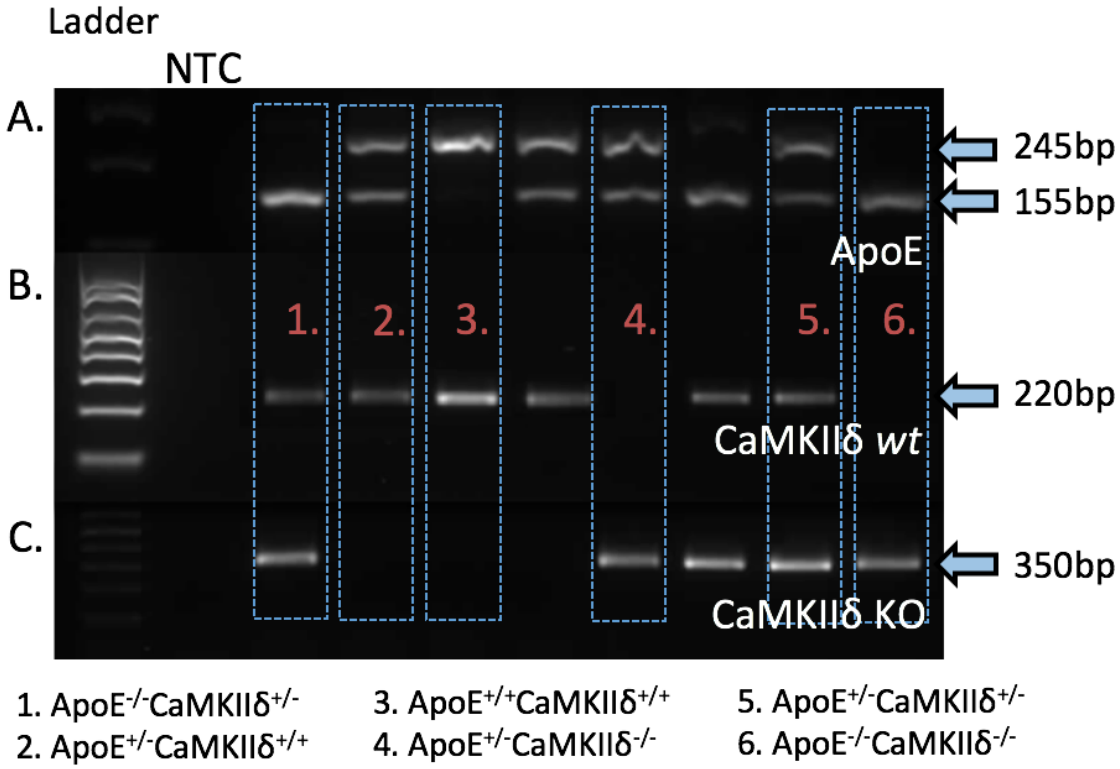

Figure 3.6: Genotyping experiment example. *DNA was extracted and RT-PCR was carried out targeting ApoE and CaMKIIδ genes. Products of PCR were loaded onto a 1.5% agarose gel alongside a no template control (NTC) and electrophoresis applied at 100 V for 60 min. Digital images were captured using the Syngene PXi 4 touch. PCR products of 155 bp and 245 bp indicated the ApoE wt allele and the ApoE mutant (KO) allele (**A**). The presence of the CaMKII wt and KO alleles is indicated by product sizes of 220 bp and 350 bp, respectively (**B-C**). 100 bp DNA marker (Invitrogen, cat.no. 15628019). Representative gels show eight animals targeted in three independent PCR reactions.*

To further validate this novel model for the upcoming experiments it was important to determine any differences in body weight and total cholesterol between control and dKO mice. Cholesterol is the major risk factor for atherosclerosis [14, 16] so it was important to identify whether knocking out CaMKIIδ had any effect on lipid transport and metabolism. At 20-weeks of age, male and female control and dKO mice were euthanised by CO_2 overdose. Mice were weighed and a blood sample was collected via cardiac puncture. The serum was extracted from the blood and total cholesterol analysed by ELISA, as described in *Section 3.2.1.3.*

There were no differences shown in body weight between ApoE$^{-/-}$ (control) and ApoE$^{-/-}$ CaMKII$\delta^{-/-}$ (dKO) mice in both males ($p = 0.17$, $n = 8$), and females ($p = 0.57$, $n = 8$) (**Figure 3.7)**. No differences were observed in total cholesterol between control and dKO mice in males ($p = 0.98$, $n = 8$) and females ($p = 0.99$, $n = 0.99$) (**Figure 3.8**). Furthermore, no differences were shown between male and female control mice ($p = 0.64$, $n = 8$), as well as any other comparison between groups.

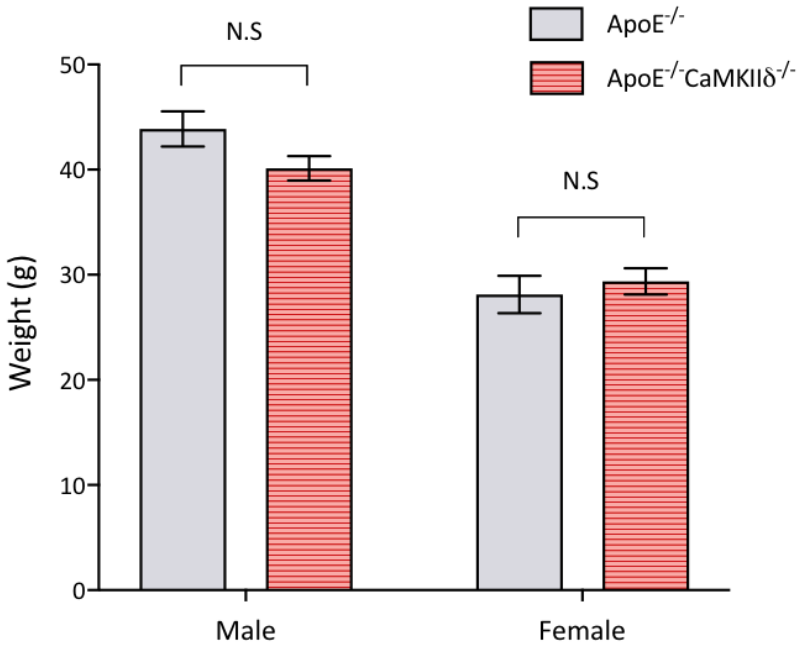

Figure 3.7: Body weight at 20-weeks age in male and female ApoE$^{-/-}$ and CaMKII$\delta^{-/-}$ mice. *At 20-weeks age ApoE$^{-/-}$ (control) and ApoE$^{-/-}$CaMKII$\delta^{-/-}$ mice were euthanised and weighed. Weights were analysed on GraphPad Prism 8. Non-significant (N.S) as determined by two-way ANOVA with Tukey's multiple comparisons post-hoc test (n = 8).*

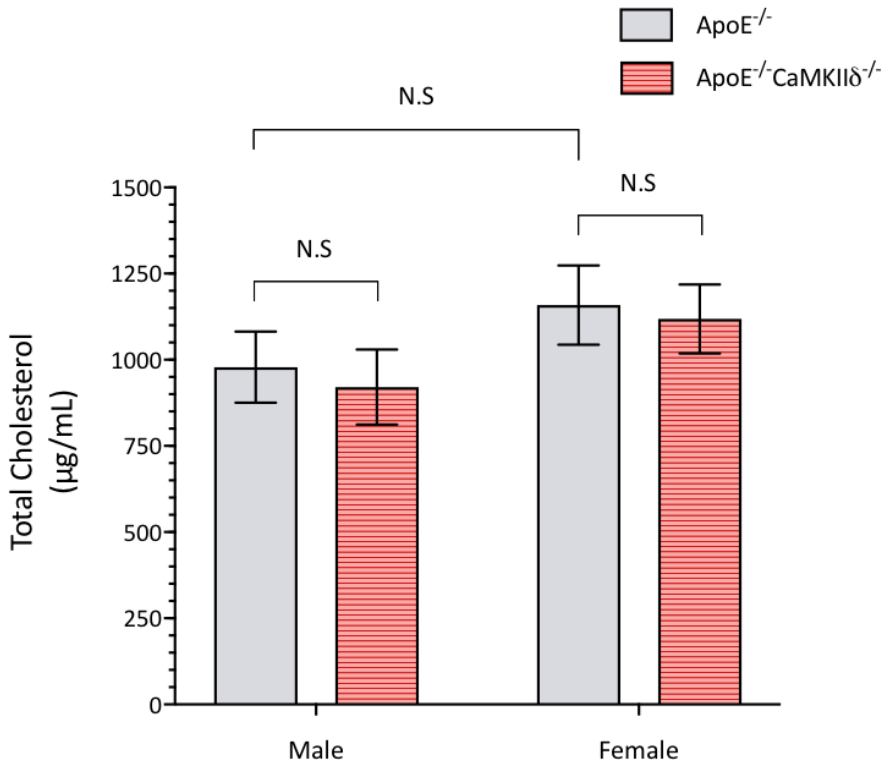

Figure 3.8: Total cholesterol at 20-weeks age in male and female ApoE$^{-/-}$ and CaMKII$\delta^{-/-}$ mice. *At 20-weeks age ApoE$^{-/-}$ (control) and ApoE$^{-/-}$CaMKII$\delta^{-/-}$ mice were euthanised and blood samples collected by cardiac puncture. Serum was extracted from blood and total cholesterol measured using the HDL and LDL/VLDL Cholesterol Assay Kit (Abcam, cat.no.65390) as detailed in Section 3.2.1.3. Total cholesterol values were analysed on GraphPad Prism 8. Non-significant as determined by two-way ANOVA with Tukey's multiple comparisons post-hoc test (n = 8).*

3.3.2 Genetic knockdown of CaMKIIδ has no effect on aortic sinus lesion size in 20-week male ApoE mice.

What was immediately striking was the difference in atherosclerosis content between male and female groups. By examination under a light microscope it was clear that both female groups contained more atherosclerosis than counterpart male groups. In the male control and dKO groups, the aortic tree, which included the aortic arch, brachiocephalic artery, left carotid and left subclavian artery, was relatively translucent in appearance. In contrast, the aortic tree from female control and dKO groups contained large opaque regions, indicative of foam cell lesions. These lesions were primarily observed around bifurcating areas of the aortic tree.

The aortic sinus of male control (ApoE$^{-/-}$CaMKII$\delta^{+/+}$) and dKO (ApoE$^{-/-}$CaMKII$\delta^{-/-}$) mice was sectioned and stained with VVG for lesion analysis (*Section 3.2.2*). Male control and double KO mice both displayed areas of intimal thickening and very small areas of foam cell lesion growth on the arterial wall within the aortic sinus valve leaflets (**Figure 3.9-10**). Furthermore, these early lesions were present at the base of the aortic sinus (0μm) and persisted through the aortic sinus trunk toward the aorta (400μm). After the area under the curve was calculated, there were no significant differences in aortic sinus lesion volume in double KO (90 $\pm$ 13 μm^3) vs control mice (126 $\pm$ 30 μm^3) (p = 0.20, Students unpaired T-test, n = 9 ApoE$^{-/-}$ CaMKII$\delta^{+/+}$, 11 ApoE$^{-/-}$CaMKII$\delta^{-/-}$) (**Figure 3.11**). This indicates that in males atherosclerosis is too early in its progression to clearly identify if CaMKIIδ is having an effect.

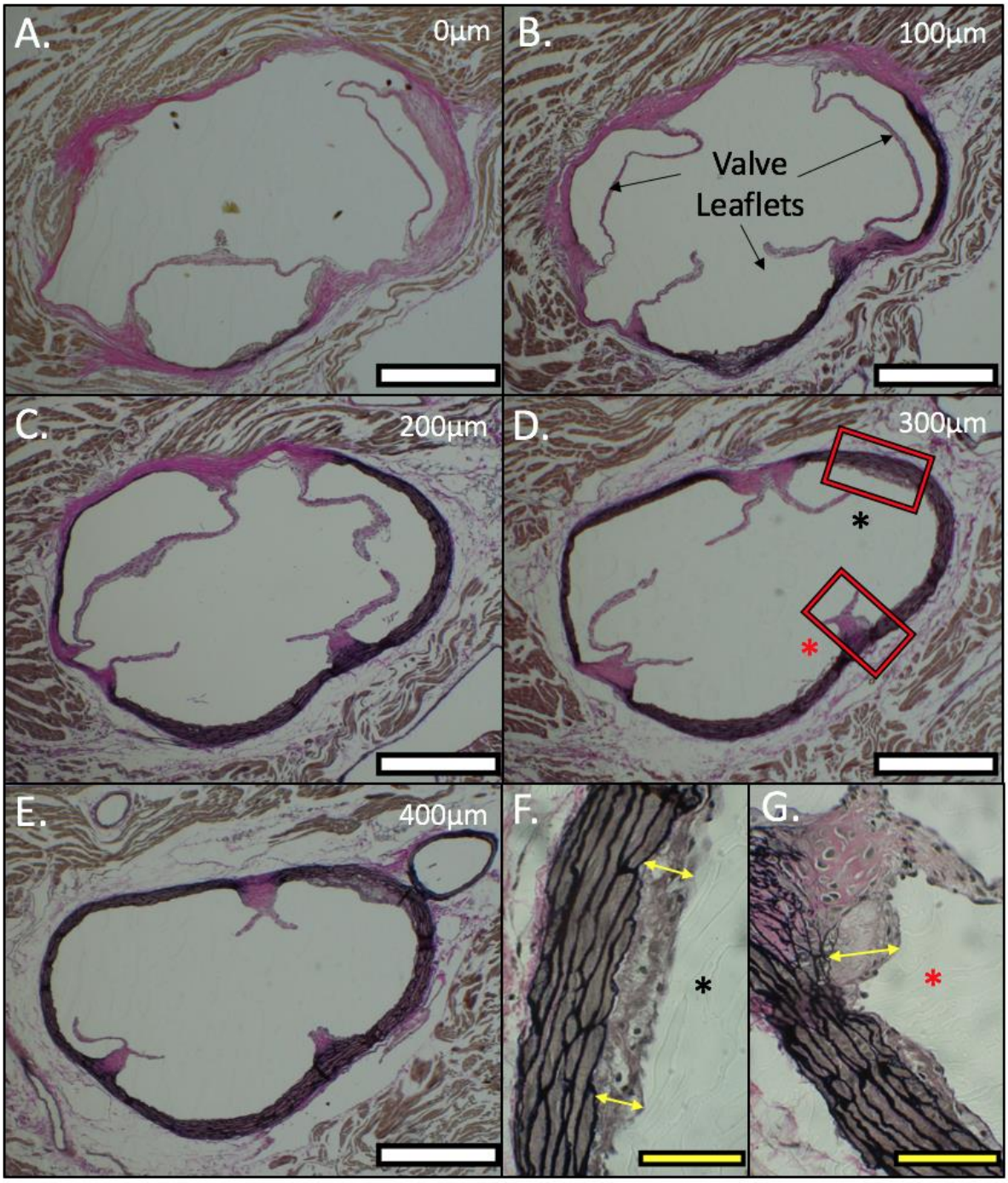

Figure 3.9: Foam cell lesions in the aortic sinus of 20-week male control (ApoE$^{-/-}$CaMKII$^{+/+}$) mice. *Male control mice were housed until 20 weeks of age. Mice were perfusion fixed with 4% PFA and the heart dissected. The heart was cut in a transverse plane below the level of the atria and embedded in paraffin wax. Shown above is a representative aortic sinus from a 20-week control male. A 5 µm section was collected at the appearance of the first two valve leaflets **(A)** and 4 more collected at 100 µm intervals throughout the aortic sinus **(B-E)**. Each section was stained with Verhoeff van Gieson and photos captured with a light microscope. The red boxes indicated by black and red asterisks correlate to zoomed in image of the vessel wall shown in **F-G**. Yellow double arrow indicated foam cell lesion growth on vessel wall. White scale bar = 200 µm, yellow scale bar = 40 µm.*

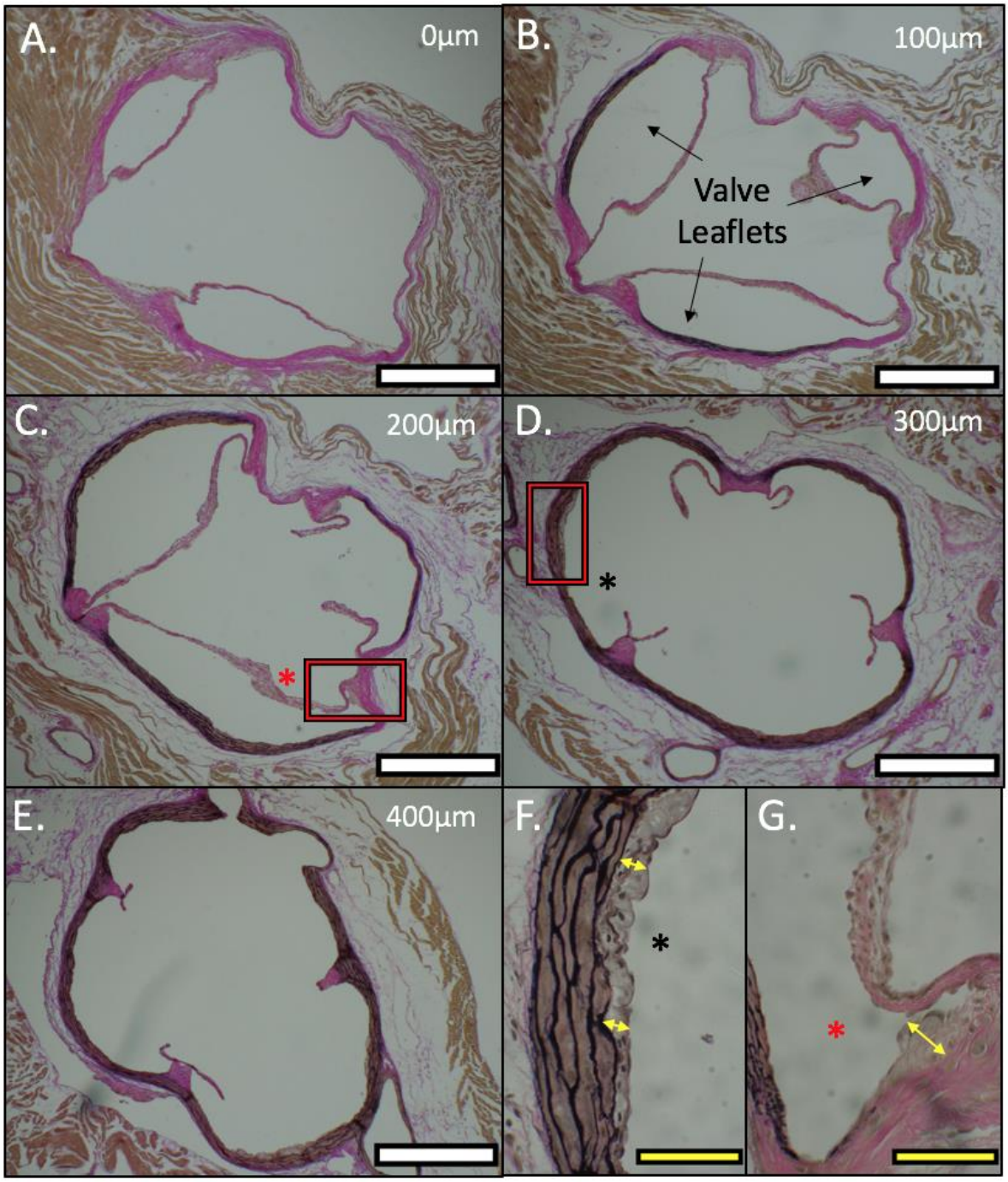

Figure 3.10: Foam cell lesions in the aortic sinus of 20-week male dKO (ApoE$^{-/-}$CaMKII$^{-/-}$) mice. *Male dKO mice were housed until 20 weeks of age. Mice were perfusion fixed with 4% PFA and the heart dissected. The heart was cut in a transverse plane below the level of the atria and embedded in paraffin wax. Shown above is a representative aortic sinus from a 20-week dKO male. A 5 µm section was collected at the appearance of the first two valve leaflets **(A)** and 4 more collected at 100 µm intervals throughout the aortic sinus **(B-E)**. Each section was stained with Verhoeff van Gieson and photos captured with a light microscope. The red boxes indicated by black and red asterisks correlate to zoomed in image of the vessel wall shown in **F-G**. Yellow double arrow indicated foam cell lesion growth on vessel wall. White scale bar = 200 µm, yellow scale bar = 40 µm.*

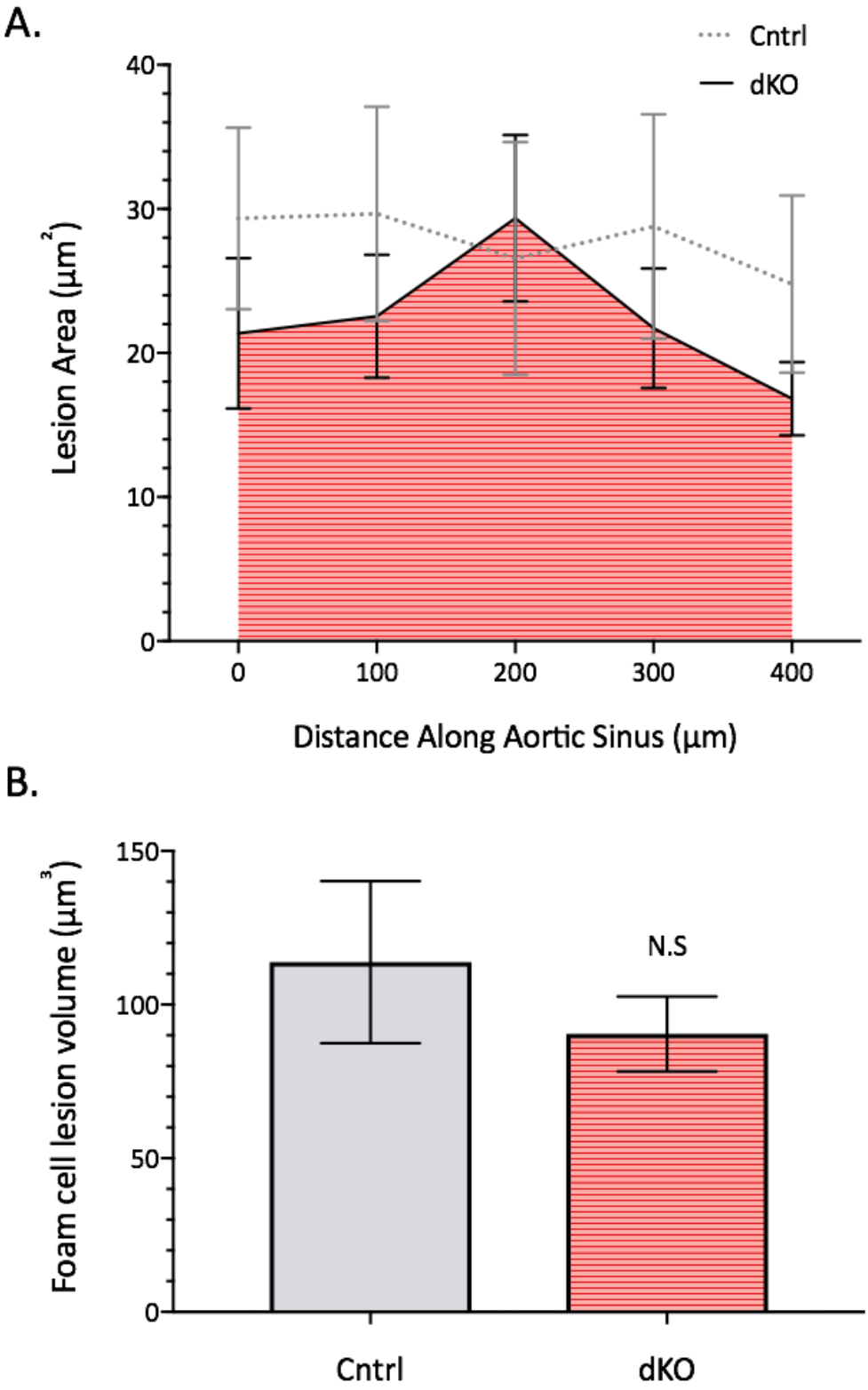

Figure 3.11: Foam cell lesion quantification in the aortic sinus of 20-week male control (ApoE$^{-/-}$ CaMKII$^{+/+}$) and dKO (ApoE$^{-/-}$CaMKII$^{-/-}$) mice. *A section was collected every 100 µm throughout the aortic sinus of each mouse and stained with Verhoeff van Gieson. Lesion area was calculated for each section along the aortic sinus (A). The area under the curve was calculated to generate foam cell lesion volume (B). Graphs show mean foam cell lesion area/volume as mean ±S.E.M. Not significant (N.S) as determined by unpaired Students t-test (n = 9-11).*

3.3.3 Genetic knockdown of CaMKIIδ reduces aortic sinus lesion size in 20-week female ApoE mice.

Genetic knockdown of CaMKIIδ had no significant effect on lesion size in the aortic sinus of male ApoE mice. However, it is known that on the C57/Bl6 background that male lesions progress slowly and in both control and dKO groups, there were only small pockets of foam lesion growth. It was next investigated whether CaMKIIδ promotes foam cell lesion growth in the aortic sinus of female ApoE$^{-/-}$ mice using the same approach described for males. The aortic sinus of female control (ApoE$^{-/-}$CaMKIIδ$^{+/+}$) and dKO (ApoE$^{-/-}$CaMKIIδ$^{-/-}$) mice was sectioned and stained for lesion analysis.

As expected for this model, female mice showed more atherosclerosis at 20-weeks of age compared to males. In the control (ApoE$^{-/-}$CaMKIIδ$^{+/+}$) group, some mice presented with large foam cell lesions that extended the length of each valve leaflet and was also present throughout the whole trunk of the aortic sinus (**Figure 3.12**). The dKO (ApoE$^{-/-}$CaMKIIδ$^{-/-}$) mice had lesions present throughout the trunk of the aortic sinus however they were sporadic and did not extend the full length of the valve leaflets (**Figure 3.13**). Foam cell lesion volume in control and dKO groups was 357 $\pm$ 55 μm^3 and 195 $\pm$ 24 μm^3, respectively (**Figure 3.14**). When compared, there was a significant decrease in lesion content in dKO group of 162 μm^3 ($P<0.05$, Students unpaired t-test, n=11 cntrl, 9 dKO).

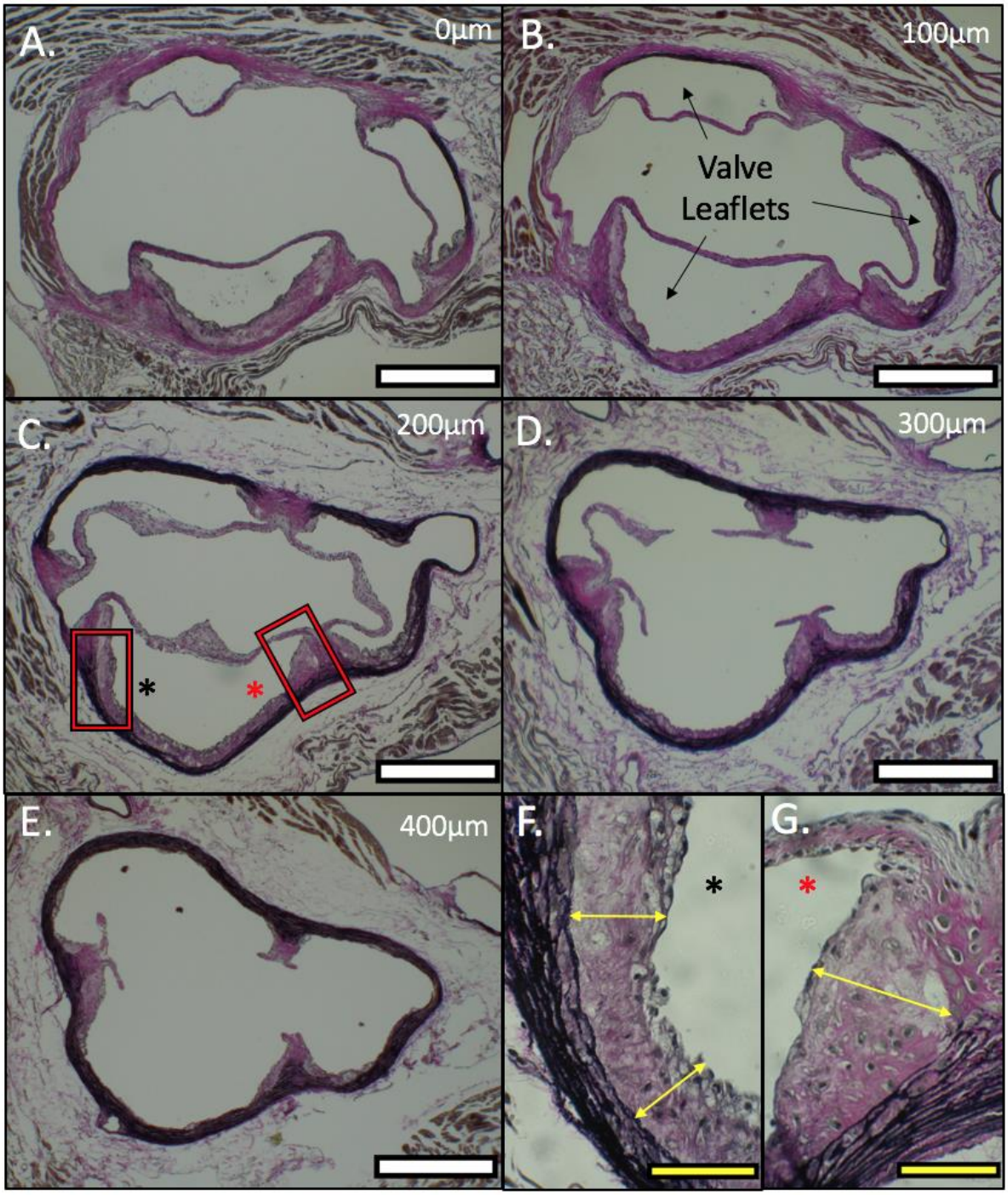

Figure 3.12: Foam cell lesions in the aortic sinus of 20-week female control (ApoE$^{-/-}$CaMKII$^{+/+}$) mice. *Female control mice were housed until 20 weeks of age. Mice were perfusion fixed with 4% PFA and the heart dissected. The heart was cut in a transverse plane below the level of the atria and embedded in paraffin wax. Shown above is a representative aortic sinus from a 20-week control female. A 5 µm section was collected at the appearance of the first two valve leaflets* ***(A)*** *and 4 more collected at 100 µm intervals throughout the aortic sinus* ***(B-E)****. Each section was stained with Verhoeff van Gieson and photos captured with a light microscope. The red boxes indicated by black and red asterisks correlate to zoomed in image of the vessel wall shown in* ***F-G****. Yellow double arrow indicated foam cell lesion growth on vessel wall. White scale bar = 200 µm, yellow scale bar = 40 µm.*

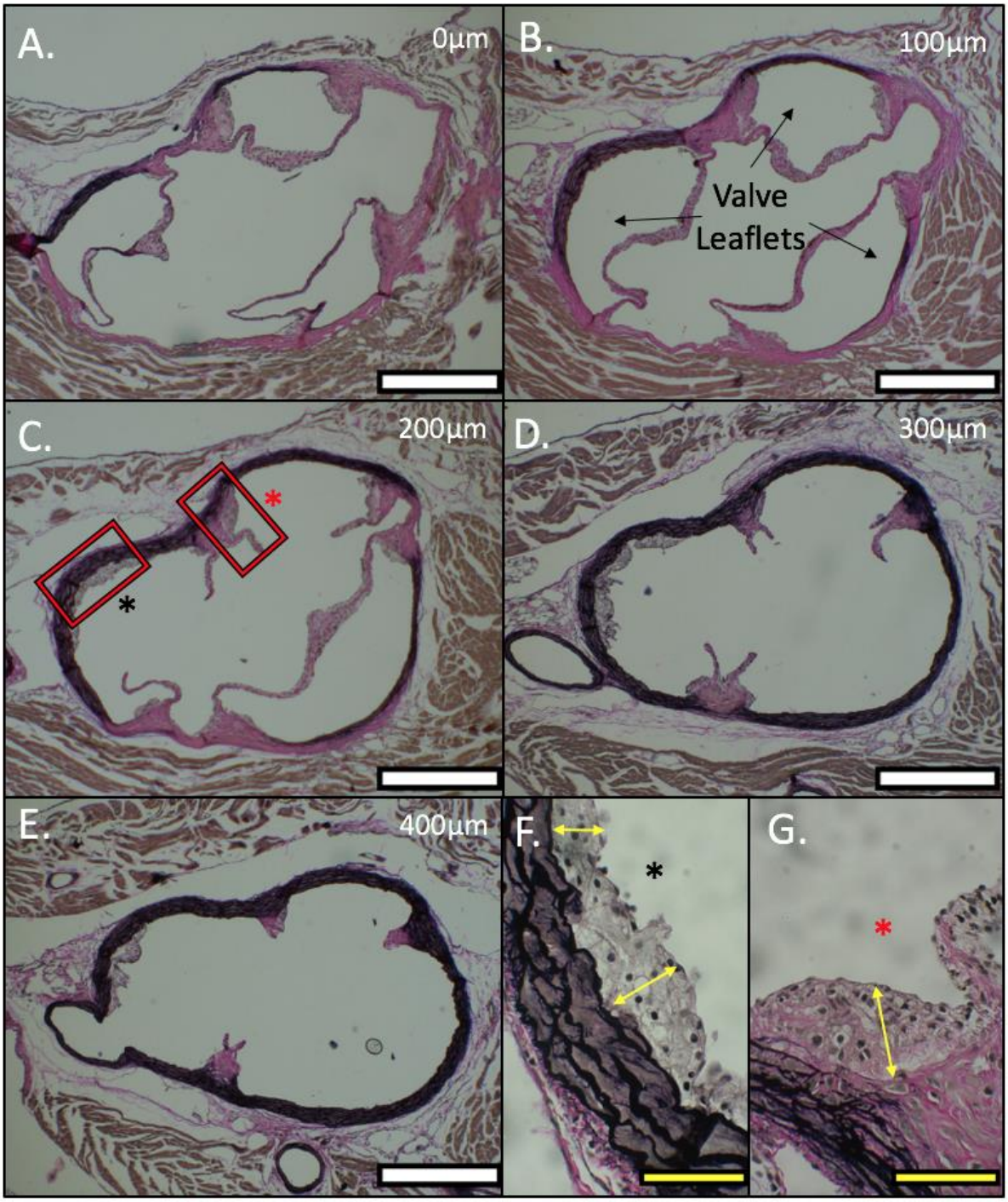

Figure 3.13: Foam cell lesions in the aortic sinus of 20-week female dKO (ApoE$^{-/-}$CaMKII$^{-/-}$) mice. *Female dKO mice were housed until 20 weeks of age. Mice were perfusion fixed with 4% PFA and the heart dissected. The heart was cut in a transverse plane below the level of the atria and embedded in paraffin wax. Shown above is a representative aortic sinus from a 20-week dKO female. A 5 µm section was collected at the appearance of the first two valve leaflets **(A)** and 4 more collected at 100 µm intervals throughout the aortic sinus **(B-E)**. Each section was stained with Verhoeff van Gieson and photos captured with a light microscope. The red boxes indicated by black and red asterisks correlate to zoomed in image of the vessel wall shown in **F-G**. Yellow double arrow indicated foam cell lesion growth on vessel wall. White scale bar = 200 µm, yellow scale bar = 40 µm.*

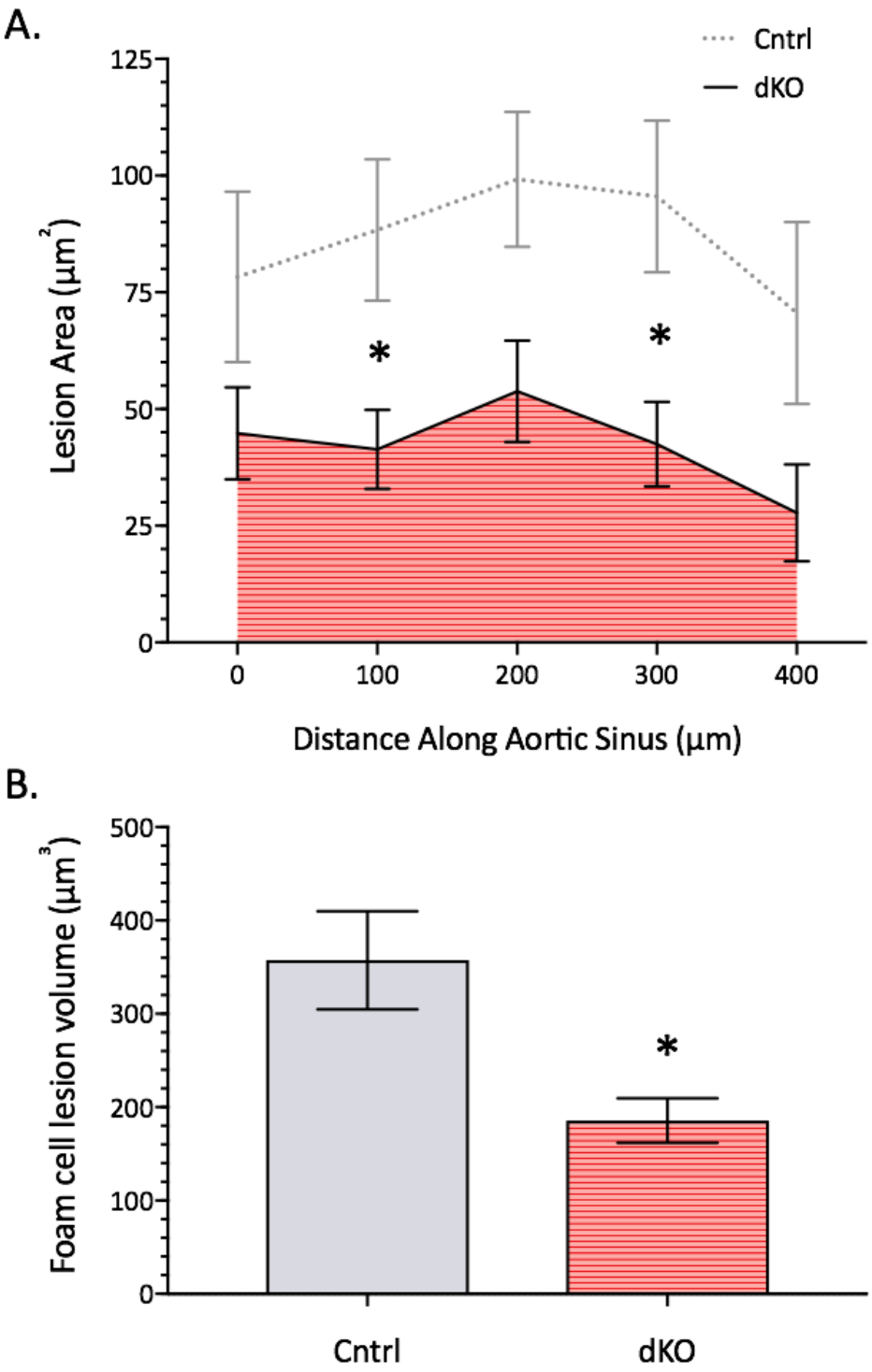

Figure 3.14: Foam cell lesion quantification in the aortic sinus of 20-week female control (ApoE$^{-/-}$ CaMKII$^{+/+}$) and dKO (ApoE$^{-/-}$CaMKII$^{-/-}$) mice. *A section was collected every 100 µm throughout the aortic sinus of each mouse and stained with Verhoeff van Gieson. Lesion area was calculated for each section along the aortic sinus (A). The area under the curve was calculated to generate foam cell lesion volume (B). Graphs show mean foam cell lesion area/volume as mean ± S.E.M.. *P < 0.05 as determined by unpaired Students t-test (n = 9-11).*

In summary, knocking the CaMKIIδ gene from our atherosclerotic mouse model (ApoE$^{-/-}$) did not have comparable effects on lesion size between males and females. At 20 weeks there was little atherosclerosis present in the aortic sinus of male groups and no difference observed between control and dKO. In contrast female groups had extensive lesions along the valve leaflet vessel wall of the aortic sinus. Interestingly, the dKO group had a striking reduction in lesion volume in the aortic sinus compared to control. Whether or not any male effect is masked due to lack of disease progression could indeed be a factor. Collectively, the strong effect observed in females where atherosclerosis is more advanced suggests the CaMKIIδ isoform plays a role in lesion growth.

3.4 Discussion

In this investigation, a genetic approach was employed by crossing ApoE$^{-/-}$ mice (atherosclerosis model) with CaMKII$\delta^{-/-}$ mice to generate a novel model ApoE$^{-/-}$CaMKII$\delta^{-/-}$ (dKO). Using this model it was identified the contribution of CaMKIIδ to atherosclerosis. Histological analysis of atherosclerosis in the aortic sinus of male and female control (ApoE$^{-/-}$ CaMKII$\delta^{+/+}$) and dKO (ApoE$^{-/-}$CaMKII$\delta^{-/-}$) groups suggests CaMKIIδ plays a role in foam cell lesion development.

What was striking was the dramatic differences in atherosclerosis between males and females. During dissection, it was noticeable that the aortic tree of male mice was translucent in appearance. In contrast, the aortic tree of female mice was opaque indicative of foam cell lesion build up within the artery wall. An extensive analysis of foam cell lesion content in the aortic sinus of males revealed there was little atherosclerosis present and no differences observed between control and dKO groups (**Figure 3.9-11)**. As our measurement was foam cell lesion area, many of the males did not present with extensive foam cell lesions so it was difficult to measure differences.

In the female groups however, there was extensive atherosclerosis development. This included extensive foam cell lesions that were present in the valve leaflets of the aortic sinus and extended the through the trunk of the aortic sinus (0 µm – 400 µM) (**Figure 3.12-14**). When groups were quantified there was roughly three times more lesion content in combined female control and dKO groups compared to male counterpart groups.

The finding that there is more atherosclerosis present in the aortic sinus of female mice at 20-weeks is not novel. Males are more resistant to the development of atherosclerosis and different effects are seen between sex when ApoE$^{-/-}$ mice are bred over different genetic backgrounds [236-238]. This includes the C57/Bl6 strain, which was the background strain for the current experiments [239]. Regardless of differences in disease progression we were interested in the role CaMKIIδ played in the development of atherosclerosis.

Female dKO mice had significantly less foam cell lesion in the aortic sinus compared to female control mice (**Figure 3.14**). Both groups had lesions present that extended the length of the aortic sinus however the lesions from control group were more progressed. Measuring lesion content in female groups was easy due to the large continuous lesions present. In contrast the small pockets of lesions present in male groups were more challenging to measure. It is likely that lack of disease progression is masking any effect of CaMKIIδ. In future, it would be useful to age mice until they reach a stage of lesion progression seen in the female counterpart group at 20-weeks and identify any differences at this time point. Regardless of the results shown by male, the strong effect seen between female groups suggest CaMKIIδ is a key player in foam cell lesion development.

As we were establishing a novel mouse model it was important body weight and total cholesterol was measured between male and female control and dKO mice. Total cholesterol is a risk factor for the development of atherosclerosis so it was important to identify whether knocking out the CaMKIIδ had any effects on cholesterol metabolism/ transport. Body weight and total cholesterol was not different between control and dKO groups in males and female (**Figure 3.7-8**). As cholesterol levels were not different it was not required to investigate the serum lipid profile in more depth by looking at HDL and LDL-C/VLDL-C. This suggests that CaMKIIδ is not playing a role in atherosclerosis by altering cholesterol metabolism.

Previously, we showed global inhibition of CaMKII with KN-93 reduced foam cell lesion development. This new model is advantageous over the former as it is selectively blocking CaMKIIδ expression while preserving the expression and physiological actions of the other isoforms. A limitation of the model in the context of the whole PhD is that we are interested in splice variants of the CaMKIIδ isoform. This is because there is evidence for splice variant-

specific functions. If it was investigated what splice variant of CaMKIIδ is contributing to atherosclerosis we would have to design specific siRNAs against the different variants.

Interestingly, some of the dKO mice from breeding litters displayed an ataxic phenotype. This neurological behaviour was unexpected as CaMKIIα and β are the main neural isoforms so it was expected any brain function would be preserved when knocking out CaMKIIδ. Even though CaMKIIα and β are the predominant cardiovascular isoform there has been some expression of δ found, however it has not been linked to any main function yet. This ataxic behaviour could be linked to any of the splice variants of CaMKIIδ that may be present in the brain. This adverse phenotype is not desirable in the context of drug discovery, suggesting a more targeted approach is required.

In summary, this is the first study to develop an atherosclerotic mouse model with a deletion in the CaMKIIδ gene. Collectively, results obtained from the aortic sinus of control and dKO mice suggest CaMKIIδ plays a role in foam cell lesion growth. Importantly, there were ataxia issues in some of the dKO mice suggesting one of the CaMKIIδ variants may be playing a physiological role in the brain. For a more targeted investigation next, we need to over express a variant of CaMKIIδ in the dKO mice and identify the contribute to lesion growth.

Chapter 4

AAV-Mediated Overexpression of CaMKIIδ_2 in Ligated Carotid Arteries of ApoE$^{-/-}$CaMKII$\delta^{-/-}$ Mice.

Contents

4.3 Results

4.3.1 Validation of CaMKIIδ_2-/control-mCherry AAV particles in vitro.

4.3.2 Ligation of the left carotid artery of ApoE$^{-/-}$CaMKII$\delta^{-/-}$ mice causes gross morphological changes to the vascular wall.

4.3.2 Ligation of the left carotid artery in ApoE$^{-/-}$CaMKII$\delta^{-/-}$ mice rapidly promotes foam cell lesion development and arterial wall remodeling wall.

4.3.4. Detection of mCherry fluorescence in the carotid arteries of ApoE$^{-/-}$ CaMKII$\delta^{-/-}$ mice transduced with CaMKIIδ_2- and control-mCherry.

4.3.5. CaMKIIδ_2 has no effect on vessel wall hypertrophy in response to ligation of the left carotid artery in ApoE$^{-/-}$CaMKII$\delta^{-/-}$ mice.

4.3.6. Examining the effect of CaMKIIδ_2 on foam cell lesion growth in an accelerated model of atherosclerosis.

4.3.7. Evaluating stenosis in the ligated carotid arteries of ApoE$^{-/-}$CaMKII$\delta^{-/-}$ mice transduced with CaMKIIδ_2- and control-mCherry.

2.4 Discussion

4.1 Introduction

Atherosclerosis is a multifactorial disease characterised by the formation of foam cell lesions on the inner layer of the arterial wall [13]. The development of foam cell lesions in the coronary arteries and aortic tree are responsible for ischaemic attacks including myocardial infarction (MI) and stroke [23, 243]. Current therapies targeted towards reducing atherosclerosis include the use of statins. Statins have been successful at reducing cardiac event mortality and morbidity [113, 124, 125, 127], however, even when target LDL-C levels are met, there remains a residual risk for a cardiovascular event [224]. It is critical that alternative treatments are developed that can be used alongside statins to target atherosclerosis. Such treatments could be those that target cellular mechanisms which promote lesion growth.

In vascular smooth muscle cells (VSMCs) and endothelial cells (ECs), calcium/calmodulin-dependent protein kinase II (CaMKII) has emerged as a critical regulator of cellular function in health and disease [244, 245]. The predominant isoforms expressed in vascular cells are CaMKIIδ and γ (*Chapter* 2) [185, 197, 198]. The differentiation between each isoform is critical as the δ and γ isoforms have shown contrasting roles in vascular function. In particular, δ promotes cellular functions that drive vascular pathology, whereas, γ has been shown to promote vascular health [213, 219, 221, 246].

The δ and γ isoforms exist as a number of splice variants, $\delta_{1\text{-}11}$, $\gamma_{1\text{-}3}$ [197, 199, 200, 203]. These variants have only been identified in cells but, of interest, the δ_2 and δ_6 have been investigated in relation to variant specific function. CaMKIIδ_2 has been shown to promote VSMC proliferation and migration [219, 220]. In contrast, CaMKIIδ_6 has been associated with thrombin-induced increase in endothelial cell permeability and expression of vascular cell adhesion molecules (e.g. VCAM-1) [212, 218]. Collectively, these functions in VSMCs and ECs are mechanisms that contribute to foam cell lesion development.

CaMKII function is yet to be investigated in a model of atherosclerosis (ApoE$^{-/-}$). Some of the previous research in CaMKII employed AAV-mediated techniques, and these approaches have been effective at unravelling some of the functions of CaMKII in pathology [181, 213, 247].

Already, it has been shown that CaMKIIδ promotes lesion development in the aortic sinus of ApoE$^{-/-}$ mice using a genetic knockout model (ApoE$^{-/-}$CaMKIIδ$^{-/-}$) (*Chapter 3*). To provide unequivocal evidence of CaMKIIδ involvement, it is now important to over-express the δ isoform using an AAV-mediated approach to fully exemplify CaMKIIδ contribution to foam cell lesion growth.

4.2 Approach

So far, the results gathered suggest CaMKIIδ plays a role in atherosclerosis. In Chapter 3, it was shown that female ApoE$^{-/-}$CaMKII$\delta^{-/-}$ had a strikingly reduced foam cell lesion content in the aortic sinus at 20-weeks of age compared to control females (ApoE$^{-/-}$CaMKII$\delta^{+/+}$). In both male ApoE$^{-/-}$CaMKII$\delta^{-/-}$ (dKO) and ApoE$^{-/-}$CaMKII$\delta^{+/+}$ (control) groups, there was minimal atherosclerosis in the aortic sinus so the disease was not progressed enough to measure any difference.

To provide further mechanistic evidence that CaMKIIδ promotes foam cell lesion development, an over-expression approach was employed. More specifically, AAV particles encoding either CaMKIIδ_2 or a scrambled sequence (control) were grown as detailed in *Section 4.2.1*-2. The CaMKIIδ_2 variant was chosen for two main reasons. Firstly, from the limited literature that has focused on a specific variant, CaMKIIδ_2 is described as causing cellular pathology including VSMC proliferation and EC dysfunction [212, 218-220]. Secondly, in *Chapter 2,* the δ_2 was shown to be present in human vascular cells as well as the atherosclerotic arteries of ApoE$^{-/-}$ mice.

ApoE$^{-/-}$CaMKII$\delta^{+/-}$ mice were mated and offspring litters were genotyped as described in *Section 3.2.1.1*. At 16-weeks of age, the carotid artery of ApoE$^{-/-}$CaMKII$\delta^{-/-}$ mice was ligated to disturb blood flow and accelerate atherosclerosis [248-251]. AAV particles harbouring either CaMKIIδ_2- or control-mCherry were then introduced into the tissue of the ligated artery. After surgery and recovery, the mice were returned to housing until mice were 20-weeks of age. At this time, mice were euthanised and perfused-fixed as previously described (WHERE). Both the left ligated carotid and right non-ligated carotid artery were dissected and processed through histology. The carotid arteries of CaMKIIδ_2 and control groups were analysed for foam cell lesion area, stenosis (%) and vessel remodelling which was the medial wall thickness.

4.2.1 Cloning CaMKII into pAAV-mCherry

To develop a CaMKII expressing AAV particle, initially, two plasmids containing the CaMKIIδ_2 and CaMKIIγ_3 open reading frames (ORFs) were purchased from GenScript® The CaMKIIδ_2 sequence was selected as it is a predominant splice variant in the vasculature of humans and a mouse model of atherosclerosis (ApoE$^{-/-}$) as previously discussed (where). While the δ isoform is the primary target for investigation, an additional variant of the "protective" γ_3 sequence was cloned and developed into a virus, to act as a method control and to be used in an independent parallel experiment.

The backbone plasmid (pAAV-hSyn-hM4D(Gi)-mCherry (Addgene)) was digested and the CaMKII sequences amplified by PCR. Amplified CaMKII inserts were ligated into the virus backbone for plasmid transformation (**Fig. 4.1**).

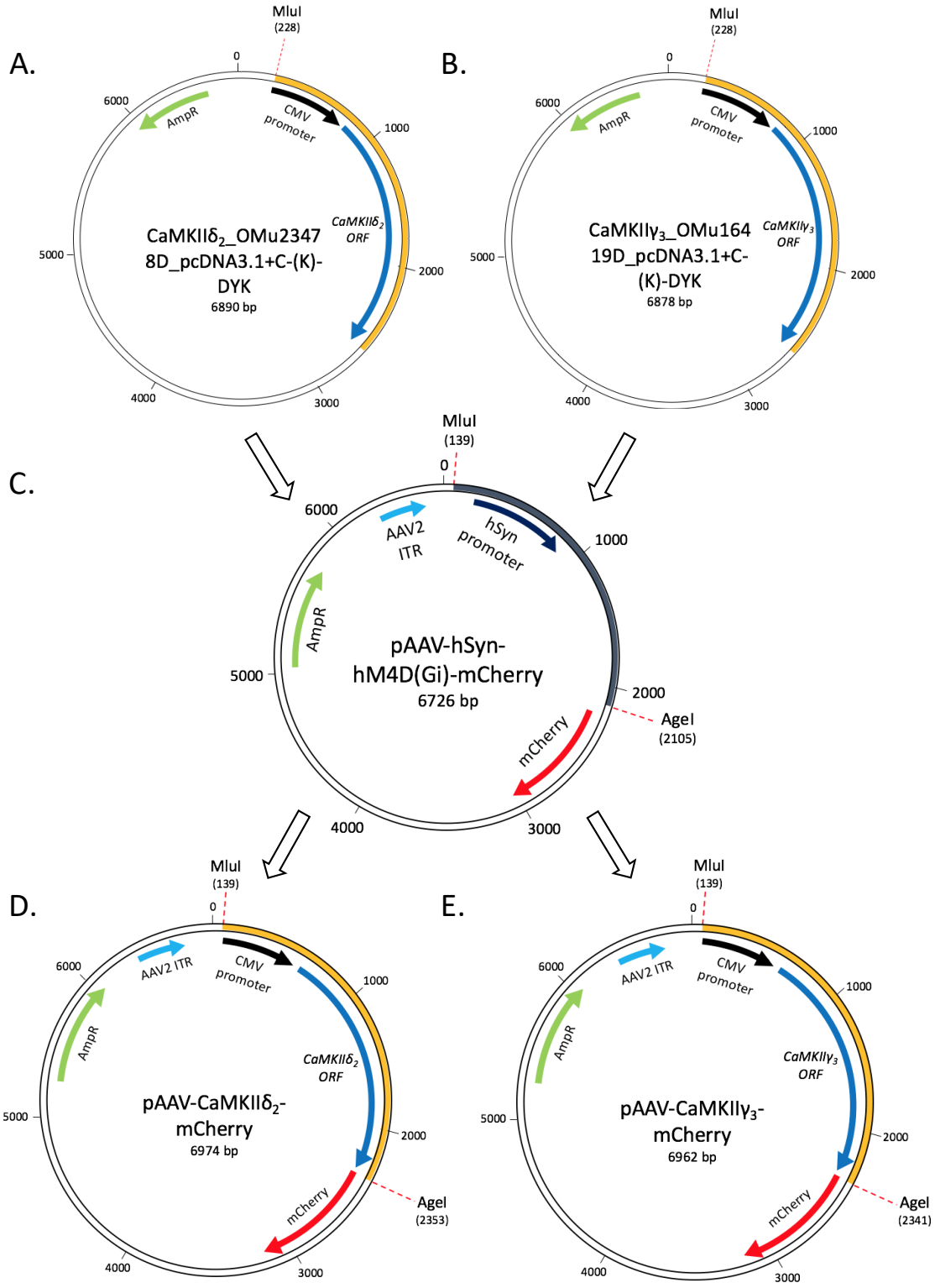

Figure 4.1: Summary of CaMKIIδ_2 and γ_3 cloning procedure. *CaMKIIδ_2 and γ_3 ORFs were purchased as pcDNA3.1+C-(K)-DYK vectors (A-B) and amplified via PCR. The pAAV-hSyn-hM4D(Gi)-mCherry backbone plasmid (GenScript) (C) was digested utilising restriction sites MluI (139) and AgeI (2105). Amplified CaMKIIδ_2 and γ_3 ORFs were ligated into the digested backbone resulting in pAAV-CaMKIIδ_2/γ_3-mCherry vectors (D-E).*

4.2.1.1 Digest of AAV-backbone vector

The pAAV-hSyn-hM4D(Gi)-mCherry plasmid (Genscript) was used as the virus backbone (**Fig. 4.2)**. The plasmid was digested by utilising restriction enzyme sites MluI (139) and AgeI (2105) to cut out a 1966 bp segment of the plasmid that includes the hSyn promoter.

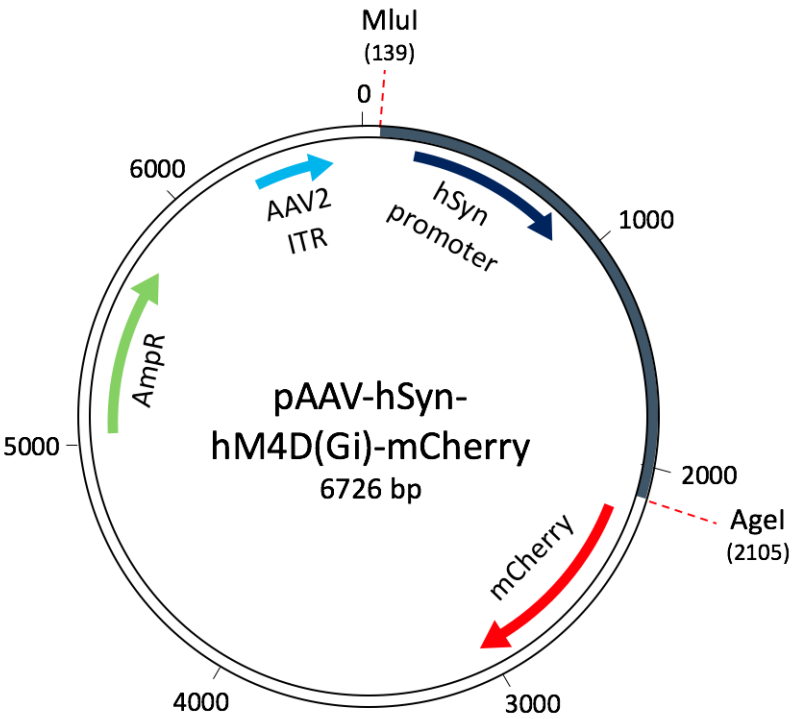

Figure 4.2: Basic structure of pAAV-hSyn-hM4D(Gi)-mCherry. *The 6726 bp plasmid encodes the hSyn promoter, mCherry reporter gene, ampicillin resistance gene and inverted terminal repeat sequence (ITR). MluI (139) and AgeI (2105) are restriction enzymes which flank a 1966 bp segment.*

Firstly, 12 µL (2 µg) of pAAV-hSyn-hM4D(Gi)-mCherry was mixed with 5 µL cut-smart buffer (10X) and 29 µL DEPC treated water in a 1.5 ml microcentrifuge tube. 2 µL of each restriction enzyme; MluI (cata.no. R31985) and AgeI-HF (cata.no. R35525), were added to the buffer mix and incubated for 15 mins at 37°C. Following this, the reaction was inactivated by heating to 65°C for 5 mins. **Figure 4.3** shows the plasmid digest products electrophoresed through a 1% agarose gel. The plasmid treated with restriction enzymes MluI/AgeI contains two bands which indicate the cut-out insert (1966 bp) and the rest of the plasmid (4760 bp). The top DNA fragment containing the backbone of the plasmid without the insert was excised from the gel and stored in a 1.5 ml microcentrifuge tube at 4°C for DNA extraction.

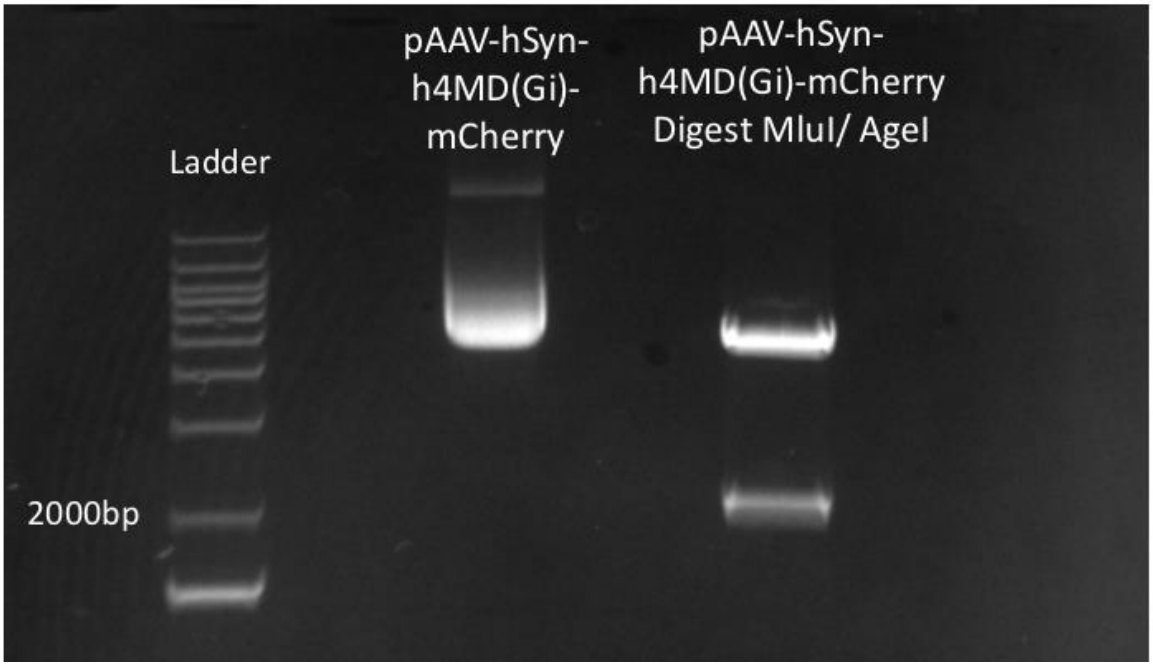

Figure 4.3: pAAV-hSyn-hM4D(Gi)-mCherry digest. *1 µg of pAAV-hSyn-hM4D(Gi)-mCherry plasmid, either non-treated or digested with MluI and AgeI, was loaded into a 1% agarose gel containing SYBR safe DNA stain and electrophoresis performed at 90 V for 90 mins. Photo captured on Syngene imager.*

4.2.1.2 Amplification of CaMKII Open Reading Frames (ORFs)

The CaMKIIδ_2 and γ sequences were purchased as the pcDNA3.1+C-(K)-DYK vectors (Genscript) (**Fig. 4.4**). Plasmid vectors containing CaMKII insert sequences were reconstituted in 100 µL DEPC-treated water to a concentration of 100 ng/µL.

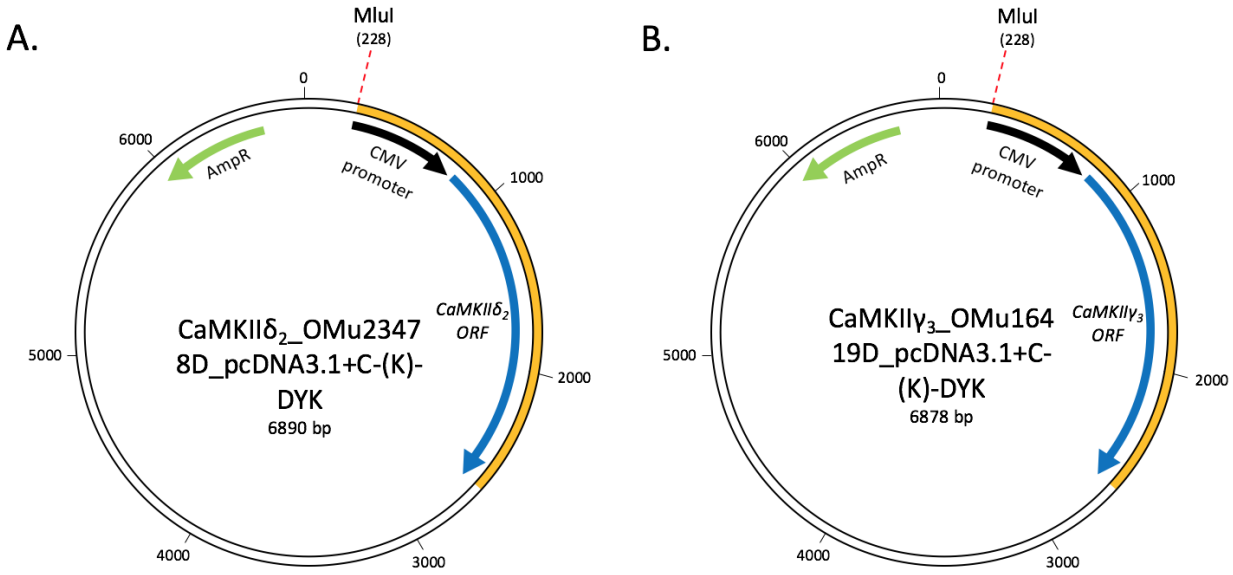

Figure 4.4: Basic structure of pcDNA3.1+C-(K)-DYK. *The CaMKIIδ_2 (A) and γ_3 (B) ORFs were encoded within each plasmid. Other features of the plasmid include the ampicillin resistance gene and restriction enzyme site MluI (228) upstream of CMV promoter and CaMKIIδ_2/γ_3 ORF.*

PCR was carried out to amplify CaMKIIδ_2 and γ_3 ORFs including the CMV promoter. The forward primer (MluI-CMV-fwd: 5'GATATACGCGTTGACATTGATTATTGAC-3') is the same for both δ_2 and γ_3 sequences, utilising the MluI restriction enzyme site upstream of the CMV promoter in the pcDNA3.1+C-(K)-DYK vector. The AgeI restriction enzyme site was added for both the δ_2 and γ_3 reverse primer (AgeI-OMu23478D-CaMKIIδ_2-Rev: 5'-GTATACCGGTAATCGATGTTTTGCCAC-3' and AgeI-OMu16419D-CaMKIIγ_3-Rev: 5'-GTATACCGGTAATCCTGTAGCGGTGC-3'). This was to allow ligation of amplified δ_2 and γ_3 PCR products into the digested pAAV-hSyn-hM4D(Gi)-mCherry backbone in a later step (**Section 4.2.1.4**).

For each PCR reaction, 12.5 µL KAPA HiFi mastermix (cat.no. KRO370) was mixed with 10 µL DEPC-treated water and 1 µL (2 ng) of pcDNA3.1+C-(K)-DYK vector. 0.75 µL of each respective forward and reverse primer for δ_2 and γ_3 was added to the mastermix and PCR performed under conditions shown in **Table 4.1**.

Table 4.1: PCR conditions for CaMKIIδ_2 and γ_3 amplification from pcDNA3.1+C-(K)-DYK vector

	98°C – 30 sec	-
Denaturing	98°C – 10 sec	X 35 cycles
Annealing	63°C – 20 sec	
Elongation	72°C – 60 sec	
	72°C – 5 min	-

Once PCR cycling had terminated, the PCR products were loaded into a 1% agarose gel and electrophoresed at 90 V for 1 hr. **Figure 4.5** shows the amplified CaMKIIδ_2 and γ_3 products indicated by the white bands at sizes 2214 bp and 2207 bp, respectively. The amplified DNA fragment was excised out of the gel and stored in a 1.5 ml microcentrifuge tube at 4°C for DNA extraction.

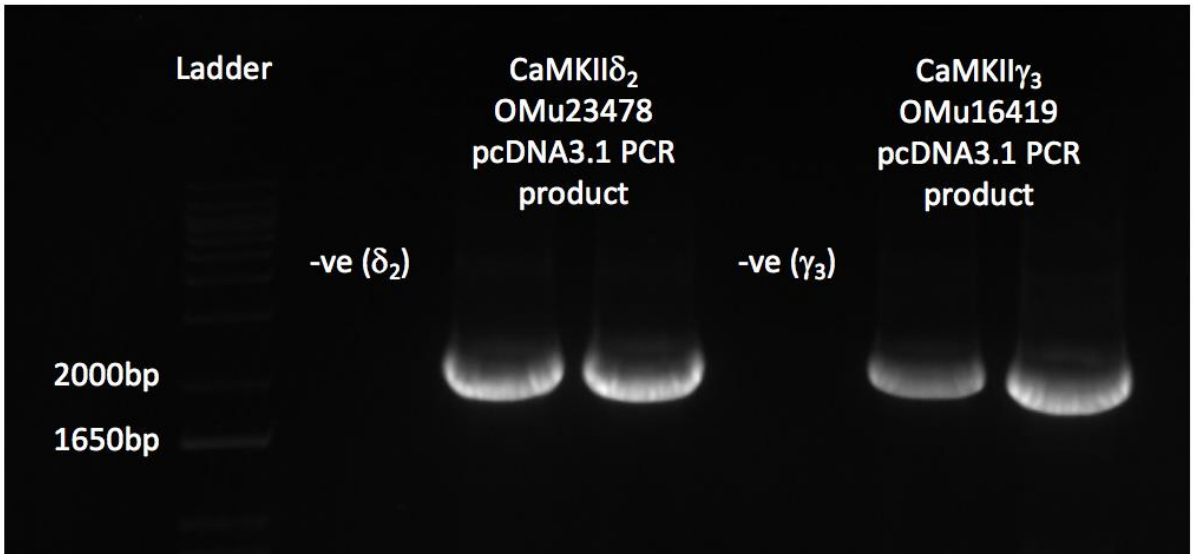

Figure 4.5: PCR amplification of CaMKIIδ_2 and γ_3 ORFs in pcDNA3.1+C-(K)-DYK vector. *PCR targeting CaMKIIδ_2 and γ_3 ORFs was carried out in duplicate. The total PCR product for each reaction was loaded into a 1% agarose gel (with SYBR safe DNA stain) alongside negative controls (-ve) and run at 90V for 60 mins. Photo captured on Syngene imager.*

4.2.1.3 DNA gel extraction, digestion and purification of CaMKII

The DNA fragments from the digested backbone vector and amplified CaMKII ORFs were extracted from the gel using the QIAquick Gel Extraction Kit (cata.no. 29704 – Qiagen). Each gel fragment was weighed and incubated in 3X the gel volume of buffer QG at 50°C for 10 mins. Following incubation, 1X gel volume of isopropanol was added to buffer and transferred to a spin column. The samples were centrifuged at 12000 x g and flow through was discarded. 750 µL of wash buffer PE was added to each column and centrifuged at 12000 x g for 1 min or until all residual buffer had flowed through. Each column was eluted into a sterile 1.5 ml microcentrifuge tube. 40 µL of DEPC-treated water was added to each column and centrifuged at 12000 x g for 1 min. DNA concentrations were calculated using the Nanodrop.

Once the CaMKIIδ_2 and γ_3 PCR fragments were extracted from the gel, they were digested using the MluI and AgeI restriction sites to allow ligation into the pAAV-hSyn-hM4D(Gi)-mCherry plasmid. 5 µL of cut-smart buffer was mixed with 1 µL AgeI and MluI restriction enzymes. 2 µg of CaMKIIδ_2 or γ_3 PCR product was added to the buffer and adjusted with DEPC-treated water to a final volume of 50 µL. Each sample was incubated for 15 min at 37°C.

Following digestion, the CaMKIIδ_2 and γ_3 DNA fragments were purified using the QIAquick PCR kit (cata.no. 28104 - Qiagen). 250 µL of buffer PB (Qiagen) was added to 50 µL PCR digest product and mixed. The resulting sample was transferred to a column for DNA binding and centrifuged at 15,000 x g for 30 sec. The flow-through was discarded and the column washed with 750 µL buffer PE (Qiagen) and centrifuged in the same manner. The column was applied to a fresh microcentrifuge tube and 35 µL DEPC-treated water was added and centrifuged for 1 min at 15,000 x g to elute DNA. DNA concentrations were calculated using the Nanodrop.

4.2.1.4 Plasmid Ligation

Prior to plasmid ligation, the digested backbone pAAV-hSyn-hM4D(Gi)-mCherry was treated with recombinant shrimp alkaline phosphatase (rSAP). This was to prevent self-ligation of the digested plasmid. 2 µL of cut-smart buffer was incorporated with 0.25 µL rSAP and 200 ng of digested pAAV-hSyn-hM4D(Gi)-mCherry up to a volume of 20 µL. The sample was incubated for 30 min at 37°C and then heat inactivated for 5 min at 65°C.

To set up ligation reaction, 30 ng of digested and rSAP-treated vector backbone was mixed with 5 µL of T_4 ligase and 90 ng PCR digest (CaMKIIδ_2 or γ_3). The reaction was incubated for 15 mins at room temperature and then overnight at 4°C. A simplified map of the ligated pAAV-CaMKIIδ_2-mCherry and pAAV-CaMKIIγ_3-mCherry plasmid can be seen in **Figure 4.6**.

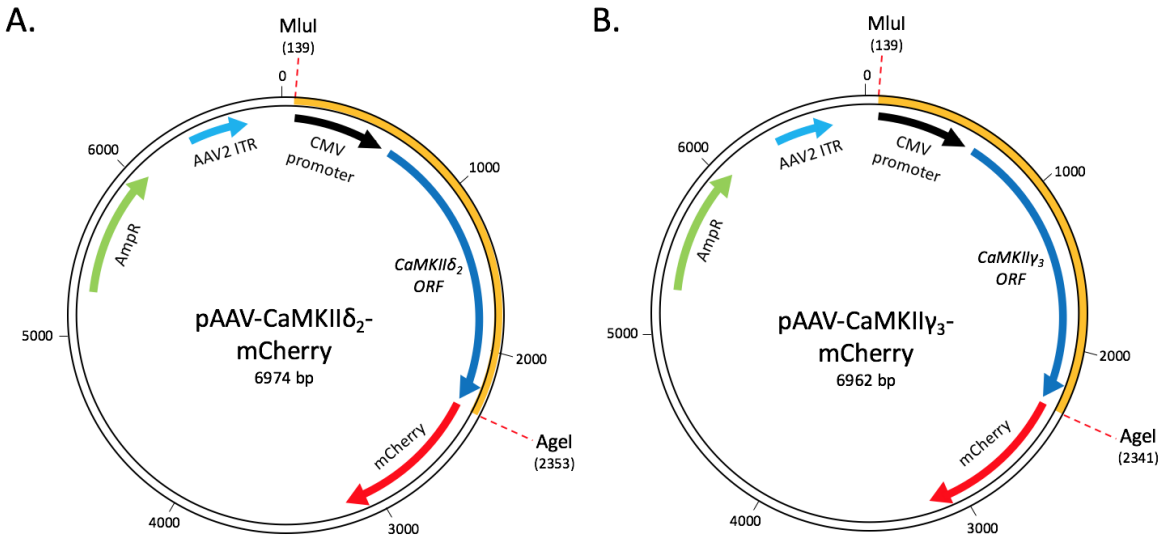

Figure 4.6: Structure of the developed pAAV-CaMKIIδ_2/γ_3-mCherry plasmid. *The 6726 bp plasmid encodes the hSyn promoter, mCherry reporter gene, ampicillin resistance gene and inverted terminal repeat sequence (ITR). MluI (139) and AgeI (2105) are restriction enzymes which flank a 1966 bp segment. Original figure made on Microsoft PowerPoint.*

4.2.1.5 Plasmid Transformation

The One Shot® Top10 competent E. coli (cata.no. C4040-10) were used to transform the newly ligated pAAV-CaMKIIδ_2/γ_3-mCherry plasmids. A 50 µL vial of One-Shot cells for each transformation was thawed on ice. 5 µL of each ligation reaction was added to a vial of cells, mixed gently and incubated on ice for 30 mins. Following this, each vial was transferred to a water bath for exactly 30 secs before being returned to ice. 250 µL of pre-warmed S.O.C (super optimal broth with catabolite repression, Thermofisher) media was added to each vial before shaking at 225 rpm for 1 hr at 37°C. 50 µL from each transformation vial was inoculated onto separate LB agar plates (100 µg/ml ampicillin). The plates were inverted and incubated overnight at 37°C.

The following day the plates were observed for colony growth. Two new LB agar plates (100 µg/ml Amp) were divided into seven segments. Seven separate colonies were swabbed from each of the pAAV-CaMKIIδ_2/γ_3-mCherry plates and streaked onto the fresh segmented plates. Additionally, each colony was run for PCR in the same manner as was used to amplify the CaMKIIδ_2/γ_3 ORFs from the pcDNA3.1+C-(K)-DYK vectors. **Figure 4.7** shows the amplified CaMKIIδ_2 and γ_3 ORF indicated by the white bands at sizes 2214 bp and 2207 bp, respectively. This confirmed that pAAV-CaMKIIδ_2/γ_3-mCherry had been successfully transformed into the colonies.

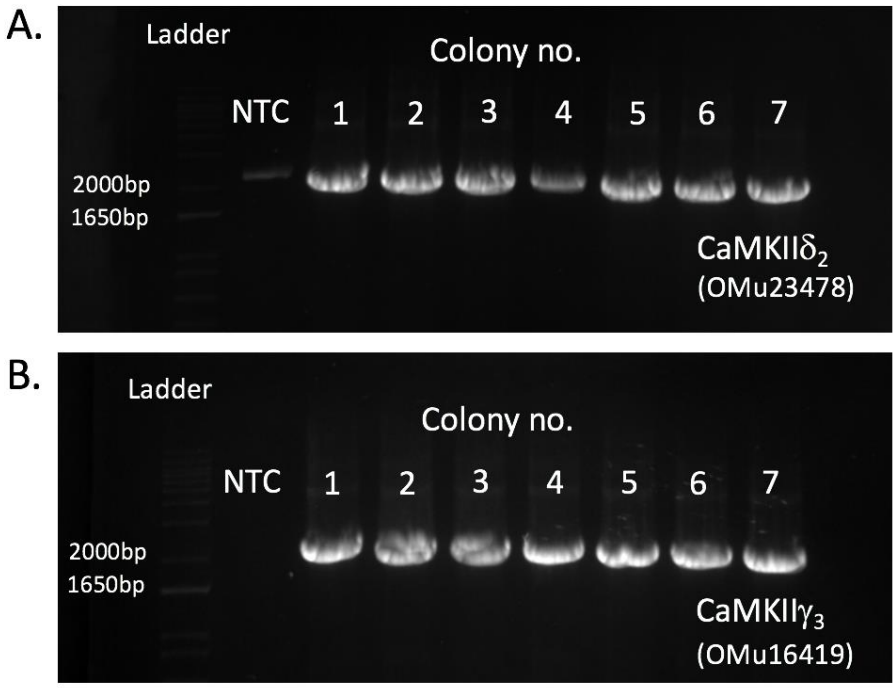

Figure 4.7: PCR of CaMKIIδ_2 and γ_3 ORFs after ligation into pAAV-hSyn-hM4D(Gi)-mCherry. *E. coli were grown and transformed overnight with either pAAV-CaMKIIδ_2-mCherry (A), or pAAV-CaMKIIγ_3-mCherry (B). Seven separate colonies from each transformation were swabbed and run for PCR targeting CaMKIIδ_2 (OMu23478) or CaMKIIγ_3 (OMu16419). Total PCR products were loaded onto a 1% agarose gel (SYBR safe DNA stain) and electrophoresed at 90 V for 60 mins.*

4.2.1.6 Plasmid midi prep

After confirming the colonies were successfully transformed with pAAV-CaMKIIδ_2/γ_3-mCherry, a midiprep was carried out. Using a plastic loop, 100 ml LB media containing ampicillin (100 µg/ml) was inoculated with either the pAAV-CaMKIIδ_2-mCherry, pAAV-CaMKIIγ_3-mCherry, DJ or helper plasmids (catalog.no.VPK-400-DJ). The DJ and P-helper plasmids are co-transfected with pAAV-CaMKIIδ_2-mCherry to facilitate AAV production. Additionally, these plasmid constructs contain the ampicillin resistance gene so only bacteria successfully transformed are expected to grow. Flask cultures were put onto a shaker at 225 RPM overnight at 37°C.

The Purelink^{TM} HiPure Plasmid DNA Purification Kit (Catalog.no. K2100-2) was used for plasmid extraction and purification. The following day, each flask was transferred to two 50 ml conical tubes and spun down at 4000 x g for 40 mins at 4°C. The supernatant was discarded and 4 ml resuspension buffer with RNase A was added to the cell pellet and mixed until homogenous. Following this, 4 ml lysis buffer was incorporated into the cell suspension and gently inverted before incubation at room temperature for 5 mins. After incubation, 4 mL of precipitation buffer was added and immediately mixed by inversion. The cell lysate was centrifuged at 12,000 x g for 10 min.

Following centrifugation, the supernatant fraction from the prepared cell lysate was loaded onto an equilibrated column. Once this had drained, 20 ml of wash buffer was run through the column to wash the bound DNA. A fresh 15 ml centrifuge tube was placed under the column and 5ml of elution buffer was added to the column to elute the DNA. 3.5 ml isopropanol was mixed thoroughly with elution tube and centrifuged at 12000 x g for 5 min at 4°C. The supernatant was discarded, the DNA pellet resuspended in 3 ml 70% ethanol and centrifuged at 12000 G for 10 mins. The supernatant was carefully removed and the DNA pellet air dried for 10 mins. 100 µL DEPC-treated water was added to the pellet and left overnight at 4°C. A sample from each plasmid midi prep was run on a 1% agarose gel to identify plasmid size *(***Figure 4.8***).* The following day, the DNA concentration of cloned plasmids from each midi prep was calculated using a Nanodrop and stored at -80°C.

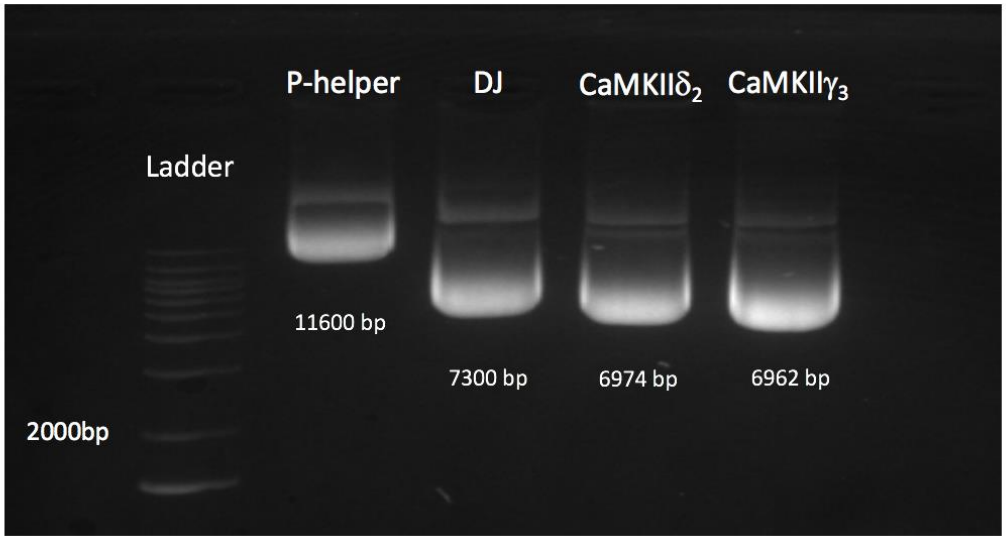

Figure 4.8: Confirmation of plasmid midi prep. *A midi prep for pAAV-CaMKIIδ_2-mCherry, pAAV-CaMKIIγ_3-mCherry, DJ or helper plasmid was carried out. A 3 µL sample of each plasmid was loaded into a 0.5% agarose gel (SYBR safe DNA stain) and electrophoresed at 70 V for 2 hrs. Photo captured on Syngene imager.*

4.2.2 Cell Culture

4.2.2.1 Transfection of 293 AAV cells

To generate the CaMKIIδ_2- and γ_3-expressing particles, 293AAV cells were used (Cat.no. AAV-100 CELLBIOLABS). The 293AAV cell line are terminally differentiated, originating from primary embryonic human kidney transformed with adenovirus type 5 DNA. The transformed DNA encodes genes important for transactivation of viral promoters to drive replication. To achieve a high titre of virus the AAV-DJ Helper Free Packaging System (Cata.no. VPK-400-DJ CELLBIOLABS) was used. This kit provides two plasmids, pHelper and DJ, which assist 293AAV cells with the other required proteins for effective viral gene production and packaging.

To mediate transfection, the Lipofectamine 3000 kit was used. Alongside CaMKII transfections an additional control AAV particle was generated in a parallel experiment. This AAV particle contains a section of the LacZ sequence. For each transfection (pAAV-CaMKIIδ_2-mCherry/pAAV-CaMKIIγ_3-mCherry/pAAV-LacZ-mCherry) two T175 flasks of 293AAV cells were grown to 70-80% confluence. Initially, two tubes (A-B) for each of the transfections were set up according to **Table 4.2** and incubated for 5 min. Following this, tube A was incorporated into tube B, mixed gently, and incubated for a further 5 min.

Table 4.2: Summary for transfection of 293AAV cells using Lipofectamine 3000.

	Component	2 X T175 Flasks
Tube A	DJ	27.6 µg
	pHelper	27.6 µg
	CaMKIIδ_2/CaMKIIγ_3/LacZ (control)	27.6 µg
	P3000 Reagent	172.5 µL
	DMEM (no serum)	Adjust total volume to 3000 µL
Tube B	Lipofectamine Reagent	250 µL
	DMEM (no serum)	2750 µL
		Total volume 3000 µL

Each transfection mix was added drop by drop to the appropriate T175 flask while swirling gently. The flasks were returned to the incubator at 37°C with 5% CO_2, and incubated for 72 hours. At this time, the flasks were viewed under a ZOE Fluorescent Cell Imager (cat.no. 1450031, BIORAD) with red filter and photos captured (**Figure 4.9**). The red glowing cells are indicative of mCherry expression and a successful transfection of pAAV-CaMKIIδ_2-mCherry (**A**), pAAV-CaMKIIγ_3-mCherry (**B**) and pAAV-LacZ-mCherry (**C**). Each flask was then prepared for AAV purification.

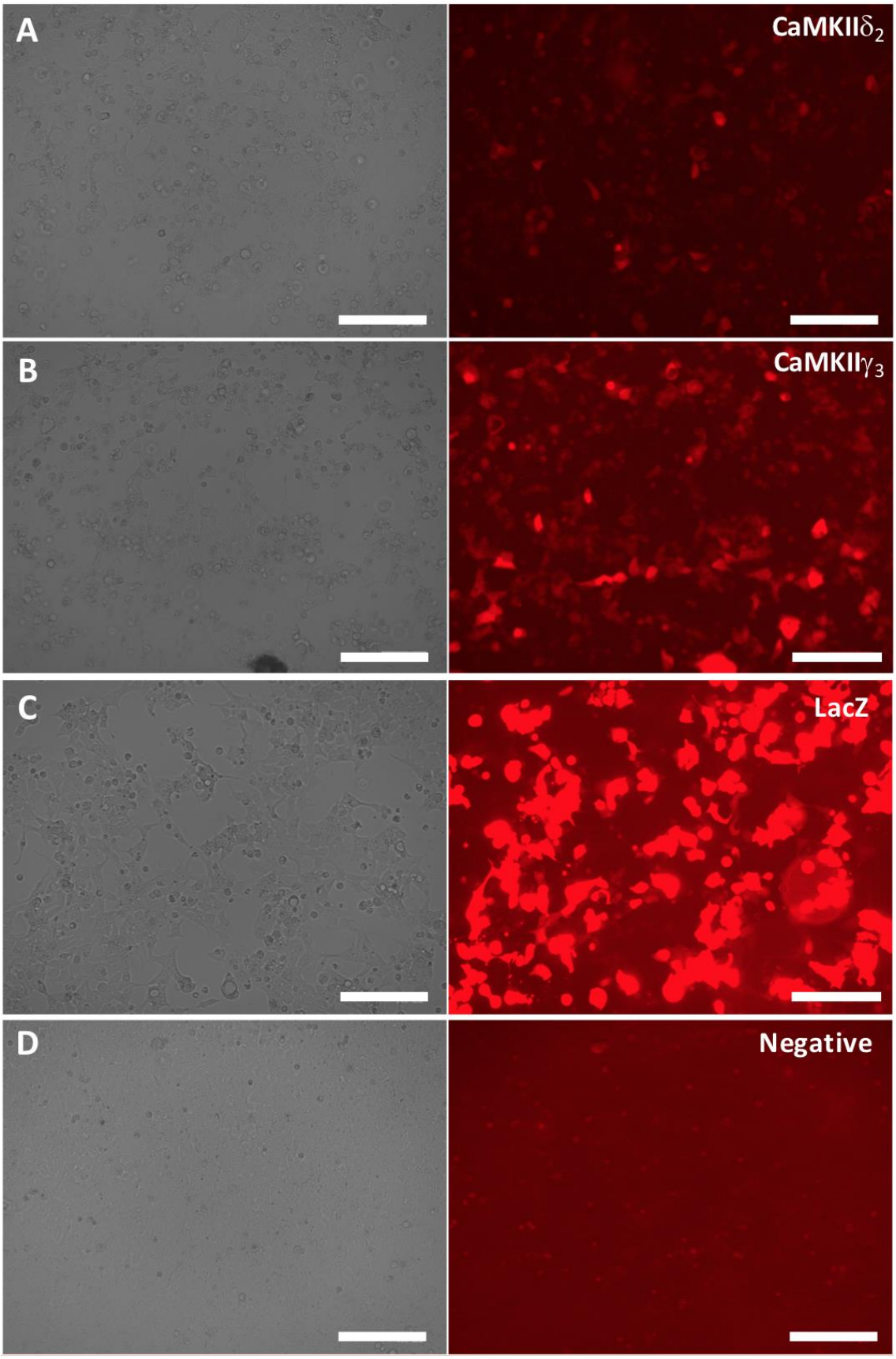

Figure 4.9: Transfection of 293 AAV cells for viral production. *Cells were co-transfected with DJ, helper plasmid and either pAAV-CaMKIIδ_2-mCherry (A), pAAV-CaMKIIγ_3-mCherry (B), LacZ-mCherry (C) or nothing (D). 72-hrs post-transfection, cells were viewed and photos captured using the ZOE Fluorescent Cell Imager (cat.no. 1450031 BIORAD). A positive transfection was confirmed by red glowing cells indicating mCherry expression.*

4.2.2.2 AAV Purification

72 hrs post-transfection 0.5 M EDTA was added to the flask to alleviate cell adhesion and pull cells into suspension. The media was harvested into a 15 ml conical tube and centrifuged at 1000 x g for 5 mins to pellet transfected cells. The pellet was resuspended in 2.5 ml serum-free DMEM and subjected to four rounds of freeze/thaw cycling using dry ice-ethanol bath and 37°C water bath. The tube was centrifuged at 10,000 x g for 10 mins and the AAV-containing supernatant collected and transferred to a fresh 15 ml tube.

To extract AAV particles from cells at 72 hrs post-transfection, the ViraBind™ AAV Purification Kit (cata.no. VPK-140 CELLBIOLABS) was used. 25 µL of AAV Reagent A was added to 2.5 ml of viral supernatant and incubated at 37°C for 30 mins. The tube was centrifuged at 5000 x g for 15 mins and the supernatant transferred to a fresh 10 ml tube. Following this, 125 µL of pre-warmed (37°C) Reagent B was added to the viral supernatant and incubated at 37°C for 30 mins. The tube was centrifuged at 10,000 x g for 10 mins and the supernatant transferred to a sterile 15 ml conical tube.

The AAV-containing supernatant was resuspended in 300 µL of Purification Matrix and mixed at room temperature for 30 mins on an orbital shaker. Immediately after, the tube was centrifuged at 1000 x g for 10 mins to pellet the purification matrix. The supernatant was discarded and the purification matrix was washed with 2.5 ml purification buffer. The tube was centrifuged at 1000 G for 10 mins and the supernatant carefully removed. 0.5 ml of elution buffer was added to extract purified AAVs and the mixture was incubated on an orbital shaker for 10 mins at 4°C. Post-incubation, the conical tube was centrifuged at 1000 x g for 10 mins and the eluted AAV-containing supernatant carefully collected.

The supernatant was applied to the sample reservoir in a centrifugal concentrator and centrifuged at 2000 x g for 5 mins. Flow-through was discarded until 100 µL remained in the sample reservoir. 400 µL PBS was added to the concentrator and centrifuged again at 2000 x g until 100 µL remained and this step repeated one more time. The sample reservoir was inverted over a sterile 1.5 ml microcentrifuge tube and centrifuged at 1000 x g for 30 secs to collect concentrated AAV sample. A 5 µL sample of each AAV was taken to calculate the titre and the remaining AAVs stored at -80°C.

4.2.2.3 AAV Titration

To calculate the physical titre for each AAV, qPCR using SYBR Green PowerUp was carried out. The AAV2 inverted terminal repeat (ITR) sequence was targeted by qPCR as the viral marker; ITR primer pair fwd: 5'-GGAACCCCTAGTGATGGAGTT-3', rev: CGGCCTCAGTGAGCGA-3'.

Firstly, the 5 µL samples kept aside were diluted 1:80 and 1:5000 with DEPC-treated water. Each diluted sample was set up for qPCR as shown in **Table 4.3**. Additionally, another set of reactions were set up using plasmid standards ranging from concentrations 2 X 10^3 molecules / µL to 2 X 10^9 molecules / µL.

Table 4.3: qPCR components for calculating virus titre

PCR Component	**Volume (µL) per reaction**
SYBR Green	10
100 µM ITR fwd	0.1
100 µM ITR rev	0.1
DEPC-treated water	4.8
Sample	5

Each reaction was carried out in triplicate. 15 µL qPCR mastermix was added to each well in a 96 well plate and kept on ice. 5 µL of diluted AAV sample or standard was added to a well and the plate lid attached. The 96 well-plate was spun on a benchtop centrifuge and loaded into the Applied Biosystems StepOne Plus RTPCR system and PCR performed under the conditions shown in **Table 4.4**.

Table 4.4: PCR conditions for AAV titration

Denaturing	98°C – 15 sec	X 40 cycles
Annealing	63°C – 30 sec	
Elongation	72°C – 30 sec	

The mean cycle threshold (C_T) value was calculated between each of the triplicate reactions for standards and diluted samples. A standard curve was constructed from known standards on Graphpad Prism. The C_T value for each diluted sample was inserted into the standard curve

equation to calculate x as shown in example equation 1. The x value was log transformed and multiplied by the dilution factor to transform the units into genome copies per ml (GC/ml).

Equation 4.1:

$Y(C_T) = -2.997x + 37.85$

$X = (C_T – 37.85)/-2.997$

4.2.2.4 Transfection of CaMKII-mCherry into HCASMCs and HUVECs

Human coronary artery smooth muscle cells (HCASMCs), human umbilical vein endothelial cells (HUVECs) and human coronary artery endothelial cells (HCAECs) were cultured in specialised growth medium with 10% fetal bovine serum (FBS) and 1% pen/strep as described in *Section 2.2.1*.

24 hr before transduction, HCASMCs and HUVECs were seeded into individual 6-well plates at a concentration of 5 x 10^5 cells/ml. 20 µL of respective media containing $5x10^{12}$ PFUs of either CaMKIIδ_2, CaMKIIδ_6 or control AAV was added to each well drop by drop. Cells were returned to the incubator for 48 hrs. After this time, HUVECs and HCASMC were harvested for total RNA and RT-PCR was performed targeting huV1 as previously described in *Section 2.2.1.*

4.2.3 Animal Work

Fourteen ApoE-/-CaMKIIδ-/- mice were housed at the Hercus-Taieri Research Unit (HTRU) under a 12:12 hr lighting schedule with ad libitum access to food and water. At 14-weeks of age, mice were switched from a regular chow diet (5 % energy from fat) to a high-fat diet (HFD) (40 % energy from fat). At 16-weeks of age, the left carotid artery (LCA) was accessed by surgery and ligated with a suture to disrupt blood flow and promote atherogenesis. AAVs expressing either CaMKIIδ2-mCherry or control-mCherry were introduced to the left carotid artery of the mice. The surgical manipulation of the carotid artery and AAV instilment in these mice was approved by the University of Otago Animal Ethics Committee (AEC) (19-58).

4.2.3.1 Carotid artery surgery and AAV overexpression

Prior to induction of anaesthesia, analgesia was provided to each mouse by subcutaneous injection of carprofen (5 mg/kg). At the time of surgery, anaesthesia of the mouse was induced by intraperitoneal (IP) administration of a ketamine (75mg/kg) and medetomidine (1mg/kg). After surgical anaesthesia was induced and confirmed by the pedal-withdrawal reflex, the fur around the neck and clavicle was removed by depilatory cream and a local injection of lignocaine (5 mg/kg) administered. The mouse was then transferred to the operating theatre for surgery employing full aseptic techniques.

An incision was made in the mouse neck midline from the level of the sternum to the mandible. Using blunt dissection, the skin was separated from underlying submandibular gland and other soft tissues. The sternomastoid muscle was located under the submandibular gland and retracted to the left side to access the bifurcation of the LCA. The LCA was freed of the vagus nerve and other surrounding tissues. A 6-0 silk suture was placed around the artery and a piece of nylon with a diameter of 400 µm below the level of the bifurcation was tied to impede blood flow. The piece of nylon was removed so that the area ligated was similar between mice. Although this manipulation is a partial ligation, it will be referred to just as ligated artery in the following sections.

50 µL of 30% Pluronic f-127 suspending either CaMKII or control ($3X10^8$ PFU gel) was applied to the adventitial surface of the LCA. The sternomastoid muscle and submandibular gland was

carefully replaced and the skin wound closed by application of tissue glue. Anaesthesia was reversed with subcutaneous administration of antisedan (5 mg/kg). Additionally, a saline bolus (1 ml) was administered to maintain the hydration status of the mouse. The recovery of each mouse was closely monitored for the next 4 hrs in a warming chamber before returning to the animal facility until 20-weeks of age.

4.2.3.2 Histology

Four-weeks post-surgery (20-weeks of age), mice were euthanised by CO_2 overdose at a flow rate of 8.5 L/min. Once breathing had ceased, mice were left for an additional 2 mins of CO_2 and then death was confirmed by the pedal withdrawal reflex. Each mouse was set on a dissection board and cardiac perfusion was carried out as described in **Section 2.2.2**.

After tissue fixation by cardiac perfusion of 4% PFA the aortic tree was located in the thoracic cavity and excised from the mouse as previously described in Section 2.2.2.1. The carotid arteries were cut off the aortic tree above the level of the aortic arch and above the carotid artery bifurcation as shown in **Figure 4.10**.

The left-ligated and AAV-transduced carotid artery was embedded alongside the non-ligated contralateral right artery. The carotid arteries were orientated with the external and internal carotid bifurcation facing down against the block mould. In this way, sections were cut from the carotid bifurcation toward the aortic arch. The block was trimmed at 20 µm until the two lumens of the internal and external carotid arteries converged. A 5 µm section was collected and then three more sections at 200 µm along the aortic tree (0 µm, 200 µm, 400 µm and 600 µm).

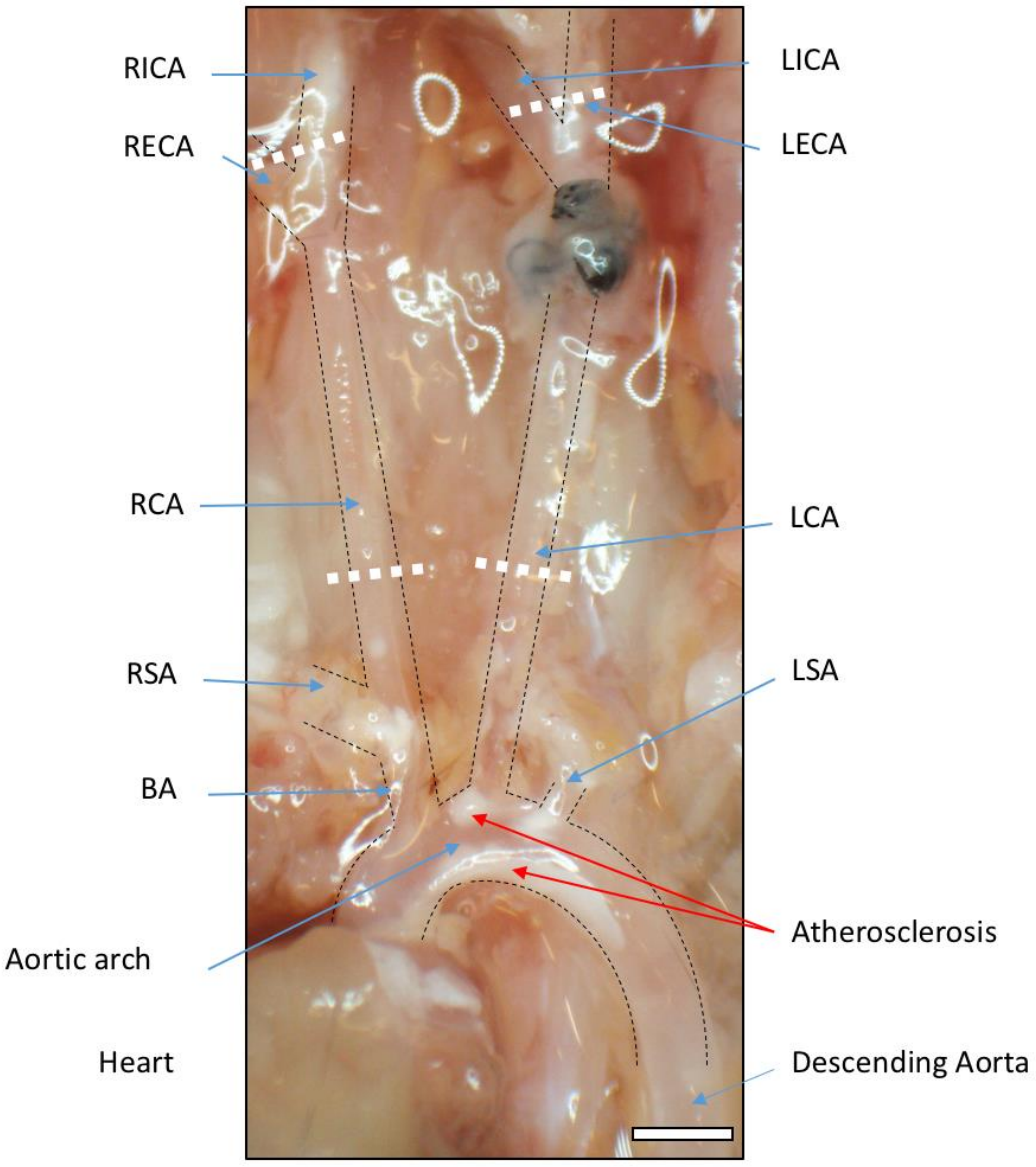

Figure 4.10: Intact aortic arch from a control-mouse at 20-weeks age. *At 20-weeks age mice were euthanised by CO_2 overdose and then perfusion fixed with 4% PFA. Excess adipose tissue was trimmed away from the aortic arch and associated branches. Black dotted line shows outline of the aortic tree. White dotted lines show where the carotid artery was dissected. Anatomy of the aortic tree indicated by blue arrows; right internal carotid artery (RICA), right external carotid artery (RECA), right carotid artery (RCA), right subclavian artery (RSA), brachiocephalic artery (BA), left subclavian artery (LSA), left carotid artery (LCA), left external carotid artery (LECA) and left internal carotid artery (LICA). Red arrows indicate regions of foam cell lesion growth. Scale bar = 1000 µm.*

4.2.3.2 Fluorescent microscopy

Whole transverse carotid sections were illuminated using a CoolLED fluorescence illuminator on an Olympus BX-50 (Olympus Corporation, Tokyo, Japan) compound widefield fluorescence microscope and digitally photographed with a Spot-RT slider (SPOT Imaging Solutions: Diagnostic Instruments, Inc., Sterling Heights, MI) cooled digital microscope camera. Illumination and exposure conditions were carefully controlled to eliminate sample to sample variation.

4.2.4 Statistics

All data was analysed on GraphPad Prism 8 ad is expressed as mean $\pm$ SEM. Significant differences were determined by Students unpaired t-test.

4.3 Results

4.3.1 Validation of CaMKIIδ_2-/control-mCherry AAV particles in vitro.

Before any AAV particles expressing CaMKIIδ_2- or control-mCherry were transduced into the carotid arteries of ApoE$^{-/-}$ mice, they were first tested *in vitro*. The primary objective of producing the AAV particles was to over-express CaMKIIδ_2 in the carotid artery, so, a human vascular cell culture model was used mimic cell groups more closely.

Human coronary artery smooth muscle cells (HCASMCs) and human umbilical vein endothelial cells (HUVECs) were cultured, as previously described, and 5 x 10^8 PFU of either CaMKIIδ_2-, CaMKIIδ_6-, or control-mCherry was transduced and incubated for 24 hr. An additional AAV variant CaMKIIδ_6, generated in a previous experiment was also included to serve as an additional control of a validated variant. Post-24 hr, total RNA was extracted and RT-PCR performed targeting huV1 (δ_2 and δ_6 variants) in a thermocycler. Products of PCR were visualised by agarose gel electrophoresis (*Section 2.2.3*).

Figure 4.11 shows the relative mRNA level of CaMKIIδ_2- and CaMKIIδ_6- in human vascular cells. In both HCASMCs and HUVECs, the presence of a band at 130 bp and 190 bp, indicated by the blue arrows is indicative of the CaMKIIδ_2 and CaMKIIδ_6 transcript, respectively. In HCASMCs and HUVECs transduced with CaMKIIδ_2 there was an observed increased intensity in band product. In addition, CaMKIIδ_6 transduced HCASMCs and HUVECs had a band present at 190 bp, which was not present in the other groups. These findings validate that the AAV-CaMKIIδ_2- or CaMKIIδ_6 mCherry are promoting CaMKIIδ expression levels.

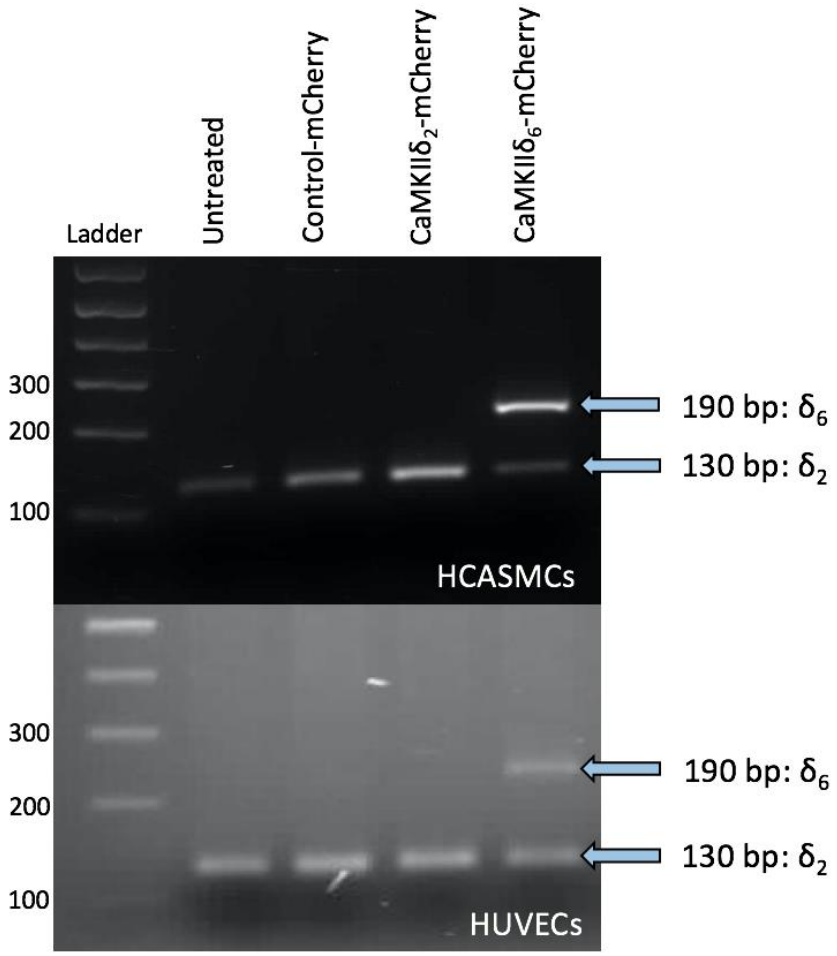

Figure 4.11: DNA agarose gel showing CaMKIIδ variant levels in HUVECs and HCASMCs transduced with either control-, CaMKIIδ$_2$- or CaMKIIδ$_6$-mCherry. *HUVECs and HCASMCs were left untreated or transduced with 5 x 10^8 PFU of either control-, CaMKIIδ$_2$- or CaMKIIδ$_6$-mCherry and incubated for 24 hr. Total RNA was extracted and 100 ng cDNA used in RT-PCR targeting the huV1 primer set. PCR products were loaded into a 1.5% agarose gel and electrophoresis run at 90 V for 1 hr. 100 bp DNA marker (Invitrogen cat.no. 15628019).*

4.3.2 Ligation of the left carotid artery (LCA) of ApoE$^{-/-}$CaMKII$\delta^{-/-}$ mice causes gross morphological changes to the vascular wall.

At 16-weeks of age, the LCA of ApoE$^{-/-}$CaMKII$\delta^{-/-}$ mice fed a HFD for the previous 2-weeks was surgically accessed and ligated to increase shear stress and promote atherogenesis. 5 x 10^8 PFU of either control- or CaMKIIδ_2- was applied to the arterial tissue via a pluronic gel. The incision was closed and the mice monitored over recovery before being returned to animal housing. Eight mice did not survive the experiment. In the two-day post-surgical monitoring period, four mice from each control and dKO group were euthanised for welfare reasons. These mice showed signs of head nodding, irritation, vocalisation and ataxia indicative of some degree of stroke.

At 20-weeks of age, the mice were perfused fixed as described in *Section 3.2.1.2* and the left ligated and right non-ligated carotid artery dissected and laid flat under a dissection microscope. **Figure 4.12** shows four sets of left and right carotid arteries from ApoE$^{-/-}$CaMKII$\delta^{-/-}$ mice treated with either CaMKIIδ_2- (CaMKIIδ_2) or control-mCherry (control) AAVs (n = 4/8). What became immediately striking was the variation in the appearance of the left ligated carotid artery. In both control and CaMKIIδ_2 groups there was a range of atherosclerosis from small pockets of foam cell lesion growth to extensive atherosclerotic lesions and vascular remodelling. Interestingly, in the CaMKIIδ_2 treated mice, three out of eight left ligated carotid arteries had evidence of thrombolysis, indicated by the appearance of clotted blood through the vascular wall (**Figure 4.12E & H**).

In contrast, by gross observation, the non-ligated right carotid artery had a more translucent and this was consistent between and across groups. **Figure 4.12I** highlights the importance of distinguishing between perivascular adipose tissue, fat on the outside of the artery, and foam cell lesion growth when making observations of atherosclerosis in the arteries.

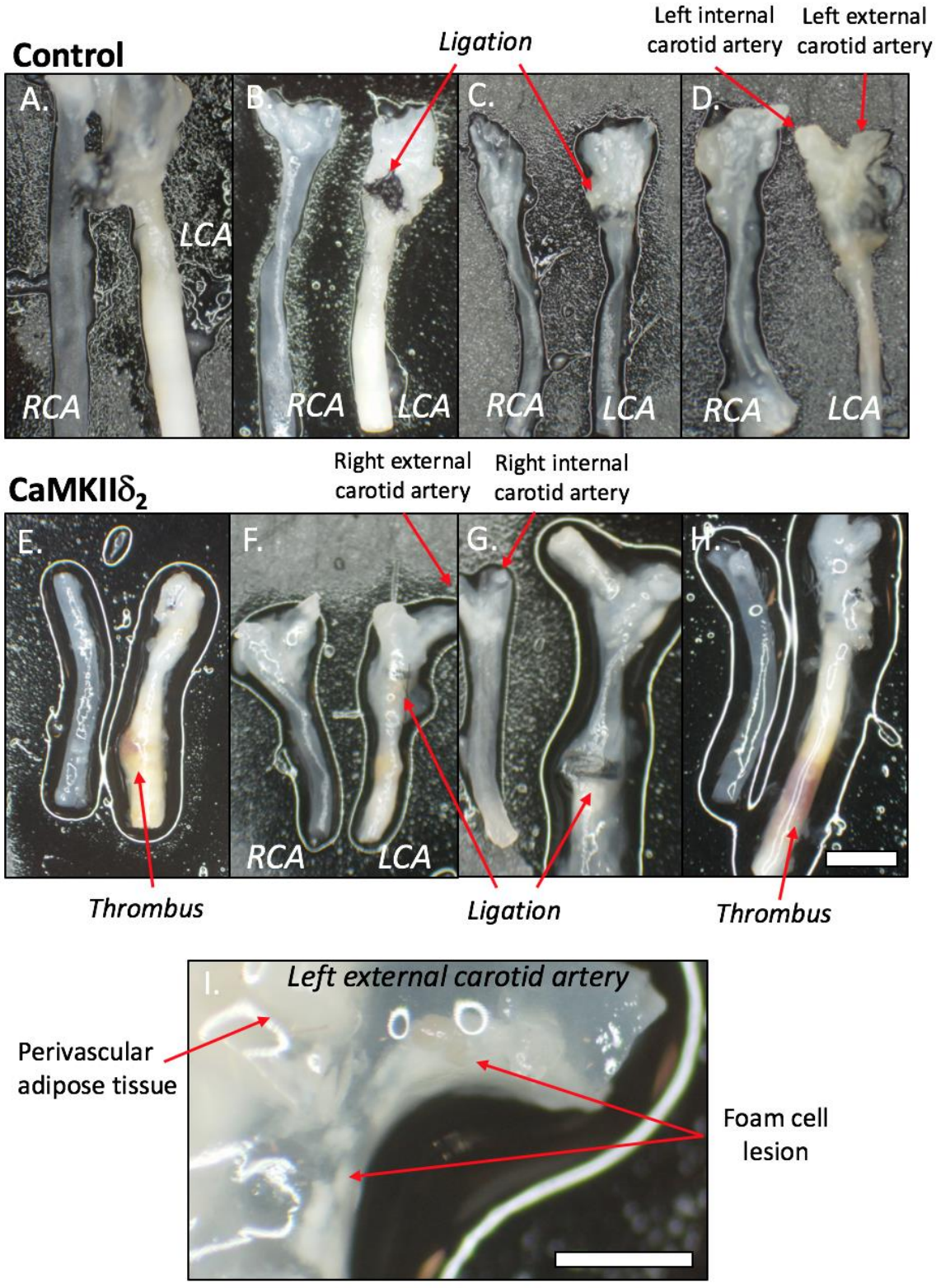

Figure 4.12: Dissected left-ligated and right carotid arteries from ApoE$^{-/-}$CaMKIIδ$^{-/-}$ mice treated with either control- or CaMKIIδ$_2$-mCherry. *Mice were perfusion fixed with 4% PFA and left (LCA) and right carotid arteries(RCA) dissected. Anatomical features of the carotid artery include foam cell lesions, perivascular adipose tissue, thrombus and ligation tie indicated by red arrows and labels. Scale bar for top panels = 1000 µm, bottom photo = 200 µm. Representative panels show four out of eight mice for each treatment group (n = 8).*

4.3.3 Ligation of the carotid artery in ApoE$^{-/-}$CaMKII$\delta^{-/-}$ mice rapidly promotes foam cell lesion development and arterial wall remodeling.

AAV-transduced left-ligated and right carotid artery of ApoE$^{-/-}$CaMKII$\delta^{-/-}$ mice were embedded in paraffin wax as described in *Section 4.2.3.2.* The carotid artery was sectioned in a cross-sectional plane from the bifurcation of the external and internal carotid artery toward the aortic arch. The non-ligated right carotid artery was used in a later experiment to assess specificity of mCherry expression.

Figure 4.13-14 are representative images of sections collected along the carotid artery of four mice transduced with either control- or CaMKIIδ_2-mCherry, respectively (n = 8 total). In the left carotid artery of mice transduced with control-mCherry, there were variable amounts of foam cell lesions present to different degrees of progression. In **Figure 4.13A** there is foam cell lesion present around the majority of the inner wall of the carotid artery. Furthermore, foam cell lesions are also present in the subsequent section (**A2**) but then are not present to the same extent in the last two sections (**A3-4**). Contrast this with representative section **D1-4** where there is an area of foam cell lesion development present in the first section but no observable lesions in the subsequent three sections (**D2-4**).

In the sections from mice transduced with CaMKIIδ_2-mCherry, there was atherosclerosis present (**Figure 4.14**). Foam cell lesions present in the carotid artery, ranging from medium size lesions that occupied one side of the vessel wall (**B2**), to large continuous lesions, which occupied a large area of the lumen space (**A2**). Like the control mice, in the latter section, foam cell lesion content seemed to decrease dramatically and in some sections in these mice there was no observable lesion growth (**Figure 3.14A4, B3, B4, D4**). Interestingly, in **Figure 3.14C1-C4,** instead of the characteristic grey 'soap bubble' like cells composing the lesions there was a growth in the lumen which was a combination of brown and pink stained tissue indicating VSMCs and extracellular matrix. This is likely inward remodelling (proliferation of VSMCs) in response to a dramatic change in flow/ shear stress patterns.

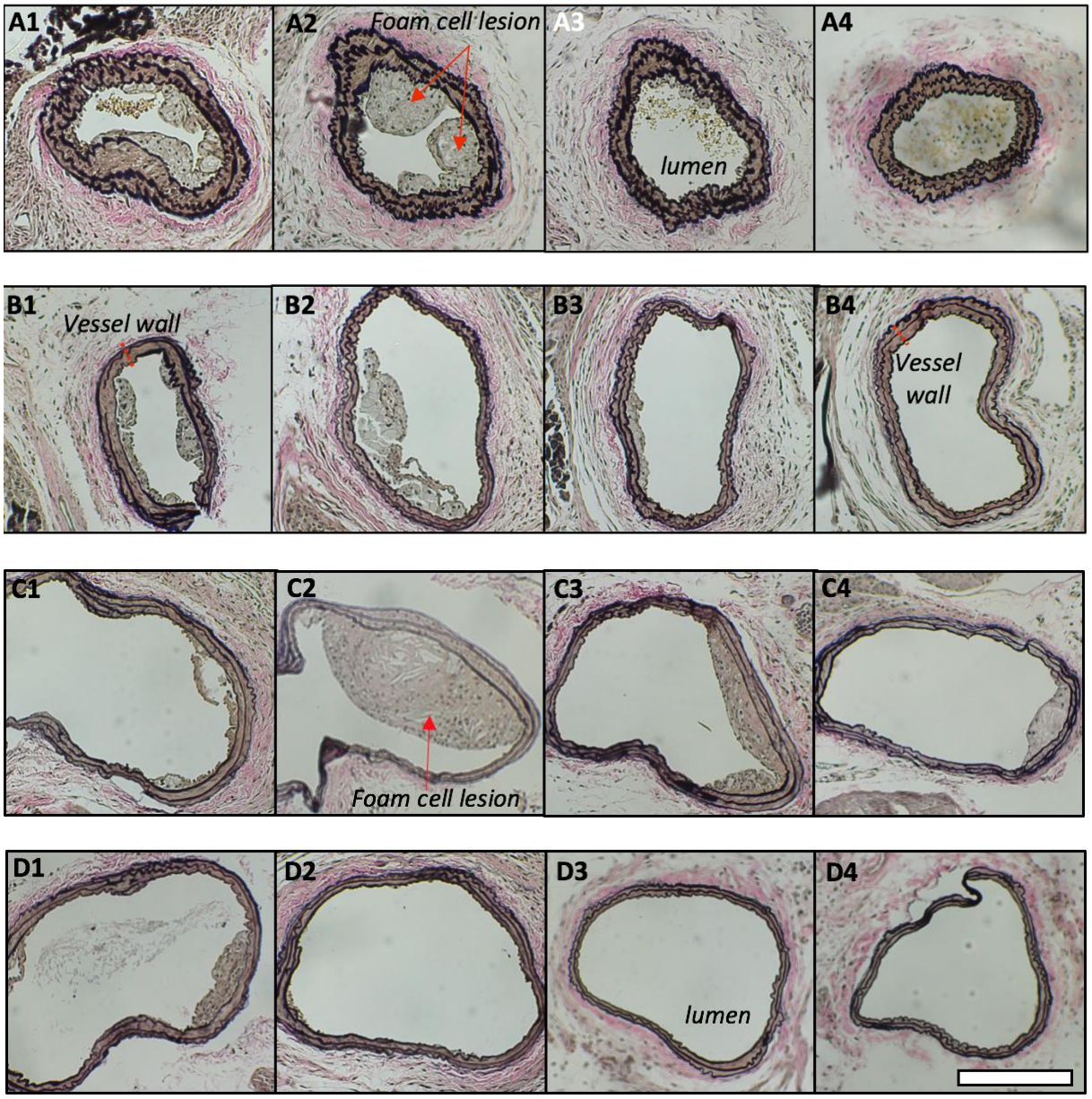

Figure 4.13: Foam cell lesions in the left-ligated carotid artery of ApoE$^{-/-}$CaMKIIδ$^{-/-}$ mice transduced with control-mCherry. At 16-weeks of age ApoE$^{-/-}$CaMKIIδ$^{-/-}$ mice underwent surgical ligation of the left carotid artery. 5 x 10^8 PFUs of control-mCherry was applied to the left carotid artery in a pluronic gel (20%). Mice were euthanised at 20-weeks and perfusion fixed with 4% PFA. Four 5 µm section were collected in 200 µm intervals from the internal and external carotid bifurcation toward the aortic arch (**1-4**). Sections were stained with Verhoeff van Gieson. Shown above in each panel (**A-D**) is a representative of the carotid artery sections from four out of eight control-treated mice. Red arrows indicate foam cell lesions. White scale bar = 200µm.

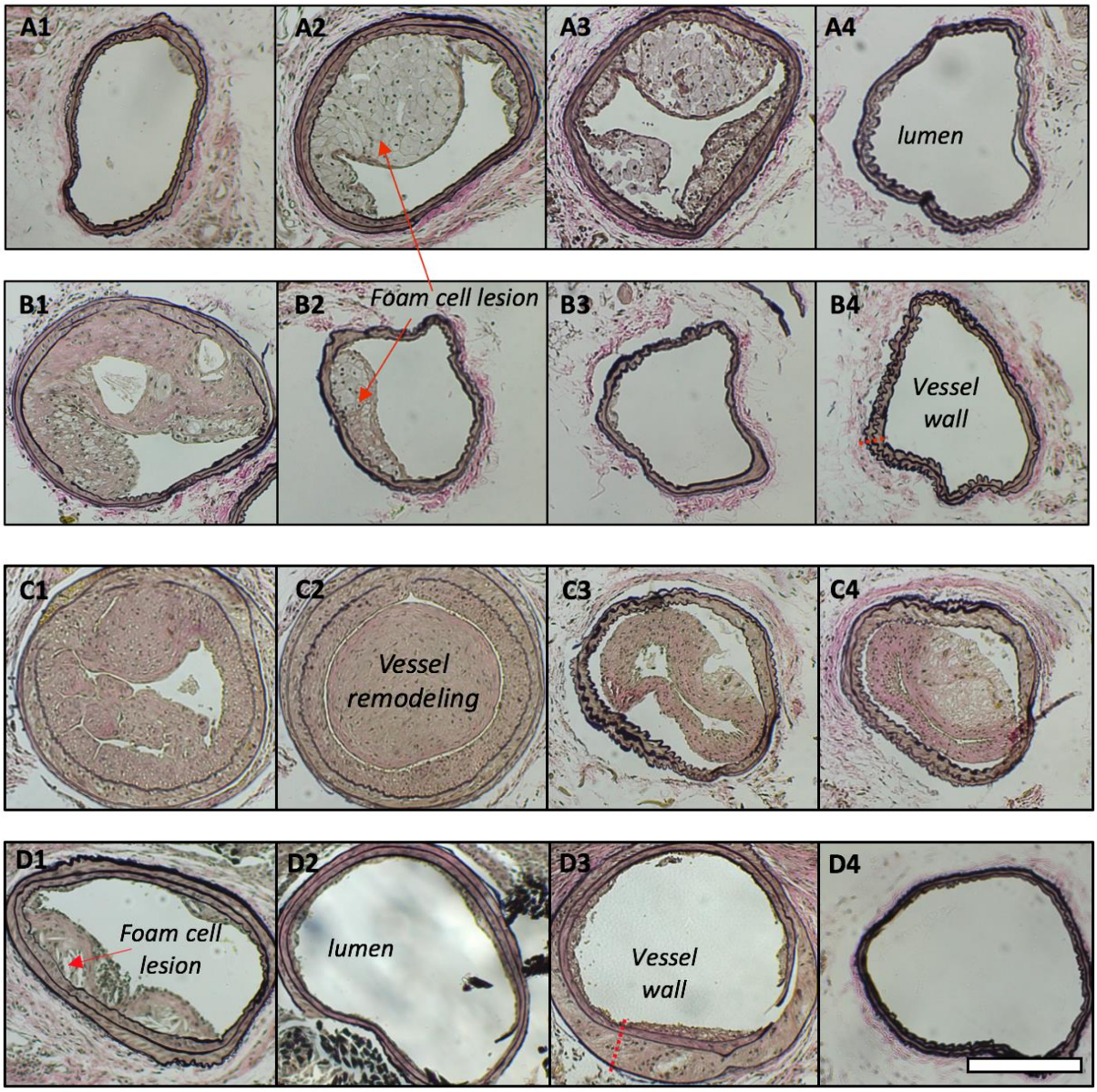

Figure 4.14: Foam cell lesions in the left-ligated carotid artery of ApoE$^{-/-}$CaMKII$\delta^{-/-}$ mice transduced with CaMKIIδ_2-mCherry. *At 16-weeks of age ApoE$^{-/-}$CaMKII$\delta^{-/-}$ mice underwent surgical ligation of the left carotid artery. 5 x 10^8 PFUs of* CaMKIIδ_2-mCherry *was applied to the left carotid artery in a pluronic gel (20%). Mice were euthanised at 20-weeks and perfusion fixed with 4% PFA. Four 5 µm sections were collected in 200 µm intervals from the internal and external carotid bifurcation toward the aortic arch (**1-4**). Sections were stained with Verhoeff van Gieson. Shown above in each panel (**A-D**) is a representative of the carotid artery sections from four out of eight control-treated mice. Red arrows indicate foam cell lesions. White scale bar = 200 µm.*

4.3.4 Detection of mCherry fluorescence in the carotid arteries of ApoE$^{-/-}$ CaMKII$\delta^{-/-}$ mice transduced with CaMKIIδ_2- and control-mCherry.

To confirm a successful AAV transduction, the left-AAV-transduced and right carotid artery of ApoE$^{-/-}$ CaMKII$\delta_2^{-/-}$ were analysed for mCherry fluorescence. CaMKIIδ_2 and control AAV particles contained a red mCherry tag that allowed detection of virus transduction in the vascular wall. Four sections of the left and right carotid arteries of mice were cut along the length of the carotid artery. The right non-ligated artery was used to identify whether the AAV transduction was specific to the left carotid artery. Carotid sections were illuminated using a CoolLED fluorescence illuminator on an Olympus BX-50 (Olympus Corporation, Tokyo, Japan) and digital images captured.

Figure 4.15 shows the left-ligated and right carotid artery of a CaMKIIδ_2 mouse both, stained with VVG (**1.A-D** & **3.A-D**) and imaged under a fluorescent microscope (**2.A-D** & **4.A-D**). There was red fluorescence in the vessel wall of the left carotid artery sections indicating mCherry expression. Furthermore, in the right non-treated sections, there was also red fluorescence (**4.A-D**). This suggests the virus was not localised to the left carotid artery. Interestingly, there was no red fluorescence in the foam cell lesion region of the sections. A carotid artery and aortic sinus section from an untreated control mouse was also imaged. In these control sections, under low emission there was still some red fluorescence. This was surprising and indicates the vascular wall has an element of auto-fluorescence.

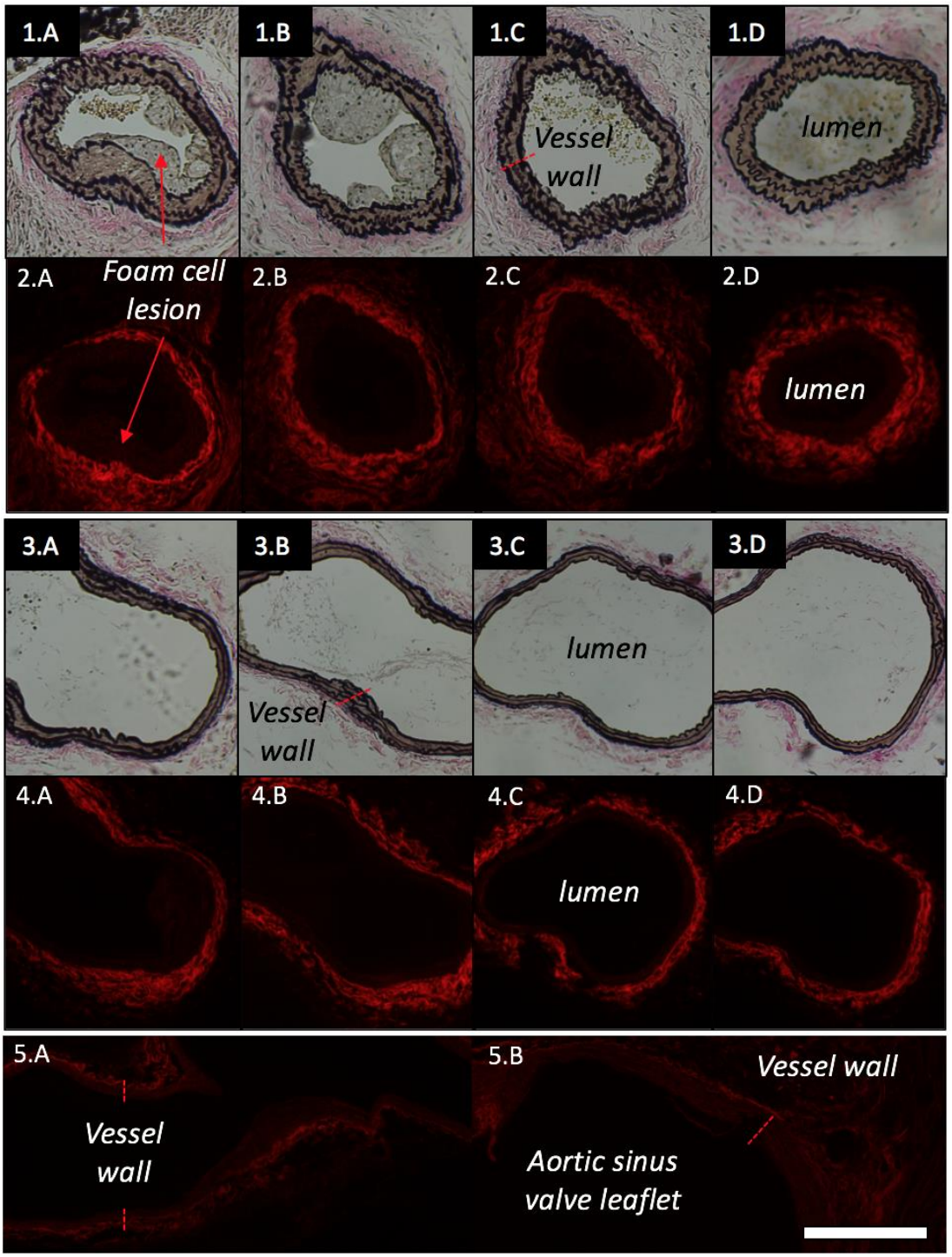

Figure 4.15: Detection of mCherry fluorescence in the left ligated and right non-ligated carotid artery of control and CaMKIIδ_2 mice. At 16-weeks of age ApoE$^{-/-}$CaMKII$\delta^{-/-}$ mice underwent surgical ligation of the left carotid artery. 5 x 10^8 PFUs of CaMKIIδ_2-mCherry was incubated over the left carotid artery in a pluronic gel (20%). Mice were euthanised at 20-weeks and perfusion fixed with 4% PFA. Four 5 µm sections of the left and right carotid artery were collected in 200 µm intervals from the internal and external carotid bifurcation toward the aortic arch (1.A-D left carotid, & 3.A-D right carotid). Carotid sections were illuminated using a CoolLED fluorescence illuminator on an Olympus BX-50 (Olympus Corporation, Tokyo, Japan) compound widefield fluorescence microscope and digitally photographed with a Spot-RT slider (SPOT Imaging Solutions: Diagnostic Instruments, Inc., Sterling Heights, MI) cooled digital microscope camera (2.A-D left carotid, 4.A-D right carotid, 5.A control carotid, 5.B control aortic sinus. Red arrows indicated foam cell lesions. The red dotted line shows the vessel wall region (5B). Scale bar = 200 µm.

4.3.5 CaMKIIδ_2 has no effect on vessel wall hypertrophy in response to ligation of the left carotid artery in ApoE$^{-/-}$CaMKII$\delta^{-/-}$ mice.

The primary focus of the current experiment was to identify the impact of CaMKIIδ_2 on foam cell lesion growth in the carotid arteries of ApoE$^{-/-}$CaMKII$\delta^{-/-}$ mice. CaMKIIδ_2 has been shown to play a role in proliferative response of VSMCs after arterial injury [219]. Therefore, firstly it was measured if CaMKIIδ_2 promotes hypertrophy of the vessel wall after ligation of the left carotid artery.

The left carotid artery of mice from control- and CaMKIIδ_2-mCherry groups was sectioned and stained with VVG as previously described (*Section 4.2.3.2*). Vessel wall width was indicated by the boundary of the IEL stained black (**Figure 4.13-14**). In both control and CaMKIIδ_2 groups, there were sections containing extensive hypertrophy of the vessel wall (**Figure 4.13A1 & C2, Figure 3.14C2 & D3**). In contrast there were also sections that displayed no hypertrophy and the IEL remained tightly bound (**Figure 13B3 & D4, Figure 14A4 & D4**).

Eight regions of the vessel wall were measured on all four sections in both mice groups and the mean was calculated. There were no significant differences in vessel wall width in the 0 µm, 200 µm, 400 µm and 600µm section between CaMKIIδ_2 and control groups (N.S, p = 0.3, 0.5, 0.9,0.6, respectively, n = 8) (**Figure 4.16**). Furthermore, vessel width was around 30 µM in both groups and did not change over the length of the carotid artery. This indicates that CaMKIIδ_2 does not promote hypertrophy of the carotid artery wall.

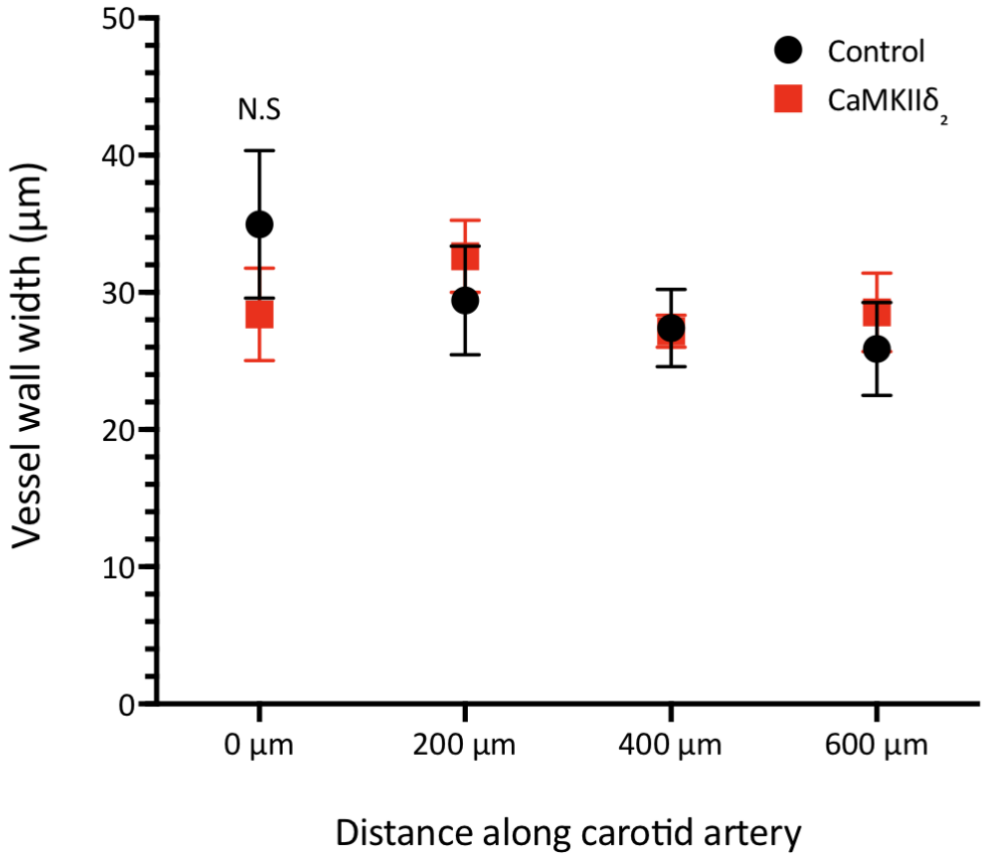

Figure 4.16: Vessel wall width quantification in the left-ligated carotid artery of ApoE$^{-/-}$CaMKIIδ$^{-/-}$ mice transduced with control- or CaMKIIδ$_2$-mCherry. *Four 5 µM sections were cut in 200 µm intervals throughout the carotid artery from the internal and external carotid bifurcation toward the aortic arch (0 µM, 200 µM, 400 µM, 600 µM). Sections were stained with VVG and eight measurements of the vessel wall width were taken per section and the mean calculated. Graph shows vessel wall width (µM) as mean ±S.E.M. Not significant (N.S) as determined by unpaired Students t-test (n = 8).*

4.3.6 Examining the effect of CaMKIIδ_2 on foam cell lesion growth in an accelerated model of atherosclerosis.

Next, it was investigated if CaMKIIδ_2.has any effect on foam cell lesion growth in the left-ligated carotid arteries of ApoE$^{-/-}$CaMKII$\delta^{-/-}$ mice. Carotid artery sections were stained with VVG and foam cell lesion area was measured (0 µm, 200 µm, 400 µm, 600 µm sections). Shown in **Figure 4.13-14** and indicated by the red arrows are foam cell lesions present in the carotid artery of ApoE$^{-/-}$CaMKII$\delta^{-/-}$ mice transduced with either control- or CaMKIIδ_2-mCherry, respectively. There was foam cell lesion development in the carotid artery of both groups and lesions ranged in progression.

Although the mean foam cell lesion area was higher across all four sections in the CaMKIIδ_2, there were no significant differences compared to control group (n = 8, N.S, p = 0.4, 0.5, 0.2, 0.3, respectively) (**Figure 4.17**). The area under the curve was measured across all four sections to calculate foam cell lesion volume. In control and CaMKIIδ_2 mice the mean foam cell lesion volume was 387 $\pm$ 92 µm^3 and 594 $\pm$ 128 µm^3. When each group was compared there was no significant difference in foam cell lesion volume (N.S, p = 0.2, n =8) (**Figure 4.17**).

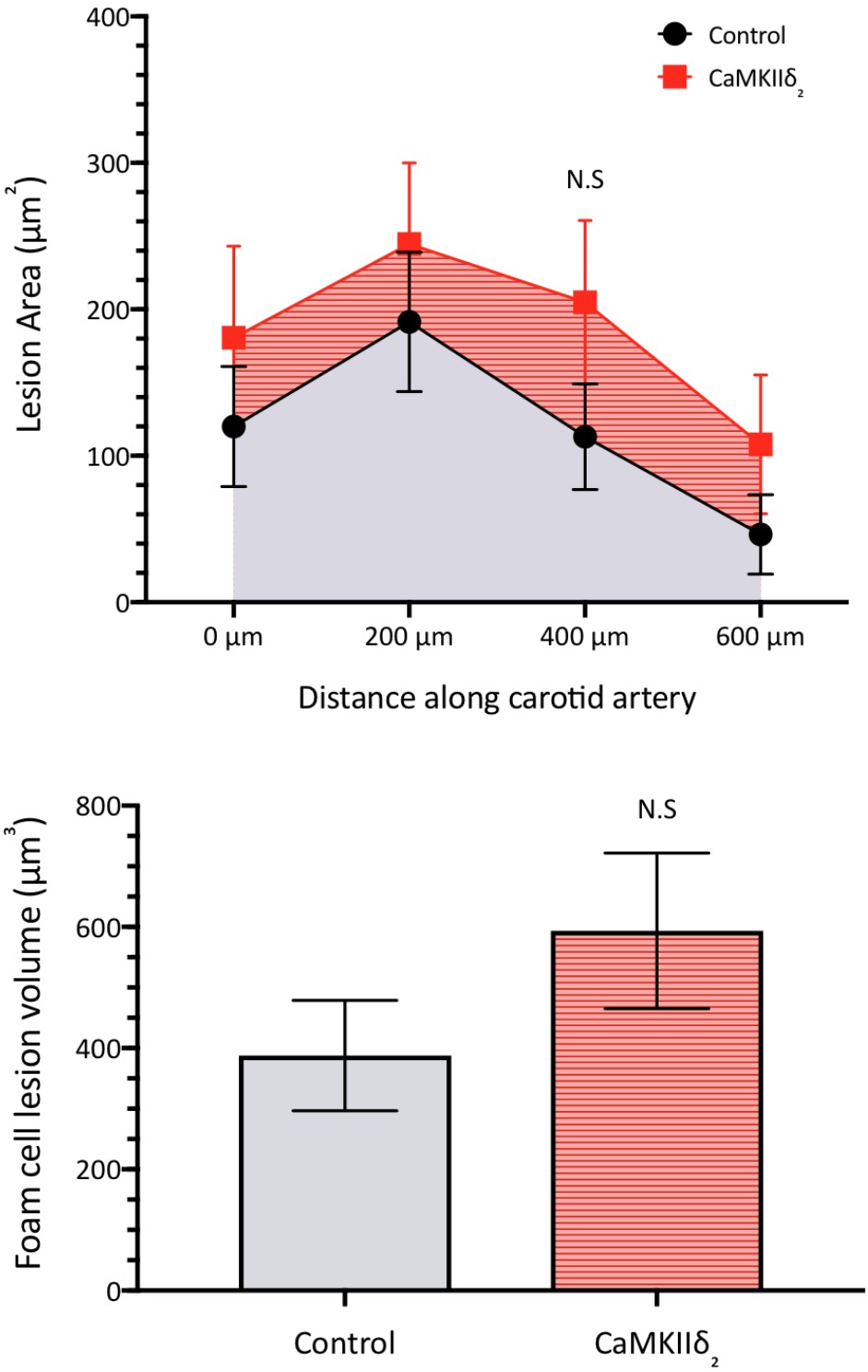

Figure 4.17: Foam cell lesion quantification in the left-ligated carotid artery of ApoE$^{-/-}$CaMKIIδ$^{-/-}$ mice transduced with control- or CaMKIIδ$_2$-mCherry. *Four 5 µM sections were cut in 200 µm intervals throughout the carotid artery from the internal and external carotid bifurcation toward the aortic arch (0 µM, 200 µM, 400 µM, 600 µM). Sections were stained with VVG and foam cell lesion area measured in each section (Above). The area under the curve was measured to calculate foam cell lesion volume (Below) Data on graphs is presented as mean foam cell lesion ± S.E.M. Not significant (N.S) as determined by unpaired Students t-test (n = 8).*

4.3.7 Evaluating stenosis in the ligated carotid arteries of ApoE$^{-/-}$CaMKII$\delta^{-/-}$ mice transduced with CaMKIIδ_2- and control-mCherry.

The CaMKIIδ_2 mice did not show a significant increase in foam cell volume compared to control, regardless of having higher mean foam cell areas for each set of sections (**Figure 4.17**). Even though foam cell lesion was the primary investigation, it was next identified if there were differences in stenosis along the carotid artery between control- and CaMKIIδ_2 mice. Stenosis is a useful functional measurement as it provides an indication of the physical obstruction the foam cell lesion relative to the size of the lumen.

The inner circumference of the left-ligated carotid artery sections from control- and CaMKIIδ_2-mCherry mice was measured to calculate lumen area. Using the foam cell lesion area data and lumen area stenosis (%) was calculated as shown in **Figure 4.18**. Both groups showed a similar trend in stenosis as seen in foam cell lesion area with an increase from 0 µm to 200 µm and then a steady decline to 600 µm. The mean stenosis percentages in the control- group was 10.4 $\pm$ 4.3 % (0 µm), 25.4 $\pm$ 9.8 % (200 µm), 16.3 $\pm$ 9.4 (400 µm) and 10.5 $\pm$ 9.8 % (600 µm). In comparison the mean stenosis of the CaMKIIδ_2 group was 27.7 $\pm$ 12.3 % (0 µm), 43.5 $\pm$ 12.2 % (200 µm), 32.4 $\pm$ 11.5 (400 µm) and 19.7 $\pm$ 11.6 % (600 µm). Although mean stenosis in CaMKIIδ_2 group was higher than control group across all four sections, there were no significant differences (n = 8, N.S, p = 0.2, 0.3, 0.3, 0.6, respectively).

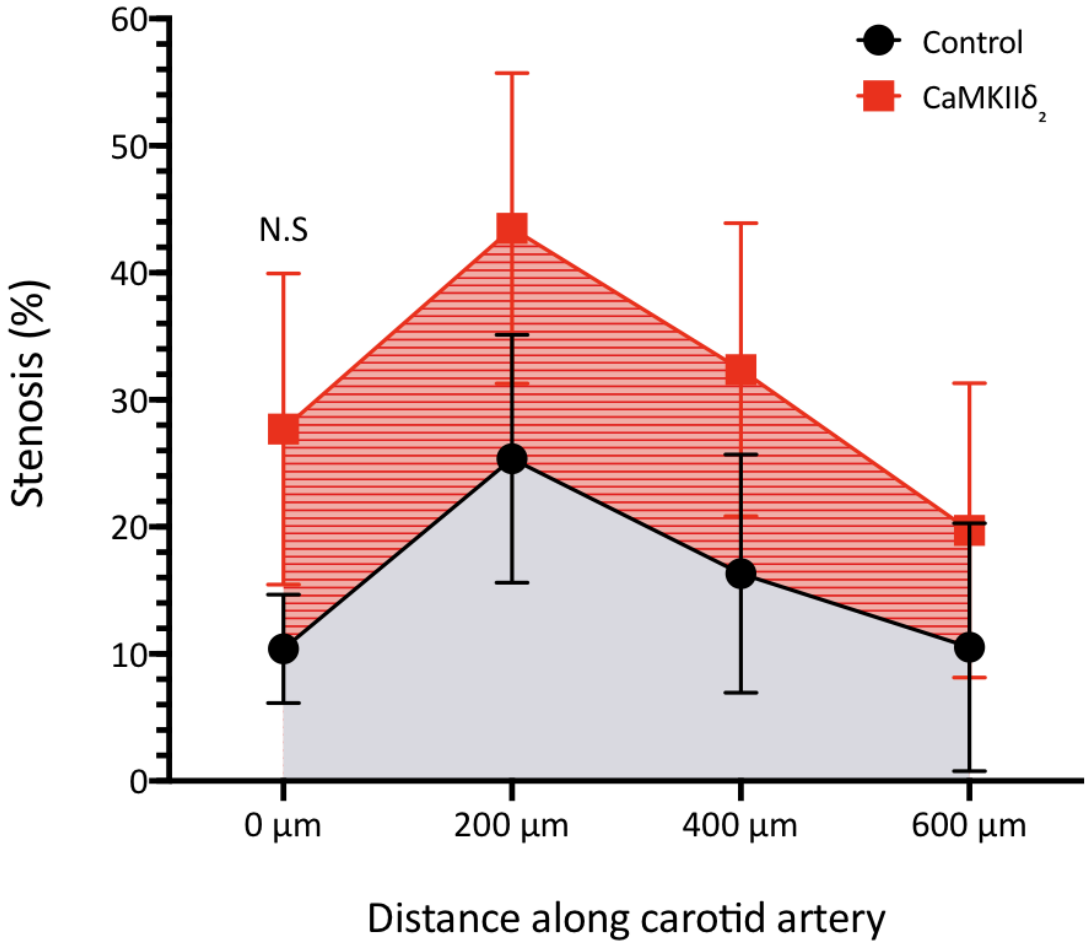

Figure 4.18: Stenosis quantification in the left-ligated carotid artery of ApoE$^{-/-}$CaMKIIδ$^{-/-}$ mice transduced with control- or CaMKIIδ$_2$-mCherry. *Four 5 µm sections were cut in 200 µm intervals throughout the carotid artery from the internal and external carotid bifurcation toward the aortic arch (0 µm, 200 µm, 400 µm, 600 µm). Sections were stained with VVG. The inner circumference of the lumen was measured to calculate lumen area. Foam cell lesion area was divided by lumen area to calculate stenosis (%). Data on graphs is presented as mean foam cell lesion ± S.E.M. Not significant (N.S) as determined by unpaired Students t-test (n = 8).*

4.4 Discussion

In this final chapter, an AAV-mediated overexpression approach was employed to identify the contribution of CaMKIIδ_2 to foam cell lesion development. CaMKIIδ_2-expressing AAV particles were introduced to the left-ligated carotid artery of ApoE$^{-/-}$CaMKII$\delta^{-/-}$ mice. Ligation of the carotid artery alters blood flow and shear stress, creating a local milieu that promotes atherogenesis [34, 35, 250-252]. After 4-weeks the carotid arteries were processed for histology and sections analysed for foam cell lesion area/volume (μm^2, μm^3), stenosis (%), and vessel wall width.

Foam cell lesions were variable in the carotid arteries of CaMKIIδ_2- and control-mCherry mice, indicated by the high SEM for mean lesion area for each section (**Figure 4.17**). In both groups, lesions ranged from small pockets of growth containing a small number of foam cells, to extensive foam cell lesions, that had a more advanced phenotype (**Figure 4.13-14**). This included the appearance of lipid pool accumulation and fibrous cap formation (**Figure 4.13C2**, & **Figure 4.14A2, B1, A2**). This is likely to reflect differences in consumption of the high-fat diet between mice. LDL-C is the major risk factor for the development of atherosclerosis [14-16]. LDL-C entry and exit in foam cells is tightly regulated and when lipid accumulation exceeds storage capabilities, lipid pooling occurs [62-64].

Next, it was analysed what influence CaMKIIδ_2-mCherry transduction had in the surgically-induced pro-atherogenic environment. After four-weeks of incubation there was red fluorescence detected in the vascular wall of the left ligated carotid artery of both control- and CaMKIIδ_2-mCherry groups (**Figure 4.15**). This indicated the AAVs had successfully transduced into the vascular wall. CaMKIIδ_2-mCherry mice had increased foam cell lesion area in the four sections analysed along the length of the carotid artery compared to control-mCherry mice. However, when this data was compared to control group, there were no significant differences in foam cell area or volume (**Figure 4.17**). The lack of significance in lesion area and volume between groups is likely to reflect a low n number. Initially, twenty animals were randomly allocated into either control-mCherry, or CaMKIIδ_2-mCherry groups (n = 10). However, problems with recovery meant four mice across both groups were euthanised for welfare reasons, which will be discussed later. With the low n numbers and trending significance in mind, this data suggests CaMKIIδ_2 is likely to promote foam cell lesion

development, however, a full sample size is required to determine whether there is a significant effect.

To gain some idea of the functional impact foam cell lesions were causing on blood flow in the carotid artery, stenosis was calculated. Stenosis is a useful measurement as it calculates what area of the lumen is occupied by foam cell lesions. This is important as impeding blood flow is a major mechanism of ischaemic injury such as stroke [253, 254]. For example, if lesion area is extensive but lumen area is large, there is less stenosis than if that same lesion was present in a smaller artery. Stenosis (%) along the length of the carotid artery showed a similar trend to foam cell lesion area in both groups. This was an initial increase 0 μm – 100 μm followed by a reduction over the 400 μm and 600 μm measurement points (**Figure 4.17**). Although there were no significant differences between groups, likely due to low n numbers, the stenosis area was higher on average across each measurement point of the carotid artery in CaMKIIδ_2 groups.

In Chapter 3, CaMKIIδ knock out resulted in a reduction in foam cell lesion development in the aortic sinus. Therefore, in this experiment, it was hypothesised CaMKIIδ_2 would augment carotid artery foam cell lesion development. The CaMKIIδ isoform is the predominant subtype expressed in cells of the vascular wall and has been linked to endothelial and VSMC pathology [181, 212, 218, 219, 255]. From what is known about variant specific functions the δ_2 has shown roles in VSMC proliferation and migration whereas δ_6 has been associated with endothelial dysfunction [212, 219, 220]. In these studies, the pathologies were examined in an independent setting, however, the mechanisms involved collectively contribute to the pathogenesis of atherosclerosis [13]. It is reasonable to then speculate that CaMKIIδ_2 is most likely contributing to foam cell lesion growth through its effects in VSMCs rather than in endothelial cells. This is also evidenced as mCherry fluorescence was localised to the media layer of the artery wall rather than cells on the luminal surface (**Figure 4.15**). In the production of the CaMKIIδ_2 , an additional variant δ_6 was generated in parallel. In the future, it would be interesting to transduce CaMKIIδ_6, a variant known to promote endothelial dysfunction, into the left-ligated carotid arteries in a similar manner to identify and compare the relative contribution to foam cell lesion development.

Across the foam cell lesion area and stenosis data, what was evident was the variation in both groups suggesting optimisation of the model is still required. Already, it has been discussed that differences in the amount of HFD eaten are likely to contribute to more advanced lesion characteristics, and this is the same with foam cell lesion progression [162, 256]. Another reason for the variation in data is the extent of ligation. For the purpose of these experiments, ligating the carotid artery was used to alter shear stress to promote endothelial dysfunction and atherogenesis [249-251]. In the surgical procedure, ligation of the left-carotid artery was achieved by tying a piece of silk around the artery and a piece of nylon, which was later removed, so the area reduced was the same between mice (*Section 4.2.3.1*). However, the manipulation was carried out under microscope on a relatively small region of the mouse aortic tree, so it is likely there is an element of surgical error. In addition, the initial ligations may have been similar at the time of surgery, but under conditions of high pressure, pulsatile flow could have loosened the ligation over the following four-week period. Together, the variation in how individual mice respond to HFD and the potential surgical error result in a high SEM in both groups suggesting further refinement of the technique is required.

Further to these technical issues, the variation in data could also be confounded by sex differences. Male and female data groups were pooled in this study. Female ApoE$^{-/-}$ mice on a C57/Bl6 background develop atherosclerosis at a faster rate than males [236, 237, 239] (**Figure 3.14**). Because of these sex differences in lesion progression, atherosclerosis assessment in the ApoE$^{-/-}$ mouse should be grouped as males and females. In the case of this experiment, mice were fed a HFD and the left carotid artery ligated to promote atherosclerosis. Both diet and surgical manipulation are strong stimuli for atherosclerosis so it is possible sex as a driver was overridden by these other factors over this four-week period, however it cannot be discounted [162, 256, 257]. In future experiments, increasing the n number to allow for sex-dependent analysis of data may also help to reduce variation.

An important aspect of the model used in this study is that the ligation was performed on an atherosclerotic background (ApoE$^{-/-}$CaMKII$\delta^{-/-}$). Without the elevated LDL-C levels, wild-type mice do not develop atherosclerosis even with surgical manipulation [158, 249, 258, 259]. Carotid ligations are also used in models of flow remodeling. In these vascular diseases, the structure of the vascular wall changes to compensate for changes in flow and blood pressure. Collectively, these studies have used a range of approaches from partial to complete ligations

and have applied the ligation to different regions of the carotid branches including the internal and external carotid artery [249, 259-262]. In wild-type mice, ligation of the carotid artery causes injury to the vascular wall promoting the release of inflammatory mediators which promote VSMC phenotype switch from contractile to synthetic [263]. The synthetic phenotype is characterised by increased proliferation, migration and ECM production [72]. This leads to the expansion of the intimal region of the artery wall, termed neo-intima, as VSMCs migrate to the intima and generate ECM [262].

With these other ligation approaches in mind, it was expected that there may be some elements of vascular remodeling independent of foam cell lesion growth and, indeed, this was observed in some of the carotid sections (**Figure 4.13-14**). It was important we could differentiate between foam cell lesion development and vascular remodeling [264]. This was achieved by using the VVG stain which stained foam cells grey and VSMCs and ECM brown and pink, respectively. Vascular remodeling in both groups of mice ranged from hypertrophy of the media wall layer (**Figure 4.13 B4** & **C3**) to striking neo-intima (**Figure 4.14 B1** & **C4**). formation shown by pink and brown staining. As we saw some remodeling in the carotid artery sections across both groups, vessel wall width was measured to identify if CaMKIIδ_2 contributed to remodelling in this atherosclerotic model (ApoE$^{-/-}$). CaMKIIδ_2 had no significant effect on vessel wall hypertrophy (**Figure 4.16).** This is in contrast with the current literature that has shown in models of flow remodelling that CaMKIIδ_2 mediates the proliferative response in response to arterial injury [181, 220, 259]. The fact this difference was not seen could reflect a volatile environment that promotes lesion formation over vascular remodelling.

The ligation method is clearly a sensitive technique. In the current experiment a partial ligation was applied to increase shear stress to promote atherogenesis [248, 250-252]. In other non-atherosclerotic models, more extensive ligations are used to induce vascular remodeling, which suggests there is a fine line for using this technique to study the pathogenesis of atherosclerosis. Both diseases involve similar mechanisms for pathogenicity (e.g. VSMC proliferation) so it is unlikely foam cell lesion can occur without some level of vascular remodeling. In this experiment, significant ligations to the carotid artery resulted in adverse effects. In the two-day post-operative recovery period four mice across both groups displayed neurological issues including fatigue and ataxia and mice were euthanised for welfare reasons.

These neurological issues are phenotypes commonly seen in stroke. Although stroke was not examined by post-mortem examination, there was some evidence in the 20-week carotid arteries to suggest this is likely. In the carotid artery of some mice there was extensive atherosclerosis and the presence of clotted blood (**Figure 4.12E & H**), indicating thromboembolytic activity, a common mechanism for stroke [265, 266]. Regardless of the small surgical risks associated with ischaemic injury, the carotid artery ligation serves as an excellent tool for studying the pathogenesis of atherosclerosis.

The mCherry tag was identified under fluorescent microscope to check for a positive transduction four-weeks post-surgery (**Figure 4.15**). Carotid artery sections from the control- and CaMKIIδ_2 groups displayed bright red fluorescence in the vascular wall, indicative of a positive AAV transduction. AAV delivery was in a pluronic gel and applied locally to the left-ligated carotid artery. The non-ligated contralateral artery served as a control to identify if the AAV had been delivered specifically to the left carotid artery. Detection of red fluorescence in the medial wall layer of the right carotid artery in indicated that the AAV was not specific and had infiltrated other tissues (**Figure 4.15 4A-D**). A limitation of this experiment is that elements of the vasculature were causing auto-fluorescence. In a control non AAV-treated carotid artery and aortic sinus, there was a small level of red fluorescence in the vascular wall (**Figure 4.15 5A-B**). Interestingly, mCherry expression was consistently located to the media and adventitia, whereas there was no red fluorescence in any of the foam cell lesions. This could reflect poor infiltration of AAV virus but also the mCherry signal may have faded between surgery and sectioning of the carotid artery. Loss of fluorescent signals is a problem commonly faced with paraffin embedded tissue. In future, it would be useful in addition, to clamp and seal off the artery and inject the AAVs into the lumen to promote transduction on the luminal side of the vascular wall. Even though the use of mCherry has its limitations, poor transduction of AAV is less likely in the current study given the trend in data between groups.

In summary, the results presented in this chapter did not show CaMKIIδ_2 promoted foam cell lesion development. This is likely in part, to reflect low n numbers due to early euthanasia of mice post-surgery on welfare grounds. Given the trend in data of CaMKIIδ_2 compared to control groups for foam cell lesion area and stenosis, it is enticing to speculate with a full set of animals CaMKIIδ_2 is likely to promote atherosclerosis. This is the first time the carotid ligation approach has been employed in the laboratory and the data suggests that further

optimisation of this model is required. Alongside increasing n numbers, this includes sex differences, consistency with ligation and improvements with transduction and detection of AAV-mCherry. With further optimisation, this model will serve as an excellent tool for experiments that use a similar approach. To our knowledge this is the first study to identify the contribution of CaMKII to foam cell lesion development in a carotid artery ligation model.

Chapter 5

5.1 Addressing primary aims

The overarching aim of this project was to investigate the role of CaMKII in the early development of atherosclerosis. Summarised below are the main findings in the context of our initial aims.

Aim 1: Identify the major isoforms of CaMKII in human cells of the vasculature and the arteries of atherosclerotic mice ($ApoE^{-/-}$).

Previously we showed that a systemic inhibition of CaMKII by the pharmacological compound KN-93 leads to a reduction in foam cell lesion development. A limitation with this study is it was a global inhibition of all CaMKII isoforms thus all of the important physiological functions that they effect across the different tissues of the body would be impacted. Using RT-PCR, it was identified that CaMKII$\delta_{1,2,3,6}$ and CaMKIIγ were the predominant isoforms and the variants present in cultured human vascular endothelial cells and smooth muscle cells and the arteries of atherosclerotic mice ($ApoE^{-/-}$). CaMKIIδ_2 was the predominant form across all samples tested inclusive of cells or tissue. Interestingly, Western blotting showed high expression of CaMKIIδ, but not gamma, in $ApoE^{-/-}$ mice at 13-weeks, before any lesion growth and this expression persisted at 20-weeks, where lesions are extensive. Together, this data suggested that CaMKIIδ was the most likely isoform, and within that isoform, variant 2, to contribute to the underlying pathogenesis of atherosclerosis.

Aim 2: To knockout the predominant CaMKIIδ isoform in $ApoE^{-/-}$ mice and generate the $ApoE^{-/-}$CaMKII$\delta^{-/-}$ mouse model to identify the contribution of this specific isoform to foam cell lesion development.

As we identified CaMKIIδ was the predominant isoform in human vascular cells and the arteries of an atherosclerosis model ($ApoE^{-/-}$ mouse), we next employed a genetic approach

to further test our hypothesis. ApoE$^{-/-}$ mice were crossed with CaMKII$\delta^{-/-}$ mice to generate the novel ApoE$^{-/-}$CaMKII$\delta^{-/-}$ (dKO) model. Levels of foam cell lesion content in the aortic sinus of female groups was significantly greater than male counterpart groups. A histological examination revealed a strikingly significant reduction in foam cell lesion area/ volume in the aortic sinus of female ApoE$^{-/-}$CaMKII$\delta^{-/-}$ mice compared to female ApoE$^{-/-}$ (control) mice. Collectively, this indicates CaMKIIδ signalling promotes foam cell lesion development.

Aim 3: To overexpress CaMKIIδ_2 by AAV transduction, in surgically-ligated carotid arteries of ApoE$^{-/-}$ mice to examine the impact of CaMKIIδ in foam cell lesion development.

To further test the contribution of CaMKIIδ in the early stages of atherosclerosis, an AAV-mediated over-expression protocol was carried out. At 16-weeks, the left carotid artery of ApoE$^{-/-}$CaMKII$^{-/-}$ mice on a high-fat diet was ligated to increase shear stress and promote the development of foam cell lesions. AAV-mCherry particles encoding either the CaMKIIδ_2 or control sequence were introduced to the ligated artery and left to incubate for four weeks. At 20-weeks carotid arteries of mice displayed a range of foam cell lesions with respect to size and morphology. The mean foam cell lesion area was higher in CaMKIIδ_2-mCherry group across the length of the carotid artery however, no significant differences were observed when compared to control-mCherry group. This is likely due to low n numbers due to stroke-related events induced by the ligation from surgery.

5.2 Limitations

There were a number of limitations that need to be discussed and kept in mind when moving forward with future experiments. Initially, it was tested what the predominant isoforms of CaMKII were in vascular cells. After RT-PCR was used to detect CaMKIIδ and γ variants, Western blotting was used to identify the expression levels. The antibodies used for WB are not perfect. In both the δ- and γ-probed membranes consistently, there was the appearance of other bands apart from our target size. This suggests the antibody is not specific but picking up proteins that share similar motifs. Therefore, a consistent method for the procedure and analysis should be taken to avoid any other variation.

The CaMKIIδ knockout model used in *Chapter 3* also had its limitations. We were interested in the function of CaMKIIδ in atherosclerosis, a disease of the arteries, however the model used was a global knockdown. We did not measure any other off target effects that are occurring in other tissues of the body. This is important as there was evidence in litters bred from the dKO colonies to suggest that some mice had adverse effects. These were neurological issues such as ataxia as well as developmental problems including malocclusion. These adverse effects highlight the need for a more specific approach in future studies.

The carotid artery ligation method was effective at providing a pro-atherogenic environment where we could introduce AAV particles encoding CaMKIIδ_2 and measure the contribution to foam cell lesion growth. Looking back at the model there are still areas for refinement before we utilise this model in the future. Firstly, we need a more consistent ligation approach, to avoid high variation in carotid artery foam cell content. Secondly, a more robust introduction of the AAV to the carotid artery tissue is required as we only saw AAVs after 4-weeks in the tunica media compartment. Also low n-numbers due to unexpected adverse effects meant that strong conclusions could not be drawn at times.

5.3 Moving forward

No other work to our knowledge has investigated the contribution of CaMKII to the development of atherosclerosis. In this thesis, it was identified that CaMKIIδ promotes foam cell lesion formation (Figure 5.1). This was achieved by using standard molecular biology techniques (PCR &WB) and by employing modern genetic approaches and manipulations. Like all thorough research, addressing the primary aims have only opened up more avenues for future investigation.

5.3.1 What cell group is the major contributor?

This work has provided foundation evidence that CaMKIIδ contributes to atherosclerosis. Atherosclerosis is a complicated pathology that involves a number of contributing cell groups including ECs, VSMCs and macrophages [13]. The cell groups under investigation in Chapter 2 were ECs and VSMCs and it was shown CaMKIIδ is the predominant isoform. CaMKIIδ has roles in VSMC proliferation/ migration as well as endothelial dysfunction [212, 218-220, 244]. Both of these pathologies are involved in atherosclerosis and this is the likely mechanism by which CaMKIIδ is having its effect.

Now that it has been identified that CaMKIIδ contributes to foam cell lesion development, we can now determine what cell group is the biggest contributor. In *Chapter 3,* knockout of CaMKIIδ led to a significant reduction in aortic sinus foam cell lesion content. In this model, all the splice variants of CaMKIIδ and any pathological role they play, were knocked out of all cell groups. Compare this with the over-expression experiment in *Chapter 4*. In this approach, CaMKIIδ_2 was overexpressed in the carotid arteries of ApoE$^{-/-}$CaMKII$\delta^{-/-}$ mice. While the results here showed a trend that CaMKIIδ promoted carotid foam cell lesion growth, they were not significantly different from control. The fact these two experiments showed contrasting significance could reflect the fact we have only used one of the eleven identified CaMKIIδ variants [197, 199, 200, 202]. The variant used in this study, CaMKIIδ_2, is important in the regulation of proliferation and migration in VSMCs [219, 220, 259, 267]. The other well-documented variant CaMKIIδ_6 has been more closely associated with endothelial dysfunction

[212]. In a future experiment, it would be worth overexpressing other variants in the carotid arteries of ApoE$^{-/-}$CaMKII$\delta^{-/-}$ mice including CaMKIIδ_6 and then both δ_2 and δ_6 to get a better understanding of the pathological variants and their contribution to atherogenesis. In addition, to move forward with the current study, it is critical we identify the impact of endothelial specific CaMKIIδ signalling plays in comparison with CaMKII activity in VSMCs. This can be achieved through the use of Cre-recombinase technology to specifically knockout δ isoform in endothelial or VSMCs by using a cell specific promoter [268, 269].

5.3.2 CaMKIIγ

The aim of the current study was to identify the isoform most-likely contributing to early lesion development. Our data indicated it was CaMKIIδ promoting atherogenesis, however, it was not the only isoform present. CaMKIIγ was the other isoform expressed in vascular cells (*Chapter 2*). CaMKIIγ is of particular interest because of the contrasting functions it has shown to play in comparison with CaMKIIδ. CaMKIIγ has been shown to inhibit VSMC proliferation and is important in maintenance of the VSMC contractile phenotype by regulating ion channel function and phosphorylating myosin filaments to promote tone [213, 221, 223]. Clearly both these isoforms are important in balancing two functional ends of phenotype diversity.

VSMC proliferation is a major mechanism of foam cell lesion development. With CaMKIIγ functions in maintenance of the contractile phenotype, it is intriguing to speculate CaMKIIγ protects against the development of foam cell lesions. In line with other experiments of vascular remodelling CaMKIIγ overexpression by AAV led to a reduction in remodelling and promoted contraction [213]. Going forward, it would be worth knocking out CaMKIIγ in the ApoE$^{-/-}$ mice and using a similar approach as the methods used for the current thesis, analyse foam cell lesion development.

5.3.3 Post-translational modifications of CaMKII

The two aspects of studying protein physiology include expression and activity. In the present study we were interested in the expression profile of the predominant CaMKII isoforms. It is important to keep in mind expression levels do not always directly relate to activity. CaMKII

displays a unique mechanism of activation which is tightly regulated. In the inactive state the regulatory domain is tightly bound to the catalytic state preventing activity. An elevation in intracellular Ca^{2+} leads to the formation of Ca^{2+}-calmodulin complex, which binds the regulatory domain, relieving the auto-inhibitory interaction to carry out kinase function [187]. CaMKII remains active until Ca^{2+} is extruded from the cell (*Section 1.5.1*). Under conditions of prolonged activation CaMKII can undergo inter-subunit auto-phosphorylation of the regulatory domain which prevents the auto-inhibitory properties and the enzyme is chronically active [188, 189].

In this state of chronic activation, depending on the local environment, CaMKII can also undergo additional post-translational modifications including oxidation, nitrosylation and O-GlyNAcylation [180, 191, 192]. Most of the work on CaMKII in the heart has focused on targeting these post-translational modifications to protect against the detrimental cellular effects of chronic CaMKII activation [178, 180, 191, 192, 196]. However, in these studies using KN-93 as the CaMKII inhibitor remains a limitation as it only blocks the inactive form of CaMKII by competing for the calmodulin binding domain to prevent future activation and the addition of any post-translational modifications [270]. Hence, any activated CaMKII will remain active following KN-93 treatment. A better inhibitor that should be routinely used for CaMKII research is autocamtide-2-related inhibitory peptide (AIP). This has benefits over KN-93 as its mechanism of action is to block the ATP binding site within the catalytic domain [271]. We have previously started to investigate post-translational modifications of CaMKII in atherosclerosis. In this study, we have shown that the levels of P-CaMKII do not change from early lesion (13-weeks) to mid-lesion (20-weeks) phase (MSc, Worthington, 2016). Increased oxidative and nitrosative stress are fundamental elements to the atherosclerotic milieu [272, 273]. Therefore, in future, it would be useful to identify whether the levels of oxidation and nitrosylation of CaMKII contribute to lesion progression. There are already oxidative and nitrosative mutants of CaMKII that exist and these can be introduced into the AAV model that is now established.

The work carried out in this thesis has been instrumental in establishing this model in the lab, and in New Zealand. With further optimisation, the model can be used to establish the role of not only other CaMKII variants, but also these mutants that are resistant to post-translational modifications.

5.3.4 Feasibility of CaMKIIδ as a therapeutic target

This work has made a significant contribution in identifying CaMKII as a therapeutic target for treating the early development of atherosclerosis. While these results are promising, it is still important to evaluate how this approach would be targeted in the clinic for the treatment of human atherosclerosis. A major difficulty with treating the disease is it is silent for decades before any symptoms manifest and importantly, these first symptoms can be life threatening [274, 275]. In the current study we identified that CaMKII inhibition protects against atherosclerosis during the foam cell lesion phase. This is an early event in the development of atherosclerosis and in the clinic atherosclerosis is mainly seen in its advanced stage [95]. It is not known how CaMKII inhibition effects atherosclerosis after the foam cell lesion phase. Therefore, it is important in the future we investigate how CaMKII promotes lesion growth after the foam cell phase and also differentiation of the lesion. Like most diseases, early treatment is best and for this treatment better screening and earlier detection of atherosclerosis is required so the disease can be treated at an earlier stage. If CaMKII was to be a target for early stage atherosclerosis, it would be imperative that the treatment be targeted to the coronary arteries because systemically it would target CaMKII in other tissues which for a long-term treatment may not be ideal.

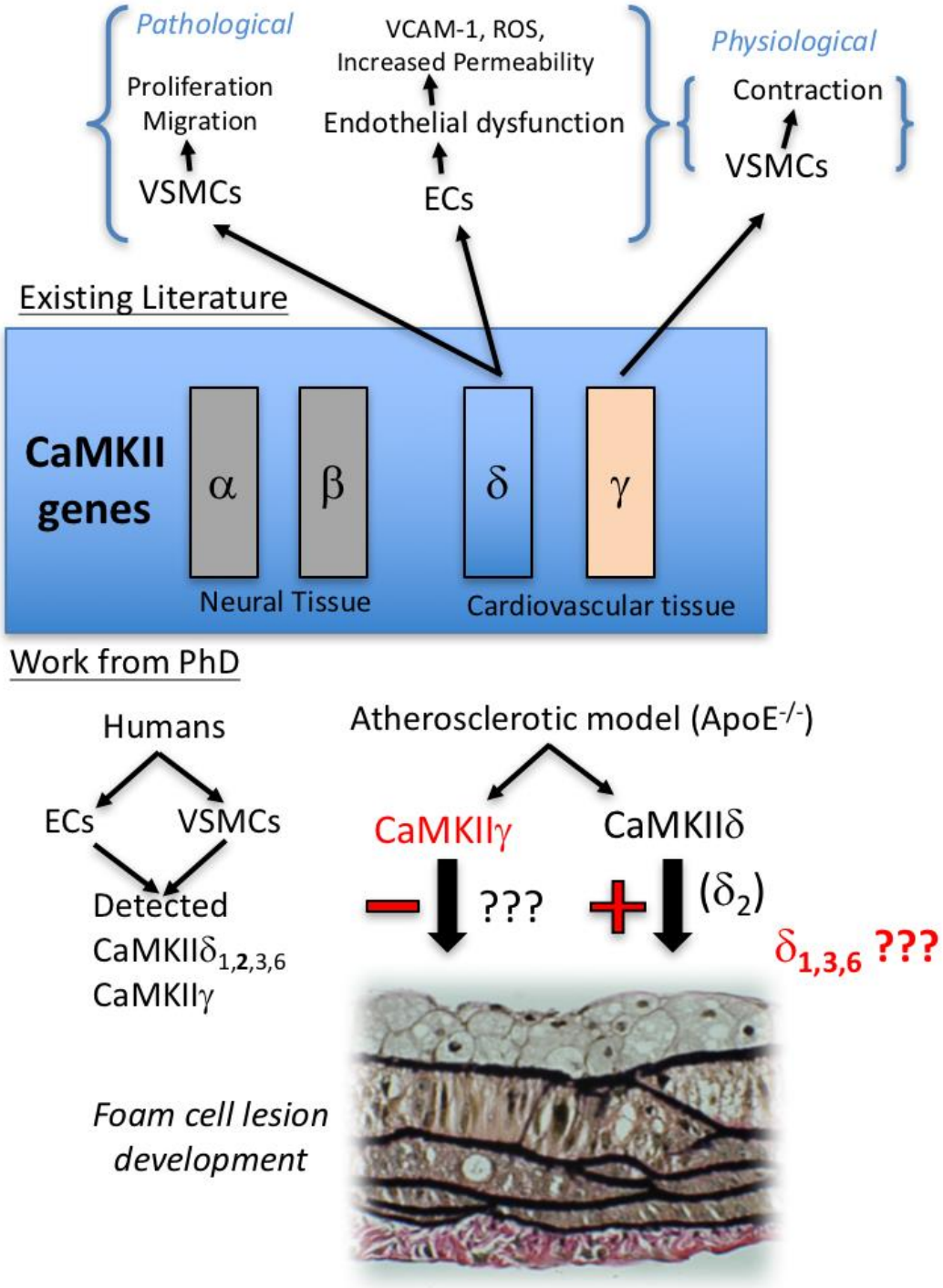

Figure 5.1 Summary of the contribution of PhD work to current CaMKII literature. There are four separate genes that encode CaMKII isoforms α, β, δ and γ. The α and β isoforms are predominantly expressed in the nervous system and have important roles in brain function. The δ and γ isoforms are expressed in cardiovascular tissue. Furthermore, the δ isoform has pathological roles in promoting endothelial dysfunction and increasing the synthetic phenotype in VSMCs. In contrast the γ isoform has received little attention, however it has important functions in VSMC contraction. In this PhD we have identified CaMKIIδ variants 1, 2, 3 and 6 are present in human vascular cells (ECs and VSMCs) as well as atherosclerotic arteries of ApoE$^{-/-}$ mice. CaMKIIδ promotes lesion development mediated at least in part by the δ_2 variant. The contribution of the other δ variants 1, 3 and 6, remains to be identified. Whether CaMKIIγ is protective against the development of atherosclerosis is not known.

5.3 Conclusions

Atherosclerosis is the most significant cardiovascular disease characterised by the formation of fat-filled lesions on the arterial wall. In this novel study, we have utilised a number of molecular, genetic and viral-mediated approaches to identify that CaMKIIδ promotes atherosclerosis. These results provide a strong foundation to continue researching CaMKII function in the pathogenesis of atherosclerosis to explore the therapeutic potential.

References

1. *Global, regional, and national age-sex-specific mortality for 282 causes of death in 195 countries and territories, 1980-2017: a systematic analysis for the Global Burden of Disease Study 2017.* Lancet, 2018. **392**(10159): p. 1736-1788.
2. Pugsley, M.K. and R. Tabrizchi, *The vascular system. An overview of structure and function.* J Pharmacol Toxicol Methods, 2000. **44**(2): p. 333-40.
3. *The Circulatory System*, in *Mathematical Physiology: II: Systems Physiology*, J. Keener and J. Sneyd, Editors. 2009, Springer New York: New York, NY. p. 471-522.
4. Corso, P.F., *Variations of the arterial, venous and capillary circulation of the soft tissues of the head by decades as demonstrated by the methyl methacrolate injection technique, and their application to the construction of flaps and pedicles.* Probl Sovrem Neirokhirurgii, 1961. **27**: p. 160-84.
5. Tennant, M. and J.K. McGeachie, *Blood vessel structure and function: a brief update on recent advances.* Aust N Z J Surg, 1990. **60**(10): p. 747-53.
6. Vanhoutte, P.M. and T. Scott-Burden, *The endothelium in health and disease.* Texas Heart Institute journal, 1994. **21**(1): p. 62-67.
7. Vane, J.R. and R.M. Botting, *The role of chemical mediators released by the endothelium in the control of the cardiovascular system.* Int J Tissue React, 1992. **14**(2): p. 55-64.
8. Tucker, W.D., Y. Arora, and K. Mahajan, *Anatomy, Blood Vessels*, in *StatPearls*. 2021, StatPearls Publishing

9. Lacolley, P., et al., *The vascular smooth muscle cell in arterial pathology: a cell that can take on multiple roles.* Cardiovasc Res, 2012. **95**(2): p. 194-204.
10. Gomez, D. and G.K. Owens, *Smooth muscle cell phenotypic switching in atherosclerosis.* Cardiovasc Res, 2012. **95**(2): p. 156-64.
11. Maiellaro, K. and W.R. Taylor, *The role of the adventitia in vascular inflammation.* Cardiovasc Res, 2007. **75**(4): p. 640-8.
12. Fleming, R.M., *The Pathogenesis of Vascular Disease*, in *Textbook of Angiology*, J.B. Chang, Editor. 2000, Springer New York: New York, NY. p. 787-798.
13. Singh, R.B., et al., *Pathogenesis of atherosclerosis: A multifactorial process.* Exp Clin Cardiol, 2002. **7**(1): p. 40-53.
14. Gordon, T., et al., *Lipoproteins, cardiovascular disease, and death. The Framingham study.* Arch Intern Med, 1981. **141**(9): p. 1128-31.
15. Kannel, W.B., et al., *Factors of risk in the development of coronary heart disease--six year follow-up experience. The Framingham Study.* Ann Intern Med, 1961. **55**: p. 33-50.
16. Stamler, J., D. Wentworth, and J.D. Neaton, *Is relationship between serum cholesterol and risk of premature death from coronary heart disease continuous and graded? Findings in 356,222 primary screenees of the Multiple Risk Factor Intervention Trial (MRFIT).* Jama, 1986. **256**(20): p. 2823-8.
17. Mozaffarian, D., et al., *Heart disease and stroke statistics--2015 update: a report from the American Heart Association.* Circulation, 2015. **131**(4): p. e29-322.
18. Grundy, S.M., et al., *Assessment of cardiovascular risk by use of multiple-risk-factor assessment equations: a statement for healthcare professionals from the American Heart Association and the American College of Cardiology.* Circulation, 1999. **100**(13): p. 1481-92.

19. Wilson, P.W., et al., *Prediction of coronary heart disease using risk factor categories.* Circulation, 1998. **97**(18): p. 1837-47.
20. Ross, R., J. Glomset, and L. Harker, *Response to injury and atherogenesis.* Am J Pathol, 1977. **86**(3): p. 675-84.
21. Ference, B.A., et al., *Low-density lipoproteins cause atherosclerotic cardiovascular disease. 1. Evidence from genetic, epidemiologic, and clinical studies. A consensus statement from the European Atherosclerosis Society Consensus Panel.* Eur Heart J, 2017. **38**(32): p. 2459-2472.
22. Dayton, S. and S. Hashimoto, *Movement of labeled cholesterol between plasma lipoprotein and normal arterial wall across the intimal surface.* Circ Res, 1966. **19**(6): p. 1041-9.
23. Fuster, V., et al., *The pathogenesis of coronary artery disease and the acute coronary syndromes (2).* N Engl J Med, 1992. **326**(5): p. 310-8.
24. Ignarro, L.J., et al., *Mechanism of vascular smooth muscle relaxation by organic nitrates, nitrites, nitroprusside and nitric oxide: evidence for the involvement of S-nitrosothiols as active intermediates.* J Pharmacol Exp Ther, 1981. **218**(3): p. 739-49.
25. Pellacani, A., H.R. Brunner, and J. Nussberger, *Plasma kinins increase after angiotensin-converting enzyme inhibition in human subjects.* Clin Sci (Lond), 1994. **87**(5): p. 567-74.
26. Davies, P.F., et al., *Spatial relationships in early signaling events of flow-mediated endothelial mechanotransduction.* Annu Rev Physiol, 1997. **59**: p. 527-49.
27. Luscher, T.F. and M. Barton, *Biology of the endothelium.* Clin Cardiol, 1997. **20**(11 Suppl 2): p. Ii-3-10.
28. Yanagisawa, M., et al., *A novel potent vasoconstrictor peptide produced by vascular endothelial cells.* Nature, 1988. **332**(6163): p. 411-5.
29. Li, Q., et al., *Comparative vasoconstrictor effects of angiotensin II, III, and IV in human isolated saphenous vein.* J Cardiovasc Pharmacol, 1997. **29**(4): p. 451-6.
30. Carreau, A., C. Kieda, and C. Grillon, *Nitric oxide modulates the expression of endothelial cell adhesion molecules involved in angiogenesis and leukocyte recruitment.* Exp Cell Res, 2011. **317**(1): p. 29-41.
31. De Caterina, R., et al., *Nitric oxide decreases cytokine-induced endothelial activation. Nitric oxide selectively reduces endothelial expression of adhesion molecules and proinflammatory cytokines.* J Clin Invest, 1995. **96**(1): p. 60-8.
32. Vita, J.A., et al., *Coronary vasomotor response to acetylcholine relates to risk factors for coronary artery disease.* Circulation, 1990. **81**(2): p. 491-7.
33. Vanhoutte, P.M., et al., *Endothelial dysfunction and vascular disease.* Acta Physiol (Oxf), 2009. **196**(2): p. 193-222.
34. McLenachan, J.M., et al., *Early evidence of endothelial vasodilator dysfunction at coronary branch points.* Circulation, 1990. **82**(4): p. 1169-73.
35. Sheikh, S., et al., *Exposure to fluid shear stress modulates the ability of endothelial cells to recruit neutrophils in response to tumor necrosis factor-alpha: a basis for local variations in vascular sensitivity to inflammation.* Blood, 2003. **102**(8): p. 2828-34.
36. Burke, A.P., et al., *Coronary risk factors and plaque morphology in men with coronary disease who died suddenly.* N Engl J Med, 1997. **336**(18): p. 1276-82.
37. Hao, H., G. Gabbiani, and M.L. Bochaton-Piallat, *Arterial smooth muscle cell heterogeneity: implications for atherosclerosis and restenosis development.* Arterioscler Thromb Vasc Biol, 2003. **23**(9): p. 1510-20.
38. Lin, S.J., K.M. Jan, and S. Chien, *Role of dying endothelial cells in transendothelial macromolecular transport.* Arteriosclerosis, 1990. **10**(5): p. 703-9.

39. Khan, B.V., et al., *Nitric oxide regulates vascular cell adhesion molecule 1 gene expression and redox-sensitive transcriptional events in human vascular endothelial cells.* Proc Natl Acad Sci U S A, 1996. **93**(17): p. 9114-9.
40. Min, J.K., et al., *TNF-related activation-induced cytokine enhances leukocyte adhesiveness: induction of ICAM-1 and VCAM-1 via TNF receptor-associated factor and protein kinase C-dependent NF-kappaB activation in endothelial cells.* J Immunol, 2005. **175**(1): p. 531-40.
41. Galkina, E., et al., *Lymphocyte recruitment into the aortic wall before and during development of atherosclerosis is partially L-selectin dependent.* The Journal of experimental medicine, 2006. **203**(5): p. 1273-1282.
42. van Furth, R. and Z.A. Cohn, *The origin and kinetics of mononuclear phagocytes.* J Exp Med, 1968. **128**(3): p. 415-35.
43. Khan, B.V., et al., *Modified low density lipoprotein and its constituents augment cytokine-activated vascular cell adhesion molecule-1 gene expression in human vascular endothelial cells.* J Clin Invest, 1995. **95**(3): p. 1262-70.
44. van der Valk, F.M., et al., *Oxidized Phospholipids on Lipoprotein(a) Elicit Arterial Wall Inflammation and an Inflammatory Monocyte Response in Humans.* Circulation, 2016. **134**(8): p. 611-24.
45. Curtiss, L.K. and P.S. Tobias, *Emerging role of Toll-like receptors in atherosclerosis.* Journal of lipid research, 2009. **50 Suppl**(Suppl): p. S340-S345.
46. Shuang, C., et al., *Differential expression of Toll-like receptor 2 (TLR2) and responses to TLR2 ligands between human and murine vascular endothelial cells.* J Endotoxin Res, 2007. **13**(5): p. 281-96.
47. Doyle, S.E., et al., *Toll-like receptors induce a phagocytic gene program through p38.* The Journal of experimental medicine, 2004. **199**(1): p. 81-90.
48. Zhang, W., et al., *Sphingosine-1-phosphate receptor-2 mediated NFκB activation contributes to tumor necrosis factor-α induced VCAM-1 and ICAM-1 expression in endothelial cells.* Prostaglandins & other lipid mediators, 2013. **106**: p. 62-71.
49. Tan, S.M., et al., *Effect of integrin beta 2 subunit truncations on LFA-1 (CD11a/CD18) and Mac-1 (CD11b/CD18) assembly, surface expression, and function.* J Immunol, 2000. **165**(5): p. 2574-81.
50. Dobrina, A., et al., *Mechanisms of eosinophil adherence to cultured vascular endothelial cells. Eosinophils bind to the cytokine-induced ligand vascular cell adhesion molecule-1 via the very late activation antigen-4 integrin receptor.* The Journal of clinical investigation, 1991. **88**(1): p. 20-26.
51. Elices, M.J., et al., *VCAM-1 on activated endothelium interacts with the leukocyte integrin VLA-4 at a site distinct from the VLA-4/fibronectin binding site.* Cell, 1990. **60**(4): p. 577-84.
52. Carman, C.V. and T.A. Springer, *A transmigratory cup in leukocyte diapedesis both through individual vascular endothelial cells and between them.* The Journal of cell biology, 2004. **167**(2): p. 377-388.
53. Martinez, F.O., et al., *Transcriptional profiling of the human monocyte-to-macrophage differentiation and polarization: new molecules and patterns of gene expression.* J Immunol, 2006. **177**(10): p. 7303-11.
54. Kunjathoor, V.V., et al., *Scavenger receptors class A-I/II and CD36 are the principal receptors responsible for the uptake of modified low density lipoprotein leading to lipid loading in macrophages.* J Biol Chem, 2002. **277**(51): p. 49982-8.

55. Febbraio, M., et al., *Targeted disruption of the class B scavenger receptor CD36 protects against atherosclerotic lesion development in mice.* J Clin Invest, 2000. **105**(8): p. 1049-56.
56. Choi, S.H., et al., *Lipoprotein accumulation in macrophages via toll-like receptor-4-dependent fluid phase uptake.* Circ Res, 2009. **104**(12): p. 1355-63.
57. Kruth, H.S., et al., *Macropinocytosis is the endocytic pathway that mediates macrophage foam cell formation with native low density lipoprotein.* J Biol Chem, 2005. **280**(3): p. 2352-60.
58. Gerrity, R.G., et al., *Dietary induced atherogenesis in swine. Morphology of the intima in prelesion stages.* Am J Pathol, 1979. **95**(3): p. 775-92.
59. Gerrity, R.G. and H.K. Naito, *Ultrastructural identification of monocyte-derived foam cells in fatty streak lesions.* Artery, 1980. **8**(3): p. 208-14.
60. Wang, N., et al., *ATP-binding cassette transporter A1 (ABCA1) functions as a cholesterol efflux regulatory protein.* J Biol Chem, 2001. **276**(26): p. 23742-7.
61. Wang, N., et al., *ATP-binding cassette transporters G1 and G4 mediate cellular cholesterol efflux to high-density lipoproteins.* Proceedings of the National Academy of Sciences of the United States of America, 2004. **101**(26): p. 9774-9779.
62. Westerterp, M., et al., *Deficiency of ATP-binding cassette transporters A1 and G1 in macrophages increases inflammation and accelerates atherosclerosis in mice.* Circ Res, 2013. **112**(11): p. 1456-65.
63. Yvan-Charvet, L., et al., *Combined deficiency of ABCA1 and ABCG1 promotes foam cell accumulation and accelerates atherosclerosis in mice.* J Clin Invest, 2007. **117**(12): p. 3900-8.
64. Guyton, J.R. and K.F. Klemp, *Development of the atherosclerotic core region. Chemical and ultrastructural analysis of microdissected atherosclerotic lesions from human aorta.* Arterioscler Thromb, 1994. **14**(8): p. 1305-14.
65. Tsukano, H., et al., *The endoplasmic reticulum stress-C/EBP homologous protein pathway-mediated apoptosis in macrophages contributes to the instability of atherosclerotic plaques.* Arterioscler Thromb Vasc Biol, 2010. **30**(10): p. 1925-32.
66. Seimon, T.A., et al., *Atherogenic lipids and lipoproteins trigger CD36-TLR2-dependent apoptosis in macrophages undergoing endoplasmic reticulum stress.* Cell metabolism, 2010. **12**(5): p. 467-482.
67. Schrijvers, D.M., et al., *Phagocytosis of apoptotic cells by macrophages is impaired in atherosclerosis.* Arterioscler Thromb Vasc Biol, 2005. **25**(6): p. 1256-61.
68. Han, S., et al., *Macrophage insulin receptor deficiency increases ER stress-induced apoptosis and necrotic core formation in advanced atherosclerotic lesions.* Cell Metab, 2006. **3**(4): p. 257-66.
69. Stary, H.C., et al., *A definition of advanced types of atherosclerotic lesions and a histological classification of atherosclerosis. A report from the Committee on Vascular Lesions of the Council on Arteriosclerosis, American Heart Association.* Circulation, 1995. **92**(5): p. 1355-74.
70. Frid, M.G., et al., *Myosin heavy-chain isoform composition and distribution in developing and adult human aortic smooth muscle.* J Vasc Res, 1993. **30**(5): p. 279-92.
71. Li, L., et al., *SM22 alpha, a marker of adult smooth muscle, is expressed in multiple myogenic lineages during embryogenesis.* Circ Res, 1996. **78**(2): p. 188-95.
72. Rensen, S.S., P.A. Doevendans, and G.J. van Eys, *Regulation and characteristics of vascular smooth muscle cell phenotypic diversity.* Neth Heart J, 2007. **15**(3): p. 100-8.
73. Wang, Z., M.R. Castresana, and W.H. Newman, *NF-kappaB is required for TNF-alpha-directed smooth muscle cell migration.* FEBS Lett, 2001. **508**(3): p. 360-4.

74. Ikeda, U., et al., *Interleukin 6 stimulates growth of vascular smooth muscle cells in a PDGF-dependent manner.* Am J Physiol, 1991. **260**(5 Pt 2): p. H1713-7.
75. Morimoto, S., et al., *Interleukin-6 stimulates proliferation of cultured vascular smooth muscle cells independently of interleukin-1 beta.* J Cardiovasc Pharmacol, 1991. **17 Suppl 2**: p. S117-8.
76. Graf, K., et al., *Mitogen-activated protein kinase activation is involved in platelet-derived growth factor-directed migration by vascular smooth muscle cells.* Hypertension, 1997. **29**(1 Pt 2): p. 334-9.
77. Mason, D.P., et al., *Matrix metalloproteinase-9 overexpression enhances vascular smooth muscle cell migration and alters remodeling in the injured rat carotid artery.* Circ Res, 1999. **85**(12): p. 1179-85.
78. Galis, Z.S., et al., *Increased expression of matrix metalloproteinases and matrix degrading activity in vulnerable regions of human atherosclerotic plaques.* J Clin Invest, 1994. **94**(6): p. 2493-503.
79. Lutgens, E., et al., *Biphasic pattern of cell turnover characterizes the progression from fatty streaks to ruptured human atherosclerotic plaques.* Cardiovasc Res, 1999. **41**(2): p. 473-9.
80. Allahverdian, S., et al., *Contribution of intimal smooth muscle cells to cholesterol accumulation and macrophage-like cells in human atherosclerosis.* Circulation, 2014. **129**(15): p. 1551-9.
81. Mietus-Snyder, M., M.S. Gowri, and R.E. Pitas, *Class A scavenger receptor up-regulation in smooth muscle cells by oxidized low density lipoprotein. Enhancement by calcium flux and concurrent cyclooxygenase-2 up-regulation.* J Biol Chem, 2000. **275**(23): p. 17661-70.
82. Beyea, M.M., et al., *The oxysterol 24(s),25-epoxycholesterol attenuates human smooth muscle-derived foam cell formation via reduced low-density lipoprotein uptake and enhanced cholesterol efflux.* J Am Heart Assoc, 2012. **1**(3): p. e000810.
83. Amento, E.P., et al., *Cytokines and growth factors positively and negatively regulate interstitial collagen gene expression in human vascular smooth muscle cells.* Arterioscler Thromb, 1991. **11**(5): p. 1223-30.
84. Stary, H.C., *Changes in components and structure of atherosclerotic lesions developing from childhood to middle age in coronary arteries.* Basic Res Cardiol, 1994. **89 Suppl 1**: p. 17-32.
85. Group, P.R., *Natural history of aortic and coronary atherosclerotic lesions in youth. Findings from the PDAY Study. Pathobiological Determinants of Atherosclerosis in Youth (PDAY) Research Group.* Arterioscler Thromb, 1993. **13**(9): p. 1291-8.
86. Stary, H.C., *Natural history and histological classification of atherosclerotic lesions: an update.* Arterioscler Thromb Vasc Biol, 2000. **20**(5): p. 1177-8.
87. Paulsson, G., et al., *Oligoclonal T cell expansions in atherosclerotic lesions of apolipoprotein E-deficient mice.* Arterioscler Thromb Vasc Biol, 2000. **20**(1): p. 10-7.
88. Zhou, X. and G.K. Hansson, *Detection of B cells and proinflammatory cytokines in atherosclerotic plaques of hypercholesterolaemic apolipoprotein E knockout mice.* Scand J Immunol, 1999. **50**(1): p. 25-30.
89. Ohayon, J., et al., *Necrotic core thickness and positive arterial remodeling index: emergent biomechanical factors for evaluating the risk of plaque rupture.* Am J Physiol Heart Circ Physiol, 2008. **295**(2): p. H717-27.
90. Fujii, K., et al., *Intravascular ultrasound assessment of ulcerated ruptured plaques: a comparison of culprit and nonculprit lesions of patients with acute coronary syndromes*

and lesions in patients without acute coronary syndromes. Circulation, 2003. **108**(20): p. 2473-8.
91. Budoff, M.J., et al., *Comparison of spiral and electron beam tomography in the evaluation of coronary calcification in asymptomatic persons.* Int J Cardiol, 2001. **77**(2-3): p. 181-8.
92. Janowitz, W.R., et al., *Differences in prevalence and extent of coronary artery calcium detected by ultrafast computed tomography in asymptomatic men and women.* Am J Cardiol, 1993. **72**(3): p. 247-54.
93. Taylor, A.E., D.C. Johnson, and H. Kazemi, *Environmental tobacco smoke and cardiovascular disease. A position paper from the Council on Cardiopulmonary and Critical Care, American Heart Association.* Circulation, 1992. **86**(2): p. 699-702.
94. Glantz, S.A. and W.W. Parmley, *Passive smoking and heart disease. Epidemiology, physiology, and biochemistry.* Circulation, 1991. **83**(1): p. 1-12.
95. Bellamy, C.M., et al., *Histopathological examination of specimens removed during directional coronary atherectomy in patients presenting with crescendo angina show mural thrombus.* Postgraduate Medical Journal, 1993. **69**(808): p. 112-114.
96. Arai, A.E., et al., *Metabolic adaptation to a gradual reduction in myocardial blood flow.* Circulation, 1995. **92**(2): p. 244-52.
97. Lampe, F.C., et al., *Chest pain on questionnaire and prediction of major ischaemic heart disease events in men.* Eur Heart J, 1998. **19**(1): p. 63-73.
98. Corrado, D., G. Thiene, and N. Pennelli, *Sudden death as the first manifestation of coronary artery disease in young people (less than or equal to 35 years).* Eur Heart J, 1988. **9 Suppl N**: p. 139-44.
99. Perrone-Filardi, P., et al., *Cardiac computed tomography and myocardial perfusion scintigraphy for risk stratification in asymptomatic individuals without known cardiovascular disease: a position statement of the Working Group on Nuclear Cardiology and Cardiac CT of the European Society of Cardiology.* Eur Heart J, 2011. **32**(16): p. 1986-93, 1993a, 1993b.
100. Sigurdsson, E., et al., *Unrecognized myocardial infarction: epidemiology, clinical characteristics, and the prognostic role of angina pectoris. The Reykjavik Study.* Ann Intern Med, 1995. **122**(2): p. 96-102.
101. Jónsdóttir, L.S., et al., *Incidence and prevalence of recognised and unrecognised myocardial infarction in women. The Reykjavik Study.* Eur Heart J, 1998. **19**(7): p. 1011-8.
102. Taylor, R.S., et al., *Exercise-based rehabilitation for patients with coronary heart disease: systematic review and meta-analysis of randomized controlled trials.* Am J Med, 2004. **116**(10): p. 682-92.
103. Heran, B.S., et al., *Exercise-based cardiac rehabilitation for coronary heart disease.* Cochrane Database Syst Rev, 2011(7): p. Cd001800.
104. Napoli, C. and V. Sica, *Statin treatment and the natural history of atherosclerotic-related diseases: pathogenic mechanisms and the risk-benefit profile.* Curr Pharm Des, 2004. **10**(4): p. 425-32.
105. Fihn, S.D., et al., *2012 ACCF/AHA/ACP/AATS/PCNA/SCAI/STS Guideline for the diagnosis and management of patients with stable ischemic heart disease: a report of the American College of Cardiology Foundation/American Heart Association Task Force on Practice Guidelines, and the American College of Physicians, American Association for Thoracic Surgery, Preventive Cardiovascular Nurses Association, Society for Cardiovascular Angiography and Interventions, and Society of Thoracic Surgeons.* J Am Coll Cardiol, 2012. **60**(24): p. e44-e164.

106. Mancini, G.B., et al., *Canadian Cardiovascular Society guidelines for the diagnosis and management of stable ischemic heart disease.* Can J Cardiol, 2014. **30**(8): p. 837-49.
107. Hollander, W., *Role of hypertension in atherosclerosis and cardiovascular disease.* Am J Cardiol, 1976. **38**(6): p. 786-800.
108. Watson, K.E., A.L. Peters Harmel, and G. Matson, *Atherosclerosis in type 2 diabetes mellitus: the role of insulin resistance.* J Cardiovasc Pharmacol Ther, 2003. **8**(4): p. 253-60.
109. *Timolol-induced reduction in mortality and reinfarction in patients surviving acute myocardial infarction.* N Engl J Med, 1981. **304**(14): p. 801-7.
110. Abrams, J., *The role of nitrates in coronary heart disease.* Arch Intern Med, 1995. **155**(4): p. 357-64.
111. Bangalore, S., S. Parkar, and F.H. Messerli, *Long-acting calcium antagonists in patients with coronary artery disease: a meta-analysis.* Am J Med, 2009. **122**(4): p. 356-65.
112. Baigent, C., et al., *Aspirin in the primary and secondary prevention of vascular disease: collaborative meta-analysis of individual participant data from randomised trials.* Lancet, 2009. **373**(9678): p. 1849-60.
113. *Randomised trial of cholesterol lowering in 4444 patients with coronary heart disease: the Scandinavian Simvastatin Survival Study (4S).* Lancet, 1994. **344**(8934): p. 1383-9.
114. Ferrari, R., S. Censi, and A. Squeri, *Treating angina.* European Heart Journal Supplements, 2019. **21**(Supplement_G): p. G1-G3.
115. Ferrari, R., R. Pavasini, and C. Balla, *The multifaceted angina.* European Heart Journal Supplements, 2019. **21**(Supplement_C): p. C1-C5.
116. Pareek, M. and D.L. Bhatt, *Dual antiplatelet therapy in patients with an acute coronary syndrome: up to 12 months and beyond.* European Heart Journal Supplements, 2018. **20**(suppl_B): p. B21-B28.
117. Lin, T.-T., et al., *Single and dual antiplatelet therapy in elderly patients of medically managed myocardial infarction.* BMC geriatrics, 2018. **18**(1): p. 86-86.
118. Thachil, J., *Antiplatelet therapy - a summary for the general physicians.* Clinical medicine (London, England), 2016. **16**(2): p. 152-160.
119. Chen, Z.M., et al., *Addition of clopidogrel to aspirin in 45,852 patients with acute myocardial infarction: randomised placebo-controlled trial.* Lancet, 2005. **366**(9497): p. 1607-21.
120. Yusuf, S., et al., *Effects of clopidogrel in addition to aspirin in patients with acute coronary syndromes without ST-segment elevation.* N Engl J Med, 2001. **345**(7): p. 494-502.
121. Abrams, J., *Hemodynamic effects of nitroglycerin and long-acting nitrates.* Am Heart J, 1985. **110**(1 Pt 2): p. 216-24.
122. Cannon, R.O., 3rd, et al., *Efficacy of calcium channel blocker therapy for angina pectoris resulting from small-vessel coronary artery disease and abnormal vasodilator reserve.* Am J Cardiol, 1985. **56**(4): p. 242-6.
123. Feliciano, L. and R.J. Henning, *Coronary artery blood flow: physiologic and pathophysiologic regulation.* Clin Cardiol, 1999. **22**(12): p. 775-86.
124. Fulcher, J., et al., *Efficacy and safety of LDL-lowering therapy among men and women: meta-analysis of individual data from 174,000 participants in 27 randomised trials.* Lancet, 2015. **385**(9976): p. 1397-405.
125. Nissen, S.E., *Effect of intensive lipid lowering on progression of coronary atherosclerosis: evidence for an early benefit from the Reversal of Atherosclerosis with Aggressive Lipid Lowering (REVERSAL) trial.* Am J Cardiol, 2005. **96**(5a): p. 61f-68f.
126. Bloch, K., *The biological synthesis of cholesterol.* Science, 1965. **150**(3692): p. 19-28.

127. Law, M.R., N.J. Wald, and A.R. Rudnicka, *Quantifying effect of statins on low density lipoprotein cholesterol, ischaemic heart disease, and stroke: systematic review and meta-analysis.* Bmj, 2003. **326**(7404): p. 1423.
128. Kolh, P., et al., *2014 ESC/EACTS Guidelines on myocardial revascularization: the Task Force on Myocardial Revascularization of the European Society of Cardiology (ESC) and the European Association for Cardio-Thoracic Surgery (EACTS). Developed with the special contribution of the European Association of Percutaneous Cardiovascular Interventions (EAPCI).* Eur J Cardiothorac Surg, 2014. **46**(4): p. 517-92.
129. Sones, F.M., Jr. and E.K. Shirey, *Cine coronary arteriography.* Mod Concepts Cardiovasc Dis, 1962. **31**: p. 735-8.
130. Rumberger, J.A., et al., *Coronary artery calcium area by electron-beam computed tomography and coronary atherosclerotic plaque area. A histopathologic correlative study.* Circulation, 1995. **92**(8): p. 2157-62.
131. Steitz, S.A., et al., *Smooth muscle cell phenotypic transition associated with calcification: upregulation of Cbfa1 and downregulation of smooth muscle lineage markers.* Circ Res, 2001. **89**(12): p. 1147-54.
132. New, S.E., et al., *Macrophage-derived matrix vesicles: an alternative novel mechanism for microcalcification in atherosclerotic plaques.* Circ Res, 2013. **113**(1): p. 72-7.
133. Huang, H., et al., *The impact of calcification on the biomechanical stability of atherosclerotic plaques.* Circulation, 2001. **103**(8): p. 1051-6.
134. Frink, R.J., et al., *Significance of calcification of the coronary arteries.* The American Journal of Cardiology, 1970. **26**(3): p. 241-247.
135. Detrano, R., et al., *Coronary calcium as a predictor of coronary events in four racial or ethnic groups.* N Engl J Med, 2008. **358**(13): p. 1336-45.
136. Achenbach, S., et al., *Noninvasive coronary angiography by retrospectively ECG-gated multislice spiral CT.* Circulation, 2000. **102**(23): p. 2823-8.
137. Schwartz, R.B., et al., *Common carotid artery bifurcation: evaluation with spiral CT. Work in progress.* Radiology, 1992. **185**(2): p. 513-9.
138. Neeland, I.J., et al., *Coronary angiographic scoring systems: an evaluation of their equivalence and validity.* American heart journal, 2012. **164**(4): p. 547-552.e1.
139. Li, P., et al., *Blooming Artifact Reduction in Coronary Artery Calcification by A New De-blooming Algorithm: Initial Study.* Sci Rep, 2018. **8**(1): p. 6945.
140. Favaloro, R.G., *Saphenous vein autograft replacement of severe segmental coronary artery occlusion: operative technique.* Ann Thorac Surg, 1968. **5**(4): p. 334-9.
141. Gruntzig, A.R., A. Senning, and W.E. Siegenthaler, *Nonoperative dilatation of coronary-artery stenosis: percutaneous transluminal coronary angioplasty.* N Engl J Med, 1979. **301**(2): p. 61-8.
142. Grech, E.D., *ABC of interventional cardiology: percutaneous coronary intervention. I: history and development.* Bmj, 2003. **326**(7398): p. 1080-2.
143. Faxon, D.P., T.A. Sanborn, and C.C. Haudenschild, *Mechanism of angioplasty and its relation to restenosis.* Am J Cardiol, 1987. **60**(3): p. 5b-9b.
144. Jin, M., et al., *Higher risk of recurrent ischemic events in patients with intracranial in-stent restenosis.* Stroke, 2013. **44**(11): p. 2990-4.
145. Stone, G.W., et al., *Paclitaxel-Eluting Stents versus Bare-Metal Stents in Acute Myocardial Infarction.* New England Journal of Medicine, 2009. **360**(19): p. 1946-1959.
146. Sianos, G., et al., *The SYNTAX Score: an angiographic tool grading the complexity of coronary artery disease.* EuroIntervention, 2005. **1**(2): p. 219-27.
147. Thuijs, D., et al., *Percutaneous coronary intervention versus coronary artery bypass grafting in patients with three-vessel or left main coronary artery disease: 10-year*

follow-up of the multicentre randomised controlled SYNTAX trial. Lancet, 2019. **394**(10206): p. 1325-1334.
148. Gnasso, A., et al., *In vivo association between low wall shear stress and plaque in subjects with asymmetrical carotid atherosclerosis.* Stroke, 1997. **28**(5): p. 993-8.
149. Dalager, S., et al., *Artery-related differences in atherosclerosis expression: implications for atherogenesis and dynamics in intima-media thickness.* Stroke, 2007. **38**(10): p. 2698-705.
150. Hollander, M., et al., *Carotid plaques increase the risk of stroke and subtypes of cerebral infarction in asymptomatic elderly: the Rotterdam study.* Circulation, 2002. **105**(24): p. 2872-7.
151. Sacco, R.L., et al., *Guidelines for prevention of stroke in patients with ischemic stroke or transient ischemic attack: a statement for healthcare professionals from the American Heart Association/American Stroke Association Council on Stroke: co-sponsored by the Council on Cardiovascular Radiology and Intervention: the American Academy of Neurology affirms the value of this guideline.* Stroke, 2006. **37**(2): p. 577-617.
152. Rothwell, P.M., et al., *Sex difference in the effect of time from symptoms to surgery on benefit from carotid endarterectomy for transient ischemic attack and nondisabling stroke.* Stroke, 2004. **35**(12): p. 2855-61.
153. Konstantinov, I.E. and G.M. Jankovic, *Alexander I. Ignatowski: a pioneer in the study of atherosclerosis.* Tex Heart Inst J, 2013. **40**(3): p. 246-9.
154. Kapourchali, F.R., et al., *Animal models of atherosclerosis.* World journal of clinical cases, 2014. **2**(5): p. 126-132.
155. Schreyer, S.A., D.L. Wilson, and R.C. LeBoeuf, *C57BL/6 mice fed high fat diets as models for diabetes-accelerated atherosclerosis.* Atherosclerosis, 1998. **136**(1): p. 17-24.
156. Lee, Y.T., et al., *Mouse models of atherosclerosis: a historical perspective and recent advances.* Lipids Health Dis, 2017. **16**(1): p. 12.
157. Vesselinovitch, D., R.W. Wissler, and J. Doull, *Experimental production of atherosclerosis in mice. 1. Effect of various synthetic diets and radiation on survival time, food consumption and body weight in mice.* J Atheroscler Res, 1968. **8**(3): p. 483-95.
158. Camus, M.C., et al., *Distribution and characterization of the serum lipoproteins and apoproteins in the mouse, Mus musculus.* J Lipid Res, 1983. **24**(9): p. 1210-28.
159. Barter, P.J., et al., *Cholesteryl ester transfer protein: a novel target for raising HDL and inhibiting atherosclerosis.* Arterioscler Thromb Vasc Biol, 2003. **23**(2): p. 160-7.
160. Zhang, S.H., et al., *Spontaneous hypercholesterolemia and arterial lesions in mice lacking apolipoprotein E.* Science, 1992. **258**(5081): p. 468-71.
161. Mahley, R.W., *Apolipoprotein E: cholesterol transport protein with expanding role in cell biology.* Science, 1988. **240**(4852): p. 622-30.
162. Nakashima, Y., et al., *ApoE-deficient mice develop lesions of all phases of atherosclerosis throughout the arterial tree.* Arterioscler Thromb, 1994. **14**(1): p. 133-40.
163. Kowala, M.C., et al., *Characterization of atherosclerosis in LDL receptor knockout mice: macrophage accumulation correlates with rapid and sustained expression of aortic MCP-1/JE.* Atherosclerosis, 2000. **149**(2): p. 323-30.
164. Ishibashi, S., et al., *Massive xanthomatosis and atherosclerosis in cholesterol-fed low density lipoprotein receptor-negative mice.* J Clin Invest, 1994. **93**(5): p. 1885-93.
165. Tangirala, R.K., E.M. Rubin, and W. Palinski, *Quantitation of atherosclerosis in murine models: correlation between lesions in the aortic origin and in the entire aorta, and*

differences in the extent of lesions between sexes in LDL receptor-deficient and apolipoprotein E-deficient mice. J Lipid Res, 1995. **36**(11): p. 2320-8.
166. Plump, A.S. and J.L. Breslow, *Apolipoprotein E and the apolipoprotein E-deficient mouse.* Annu Rev Nutr, 1995. **15**: p. 495-518.
167. Gordon, S.M., et al., *A comparison of the mouse and human lipoproteome: suitability of the mouse model for studies of human lipoproteins.* J Proteome Res, 2015. **14**(6): p. 2686-95.
168. Ha, Y.C. and P.J. Barter, *Differences in plasma cholesteryl ester transfer activity in sixteen vertebrate species.* Comp Biochem Physiol B, 1982. **71**(2): p. 265-9.
169. Dashti, M., et al., *A phospholipidomic analysis of all defined human plasma lipoproteins.* Sci Rep, 2011. **1**: p. 139.
170. Daugherty, A. and S.C. Whitman, *Quantification of atherosclerosis in mice.* Methods Mol Biol, 2003. **209**: p. 293-309.
171. Rattazzi, M., et al., *Calcification of advanced atherosclerotic lesions in the innominate arteries of ApoE-deficient mice: potential role of chondrocyte-like cells.* Arterioscler Thromb Vasc Biol, 2005. **25**(7): p. 1420-5.
172. Reddick, R.L., S.H. Zhang, and N. Maeda, *Atherosclerosis in mice lacking apo E. Evaluation of lesional development and progression.* Arterioscler Thromb, 1994. **14**(1): p. 141-7.
173. Rekhter, M.D., *How to evaluate plaque vulnerability in animal models of atherosclerosis?* Cardiovasc Res, 2002. **54**(1): p. 36-41.
174. Pamukcu, B., G.Y. Lip, and E. Shantsila, *The nuclear factor--kappa B pathway in atherosclerosis: a potential therapeutic target for atherothrombotic vascular disease.* Thromb Res, 2011. **128**(2): p. 117-23.
175. Bers, D.M., *Ca^{2+}-calmodulin-dependent protein kinase II regulation of cardiac excitation-transcription coupling.* Heart Rhythm, 2011. **8**(7): p. 1101-4.
176. Erickson, J.R., et al., *CaMKII in the cardiovascular system: sensing redox states.* Physiol Rev, 2011. **91**(3): p. 889-915.
177. De Koninck, P. and H. Schulman, *Sensitivity of CaM kinase II to the frequency of Ca2+ oscillations.* Science, 1998. **279**(5348): p. 227-30.
178. Zhang, R., et al., *Calmodulin kinase II inhibition protects against structural heart disease.* Nat Med, 2005. **11**(4): p. 409-17.
179. Zhang, T. and J.H. Brown, *Role of Ca2+/calmodulin-dependent protein kinase II in cardiac hypertrophy and heart failure.* Cardiovasc Res, 2004. **63**(3): p. 476-86.
180. Erickson, J.R., et al., *A dynamic pathway for calcium-independent activation of CaMKII by methionine oxidation.* Cell, 2008. **133**(3): p. 462-74.
181. House, S.J. and H.A. Singer, *CaMKII-delta isoform regulation of neointima formation after vascular injury.* Arterioscler Thromb Vasc Biol, 2008. **28**(3): p. 441-7.
182. Ai, X., et al., *Ca2+/calmodulin-dependent protein kinase modulates cardiac ryanodine receptor phosphorylation and sarcoplasmic reticulum Ca2+ leak in heart failure.* Circ Res, 2005. **97**(12): p. 1314-22.
183. Hoelz, A., A.C. Nairn, and J. Kuriyan, *Crystal structure of a tetradecameric assembly of the association domain of Ca2+/calmodulin-dependent kinase II.* Mol Cell, 2003. **11**(5): p. 1241-51.
184. Bennett, M.K., N.E. Erondu, and M.B. Kennedy, *Purification and characterization of a calmodulin-dependent protein kinase that is highly concentrated in brain.* J Biol Chem, 1983. **258**(20): p. 12735-44.

185. Tobimatsu, T. and H. Fujisawa, *Tissue-specific expression of four types of rat calmodulin-dependent protein kinase II mRNAs.* J Biol Chem, 1989. **264**(30): p. 17907-12.
186. Rosenberg, O.S., et al., *Structure of the autoinhibited kinase domain of CaMKII and SAXS analysis of the holoenzyme.* Cell, 2005. **123**(5): p. 849-60.
187. Hudmon, A. and H. Schulman, *Structure-function of the multifunctional Ca2+/calmodulin-dependent protein kinase II.* Biochem J, 2002. **364**(Pt 3): p. 593-611.
188. Lai, Y., et al., *Ca2+/calmodulin-dependent protein kinase II: identification of autophosphorylation sites responsible for generation of Ca2+/calmodulin-independence.* Proc Natl Acad Sci U S A, 1987. **84**(16): p. 5710-4.
189. Lucic, V., G.J. Greif, and M.B. Kennedy, *Detailed state model of CaMKII activation and autophosphorylation.* Eur Biophys J, 2008. **38**(1): p. 83-98.
190. Strack, S., et al., *Differential inactivation of postsynaptic density-associated and soluble Ca2+/calmodulin-dependent protein kinase II by protein phosphatases 1 and 2A.* J Neurochem, 1997. **68**(5): p. 2119-28.
191. Erickson, J.R., et al., *Diabetic hyperglycaemia activates CaMKII and arrhythmias by O-linked glycosylation.* Nature, 2013. **502**(7471): p. 372-6.
192. Erickson, J.R., et al., *S-Nitrosylation Induces Both Autonomous Activation and Inhibition of Calcium/Calmodulin-dependent Protein Kinase II delta.* J Biol Chem, 2015. **290**(42): p. 25646-56.
193. Zhang, T., et al., *The deltaC isoform of CaMKII is activated in cardiac hypertrophy and induces dilated cardiomyopathy and heart failure.* Circ Res, 2003. **92**(8): p. 912-9.
194. Piacentino, V., 3rd, et al., *Cellular basis of abnormal calcium transients of failing human ventricular myocytes.* Circ Res, 2003. **92**(6): p. 651-8.
195. Luo, M., et al., *Diabetes increases mortality after myocardial infarction by oxidizing CaMKII.* J Clin Invest, 2013. **123**(3): p. 1262-74.
196. Purohit, A., et al., *Oxidized Ca(2+)/calmodulin-dependent protein kinase II triggers atrial fibrillation.* Circulation, 2013. **128**(16): p. 1748-57.
197. Hoch, B., et al., *Differentiation-dependent expression of cardiac delta-CaMKII isoforms.* J Cell Biochem, 1998. **68**(2): p. 259-68.
198. Singer, H.A., H.A. Benscoter, and C.M. Schworer, *Novel Ca2+/calmodulin-dependent protein kinase II gamma-subunit variants expressed in vascular smooth muscle, brain, and cardiomyocytes.* J Biol Chem, 1997. **272**(14): p. 9393-400.
199. Edman, C.F. and H. Schulman, *Identification and characterization of delta B-CaM kinase and delta C-CaM kinase from rat heart, two new multifunctional Ca2+/calmodulin-dependent protein kinase isoforms.* Biochim Biophys Acta, 1994. **1221**(1): p. 89-101.
200. Schworer, C.M., et al., *Identification of novel isoforms of the delta subunit of Ca2+/calmodulin-dependent protein kinase II. Differential expression in rat brain and aorta.* J Biol Chem, 1993. **268**(19): p. 14443-9.
201. Krainer, A.R. and T. Maniatis, *Multiple factors including the small nuclear ribonucleoproteins U1 and U2 are necessary for pre-mRNA splicing in vitro.* Cell, 1985. **42**(3): p. 725-36.
202. Mayer, P., et al., *Novel and uncommon isoforms of the calcium sensing enzyme calcium/calmodulin dependent protein kinase II in heart tissue.* Basic Res Cardiol, 1995. **90**(5): p. 372-9.
203. Nghiem, P., et al., *Cloning and analysis of two new isoforms of multifunctional Ca2+/calmodulin-dependent protein kinase. Expression in multiple human tissues.* J Biol Chem, 1993. **268**(8): p. 5471-9.

204. Srinivasan, M., C.F. Edman, and H. Schulman, *Alternative splicing introduces a nuclear localization signal that targets multifunctional CaM kinase to the nucleus.* J Cell Biol, 1994. **126**(4): p. 839-52.
205. Kalderon, D., et al., *A short amino acid sequence able to specify nuclear location.* Cell, 1984. **39**(3 Pt 2): p. 499-509.
206. Maier, L.S., et al., *Transgenic CaMKIIdeltaC overexpression uniquely alters cardiac myocyte Ca2+ handling: reduced SR Ca2+ load and activated SR Ca2+ release.* Circ Res, 2003. **92**(8): p. 904-11.
207. Kohlhaas, M., et al., *Increased sarcoplasmic reticulum calcium leak but unaltered contractility by acute CaMKII overexpression in isolated rabbit cardiac myocytes.* Circ Res, 2006. **98**(2): p. 235-44.
208. Sag, C.M., et al., *Calcium/calmodulin-dependent protein kinase II contributes to cardiac arrhythmogenesis in heart failure.* Circ Heart Fail, 2009. **2**(6): p. 664-75.
209. Little, G.H., et al., *Critical role of nuclear calcium/calmodulin-dependent protein kinase IIdeltaB in cardiomyocyte survival in cardiomyopathy.* J Biol Chem, 2009. **284**(37): p. 24857-68.
210. Peng, W., et al., *Cardioprotection by CaMKII-deltaB is mediated by phosphorylation of heat shock factor 1 and subsequent expression of inducible heat shock protein 70.* Circ Res, 2010. **106**(1): p. 102-10.
211. Hoch, B., et al., *Identification and expression of delta-isoforms of the multifunctional Ca2+/calmodulin-dependent protein kinase in failing and nonfailing human myocardium.* Circ Res, 1999. **84**(6): p. 713-21.
212. Wang, Z., et al., *Calcium/Calmodulin-dependent protein kinase II delta 6 (CaMKIIdelta6) and RhoA involvement in thrombin-induced endothelial barrier dysfunction.* J Biol Chem, 2010. **285**(28): p. 21303-12.
213. Saddouk, F.Z., et al., *Ca2+/calmodulin-dependent protein kinase II-gamma (CaMKIIgamma) negatively regulates vascular smooth muscle cell proliferation and vascular remodeling.* Faseb j, 2016. **30**(3): p. 1051-64.
214. Pandey, D., et al., *Calcium/calmodulin-dependent kinase II mediates the phosphorylation and activation of NADPH oxidase 5.* Mol Pharmacol, 2011. **80**(3): p. 407-15.
215. Cai, H., et al., *Induction of endothelial NO synthase by hydrogen peroxide via a Ca(2+)/calmodulin-dependent protein kinase II/janus kinase 2-dependent pathway.* Arterioscler Thromb Vasc Biol, 2001. **21**(10): p. 1571-6.
216. Fleming, I., et al., *Phosphorylation of Thr(495) regulates Ca(2+)/calmodulin-dependent endothelial nitric oxide synthase activity.* Circ Res, 2001. **88**(11): p. E68-75.
217. Xia, Y., et al., *Superoxide generation from endothelial nitric-oxide synthase. A Ca2+/calmodulin-dependent and tetrahydrobiopterin regulatory process.* J Biol Chem, 1998. **273**(40): p. 25804-8.
218. Luo, S.F., et al., *Activation of ROS/NF-kappaB and Ca2+/CaM kinase II are necessary for VCAM-1 induction in IL-1beta-treated human tracheal smooth muscle cells.* Toxicol Appl Pharmacol, 2009. **237**(1): p. 8-21.
219. House, S.J., et al., *Calcium/calmodulin-dependent protein kinase II-delta isoform regulation of vascular smooth muscle cell proliferation.* Am J Physiol Cell Physiol, 2007. **292**(6): p. C2276-87.
220. Abraham, S.T., et al., *A role for Ca2+/calmodulin-dependent protein kinase II in the mitogen-activated protein kinase signaling cascade of cultured rat aortic vascular smooth muscle cells.* Circ Res, 1997. **81**(4): p. 575-84.

221. Marganski, W.A., et al., *Targeting of a novel Ca+2/calmodulin-dependent protein kinase II is essential for extracellular signal-regulated kinase-mediated signaling in differentiated smooth muscle cells.* Circ Res, 2005. **97**(6): p. 541-9.
222. Kim, I., et al., *Ca2+-calmodulin-dependent protein kinase II-dependent activation of contractility in ferret aorta.* J Physiol, 2000. **526 Pt 2**(Pt 2): p. 367-74.
223. Rokolya, A. and H.A. Singer, *Inhibition of CaM kinase II activation and force maintenance by KN-93 in arterial smooth muscle.* Am J Physiol Cell Physiol, 2000. **278**(3): p. C537-45.
224. Lieb, W., et al., *Residual cardiovascular risk in individuals on lipid-lowering treatment: Quantifying absolute and relative risk in the community.* Open Heart, 2018. **5**: p. e000722.
225. Zhou, Z.L. and M. Ikebe, *New isoforms of Ca2+/calmodulin-dependent protein kinase II in smooth muscle.* Biochem J, 1994. **299 (Pt 2)**(Pt 2): p. 489-95.
226. Miller, S.G. and M.B. Kennedy, *Distinct forebrain and cerebellar isozymes of type II Ca2+/calmodulin-dependent protein kinase associate differently with the postsynaptic density fraction.* J Biol Chem, 1985. **260**(15): p. 9039-46.
227. Bers, D.M. and E. Grandi, *Calcium/calmodulin-dependent kinase II regulation of cardiac ion channels.* J Cardiovasc Pharmacol, 2009. **54**(3): p. 180-7.
228. Erickson, J.R., *Mechanisms of CaMKII Activation in the Heart.* Front Pharmacol, 2014. **5**: p. 59.
229. Zhang, T., et al., *CaMKIIdelta isoforms differentially affect calcium handling but similarly regulate HDAC/MEF2 transcriptional responses.* J Biol Chem, 2007. **282**(48): p. 35078-87.
230. Hu, X., et al., *Ras ssDNA aptamer inhibits vascular smooth muscle cell proliferation and migration through MAPK and PI3K pathways.* Int J Mol Med, 2015. **35**(5): p. 1355-61.
231. Ferns, G.A., et al., *Inhibition of neointimal smooth muscle accumulation after angioplasty by an antibody to PDGF.* Science, 1991. **253**(5024): p. 1129-32.
232. Vandesompele, J., et al., *Accurate normalization of real-time quantitative RT-PCR data by geometric averaging of multiple internal control genes.* Genome Biology, 2002. **3**(7): p. research0034.1.
233. Elgersma, Y., J.D. Sweatt, and K.P. Giese, *Mouse genetic approaches to investigating calcium/calmodulin-dependent protein kinase II function in plasticity and cognition.* J Neurosci, 2004. **24**(39): p. 8410-5.
234. Chang, J.Y., et al., *CaMKII Autophosphorylation Is Necessary for Optimal Integration of Ca(2+) Signals during LTP Induction, but Not Maintenance.* Neuron, 2017. **94**(4): p. 800-808.e4.
235. Yin, P., et al., *Overexpression of βCaMKII impairs behavioral flexibility and NMDAR-dependent long-term depression in the dentate gyrus.* Neuropharmacology, 2017. **116**: p. 270-287.
236. Paigen, B., et al., *Comparison of atherosclerotic lesions and HDL-lipid levels in male, female, and testosterone-treated female mice from strains C57BL/6, BALB/c, and C3H.* Atherosclerosis, 1987. **64**(2-3): p. 215-21.
237. Smith, D.D., et al., *Increased aortic atherosclerotic plaque development in female apolipoprotein E-null mice is associated with elevated thromboxane A2 and decreased prostacyclin production.* J Physiol Pharmacol, 2010. **61**(3): p. 309-16.
238. Teupser, D., A.D. Persky, and J.L. Breslow, *Induction of atherosclerosis by low-fat, semisynthetic diets in LDL receptor-deficient C57BL/6J and FVB/NJ mice: comparison of lesions of the aortic root, brachiocephalic artery, and whole aorta (en face measurement).* Arterioscler Thromb Vasc Biol, 2003. **23**(10): p. 1907-13.

239. Maeda, N., et al., *Anatomical differences and atherosclerosis in apolipoprotein E-deficient mice with 129/SvEv and C57BL/6 genetic backgrounds.* Atherosclerosis, 2007. **195**(1): p. 75-82.
240. Ling, H., et al., *Requirement for Ca2+/calmodulin-dependent kinase II in the transition from pressure overload-induced cardiac hypertrophy to heart failure in mice.* J Clin Invest, 2009. **119**(5): p. 1230-40.
241. González-Navarro, H., et al., *p19(ARF) deficiency reduces macrophage and vascular smooth muscle cell apoptosis and aggravates atherosclerosis.* J Am Coll Cardiol, 2010. **55**(20): p. 2258-68.
242. Otto, C.M., et al., *Characterization of the early lesion of 'degenerative' valvular aortic stenosis. Histological and immunohistochemical studies.* Circulation, 1994. **90**(2): p. 844-53.
243. Fuster, V., et al., *Atherosclerotic plaque rupture and thrombosis. Evolving concepts.* Circulation, 1990. **82**(3 Suppl): p. Ii47-59.
244. Cai, H., D. Liu, and J.G.N. Garcia, *CaM Kinase II-dependent pathophysiological signalling in endothelial cells.* Cardiovascular Research, 2008. **77**(1): p. 30-34.
245. Singer, H.A., *Ca2+/calmodulin-dependent protein kinase II function in vascular remodelling.* J Physiol, 2012. **590**(Pt 6): p. 1349-56.
246. Toussaint, F., et al., *Vascular CaMKII: heart and brain in your arteries.* American journal of physiology. Cell physiology, 2016. **311**(3): p. C462-C478.
247. Pfleiderer, P.J., et al., *Modulation of vascular smooth muscle cell migration by calcium/calmodulin-dependent protein kinase II-delta 2.* Am J Physiol Cell Physiol, 2004. **286**(6): p. C1238-45.
248. Shin, I.J., et al., *Characterization of partial ligation-induced carotid atherosclerosis model using dual-modality molecular imaging in ApoE knock-out mice.* PLoS One, 2013. **8**(9): p. e73451.
249. Kumar, A. and V. Lindner, *Remodeling with neointima formation in the mouse carotid artery after cessation of blood flow.* Arterioscler Thromb Vasc Biol, 1997. **17**(10): p. 2238-44.
250. Chang, Z., et al., *Accelerated atherogenesis in completely ligated common carotid artery of apolipoprotein E-deficient mice.* Oncotarget, 2017. **8**(66): p. 110289-110299.
251. Nam, D., et al., *Partial carotid ligation is a model of acutely induced disturbed flow, leading to rapid endothelial dysfunction and atherosclerosis.* Am J Physiol Heart Circ Physiol, 2009. **297**(4): p. H1535-43.
252. Li, L., et al., *Tetrahydrobiopterin deficiency and nitric oxide synthase uncoupling contribute to atherosclerosis induced by disturbed flow.* Arterioscler Thromb Vasc Biol, 2011. **31**(7): p. 1547-54.
253. Padayachee, T.S., et al., *The measurement of internal carotid artery stenosis: comparison of duplex with digital subtraction angiography.* Eur J Vasc Endovasc Surg, 1997. **13**(2): p. 180-5.
254. Brott, T.G., et al., *Long-Term Results of Stenting versus Endarterectomy for Carotid-Artery Stenosis.* N Engl J Med, 2016. **374**(11): p. 1021-31.
255. Muthalif, M.M., et al., *Functional significance of activation of calcium/calmodulin-dependent protein kinase II in angiotensin II--induced vascular hyperplasia and hypertension.* Hypertension, 2002. **39**(2 Pt 2): p. 704-9.
256. Getz, G.S. and C.A. Reardon, *Diet and murine atherosclerosis.* Arterioscler Thromb Vasc Biol, 2006. **26**(2): p. 242-9.
257. Mathur, P., et al., *Gender-Related Differences in Atherosclerosis.* Cardiovasc Drugs Ther, 2015. **29**(4): p. 319-27.

258. Whitman, S.C., *A practical approach to using mice in atherosclerosis research.* Clin Biochem Rev, 2004. **25**(1): p. 81-93.
259. Zhu, L.J., et al., *Oxidative activation of the Ca(2+)/calmodulin-dependent protein kinase II (CaMKII) regulates vascular smooth muscle migration and apoptosis.* Vascul Pharmacol, 2014. **60**(2): p. 75-83.
260. Scott, J.A., et al., *The multifunctional Ca(2)(+)/calmodulin-dependent kinase IIdelta (CaMKIIdelta) regulates arteriogenesis in a mouse model of flow-mediated remodeling.* PLoS One, 2013. **8**(8): p. e71550.
261. Holt, A.W. and D.A. Tulis, *Experimental Rat and Mouse Carotid Artery Surgery: Injury & Remodeling Studies.* ISRN Minim Invasive Surg, 2013. **2013**.
262. Korshunov, V.A. and B.C. Berk, *Flow-induced vascular remodeling in the mouse: a model for carotid intima-media thickening.* Arterioscler Thromb Vasc Biol, 2003. **23**(12): p. 2185-91.
263. Marx, S.O., H. Totary-Jain, and A.R. Marks, *Vascular smooth muscle cell proliferation in restenosis.* Circ Cardiovasc Interv, 2011. **4**(1): p. 104-11.
264. Orford, J.L., et al., *The comparative pathobiology of atherosclerosis and restenosis.* Am J Cardiol, 2000. **86**(4b): p. 6h-11h.
265. Handa, N., et al., *Ischemic stroke events and carotid atherosclerosis. Results of the Osaka Follow-up Study for Ultrasonographic Assessment of Carotid Atherosclerosis (the OSACA Study).* Stroke, 1995. **26**(10): p. 1781-6.
266. Flaherty, M.L., et al., *Carotid artery stenosis as a cause of stroke.* Neuroepidemiology, 2013. **40**(1): p. 36-41.
267. Mercure, M.Z., R. Ginnan, and H.A. Singer, *CaM kinase II delta2-dependent regulation of vascular smooth muscle cell polarization and migration.* Am J Physiol Cell Physiol, 2008. **294**(6): p. C1465-75.
268. Kisanuki, Y.Y., et al., *Tie2-Cre transgenic mice: a new model for endothelial cell-lineage analysis in vivo.* Dev Biol, 2001. **230**(2): p. 230-42.
269. Mali, P., K.M. Esvelt, and G.M. Church, *Cas9 as a versatile tool for engineering biology.* Nat Methods, 2013. **10**(10): p. 957-63.
270. Sumi, M., et al., *The newly synthesized selective Ca2+/calmodulin dependent protein kinase II inhibitor KN-93 reduces dopamine contents in PC12h cells.* Biochem Biophys Res Commun, 1991. **181**(3): p. 968-75.
271. Ishida, A., et al., *A novel highly specific and potent inhibitor of calmodulin-dependent protein kinase II.* Biochem Biophys Res Commun, 1995. **212**(3): p. 806-12.
272. Kattoor, A.J., et al., *Oxidative Stress in Atherosclerosis.* Curr Atheroscler Rep, 2017. **19**(11): p. 42.
273. Patel, R.P., et al., *Cell signaling by reactive nitrogen and oxygen species in atherosclerosis.* Free Radic Biol Med, 2000. **28**(12): p. 1780-94.
274. Toth, P.P., *Subclinical atherosclerosis: what it is, what it means and what we can do about it.* Int J Clin Pract, 2008. **62**(8): p. 1246-54.
275. Simon, A. and J. Levenson, *Early detection of subclinical atherosclerosis in asymptomatic subjects at high risk for cardiovascular disease.* Clin Exp Hypertens, 1993. **15**(6): p. 1069-76.